

Schwann cell/axonal interactions in peripheral nerve

Patrick Wingfield Digby

A thesis submitted for the degree of Doctor of Philosophy

Medical Research Council

Laboratory for Molecular Cell Biology

University College London



Declaration

I, Patrick Wingfield Digby, do hereby confirm that the work presented in this thesis is my own. Where information has been derived from other sources, I confirm that this has been indicated in the thesis.

Signed



Date 19th Sept 2013

Abstract

Schwann cells are found in close proximity with axons from an early developmental stage, where, in adult nerve, they exist as either myelinating or non-myelinating Schwann cells. Reciprocal, contact-dependent signalling, between Schwann cells and axons, is central to the regulation of Schwann cell proliferation, survival and differentiation, as well as axonal survival. Cell adhesion molecules (CAMs) mediate homotypic and heterotypic interactions. They are required during development, in homeostatic nerve and in nerve repair following injury. Dysregulation of signal pathways and resulting aberrant CAM expression, can lead to irreversible Schwann cell/axonal dissociation, which is a hallmark of various peripheral neuropathies and nerve sheath tumours, e.g. neurofibromas in NF1 patients.

In this thesis, I conducted a microarray screen to identify early mediators of Schwann cell/axonal interaction, using a Large-T (LT)-expressing Schwann cell that had spontaneously lost the ability to interact with axons, termed LT-derived (LTD) cells. This analysis revealed that multiple cell adhesion genes had become dysregulated including N-cadherin, Semaphorin-4F, Necl-4, NCAM and L1-CAM. This shift in adhesion profile suggested that a transcription factor, for example Sox2, might be the genetic lesion responsible; however, Sox2 was found not to be responsible for the LTD phenotype, although over-expression of Sox2 altered N-cadherin localisation at Schwann cell-cell junctions.

Further study showed that N-cadherin was required for homotypic interactions and was an important mediator of heterotypic interactions, where heterologous N-cadherin expression in fibroblasts was sufficient to induce fibroblasts to recognise and partially associate with axons. In addition, N-cadherin was implicated in the regulation of the cell cycle; while N-cadherin silencing, in Schwann cells prior to axonal contact, was found to impede myelination *in vitro*. Finally, this work showed that N-cadherin and Semaphorin-4F operate at distinct stages of the interaction process, with N-cadherin mediating axonal recognition and Semaphorin-4F involved in stabilising the Schwann cell/axonal association.

Acknowledgements

I would like to thank Alison Lloyd for her supervision and guidance over the years and for her dedication in reading the many drafts of this thesis. I would also like to thank her for passing on the secrets behind splitting cells!

I am especially indebted to Luke Noon for his inspirational mentoring during the early years of my PhD and to Simona Parrinello, with whom I worked on parts of this project: they were both fantastic teachers and much of what I know about research I learnt from them. I am also grateful to Ilaria Napoli, Sara Ribeiro for critical reading of this manuscript, to Sinead Roberts for final proof-reading and to Melissa Collins and Charles Bradshaw for their comments on microarray analysis. I would also like to thank Laura Rosenberg, Alexi Nott and the other students of my year for all their support and for sharing the experience with me.

In addition, Andrew Vaughan's help with time-lapse microscopy was invaluable, as was George Paschalis's consistent help on various computer issues over the years; all the core staff at the LMCB have been an amazing support.

I would like to thank my mother (Belinda), grandmother (Mimi), Lydia and Nicky for their unwavering support over the years. Thank you for always being there for me, especially during the latter years when times were particularly tough.

I would also like to acknowledge my wife Kerry, without whom, it is doubtful that I would have ever finished this project. You mean everything to me - thank you.

Finally, I would like to dedicate this thesis to my father (Kelly), whose drive in life has been an inspiration to me, and also to my daughter Elisia, who continues to surprise me each and every day.

Table of contents

Declaration.....	2
Abstract.....	3
Acknowledgements.....	4
Table of contents	5
Table of figures	12
List of tables.....	16
Abbreviations and acronyms.....	17
Chapter One: Introduction	19
1.1 Chapter introduction.....	19
1.2 The scope and aims of this review	20
1.3 The biology of the peripheral nervous system (PNS)	21
1.3.1 The structure and composition of peripheral nerves	22
Glia.....	26
Fibroblasts	28
Inflammatory cells	30
Blood vessels.....	31
1.4 The biology of Schwann cells	32
1.4.1 Schwann cell development.....	32
Neural crest cells	33
Schwann cell precursors.....	34
Immature Schwann cells	34
Radial sorting and the generation of adult Schwann cells	37
Myelination	38
The regulation of myelination.....	40
A) Extracellular environment.....	40

B) Extrinsic factors and cognate receptors.....	41
C) Extrinsic modulators.....	48
D) Transcriptional regulators	49
1.4.2 Nerve homeostasis and myelination.....	54
The evolution and function of myelin.....	54
Cell adhesion molecules as mediators of Schwann cell/axonal interactions	56
General principles of cell-cell interactions	56
Cell adhesion molecules of peripheral nerve	57
Cell adhesion molecules of early Schwann cell/axonal interactions	58
N-cadherin.....	58
The structure and downstream components of N-cadherin.....	59
The classical cadherins mediates cell-cell adhesion	60
The regulation of cadherin activity	64
Semaphorin-4F	64
L1-CAM.....	66
Neural Cell Adhesion Molecule (NCAM).....	68
Structural cell adhesion molecules of myelinated nerve.....	68
The Internode	70
The compact myelin sheath.....	70
Schwann cell/axonal cell adhesion molecules of the internode.....	72
The Node of Ranvier and associated domains	74
The Node of Ranvier	74
The Paranode.....	78
The Juxtaparanode	80
Non-compact myelin extra to the Node of Ranvier	82
Schmidt-Lanterman Incisures (SLIs).....	82
Cajal bands	84

1.5 Nerve injury and pathology	87
1.5.1 Injury	87
Wallerian degeneration	88
The axonal response	89
The Schwann cell response	90
The repaired nerve.....	91
1.5.2 Demyelinating neuropathies	91
1.5.3 Neurofibromatosis type I.....	93
Neurofibromin function and Ras signalling	94
NF1: Ras activation and tumour formation.....	95
1.5.4 Neurofibromatosis type II.....	97
1.6 Conclusions and thesis goals	98
Chapter Two: Materials & Methods	101
2.1 Reference tables	101
2.1.1 Cell culture media.....	101
2.1.2 siRNA oligonucleotides.....	102
2.1.3 shRNA oligonucleotides	102
2.1.4 Primers for qRT-PCR.....	103
2.1.5 Antibodies and fluorescent dyes.....	103
2.1.6 Solutions used for molecular techniques	105
2.1.7 Solutions and buffers for Western blotting	105
2.2 Cell culture	106
2.2.1 Schwann cells	106
2.2.2 Fibroblasts	107
2.2.3 Raf-1:ER Schwann cells.....	107
2.2.4 SV40 Large-T antigen (LT) expressing Schwann cells (LTNS & LTD)...	107

2.2.5	Viral Packaging/Producer Cells	108
2.2.6	Rat dorsal-root ganglion (DRG) explants	109
2.3	Cell culture assays	109
2.3.1	siRNA transfection	109
2.3.2	Adenovirus	110
2.3.3	Retrovirus and the generation of shRNA Schwann cells	111
2.3.4	DRG cocultures for association assays.....	114
2.3.5	Myelination assay	114
2.3.6	Proliferation assays.....	115
2.4	Molecular techniques.....	115
2.4.1	Bacterial transformation	115
2.4.2	Plasmid DNA extraction.....	116
2.4.3	Determination of quantity and quality of nucleotide.....	116
2.4.4	Restriction digestion & analytic gels.....	116
2.4.5	Polymerase chain reaction (PCR).....	117
2.4.6	RNA extraction & purification.....	118
2.4.7	First-strand cDNA synthesis	118
2.4.8	Quantitative RT-PCR (qRT-PCR).....	119
2.4.9	Microarray	120
2.5	Biochemistry.....	121
2.5.1	Protein extraction & quantification	121
2.5.2	Western blotting	121
2.6	Microscopy & image processing.....	122
2.6.1	Live-cell images	122
2.6.2	Immunofluorescence	122
2.6.3	Time-lapse microscopy	123
2.6.4	Extracellular area measurements.....	123

2.6.5 Scoring Schwann cell/axonal association.....	124
2.7 Statistics.....	125
Chapter Three: A screen for mediators of Schwann cell/axonal interactions..	126
3.1 Chapter introduction.....	126
3.2 Characterising Schwann cell/axonal interactions.....	126
3.3 Schwann cell/axonal recognition	130
3.4 Large-T Schwann cell/axonal interactions.....	132
3.5 LTD cells are a non-interacting Schwann cell type	136
3.6 Expression analysis between LTNS cells and LTD cells	138
3.6.1 Array specification.....	143
3.6.2 LTNS verses LTD expression microarray.....	144
3.6.3 Analysis of quality control metrics	144
3.6.4 Pre-processing of microarray data.....	151
3.6.5 Calculating differential gene expression	152
3.6.6 Gene annotation, analysis and secondary processing.....	152
3.6.7 Functional gene annotation, cluster and enrichment analysis	156
Cell adhesion molecules.....	160
Semaphorins.....	163
Transcriptional regulators	164
3.7 Array validation by qRT-PCR.....	166
3.8 Over-expression of Sox2 in Schwann cells	166
3.8.1 Sox2 drives Schwann cell clustering by an N-cadherin-dependent mechanism	172
3.8.2 Re-expression of Sox2 in LTD cells.....	173
3.9 Chapter summary and conclusions.....	176

Chapter Four: N-cadherin mediates homotypic and heterotypic cell-cell interactions.....	178
4.1 Chapter introduction	178
4.2 Homotypic Schwann cell-cell junctions	180
4.2.1 The expression and localisation of N-cadherin in Schwann cells.....	180
4.2.2 siRNA as a tool for N-cadherin knockdown in Schwann cells.....	184
4.2.3 N-cadherin is the principal mediator of homotypic interactions	187
4.2.4 N-cadherin inhibit Schwann cell proliferation.....	191
4.3 Heterotypic Schwann cell/axonal interactions.....	195
4.3.1 N-cadherin localisation in Schwann cells, axons & heterotypic junctions.....	199
4.3.2 Schwann cells use cytoplasmic protrusions to locate, recognise and initiate association.....	199
4.4 N-cadherin expression enables fibroblast/axonal interactions.....	204
4.5 Mature Schwann cell/axonal interactions	211
4.5.1 N-cadherin expression in polarisation and myelination.....	211
4.5.2 shRNA as a tool for stable N-cadherin knockdown in Schwann cells	211
4.5.3 Loss of N-cadherin from pre-associated Schwann cells impedes progression to myelination.....	217
4.6 Chapter summary and conclusions.....	222
Chapter Five: N-cadherin and semaphorin-4F play separate but cooperative roles in heterotypic Schwann cell/axonal interactions	223
5.1 Chapter introduction	223
5.2 Sema4F and the Ras/Raf/ERK signaling pathway.....	224
5.3 Oncogenic Ras signal disrupts Schwann cell/axonal interactions	224
5.3.1 Ras activation disrupts Schwann cell/axonal interactions despite N-cadherin expression	224

5.4 Raf-ER cells: an inducible Raf for studying Schwann cell/axonal interactions	225
5.4.1 N-cadherin expression and knockdown in Raf-ER cells	227
5.5 Loss of N-cadherin and hyper-elevated Raf/ERK signalling severely disrupted heterotypic Schwann cell/axonal interactions	229
5.6 Double knockdown of semaphorin-4F and N-cadherin in Schwann cells.....	236
5.7 Chapter summary and conclusion.....	237
Chapter Six: Discussion	241
6.1 Chapter introduction.....	241
6.2 Summary of main findings.....	241
6.3 Homotypic Schwann cell-cell interactions	243
6.3.1 A role for N-cadherin	244
6.3.2 Sox2 relocalises N-cadherin to cell-cell junctions and promotes Schwann cell-cell clustering	247
6.4 Homophilic N-cadherin ligation between Schwann cells elicits an inhibitory effect on the cell-cycle	250
6.5 Early mediators of heterotypic Schwann cell/axonal interactions	253
6.5.1 A role for N-cadherin	253
6.5.2 Distinct roles for Semaphorin-4F and N-cadherin	255
6.5.3 Identifying CAMs as mediators of heterotypic interaction.....	258
6.6 N-cadherin and stable Schwann cell/axonal interactions: polarisation and myelination	263
6.8 Conclusions	266
References	267
Appendix	286

Table of figures

Figure 1.1	Schematic showing a cross-section through a large peripheral nerve ..	23
Figure 1.2	Schematic showing a cross-section through the spinal cord and depicting the dorsal root ganglion and spinal nerves.....	24
Figure 1.3	Schematic showing the two fates of mature Schwann cells.	27
Figure 1.4	Schematic showing the Schwann cell lineage.	32
Figure 1.5	Proposed model for multi-lineage peripheral nerve development.....	36
Figure 1.6	Schematic showing the role of the axon in the determination of Schwann cell fate during radial sorting	39
Figure 1.7	Schematic showing the three major classes of Neuregulin-1	42
Figure 1.8	Axonal neuregulin-1 type III operates in a binary (threshold) and dose-dependent manner to regulate Schwann cell differentiation	44
Figure 1.9	Membrane tethered axonal neuregulin (NRG)-1 Type III regulates Schwann cell differentiation and myelin thickness	46
Figure 1.10	Schematic of a pro-myelinating Schwann cell, showing the balance of factors required to initiate myelination.....	53
Figure 1.11	Schematic showing the classical view of cadherin structure.....	60
Figure 1.12	Schematic illustration showing the central role of calcium ions in generating the functional structure of the classical cadherins	61
Figure 1.13	Schematic showing the proposed linear-zipper model of cadherin homophilic adhesion	62
Figure 1.14	A theoretical model for adherens junction maturation.	63
Figure 1.15	The domain structure of class-4 semaphorins.....	65
Figure 1.16	Domain structure of L1-CAM and NCAM.....	67
Figure 1.17	Schematic showing the structure and domains of a myelinated nerve fibre.....	69
Figure 1.18	The structural components of compact myelin sheath.....	71
Figure 1.19	The cell adhesion molecules of the internode.....	72

Figure 1.20	The structure of the Node of Ranvier and its associated domains in a myelinated nerve fibre	75
Figure 1.21	Schwann cell/axonal CAM interactions at the Node of Ranvier.....	77
Figure 1.22	Cell adhesion molecules of the paranodal junction.....	79
Figure 1.23	The cell adhesion molecules of the Node of Ranvier and associated domains of myelinated fibres.....	81
Figure 1.24	Schematic depicting the Cajal bands in myelinated fibre.....	85
Figure 1.25	Schematic illustration of the events following nerve transection.....	89
Figure 1.26	Schematic showing a cross-section through a normal nerve fascicle compared to fascicle in early stages of neurofibroma formation.....	94
Figure 1.27	Receptor tyrosine kinase (RTK) activation of Ras and its downstream affects	96
Figure 1.28	Ras function and dysregulation in Neurofibromatosis type I (NF1)	97
Figure 2.1	Vector map of the pBabe-puromycin vector	108
Figure 3.1	Analysis of Schwann cell/axonal interactions	129
Figure 3.2	LTD/axonal interaction are severely impaired relative to NS and LTNS DRG cocultures.....	134
Figure 3.3	Time-lapse analysis confirmed that LTD cells were severely impaired in all aspects of axonal interaction	137
Figure 3.4	Characterisation of cell-types examined in this thesis.....	139
Figure 3.5	Schematic illustration showing the stages involved in microarray processing	145
Figure 3.6	Affymetrix quality control metrics	147
Figure 3.7	Schematic of analysis involved in secondary data processing	153
Figure 3.8	LTD cells have globally dysregulated gene expression.....	157
Figure 3.9	Validation of selected genes from the microarray analysis	167
Figure 3.10	Over-expression of Sox2 in Schwann cells strengthens N-cadherin junctions and promotes homotypic Schwann cell clustering.....	169

Figure 3.11	Sox2 over-expression does not affect N-cadherin levels in LTNS and LTD	174
Figure 4.1	Schwann cells express N-cadherin which is localised to homotypic Schwann cell-cell junctions	181
Figure 4.2	siRNA mediated N-cadherin silencing is effective, specific and transient.....	185
Figure 4.3	N-cadherin knockdown disrupts homotypic interactions in NS monocultures.....	189
Figure 4.4	N-cadherin silencing disrupts homotypic Schwann cell-cell interactions.....	192
Figure 4.5	N-Cadherin reduces Schwann cell proliferation in a density dependent manner	194
Figure 4.6	N-Cadherin knockdown disrupts heterotypic Schwann cell/axonal association & alignment.....	197
Figure 4.7	Temporal analysis of N-Cadherin localisation in Schwann cells interacting with axons.....	200
Figure 4.8	N-cadherin deficient Schwann cells showed an impaired ability to recognise and ‘grab’ axons	202
Figure 4.9	N-cadherin-expressing fibroblasts interact with axons.....	205
Figure 4.10	Fibroblasts that express N-cadherin can recognise, grab and partially associate with axons	207
Figure 4.11	N-cadherin localises along axons in established Schwann cell/axonal cocultures	212
Figure 4.12	Generating stably integrated N-cadherin shRNA Schwann cells	214
Figure 4.13	N-cadherin shRNA cells show a reduced propensity to myelinate axons	218
Figure 5.1	Ras Schwann cells failed to remain associated with axons despite N-cadherin expression localised to cytoplasmic protrusions.....	226
Figure 5.2	N-cadherin knockdown in Raf-ER cells is effective, but only at a higher concentration of siRNA	228

Figure 5.3	N-cadherin knockdown in Raf-activated Schwann cells severely disrupts interactions with axons.....	230
Figure 5.4	Schwann cell/axonal ‘grabbing’ behaviour is severely affected by loss of N-cadherin in a background of Raf/ERK activation	232
Figure 5.5	Simultaneous silencing of N-cadherin and Sema4F in NS cells after double siRNA transfection	238
Figure 5.6	Combined loss of N-cadherin and Semaphorin-4F from Schwann cells severely impairs association and alignment	239
Figure 6.1	Schematic of the mechanism by which fibroblast/Schwann cell interactions promote Schwann cell-cell clustering after injury	248
Figure 6.2	Schematic illustrating the importance of Sox2 mediated Schwann cell-cell interactions during nerve regeneration.....	249

List of tables

Table 1.1	Adhesion molecules relevant to this thesis.....	86
Table 2.1	Cell-culture media.....	101
Table 2.2	siRNA oligonucleotides.....	102
Table 2.3	shRNA oligonucleotides.....	102
Table 2.4	Primers for qRT-PCR.....	103
Table 2.5	Antibodies and fluorescent markers.....	103
Table 2.6	Solutions used for molecular techniques.....	105
Table 2.7	Solutions and buffers for Western blotting.....	105
Table 2.8	Reaction mixture for shRNA insert / vector ligation.....	112
Table 2.9	Cell plating densities for DRG cocultures.....	114
Table 2.10	Standard reaction mixture for restriction digests.....	117
Table 2.11	Standard PCR reaction mix and thermal-cycler programme.....	117
Table 2.12	First-strand cDNA synthesis.....	119
Table 3.1	Gross analysis of probesets comprising the Rat 230-2 microarray	154
Table 3.2	Summary of the types of source data used in the design of probesets for the Rat 230-2 GeneChip.....	155
Table 3.3	Analysis of data from the annotated gene list.....	155
Table 3.4	Functional annotation enrichment analysis (clusters 1 to 5).....	158
Table 3.5	List genes from functional-annotation cluster one of Table 3.4 that share common adhesion related functions.....	161
Table 3.6	Semaphorin family members and their receptors significantly changed in LTD cells.....	163
Table 3.7	List of genes involved in transcription.....	164
Table 6.1	A comparison of CAMs identified in the Spiegel et al. (2006) study against dysregulated genes in the LT microarray.....	259

Abbreviations and acronyms commonly used in this thesis

Ad-	Adenovirus
ANOVA	Analysis of variance
ANS	Autonomic nervous system
AraC	Cytosine β -D-arabinofuranoside
BDNF	Brain derived neurotrophic factor
BNB	Blood nerve barrier
bp	base pair
BrdU	5-bromo-2-deoxyuridine
BSA	Bovine serum albumin
CAM	Cell adhesion molecule
cAMP	Cyclic adenosine monophosphate
cDNA	Complementary deoxyribonucleic acid
CIP	Contact-dependent inhibition of proliferation
CMT	Charcot-Marie-Tooth disease
CNS	Central nervous system
CREB	cAMP response element binding protein
Cx32	Connexin-32
DAVID	Database for Annotation, Visualization and Integrated Discovery
db-cAMP	Dibutyryl-cAMP
Dhh	Desert hedgehog
DMEM	Dulbecco's modified eagle medium
DNF	Dermal neurofibroma
DRG	Dorsal root ganglion
Ecad	Epithelial cadherin
ECD	Extracellular domain
ECM	Extracellular matrix
EGF	Epidermal growth factor
EMT	Epithelial-mesenchymal transition
ERK	Extracellular related kinase
EST	Expressed sequence tag
Fb	Fibroblast
FC	Fold-change
FDR	False discovery rate
FGF	Fibroblast growth factor
GAP	GTPase activating protein
GAPDH	glyceraldehyde-3-phosphate dehydrogenase
GDNF	Glial cell-line derived neurotrophic factor
GEF	Guanine nucleotide exchange factor
GFAP	Glial fibrillary acidic protein
GFP	Green fluorescent protein
GPI	glycosylphosphatidylinositol
GPR	G-protein receptor
hrs	hours
IgCAM	Immunoglobulin-like cell adhesion molecule
IGF	Insulin-like growth factor
ISC	Immature Schwann cell
kb	kilobase pair
LOH	Loss of heterozygosity
LTD	Large-T derived Schwann cell
LTNS	Large-T Normal Schwann cell
MAG	Myelin-associated glycoprotein
MAPK	Mitogen activated protein kinase

MBP	Myelin basic protein
MM	Miss-match
MPZ	Myelin protein zero
mRNA	Messenger RNA
Ncad	Neural cadherin/cadherin-2 (Cdh2)
NCAM	Neural cell adhesion molecule
NCC	Neural crest cell
NCSC	Neural crest stem cell
NCV	Nerve conduction velocity
Necl	Nectin-like molecule
NF1	Neurofibromin/Neurofibromatosis type I
NF κ B	Nuclear factor kappa-light-chain-enhancer of activated B cells
NICD	Notch intracellular domain
NrCAM	Neuronal cell adhesion molecule
NRG	Neuregulin
NS	Normal Schwann cells
NT	Neurotrophin
OEC	Olfactory ensheathing cells
Oligo	Oligonucleotide
ORF	Open-reading frame
P-	Postnatal
PBS	Phosphate buffered saline
PCR	Polymerase chain reaction
PDGF	Platelet-derived growth factor
PFA	Paraformaldehyde
PI3K	Phosphatidylinositol-3-Kinase
PKA	Protein kinase A
PLL	Poly-L-lysine
PM	Perfect-match
PMP22	Peripheral myelin protein 22
PNF	Plexiform neurofibroma
PNJ	Paranodal junction
PNS	Peripheral nervous system
PXN	Periaxin
Raf-1:ER	Raf-1 estrogen receptor fusion protein
Rb	Retinoblastoma
RMA	Robust multi-array average
RPM	Revolutions per minute
RT	Reverse transcription
RTK	Receptor tyrosine kinase
S100 β	Calcium binding protein-100
SC	Schwann cell
SCE	Schwann cell specific enhancer
SCIP	Suppressed cAMP inducible POU
SCP	Schwann cell precursor
SDS-PAGE	Sodium dodecyl sulfate - polyacrylamide gel electrophoresis
Sema	Semaphorin
shRNA	short-hairpin (sh) RNA
siRNA	small interfering (si) RNA
SLI	Schmidt-Lanterman incisures
SNS	Somatic nervous system
Sox/SRY	Sex determining region-Y box protein
Tmx	4-hydroxy-Tamoxifen
UTR	Untranslated region protein-related domain
WD	Wallerian degeneration

Chapter One: Introduction

1.1 Chapter introduction

Intercellular communication is a fundamental and defining property of multi-cellular organisms, in which tight behavioural control of individual cells is asserted for the benefit of the organism as a whole (Alberts *et al.*, 2008). Direct cell-cell communications are important in all aspects of organisational behaviour. In development, cell-cell communications play essential roles in the regulation of multiple cellular processes including cell growth, proliferation, survival, migration and differentiation, all of which are required to generate the various tissue architectures comprising the body. In the adult, tissue homeostasis is tightly maintained by cell-cell communications that ensure processes of cell growth, proliferation and survival are appropriately balanced. This is essential for maintaining the size and structure of adult tissues undergoing continual turnover as well as to ensure that quiescence is maintained in non-dividing tissues.

Cell-cell communication is also essential for the detection of tissue injury and is later utilised to direct post-injury responses so that some degree of repair to damaged tissue can be accomplished. While this response can be relatively effective in some epithelial tissues, for instance wound-healing in the skin, post-trauma regeneration in more complex and differentiated tissue architectures is a rare phenomenon in mammalian biology. For example, injury to nerves of the central nervous system (CNS) invariably results in some degree of permanent paralysis with little prospect of repair (Leskovaar *et al.*, 2000). However, in contrast to the CNS, the peripheral nervous system (PNS) is capable of remarkably effective regeneration following nerve injury. A major difference between the PNS and the CNS in this regard, is the presence of Schwann cells, which associate with, ensheath and support almost all axons of the PNS (Armati, 2007; Jessen & Mirsky, 2005) (refer to page 26 for exceptions). Central to PNS recovery, following nerve injury, is the extraordinary ability of these highly specialised, differentiated Schwann cells to undergo a programme of dedifferentiation to generate proliferating stem-cell like progenitors, which then facilitate and direct the functional repair of the nerve (Harrisingh *et al.*, 2004; Parrinello *et al.*, 2010; Scherer & Salzer, 2001). This capacity for self-renewal,

more usually the reserve of stem cells, is a rare property for differentiated mammalian cells, and has only been observed in a few other mammalian cell types, including hepatocytes (Overturf *et al.*, 1997), pancreatic β -cells (Dor *et al.*, 2004) and endothelial cells.

Our understanding of the importance of Schwann cell biology to PNS nerve function has advanced considerably since their initial discovery by Theodore Schwann in 1839. However, over the next century, myelin was still generally thought of as little more than an insulating fatty layer, which was secreted by Schwann cells or indeed the axon – in fact, myelin was mistakenly named under this misapprehension, as the word is derived from the Greek *myelos*, which literally translates as marrow, i.e. implying that its origins were from the axon (Rosenbluth, 1999). The true complexity behind the bidirectional relationship elicited by Schwann cells and axons only began to emerge following Geren's (1954) seminal paper describing the repeated wrapping of the Schwann cell membrane about the axon in chick nerve myelination. Since then, the physical and signalling interdependence of Schwann cells and axons has received significant attention, especially in regard to myelination, but also during development, e.g. survival, proliferation and differentiation, as well as in later nerve homeostasis and the post-injury response discussed earlier. The importance of Schwann cell/axonal interactions in the PNS is underlined by consequences of dysregulation in the interaction programme, which can lead to cancer or a range of de-myelination neuropathies. Thus, identifying the molecular mediators involved, and determining their mechanism of action, will be central to our understanding of how this complex tissue develops, how it can regenerate following PNS nerve injury and how dysregulation results in PNS pathology. Additionally, CNS myelination shares many facets with PNS myelination, raising the intriguing possibility that mediators of PNS regeneration may in the future, be utilised in therapeutic approaches to clinically encourage CNS regeneration following injury or pathology.

1.2 The scope and aims of this review

The central theme of this introductory chapter will focus on the close reciprocal relationship that exists between Schwann cells and axons. In particular, I will

discuss the functional importance of this relationship for the PNS in terms of development, homeostasis, injury and pathology. I will begin by briefly describing the cell-types that comprise the functional PNS nerve and how these components create the radial and cylindrical architecture of peripheral nerve. I will then explore the development of the PNS in relation to Schwann cells and axons; detailing the essential roles played by contact-dependent cell-cell communication in all aspects of Schwann cell behaviour, while also emphasising the importance of the bidirectional nature of Schwann cell/axonal signalling in relation to axonal survival and regeneration. Integral to all these processes, are mediators of cell-cell signalling and adhesion; with this in mind, I will also set out our current understanding of the molecules that mediate and maintain Schwann cell/axonal interactions. I will then consider the cellular response elicited by Schwann cells following PNS injury and their role in PNS regeneration; contrasting this behaviour with the irreversible loss of Schwann cell/axonal interaction that occurs in nerve sheath tumours and various inherited de-myelinating neuropathies of the PNS. Finally, I will summarise the important principles behind Schwann cell/axonal interactions and identify deficiencies in current knowledge and outline the investigative aims and rationale of this thesis.

1.3 The biology of the peripheral nervous system (PNS)

The PNS is defined as the component of the nervous system extra to the CNS, where the CNS is defined as comprising the brain, i.e. the cerebellum, cerebrum and brainstem, as well as the spinal cord, with both structures enveloped by meninges and bathed in cerebral-spinal fluid (Purves *et al.*, 2001). Thus, while the CNS is confined to the cranial and dorsal cavities of the body, the PNS interfaces the CNS and extends bilaterally to connect with all the sensors and effectors of the body. Included within the PNS, are 31 pairs of spinal nerves, 12 pairs of cranial nerves, the autonomic nervous system and the peripheral ganglia (neuronal clusters extra to the CNS) (Bryne, 1997). While the CNS functions to receive, integrate and process information in order to execute behavioural responses, the PNS operates to bidirectionally convey information (required for that response) and instructions (the response) back and forth, respectively, between the CNS and the sensors and effectors. Examples of sensors include: Meissner's corpuscle (light touch); Merkle's

corpsule (touch); free-terminal nociceptors (pain); Pacinian corpuscle (deep pressure); Ruffini corpuscle (temperature). Examples of effectors include striated, smooth and cardiac muscle as well as various exocrine and endocrine glands (Vander *et al.*, 2001).

1.3.1 The structure and composition of peripheral nerves

In this review, I will focus on the portion of the nerve that contains nerve fibres rather than the ganglia or synapses, because this is the region in which axons are associated with Schwann cells. In cross-section, the peripheral nerve is a heterogeneous, tubular tissue; exhibiting a complex microarchitecture, constituting an array of cell-types including axons, Schwann cells, fibroblasts, endothelial cells (composing the vasculature) and various inflammatory cells, for example macrophages and mast cells.

The peripheral nerve is composed of three major compartments, the epineurium, perineurium and endoneurium (Pina-Oviedo & Ortiz-Hidalgo, 2008), which collectively protect the primary functional subunit of PNS nerve - the nerve fibre - from mechanical stresses. The nerve fibre consists of either a single axon (in myelinated fibres) or multiple axons (in non-myelinated fibres), that are ensheathed by Schwann cells, in the majority of cases (see page 26 for exceptions), and which are surrounded by a Schwann cell-derived basal lamina. In longitudinal section, both myelinated and non-myelinated fibres contain multiple Schwann cells dispersed along their length with no part of the axon exposed, even between adjacent Schwann cells. In cross-section, bundles of nerve fibres, small blood vessels, resident immune cells and fibroblasts are held within a collagenous matrix called the endoneurium, which altogether form a nerve fascicle. The nerve fascicle is delimited by an outer multi-layered sheath comprising perineurial cells and collagen-rich extracellular matrix (ECM), which collectively is called the perineurium (Choi & Kim, 2008; Parmantier *et al.*, 1999; Pina-Oviedo & Ortiz-Hidalgo, 2008). Larger nerves consists of multiple fascicles that together with larger blood vessels are contained by an outer protective sheath, composed of irregular fibrous and adipose tissue called the epineurium (Pina-Oviedo & Ortiz-Hidalgo, 2008) (**Figure 1.1**).

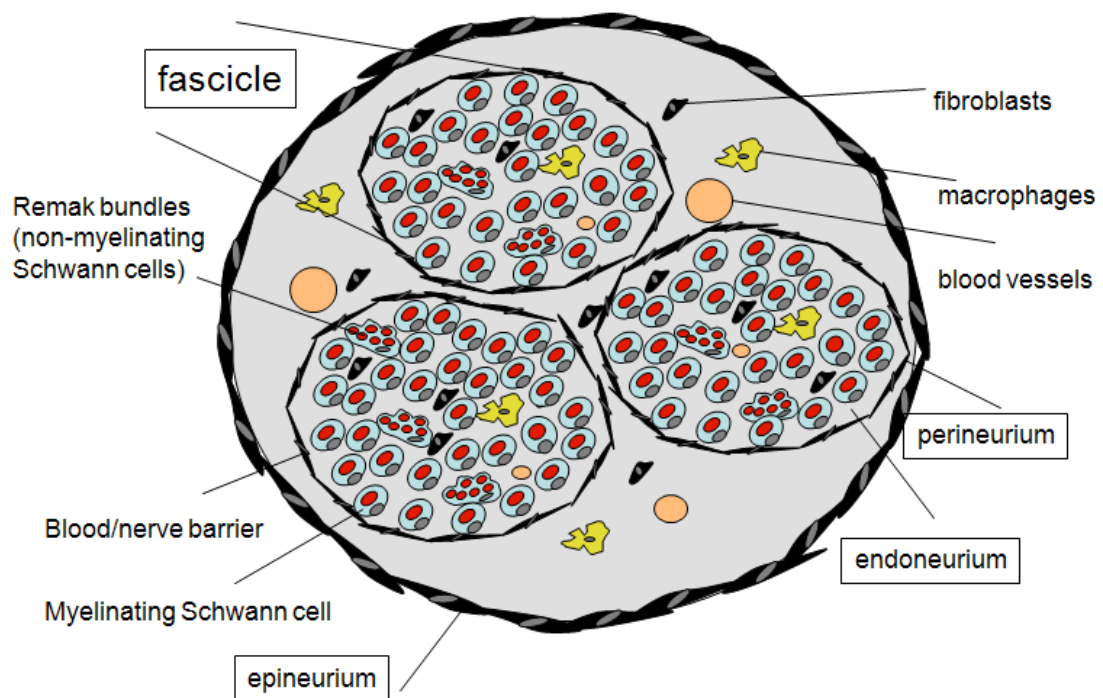


Figure 1.1 Schematic showing a cross-section through a large peripheral nerve. The nerve is enclosed by a fibrous sheath called the epineurium, which contains numerous nerve fascicles, blood vessels, epineurial fibroblasts and immune cells. Each fascicle contains both myelinating and non-myelinating fibres as well as small blood vessels, fibroblasts and immune cells, of which all reside within an extracellular matrix called the endoneurium. The fascicle is delimited by an outer perineurium that is composed of perineurial cells and collagenous extracellular matrix (ECM), which together with the endothelium of endoneurial blood vessels forms a protective blood-nerve barrier (BNB).

The PNS is composed of two functional classes of nerve fibre, referred to as afferent (sensory) and efferent (motor) fibres that convey electrical impulses to and from the CNS, respectively. In the case of spinal nerves, afferent nerve fibres enter the spinal cord through the dorsal horn, while efferent nerve fibres leave via the ventral horn; however, both types of nerve fibre merge a short distance from the spinal cord to form a single mixed spinal nerve. The cranial nerves have a slightly different arrangement, for example the olfactory nerve is composed exclusively of afferent fibres; however, in the interests of brevity they are not reviewed here. There are also important differences between the structure of afferent and efferent neurons. For instance, the cell bodies (ganglia) of afferent nerve fibres are found outside the CNS

in capsular structures called dorsal-root ganglia (DRG), which are discretely paired bilaterally along the dorsal aspect of the vertebrae, residing between the spinal cord and the confluence of afferent and efferent neurons (**Figure 1.2**).

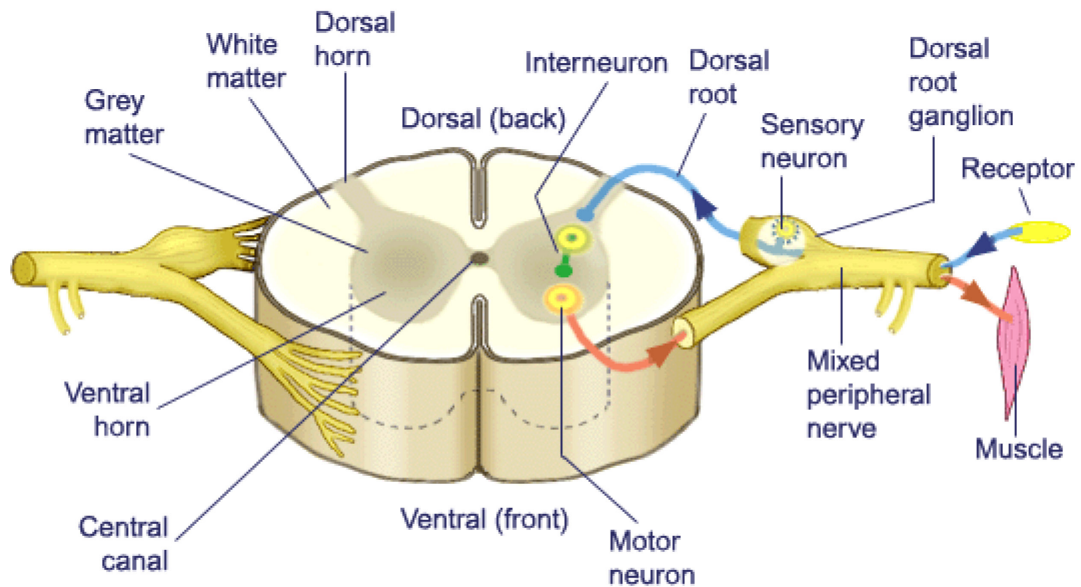


Figure 1.2 Schematic showing a cross-section through the spinal cord and depicting the dorsal root ganglion and spinal nerves. The afferent (sensory) nerve fibres (shown in blue) enter via the dorsal horn, while the efferent (motor) nerve fibres (shown in red) leave via the ventral horn. Both afferent and efferent fibres combine distal to the dorsal-root ganglion (DRG) to form a mixed peripheral (spinal) nerve (image by G. Mandl, 2012)¹.

Afferent neurons are pseudo-bipolar, projecting a single process that diverges a short distance from the ganglion into the peripheral branch, which innervates the target organ, and the central branch, which enters the spinal cord via the dorsal horn in order to synapse with CNS neurons (Mai & Paxinos, 2011). The term ‘pseudo’, in this context, refers to the fact that these neurons are derived from bipolar neuroblasts in which both axons have later fused. This arrangement allows for action potentials to effectively by-pass the cell-body, and therefore allows for sensory information to be transmitted directly from peripheral sensors to the CNS. Anatomically, both the

¹ <http://people.eku.edu/ritchisong/342notes11.html>

peripheral (myelinated and non-myelinated) and the central processes of the afferent neuron are considered to be axons rather than dendrites (Chen *et al.*, 2007).

The situation for efferent (motor) neurons is more complicated as this branch of the PNS can be divided into the somatic nervous system (SNS) or the autonomic nervous system (ANS). Neurons of the SNS have their cell bodies embedded within the CNS and directly innervate striated skeletal muscle under voluntary control of the conscious brain. In contrast, while primary neurons of the ANS also have their cell bodies encapsulated within the CNS, the projecting axon (the preganglionic fibre) synapses with the ganglion of a second neuron, which then recapitulates and transmits the signal on to the target effector via a second axonal fibre (the postganglionic fibre). The ANS differs functionally from the SNS in that the ANS is largely involuntary, i.e. signals are generated without awareness from the conscious brain. Furthermore, the ANS innervates smooth and cardiac muscle as well as glands and neurons of the gastrointestinal tract in order to regulate many vital functions of the body (Vander *et al.*, 2001).

The ANS is itself further subdivided into the sympathetic, parasympathetic and enteric subdivisions. The sympathetic and parasympathetic subdivisions often innervate the same organ (dual-innervation) and tend to exhibit functional antagonism, for example, while activity through sympathetic fibres causes an acceleration in heart contractions, constriction of pupils and stimulation of exocrine secretion, the reverse is elicited by parasympathetic fibres, i.e. a reduction in heart rate, relaxation of pupils and the inhibition of exocrine secretion. In addition, they perform separate functions, for instance sympathetic fibres innervate the adrenal medulla, which functions in an endocrine manner by releasing hormones into the blood. The arrangement of the nerves, the location of the connecting ganglion of the secondary neuron and the exit points of the nerve from the CNS, vary considerably between the sympathetic and parasympathetic nervous systems. Anatomically, sympathetic fibres leave the spinal cord from the thoracic and lumbar regions of the vertebrae, while parasympathetic nerve fibres leave from the sacral and cranial regions. The autonomic ganglia of parasympathetic nerve fibres lie within or near the target organ with little interconnectivity, while the autonomic ganglia of sympathetic

nerve fibres lie close to the spinal cord, and are extensively inter-connected by two parallel sympathetic trunk nerves that run either side of the spinal cord.

The third ANS subdivision is the enteric nervous system, which defines a neural network within the connective tissue of the gastro-intestinal (GI) tract, comprising two layers of nervous tissues, the myenteric plexus and the submucous plexus, separated by a band of circular smooth muscle. Enteric neurons form synapses extensively within and between the two nerve plexuses, as well as with both the parasympathetic and sympathetic subdivisions of the ANS and thus, indirectly with the CNS. However, most activity is coordinated through neural reflexes that are independent of the CNS (short reflexes) and contained within the GI-tract. Enteric nerve fibres innervate smooth muscle and gut epithelium, often generating waves of electrical activity that are capable of spreading rapidly throughout the GI system and beyond, i.e. to the CNS via afferent nerve fibres.

Glia

Glial cells (or neuroglia) are the accompanying cell to the neuron in both the CNS and the PNS (Vander *et al.*, 2001). Originally named from the Greek for 'glue', due to their perceived function in providing the physical matrix that support neurons, they are now also understood to be essential metabolic and cellular partners to neurons, and are vital to the function and injury response of the nervous system. The CNS and PNS have mutually exclusive glia, for instance CNS neurons are ensheathed by oligodendrocytes and supported by astrocytes, while the PNS nerve fibre is ensheathed predominantly by Schwann cells (Chen *et al.*, 2007; Corfas *et al.*, 2004; Jessen & Mirsky, 2005). This defining difference between the glial components of the CNS versus the PNS has profound consequences for regeneration as discussed later. In addition to Schwann cells, the PNS is also supported by a minority of specialised glia. These include olfactory ensheathing cells (OECs) supporting olfactory neurons; terminal glia (teloglia), which encase axons at the neuromuscular junction; enteric glia, which envelop neurons of the complex ganglia, and satellite glia that surround the soma of dorsal-root, sympathetic and parasympathetic ganglia (Jessen, 2004; Jessen & Mirsky, 2005; Murphy *et al.*, 1996).

In this review I will focus on the Schwann cell, which is the major supporting glia of the PNS.

Schwann cells were first identified by Theodore Schwann in 1839, following on from observations made by Remak the year before, who identified and distinguished the presence of both opaque and transparent fibres in the PNS (Rosenbluth, 1999). These phenomena can now be explained by the existence of two highly-specialised adult Schwann cell fates: myelinating or non-myelinating Schwann cells (**Figure 1.3**).

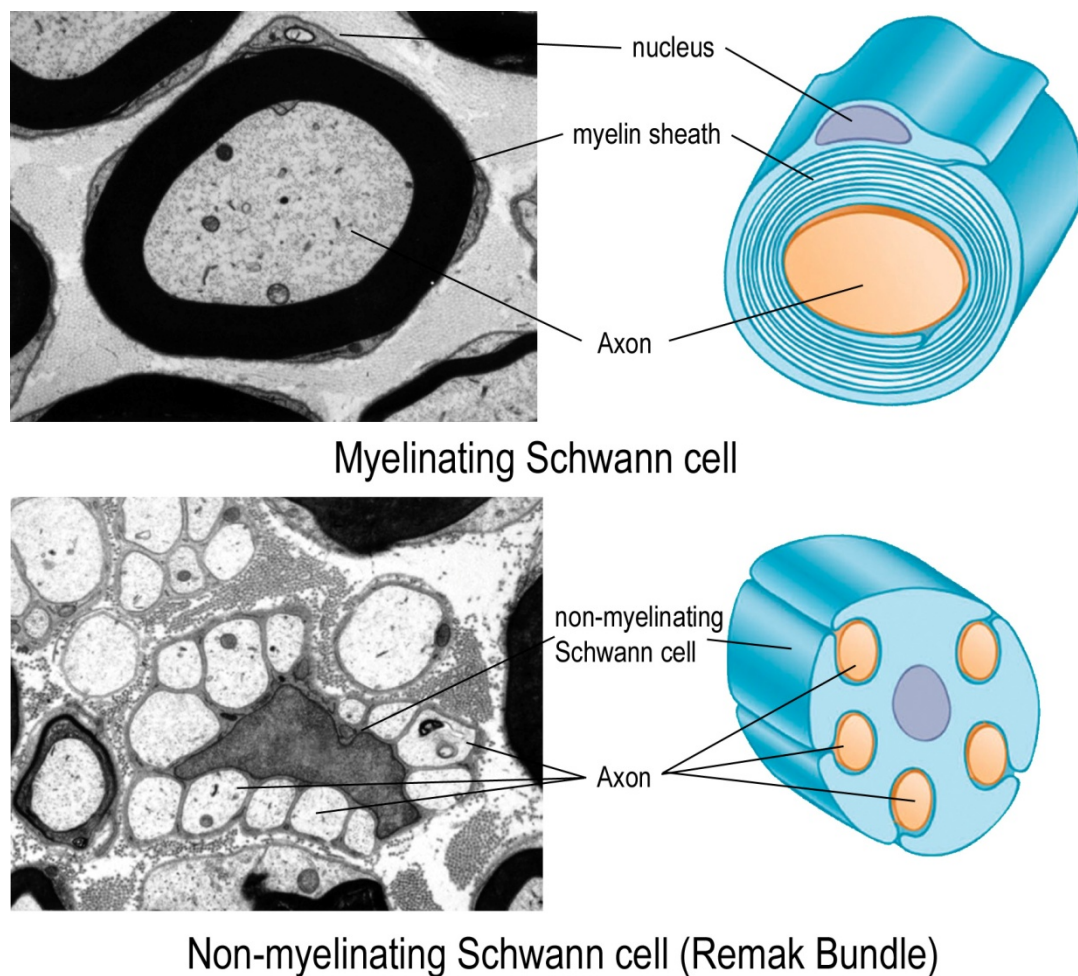


Figure 1.3 Schematic showing the two fates of mature Schwann cells. Adult Schwann cells exist as either myelinating Schwann cells, which synthesise myelin and ensheath a single axon in concentric multi-lamella sheets of membrane, or as non-myelinating Schwann cells, which do not synthesise myelin and individually ensheath multiple axons into Schwann cell/axonal families termed Remak bundles (Adapted from Jessen & Mirsky, 1999; Salzer, 2008).

Myelinating Schwann cells, which have historically been the most studied, are responsible for Remak's opaque fibres. In cross-section, myelinating Schwann cells ensheath large axons (greater than 1µm in diameter) in a one to one ratio, through concentric multilamellar wrapping of their plasma-membrane around the axon (Hartline & Colman, 2007; Sherman & Brophy, 2005). In addition, they synthesise large amounts of myelin protein and lipids, which are used to generate the two major regions of the myelin sheath: compact myelin, in which the exchange of metabolites including ion transfer is impeded, and non-compact myelin, which provide essential aqueous conduits within the sheath for metabolic exchange, both within the Schwann cell and between the Schwann cell and the axon it surrounds (Nave, 2010a; Poliak & Peles, 2003). The primary function of myelinating Schwann cells is to electrically insulate the axon that they ensheath, in order to permit significantly greater signal conduction velocities. In contrast, non-myelinating Schwann cells do not synthesise myelin but instead envelop multiple, small-calibre axons (generally less than 1µm in diameter), within invaginations of their membrane, called Remak bundles (Denisenko *et al.*, 2008; Jessen & Mirsky, 2005; Nave & Salzer, 2006; Sherman & Brophy, 2005).

Fibroblasts

Fibroblasts are 'non-vascular, non-epithelial and non-inflammatory' cells, which primarily function to construct the connective tissues that ensure the integrity of multiple organ systems within the body (Aboussekhra, 2011). They achieve this by synthesising procollagen, as well as other ECM components, which they secrete into the external *milieu*. In the case of collagen, which accounts for 30% of all protein synthesis in humans, extracellular collagen peptidases convert fibroblast-secreted procollagen into tropocollagen while lysyl oxidase and other extracellular enzymes generate the functional collagen fibrils (Di Lullo *et al.*, 2002). In contrast to epithelial cells, fibroblasts are not usually tethered to a basement membrane and thus, are generally not immobilised within the connective tissues they create. In healthy adult homeostatic tissue, fibroblasts that exhibit low-rates of basal proliferation, are found dispersed throughout the stroma of all connective tissues in the body. Upon tissue wounding or in fibroblast-associated cancers, fibroblasts generate large intracellular contractile fibres (stress-fibres) and revert to a more metabolically active

state, indicated by an abundance of rough endoplasmic reticulum (Aboussekhra, 2011). They synthesise and secrete ECM components, including collagen Type-1 fibres that will often result in tissue scarring (Polyak & Kalluri, 2010).

In the adult peripheral nerve, inactivated nerve fibroblasts are found within all three compartments of the nerve, i.e. the epineurium, perineurium, and endoneurium (Dreesmann *et al.*, 2009) at about one fibroblast to every nine Schwann cells (Jessen & Mirsky, 2005). The different compartments of the nerve contain fibroblasts that are specialised to perform specific functions. One example are perineurial cells, which are a highly-specialised fibroblast-like cell that comprises the perineurium that surrounds the nerve fascicle, and which forms a selectively-permeable barrier between the endoneurium and the epineurium and is part of the blood-nerve barrier (BNB) (Alanne *et al.*, 2009; Pina-Oviedo & Ortiz-Hidalgo, 2008). These flattened cells are held together by tight-junctions composed of zonula occludens (ZO)-1, occludin, claudin-1, and claudin-3 (Pummi *et al.*, 2004). The development of the perineurium is initiated relatively late in the Schwann cell lineage and is discussed later.

In terms of ECM and collagen synthesis, the standard injury response elicited by fibroblasts in PNS nerve appears tailored to reduce tissue scarring, which is beneficial to PNS nerve regeneration because scarring from excessive collagen Type-1 synthesis, as observed following CNS injury, presents a barrier to successful regeneration. Instead, and in contrast to fibroblast-related astrocytes in the CNS, nerve fibroblasts play a unique, conducive role in PNS regeneration. For instance, Morris *et al.* (1972) observed that perineurial fibroblasts reorganised the architecture of the regenerating nerve to generate 'mini-fascicles', absent from the pre-injured nerve, which provide a protective environment for regenerating axons (Hall, 2005). In addition, fibroblasts present in the injured nerve secrete neuregulin (NRG)-1, which has a pro-migratory effect on recently de-myelinated Schwann cells, and thus encourages the migration of Schwann cells from the proximal stump into the injury site (Dreesmann *et al.*, 2009), while ephrin-B/EphB2 signalling between Schwann cells and fibroblasts enhances homotypic Schwann cell/Schwann cell adhesional interactions and promotes directed, collective migration of Schwann cells by a Sox2-N-cadherin dependent mechanism (Parrinello *et al.*, 2010).

Inflammatory cells

The endoneurium of peripheral nerves, containing the nerve fibres, is an immune-privileged environment. This is maintained by the perineurium, that surrounds the endoneurium, and specialised endothelial cells that form the endoneurial blood vessels - both of which generate the BNB that prevents immune cells and harmful metabolites from accessing the endoneurium. However, certain restricted immune cells, termed resident immune cells, are present and are dispersed throughout the endoneurium. These include macrophages, which account for 4% of the cellular composition of the endoneurium, and a smaller number of mast cells, both of which remain inactive in normal nerve physiology (Hall, 2005). Together with Schwann cells, the resident immune cells provide a rapid response to nerve injury and are essential mediators in Wallerian degeneration (WD), i.e. the controlled disintegration of distal axons following nerve injury (refer to section 1.5.1 for a detailed analysis of WD and the injury response). Resident immune cells are primed to respond to nerve injury, where they perform different functions. In addition to recently dedifferentiated (denervated) Schwann cells, activated macrophages begin the process of phagocytising myelin debris, or 'myeloids', which are a by-product of the myelin sheath left following Schwann cell dissociation from axons (Hall, 2005). This is an essential part of the repair process, as myelin components, for example myelin-associated glycoprotein (MAG), are inhibitive to regeneration (reviewed by Filbin, 2003; Tang *et al.*, 1997). Activation of resident macrophages and mast cells is thought to be mediated by Schwann cells, through secretion of cytokines, including interleukin (IL)-1- α and tumour necrosis factor alpha (TNF- α), which build up at the nerve stump (site of injury) (Hall, 2005). Although less is known about mast cells, they are thought to be involved in mediating the breakdown of the BNB, which occurs within 48-hours after injury, through the secretion of vasoactive agents; although, endothelial cells and macrophages are also thought to play substantial roles in this through secretion of metalloproteinases and TNF- α , IL-1, respectively (Hall, 2005). The increased permeability of the BNB, together with proliferation of resident cells, results in a substantial increase in the number of macrophages, mast cells, neutrophils, and T-cells within the endoneurium (Napoli *et al.*, 2012). Infiltrating immune cells provide a secondary response to nerve injury, continuing to clear myelin debris and promote regeneration. Schwann cells are thought to play a

key role in the chemoattraction of infiltrating macrophages via the secretion of macrophage chemoattractant protein-1 (MCP-1) and leukaemia inhibitory factor (LIF) (Napoli *et al.*, 2012; Tofaris *et al.*, 2002). The authors also suggest that an autocrine-signalling cascade involving IL-6, LIF, and MCP-1 may explain the gradual accumulation of macrophage chemoattractants; thus accounting for the delayed entry of macrophages into the nerve. Following the repair of the nerve, lipid-rich macrophages remain in the epineurium for several weeks before numbers drop either by apoptosis or drainage into the lymph system (Hall, 2005).

Blood vessels

In addition to their central role in supplying oxygen and exchanging metabolites with tissues, the endothelium of the nerve, creates a protective, immune-privileged BNB, which together with the perineurium, prevents infiltration of inflammatory cells and selectively restricts the exchange of metabolites between blood and the endoneurium (Choi & Kim, 2008). The major blood vessels of the nerve run within the connective matrix of the epineurium and along the outer epineurial sheath. The immune-privileged *milieu* of the endoneurium, is serviced by small blood vessels composed of single-cell thickness endothelia held together by inter-locking tight-junctions (responsible for maintaining the BNB), that are themselves surrounded by pericytes (Joseph *et al.*, 2004). The properties of the endoneural vasculature is critical for maintaining cellular and metabolic homeostasis within the endoneurium; however, following nerve injury, the BNB must be overcome in order for immune cells, required for the phagocytosis of myelin debris, to enter the injury site and contribute to the generation of a permissive *milieu* for regeneration (Napoli *et al.*, 2012). Important questions remain as to the role of Schwann cells in the breakdown of BNB following injury (Napoli *et al.*, 2012).

1.4 The biology of Schwann cells

1.4.1 Schwann cell development

Schwann cell development is tightly coupled to the axons that they associate with (Jessen *et al.*, 2008a). The two adult Schwann cell phenotypes, myelinating and non-myelinating Schwann cells, are derived in a step-wise manner, from three transient cell populations: neural crest (NC) cells, Schwann cell precursors (SCPs) and immature Schwann cells (ISCs), each of which can be identified by a signature set of partially overlapping molecular differentiation markers (Jessen & Mirsky, 2005). In addition, ISCs differentiate to myelinating Schwann cells via a ‘pro-myelinating’ intermediate state that is dependent on Krox20 expression for further progression to the myelinated state (Jessen & Mirsky, 2005) (**Figure 1.4**).

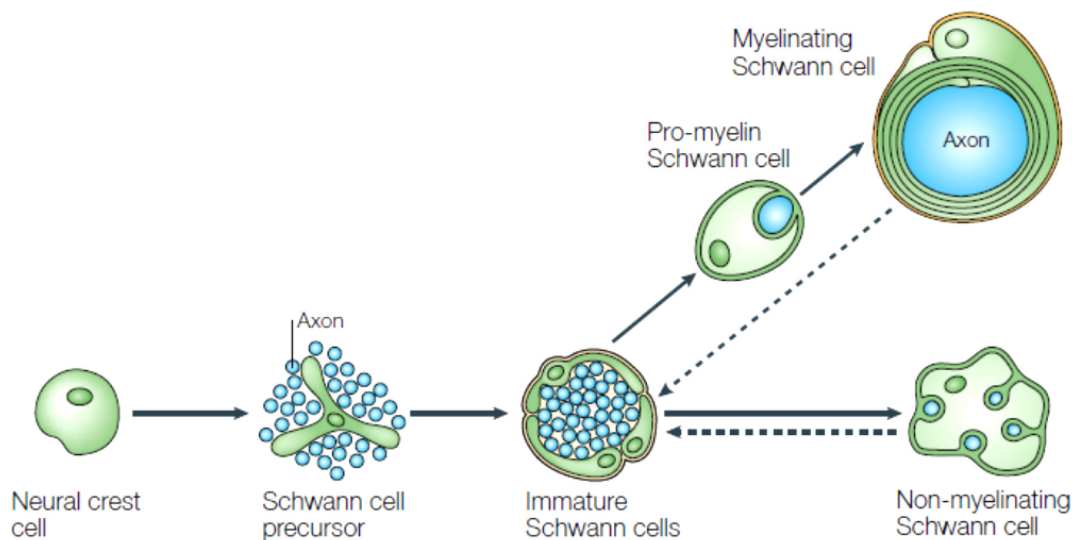


Figure 1.4 Schematic showing the Schwann cell lineage. Mature adult Schwann cells exist as either myelinating or non-myelinating Schwann cells. Their development follows a step-wise differentiation programme that encompasses a number of transient Schwann cell progenitors, comprising the multi-potent migrating neural crest (NC) cells, Schwann cell precursors (SCPs) and immature Schwann cell (ISCs). The developmental profile is remarkably plastic, with only the SCP to ISC transition considered irreversible, while differentiated adult Schwann cells remain able to readily dedifferentiate upon injury (indicated by the dashed-line) (Jessen & Mirsky, 2005).

Neural crest cells

Neural crest cells (NCCs) have been identified as the origin of nearly all Schwann cells (Jessen & Mirsky, 2005). They are formed towards the end of neurulation, a process that compartmentalises the PNS from the CNS, and are specified from the dorsal aspect of the neural tube. Following closure of the neural tube, NCCs undergo a form of epithelial-mesenchymal transition (EMT) in which they are extruded from the neural epithelium (a process known as delamination), to form a highly motile, transient population of undifferentiated cells (Jessen & Mirsky, 2005). A subset of the neural crest – neural crest stem cells (NCSC) – remains capable of extraordinary multi-potency, forming a diverse range of tissues (Joseph *et al.*, 2008; Morrison *et al.*, 1999). For instance, in addition to the glia, neural crest derivatives form the vast majority of the PNS, including ganglia and neuroendocrine tissue as well as mesectoderm (smooth muscle and bone), melanocytes and the connective tissues of the head (Garratt *et al.*, 2000; Morrison *et al.*, 1999). Importantly, neural crest do not appear to be the cell-of-origin for perineurial cells, a fibroblast-like cell that forms the perineurium, nor are they endothelial cells that form the blood vessels or pericytes that surround the endothelium (Joseph *et al.*, 2004). At this stage, all NCCs express the specification factor Sox10 as well as Activating protein (AP)-2, Ets-1, ErbB3 and the low-affinity neurotrophin receptor p75^(NTR) (Garratt *et al.*, 2000). NCCs migrate laterally to form various structures with many down-regulating Sox10, for example derivatives of facial-cranio mesenchyme; however, all glial cells and glial progenitors of the CNS and PNS continue to express Sox10 throughout embryonic development and throughout life (Jessen & Mirsky, 2005; Kuhlbrodt *et al.*, 1998). Loss of Sox10 results in the absence of Schwann cells from the nerve and conditional loss of Sox10 in immature Schwann cells prevents myelination even in the presence of the potent myelination drivers Krox20 and Oct-6 (Finzsch *et al.*, 2010). NCCs destined to form Schwann cells of the spinal nerves migrate and concentrate in regions just distal to the DRGs that line either side of the vertebrae, where they associate with the extending PNS axons of both afferent and efferent neurons. From this point onwards, all further stages in the Schwann cell lineage remain in close proximity with axons, which is essential for many aspects of PNS biology, for instance Schwann cell survival, proliferation, differentiation (Jessen & Mirsky, 2005) and also neuronal survival and function (Lemke, 2001).

Schwann cell precursors

Schwann cell-committed NCCs have generally completed their transition to SCPs by E14-E15 in the rat (E12-13 in the mouse) (Jessen & Mirsky, 2005), and can be identified by their expression of differentiation markers absent from NCCs, including F-spondin and GAP43, as well as basal expression of myelin protein zero (MPZ)/P0 (Dong *et al.*, 1995; Jessen & Mirsky, 2005; Stewart *et al.*, 2001). It is still unclear which transcriptional regulators orchestrate this transition, although as in all stages of the lineage, continued expression of Sox10 is required (as discussed earlier). At this stage, the primordial 'nerve' consists of tightly packed columns of axons and SCPs which are not serviced by a blood supply and have no basement membrane for protection (Court *et al.*, 2006; Jessen & Mirsky, 2005). PNS neurons continue to extend out axons to innervate targets, a process not complete until birth, while SCPs proliferate but remain closely associated with axons; although at this stage they do not ensheath axons (Jessen & Mirsky, 2005). During this process, SCPs appear to mantle and thus protect the axonal growth cone, as it navigates through mesenchymal tissues to locate targets for innervation, which is especially evident when neurones make growth decisions (Wanner *et al.*, 2006b). A defining feature of SCPs, distinct from later Schwann cell-types, is their essential, cell-contact dependent reliance on axons for their survival and proliferation, which is mediated through NRG1 Type III expressed on the cell-surface of the axons (Birchmeier & Nave, 2008; Dong *et al.*, 1995).

Immature Schwann cells

The majority of SCPs have differentiated to immature Schwann cells (ISCs) by E15-E17 in the rat (E13-E15 in mouse), where they start to express the differentiation markers S100 β (calcium binding protein-100), GFAP (glial fibrillary acidic protein) and O4 (lipid antigen), while down-regulating N-cadherin and cadherin-19 (Corfas *et al.*, 2004; Jessen & Mirsky, 2005). The transition from SCP to immature Schwann cells is thought to be irreversible, and ISCs are generally committed to form either myelinating or non-myelinating adult Schwann cells (although this later transition is reversible), which is achieved shortly after birth (E22-23 in rat and E20-21 in mouse) (Jessen & Mirsky, 2005). The factors regulating SCP to ISC transition are thought to

include NRG-1 Type 1 (Dong *et al.*, 1995) and Notch (Woodhoo *et al.*, 2009), both of which have been shown to control the generation of ISCs from SCPs *in vitro* and *in vivo* respectively. However, NRG1 Type I and Type II knockout mice still develop ISCs normally (Meyer *et al.*, 1997), while inactivation of Notch delays myelination and hyper-activation of Notch causes the early generation of Schwann cells *in vivo*; strongly suggesting that Notch signalling is responsible for regulating this transition (Woodhoo *et al.*, 2009).

This transition also marks a profound change in the structure of the embryonic primordial nerve, which becomes increasingly established as mesenchymal cells are recruited from the surrounding *milieu* to form a loosely-connected sheath enclosing large collections of axons and their associated glia (Parmantier *et al.*, 1999). These rudimentary perineurial cells later undergo a mesenchyme to epithelial transition and, over the proceeding weeks, the perineurium develops into a tight multi-layered sheath, secured by tight junctions, which functions as a BNB (Parmantier *et al.*, 1999). Interestingly, ISCs have been implicated in the correct formation of the mature perineurium via the secretion of desert hedgehog (Dhh). Knockout mice lacking the Dhh gene (Dhh^{-/-}) exhibit nerves in which the perineurium is malformed and immature, i.e. not a tight, multilayered sheath (Parmantier *et al.*, 1999). The first nerve fibroblasts are also observed following SCP to ISC transition, which raises intriguing questions as to their origins in the nerve. A study by Joseph *et al.* (2004), using *cre*-recombinase fate mapping, suggests that endoneurial fibroblasts might be derived from early glial progenitors. The study showed that progenitor cells, which expressed p75^{NTR}, S100 β and Dhh, i.e. an identical profile to that of SCPs, had the potential to differentiate to fibroblast rather than Schwann cell progenitors, i.e. that expressed Thy1 but not Dhh and p75^{NTR} (**Figure 1.5**). However, it remains to be determined if SCPs are the cell of origin for endoneurial fibroblasts or if fibroblasts are derived instead from a progenitor cell committed to form fibroblasts but which also happen to express SCP differentiation markers. Importantly, endoneurial fibroblasts are only found after SCPs have differentiated to ISCs, which strongly supports the theory that SCPs are able to differentiate to both glial and fibroblast progenitors (Jessen & Mirsky, 2005; Joseph *et al.*, 2004).

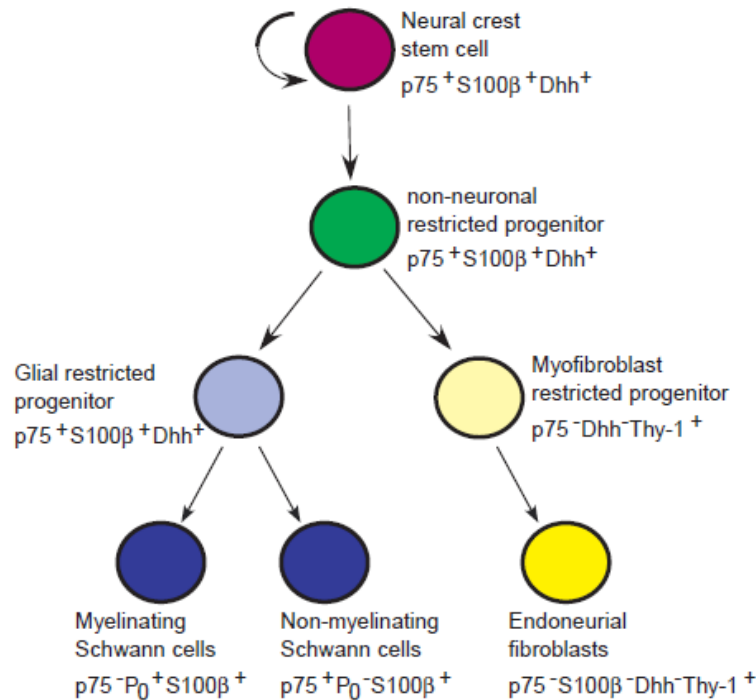


Figure 1.5 Proposed model for multi-lineage peripheral nerve development. In this model, fibroblasts share a common progenitor with Schwann cells. The progenitor expresses similar surface markers to Schwann cell precursors (SCPs), i.e. $p75^{\text{NTR}}$ (neurotrophin receptor), S100 β and Dhh (Desert hedgehog) and can generate both Schwann cell and fibroblast progenitors, where fibroblast progenitors down-regulate S100 β and $p75^{\text{NTR}}$, while up-regulating the fibroblast marker Thy1 (Joseph *et al.*, 2004).

The transition from SCP to ISC marks a significant change in glial cell morphology, with ISCs assuming a bi- or tri- polar morphology in contrast to the flattened morphology exhibited by SCP clusters (Jessen & Mirsky, 2005; Woodhoo & Sommer, 2008). This alteration in cell morphology is advantageous because it improves Schwann cell function in terms of axonal searching, interaction and manipulation, which are required at this stage in development. In addition, there is a dramatic change in the regulation of cellular survival (Jessen & Mirsky, 2005). The critical survival dependency, exhibited by SCs for axonal NRG-1, is replaced in ISCs by cell-autonomous survival circuits mediated by autocrine signalling loops, in which ISCs secrete a range of self-acting survival factors including platelet-derived growth factor (PDGF)- β , insulin-like growth factor (IGF)-2 and neurotrophin (NT)-3 (Meier *et al.*, 1999) as well as leukaemia inhibitory factor (LIF) (Dowsing *et al.*, 1999) and lysophosphatidic acid (LPA) (Li *et al.*, 2003). The requirement for

survival autonomy in ISCs and, more importantly, mature Schwann cells, reflects the essential role played by Schwann cells in the repair process, where denervated Schwann cells must survive in the absence of axons (Jessen & Mirsky, 2005) (refer to section 1.5.1 for the role of Schwann cells in the nerve repair process).

Radial sorting and the generation of adult Schwann cells

Prior to their final differentiation to mature Schwann cells, ISCs undergo a process referred to as radial sorting, in which ISCs refine large collections of multi-sized calibre axons to either large single axons that later give rise to myelinated fibres or to clusters of small-calibre axons that later give rise to non-myelinating fibres (Jessen & Mirsky, 2005; Kuhlbrodt *et al.*, 1998). Thus, the mature Schwann cell fate is not predetermined within the lineage but instead depends on the random assortment of Schwann cells with axons. Radial sorting is a highly physical process, involving manipulation of axonal bundles by Schwann cell protrusions to segregate and subdivide axons (Kuhlbrodt *et al.*, 1998). It is characterised by Schwann cell proliferation, process extensions and a morphological transition towards a spindle-like shape (Chernousov *et al.*, 2008). Radial sorting is highly reliant on the interactions between ISCs and the ECM (Court *et al.*, 2006), which is underlined by the essential requirement for laminins and integrins in this process. For instance, Schwann cells deficient in laminin had substantially reduced active forms of Rac1 (a Rho GTPase important for process extension) and cdc42 (required for cell proliferation), which greatly hindered their ability to sort axons (Chernousov *et al.*, 2008). Proliferation is an essential component of radial sorting, as the number of Schwann cells must increase to match the number of newly segregated axons which prior to de-fasciculation existed as large axonal bundles (Court *et al.*, 2006; Martin & Webster, 1973). A study by Yang *et al.* (2005), showed that combined loss of both laminin-2 and laminin-8 from ISCs resulted in the inhibition of Schwann cell proliferation and subsequent disruption to the radial sorting process. Equally, Feltri *et al.* (2002) demonstrated the importance of integrin signals to radial sorting. They used a conditional β 1-integrin Schwann cell knockout mouse and observed the presence of unsorted axonal bundles in sciatic nerves, indicating that radial sorting had been severely disrupted. NRG1 is also important for radial sorting, for example the nerves of NRG1^(+/-) mice exhibited large unsorted bundles (Taveggia *et al.*,

2005). Interestingly, some parts of the PNS, for example the sympathetic nerve fibres, are never myelinated either *in vivo* or *in vitro* and are thus, always ensheathed by non-myelinated Schwann cells (Birchmeier & Nave, 2008).

As radial sorting proceeds, the mixed bundles of unsorted, multi-sized axons are gradually sorted into either single large calibre axons (greater than 1 μm in diameter), ensheathed by a single Schwann cell (in cross-section) or multiple small calibre axons that are ensheathed by a single Schwann cell and form Schwann cell-axonal families, termed Remak bundles (**Figure 1.6**). At this stage, the adult fate of the ensheathing Schwann cell has been predetermined by the axon (Jessen & Mirsky, 2005; Woodhoo & Sommer, 2008). For instance, Schwann cells that ensheath multiple small-calibre axons later differentiate to form non-myelinating Schwann cells, which do not generate myelin or undergo compaction of their plasmamembrane. In contrast, Schwann cells that ensheath single large-calibre axons begin a complex series of processes that differentiate the Schwann cell to the myelinated state. In terms of myelinating Schwann cells, the first stage in this process is the generation of the pro-myelinating Schwann cell, in which the Schwann cell wraps the axon at least one and a half times with its plasmamembrane (Jessen & Mirsky, 2005; Topilko *et al.*, 1994). The pro-myelinating state is only readily observed in mouse models where further progression to myelination has been blocked, for instance as occurs in the nerves of the *Krox20^{-/-}* mouse (Topilko *et al.*, 1994). Importantly, while the ensheathing pro-myelin Schwann cells are committed to myelination, at this stage they have yet to initiate myelination, i.e. undergo the biosynthetic process of generating myelin and the necessary myelin proteins required for compaction of their plasmamembrane.

Myelination

The myelination programme is a highly complex process, involving significant changes to cellular biosynthesis and cell morphology as well as cell-cycle exit (Srinivasan *et al.*, 2012), and is accomplished only following an intricate, co-ordinated programme of Schwann cell/axonal interactions. For instance, the myelinating Schwann cell must synthesise large amounts of lipid-rich plasma-membrane, interlaced with an abundance of specialised myelin proteins, that is

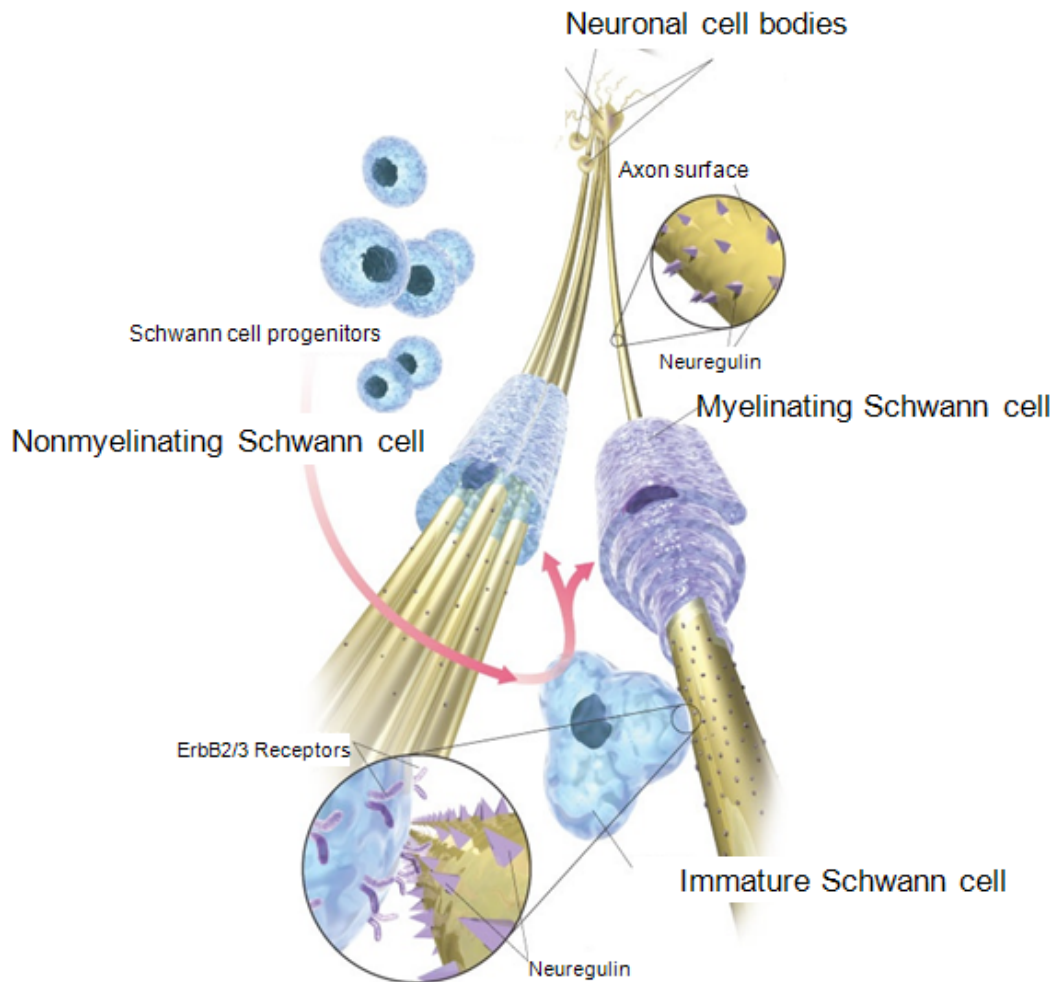


Figure 1.6 Schematic showing the role of the axon in the determination of Schwann cell fate during radial sorting. Schwann cells that randomly associate with large-calibre axons are induced to myelinate, while Schwann cells that associate with multiple small-calibre axons differentiate to non-myelinating Schwann cells. Cell-surface expressed neuregulin (NRG)-1 on the axon, which binds ErbB2/B3 receptors in Schwann cells, has been implicated in the regulation of this process (adapted from Lemke, 2006).

sufficient to wrap around the axon more than a 100 times and longitudinally extend to cover in some cases 1 mm of axon. To achieve this, the Schwann cell increases its surface area by 'several thousand-fold' over a 48-hour period (Birchmeier & Nave, 2008). Concurrent with wrapping the axon, the Schwann cell plasma-membrane must also be compacted to generate compact myelin, in which both the extracellular and intracellular regions are tightly restricted. This process of compaction is achieved by specialised myelin-specific proteins, for example MPZ, myelin basic

protein (MBP) and peripheral myelin protein-22 (PMP22), which are under the regulatory control of the master regulator of myelination, Krox20. The essential role of these proteins, and that of Krox20, are discussed in later sections. In addition, the myelinating Schwann cell must establish radial and longitudinal polarity (Simons & Trotter, 2007), for instance the radially asymmetric composition of glial CAMs expressed on the outer (ECM-facing) and inner (axonal-facing) aspects and the longitudinal specification of the axo-glial domains, i.e. the Node of Ranvier, paranode and juxtaparanode), which are essential for saltatory conduction. In addition, non-compact myelin channels must be incorporated into the myelin sheath so that the Schwann cell and the axon can be appropriately nourished (Nave, 2010a). Understanding the molecular machinery that coordinates and regulates these disparate processes to generate the functional myelinating fibre has been a matter of intense research.

The regulation of myelination

The regulation of myelination is multifaceted; consisting of a number of components that collectively switch the Schwann cell from the unmyelinated to the myelinated state.

A) Extracellular environment

Myelination requires a permissive extracellular environment, for instance the correct ECM attachments/signals and crucially, the establishment of a basal lamina around the ensheathing Schwann cell/axonal unit (Bunge *et al.*, 1986; Chernousov *et al.*, 2008; Court *et al.*, 2006). While the basal lamina undoubtedly provides structural protection for the fibre, its requirement for myelination is probably due to its role in the establishment of Schwann cell polarity (Simons & Trotter, 2007). In terms of Schwann cell-ECM attachments, the binding of Schwann cell expressed integrins with ECM fibronectin and laminin has been shown to be required for myelination (Chernousov *et al.*, 2008; Podratz *et al.*, 2001). Specifically, the binding of laminin-2, laminin-8, and laminin-10 with Schwann cell expressed integrins have all been implicated in myelination (Yu *et al.*, 2007). Furthermore, loss of integrin- β 1, known to bind various ECM components, also inhibits myelination (Feltri *et al.*, 2002). In

addition to laminins, attachment to collagens in the ECM is also required, for instance binding between alpha-4 (V) collagen (within the ECM) and Schwann cell expressed glypican-1 (a proteoglycan) is required for myelination *in vitro*, with loss of either leading to inhibition of myelination (Chernousov *et al.*, 2006).

B) Extrinsic factors and cognate receptors

Myelination requires instructive signals from the axon, one of which is known to be mediated in a juxtacrine manner via NRG-1 Type III- β 1a, which signals intracellularly through the ErbB2/B3 heterodimeric receptor-tyrosine kinase (RTK) receptor (Nave & Salzer, 2006). However, recently a second, and arguably as important, instructive signal has been reported, which is mediated through the G-protein coupled receptor (GPR)-126, which is coupled to cyclic adenosine monophosphate (cAMP); a signal known to be important for myelination. In this section, I will discuss the role played by both signals in determining the myelinated fate of Schwann cells.

Neuregulin (NRG)-1

Over the last twenty years, there has been mounting evidence for the critical role played by NRG-1 in almost all aspects of Schwann cell biology, including migration, proliferation, survival, differentiation and myelin thickness (Birchmeier & Nave, 2008; Nave & Salzer, 2006; Quintes *et al.*, 2010; Taveggia *et al.*, 2005). NRG1 formerly known as glial growth factor (GGF) was originally identified as a potent Schwann cell mitogen (Lemke & Brookes, 1984) but was also separately identified as neu differentiation factor (NDF), heregulin, acetylcholine receptor inducing activity (ARIA) and sensory and motor neuron-derived factor (SMDF) (Davies, 1998). The NRG-1 gene encodes three major classes of NRG1 isoforms: the Type I class, including heregulin, NDF and ARIA; the Type II class, including GGF; and the Type III class, including the β 1a and the β 3 (SMDF) variants, of which all share the epidermal growth factor (EGF) domain, necessary and sufficient for ErbB binding (Garratt *et al.*, 2000; Nave & Salzer, 2006).

The NRG1 gene encodes at least 15 different isoforms from multiple transcription sites and by alternative RNA splicing. All isoforms are initially expressed on the cell surface but are post-translationally modified *in situ* by various extracellular metalloproteinases, including BACE1 (β -site APP cleaving enzyme-1) and membrane-anchored ADAM (a disintegrin and metalloprotease) proteins, which extracellularly cleave NRG1 molecules near their C-terminals just distal to the membrane, rendering Type I and Type II classes of NRG1 as soluble paracrine signals (Birchmeier & Nave, 2008; Hu *et al.*, 2006). NRG1 Type III is also cleaved, however, the isoform possesses an additional hydrophobic cysteine-rich domain (CRD) towards its N-terminus that forms a second transmembrane region resistant to cleavage - giving the isoform a looped extracellular conformation. Thus, while cleavage of Type III NRG1 isoforms (proximal to the EGF domain) sterically frees the EGF domain for signalling, the CRD domain ensures that the activated isoform remains tethered to the membrane (Nave & Salzer, 2006) (**Figure 1.7**).

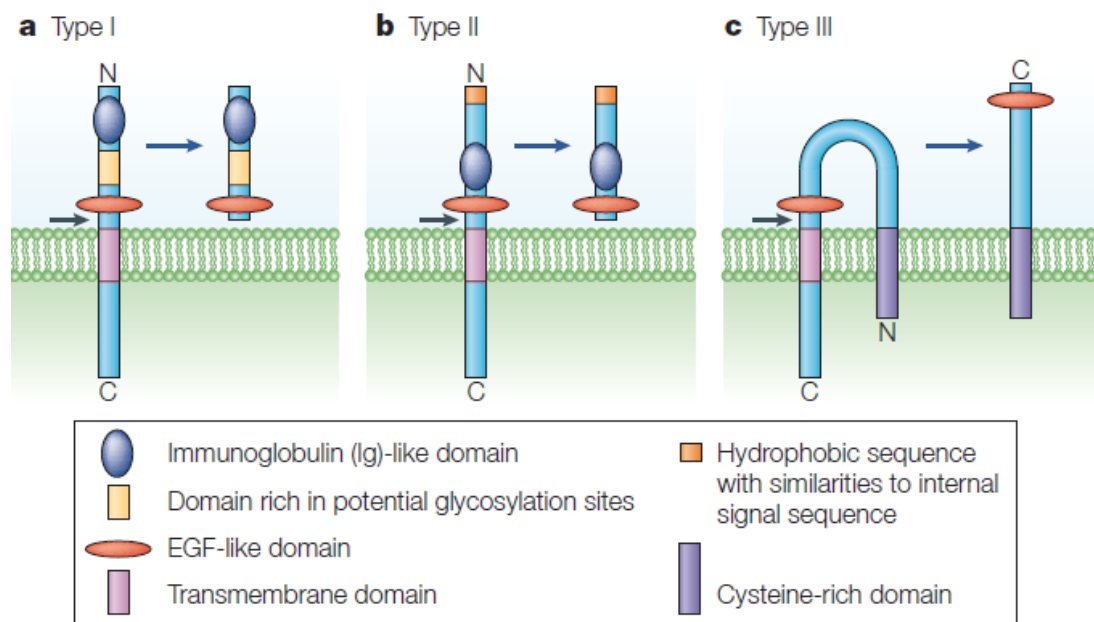


Figure 1.7 Schematic showing the three major classes of Neuregulin-1. All NRG1 isoforms are initially expressed on the axonal cell-surface and are later post-translationally cleaved by metalloprotease, for example BACE-1 (see black arrow). Cleavage releases NRG-1 Type I and Type II molecules as soluble factors that signal in a paracrine manner; however, cleavage of Type III, which is looped back on itself, results in the exposure of the EGF domain for signalling in a juxtacrine manner (Jessen & Mirsky, 2005).

Over the last decade, NRG-1 Type III β 1a has emerged as the predominant functional isoform expressed by sensory and motor neurons of the PNS (Lemke, 2001; Michailov *et al.*, 2004; Taveggia *et al.*, 2005), and is thought to be the axonal signal responsible for regulating neural crest migration, SCP survival, nerve fasciculation and Schwann cell differentiation (Jessen & Mirsky, 2005; Wolpowitz *et al.*, 2000). NRG1 Type III appears to be instrumental in the binary decision that results in the myelination of larger axons and the non-myelination of smaller axons. For some time, the mechanism that allowed Schwann cells to 'sense' the axonal diameter in order to make this decision was unknown and to date is still not completely understood. One suggestion is that the amount of axonal-expressed NRG1 Type III is correlated with the axonal diameter so that larger calibre axons with greater surface-areas will provide a correspondingly greater NRG1 stimulus to the ensheathed Schwann cell. In this hypothesis, the NRG1 Type III signal acts in both a threshold and dose-dependent manner (**Figure 1.8**).

The threshold component is binary, i.e. Schwann cells require a specific concentration of NRG1 (as provided by axons of 1 μ m or greater in diameter) to initiate myelination, without which the myelination programme is not initiated and the Schwann cell differentiates to the non-myelinating state. This theory is supported by Taveggia *et al.* (2005) and Michailov *et al.* (2004), who investigated the effect on myelination in various NRG1 mouse models. In these studies, the NRG1^(-/-) animals failed to myelinate and were characterised by malformed Remak bundles containing both large and small axons, indicative of a failure in radial-sorting, and were invariably lethal with animals not surviving post-birth. The NRG1^(+/-) nerves manifested a less severe phenotype; however, myelinated nerves were hypo-myelinated and Remak bundles were still poorly sorted. In addition, when NRG1 Type III was over expressed by axons, the resulting myelinating fibre was hyper-myelinated suggesting that the concentration of NRG1 was correlated with myelin sheath thickness. Finally, Taveggia *et al.* (2005) showed that sympathetic nerve fibres, which normally never myelinate, could be induced to myelinate by NRG1 Type III over-expression in these neurons. Taken together, these findings are consistent with NRG1 Type III acting in a dose-dependent manner in the regulation of myelin sheath thickness and lends credence to the idea of NRG1 Type III, as the

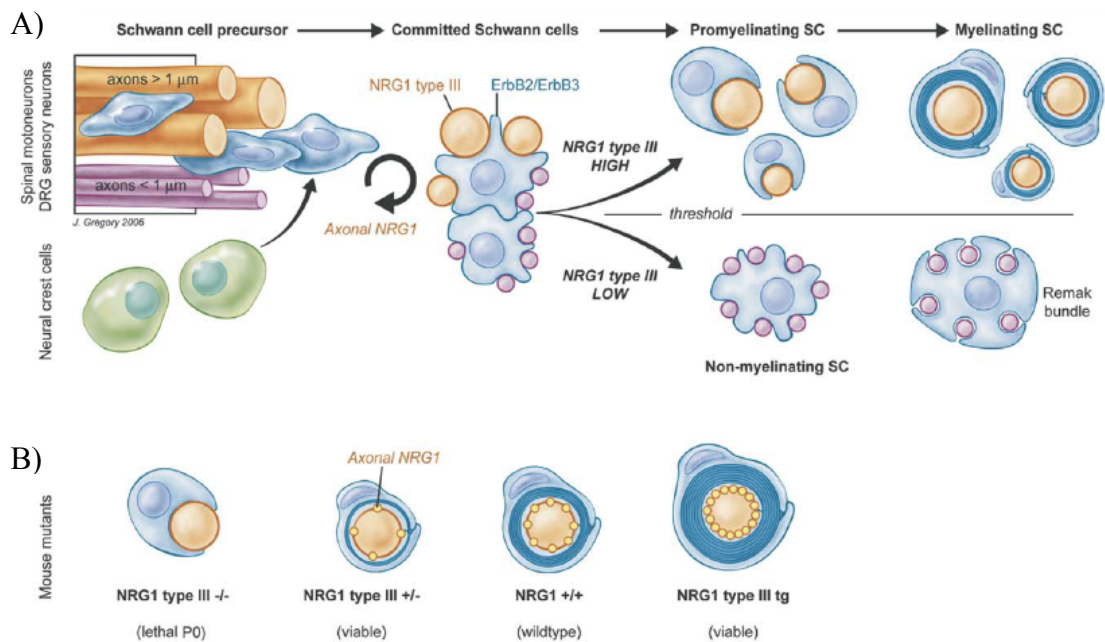


Figure 1.8 Axonal neuregulin-1 type III operates in a binary (threshold) and dose-dependent manner to regulate Schwann cell differentiation. (A) Immature Schwann cells ensheath larger axons in 1:1 ratios while ensheathing multiple smaller axons into Remak bundles in a process called radial sorting. Larger axons provide a greater NRG1 signal, which after a threshold amount commits the Schwann cell to the myelinated state. (B) The amount of NRG1 Type III above the threshold determines the extent of myelination with the $NRG1^{(-/-)}$ failing to myelinate, the $NRG1^{(+/-)}$ nerves hypomyelinated and the $NRG1$ Type III over-expressing mice having hyper-myelinated nerves (Nave & Salzer, 2006).

axon derived ‘rate-limiting factor for myelination’ (Corfas *et al.*, 2004; Michailov *et al.*, 2004; Nave & Salzer, 2006). In addition, studies have also determined the critical importance of the juxtacrine (cell-cell contact dependent) mode of NRG1 Type III signalling as soluble NRG1 failed to elicit the same effect and may even inhibit myelination (Zanazzi *et al.*, 2001).

The Neuregulin receptor

The NRG1 signal is conveyed through a heterodimeric RTK receptor composed of ErbB2 and ErbB3, which binds the EGF domain of NRG molecules (Davies, 1998; Lemke, 2001; Nave, 2010a). A third ErbB protein, ErbB4, also exists although it is minimally expressed in Schwann cells (Nave & Salzer, 2006). The ErbB2/B3

receptor is the predominant NRG-1 receptor in Schwann cells. The receptor is composed of the high-affinity (but kinase inactive) ErbB3, which recognises and binds axonal NRG1 Type III that is tethered to the axolemma. This interaction is necessary before the low-affinity (but kinase active) ErbB2 molecule can bind in *cis* with the ErbB3-NRG1 complex in order to generate the active receptor (Davies, 1998; Lemke, 2001). Heterodimerisation of ErbB2/B3 causes transphosphorylation, recruitment of SH3 adaptors and associated downstream signalling (Nave & Salzer, 2006). All components of this pathway are required for viability as NRG1, ErbB2 and ErbB3 knockout mice are all embryonic lethal, with death in NRG1 and ErbB2 null animals occurring prior to SCP generation, i.e. before E10, as a result of defects in cardiogenesis (Nave & Salzer, 2006). However, ErbB3 animals survived longer mostly because ErbB3 is not expressed in cardiac tissue and thus mutants survive until late gestation. Temporal analysis of embryonic ErbB3 null nerves revealed that by E10.5 the nerves are devoid of Schwann cell progenitors and exist as bare axons which degenerate at E18-E19 (Nave, 2010b; Riethmacher *et al.*, 1997). Importantly, while DRG neurons initially survive without Schwann cells, by E18.5 approximately 90% have died in the absence of Schwann cells (Davies, 1998), thus underlining the critical co-dependency between Schwann cells and axons.

Intracellular signalling through the ErbB2/B3 receptor

Activation of the ErbB2/B3 receptor results in the intracellular activation of known signalling cascades including the mitogen activated protein kinase (MAPK) cascade and the phosphatidylinositol-3 kinase (PI3K) cascade (Birchmeier & Nave, 2008). Understanding how Schwann cells responds to signalling through these different pathways may hold the key as to how one signal, i.e. NRG1, appears to drive seemingly opposing cellular processes and behaviours at different developmental stages (Corfas *et al.*, 2004; Nave & Salzer, 2006; Ogata *et al.*, 2004). For instance, nearly all aspects of normal Schwann cell development has been shown to require axonal NRG1 Type III and ErbB2/ErbB3 signalling through the PI3K pathway leading to activation of a number of downstream effectors including the serine-threonine kinase AKT (also known as Protein Kinase B) (Nave & Salzer, 2006) (**Figure 1.9**). Although activated to a degree, the ERK pathway is not thought to be required for axon-mediated Schwann cell survival as indicated by MEK and ERK

inhibitor studies (Maurel & Salzer, 2000). In contrast to PI3K, the ERK downstream signal can be inhibitive to myelination, where sustained ERK activation leads to down-regulation of myelin specific genes (Harrisingh *et al.*, 2004), causing demyelination, dissociation from axons and Schwann cell proliferation (Ogata *et al.*, 2004; Parrinello *et al.*, 2008). Thus, signalling through the ERK pathway takes precedence over the PI3K pathway during the injury response.

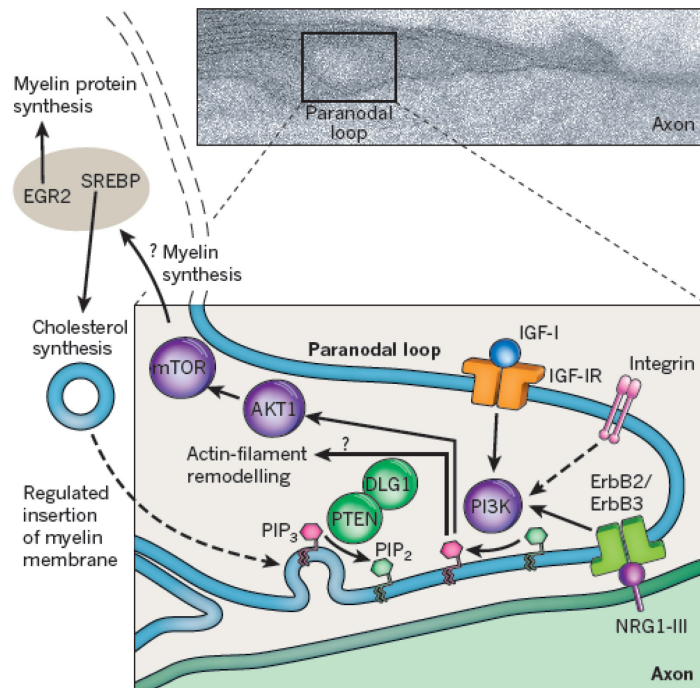


Figure 1.9 Membrane tethered axonal neuregulin (NRG)-1 Type III regulates Schwann cell differentiation and myelin thickness. The NRG1 signal is transduced through the ErbB2/B3 heterodimeric receptor-tyrosine kinase (RTK) receptor, which predominantly activates the AKT-mTOR pathway. Signalling via integrins (from the extracellular matrix) and insulin-like growth factor (IGF)-1 are also important modulators of myelination (Nave, 2010b).

G-protein coupled receptor (GPR)-126

While NRG1 has been shown to be required, it is not sufficient to instruct myelination, for instance heterologous expression of NRG1 Type III does not result in myelination *in vitro*, despite retaining its activity as a mitogen (Taveggia *et al.*, 2005). Moreover, it is still far from clear how NRG1 is exerting its downstream effects particularly in relation to a direct transcriptional link between the NRG1

signal and transcriptional activation of myelin genes (Birchmeier & Nave, 2008). Experimental elevation of intracellular cAMP in cultured Schwann cells, often by addition of the cAMP analogue forskolin, has been adopted *in vitro* for quite some time in order to mimic the axonal signal in driving Schwann cell differentiation and myelination (Monuki *et al.*, 1989; Morgan *et al.*, 1991; Scherer *et al.*, 1994). In addition, Howe & McCarthy (2000) showed that *in vivo* inhibition of PKA (protein kinase A), which is a major target of intracellular cAMP and is independent of NRG1, using a dominant negative PKA, resulted in an 80% reduction in myelinated Schwann cells (Howe & McCarthy, 2000).

The *in vivo* physiological signal that elevates cAMP during Schwann cell differentiation has until recently remained elusive. The identification of GRP-126 appears to provide an answer (Monk *et al.*, 2009). GRP-126 is expressed on the Schwann cell and has been shown to directly and transiently elevate intracellular cAMP, thus providing a second instructive signal for myelination, with importantly, a well-documented link to the transcriptional apparatus involved in the initiation of myelination (Monk *et al.*, 2009). For instance, cAMP is known to activate PKA (discussed above), which activates a number of downstream transcription factors important for Schwann cell differentiation, including nuclear factor (NF)- κ B and cAMP response element binding protein (CREB) (Arthur-Farraj *et al.*, 2011; Monk *et al.*, 2009; Monuki *et al.*, 1989). These act collectively to induce Oct-6 transcription, which together with Brn2 and Sox10 is required for the initiation of Krox20 expression and thus, myelin gene expression. The central importance of GRP-126 was initially demonstrated by GRP-126 mutant zebrafish models and later by mouse models, in which myelination in GRP-126 mutants was blocked and Schwann cell development arrested at the pro-myelinating stage (Monk *et al.*, 2009). Moreover, the addition of forskolin is sufficient to restore myelination in the zebrafish mutants, confirming that cAMP is the deficient pathway downstream of GRP-126 required for myelination. Furthermore, expression of GRP-126 was shown to be independent of NRG1, thus the authors suggest that GRP-126 signalling is required after NRG1 to initiate myelination. Further work is needed to determine the axonal ligand for GRP-126. Interestingly, a recent study by Arthur-Farraj *et al.* (2011), showed that the concentration of cAMP was important for modulating the NRG1 Type III signal, such that low cAMP favoured NRG1 as a mitogen, while high

levels of cAMP favoured NRG1 as a pro-myelinating differentiator. Importantly, loss of either the cAMP or NRG1 signal prohibits myelination, while combined cAMP and NRG1 signalling in mouse Schwann cells leads to robust myelin gene expression, for example Krox20 and MPZ, confirming the essential importance of both signals in the instruction of Schwann cell myelination (Arthur-Farraj *et al.*, 2011).

C) Extrinsic modulators

Positive modulators

Correct and timely progression to myelination requires a number of additional extrinsic factors that modulate the primary instructive signals of NRG1 and cAMP. These include, progesterone, brain derived neurotrophic factor (BDNF), glial cell line derived neurotrophic factor (GDNF) and Insulin-like growth factor 1/2 (IGF1/2) (Jessen & Mirsky, 2008b). BDNF is a neurotrophin that signals through the low-affinity p75 neurotrophin receptor (p75^{NTR}) (Chan *et al.*, 2001). Loss of either the ligand (BDNF) or receptor (p75^{NTR}) impedes myelination and results in a reduction in myelin sheath thickness and the number of myelinated fibres (Chan *et al.*, 2001; Chen *et al.*, 2006). The IGF1 signal, which is conveyed through the IGF receptor, has been implicated in modulating the cAMP signal during activation of the PI3K pathway, and thus plays a role in myelination (Ogata *et al.*, 2004). Another modulator is BACE1, involved in the cleavage and activation of the NRG1 signal (previously discussed on page 42), in which BACE1 null mice exhibit hypomyelinated nerves and radial-sorting defects (Hu *et al.*, 2006).

Negative modulators

Many of the negative regulators act to inhibit myelination by promoting the dedifferentiation of Schwann cells and in addition, commonly function as Schwann cell mitogens. Negative extrinsic factors include neurotrophin (NT)-3 and Jagged. The NT-3 receptor is the high-affinity neurotrophin receptor TrkC, whose activation inhibits myelination and stimulates Schwann cell proliferation (Chan *et al.*, 2001). Axonal expressed jagged signals via its Notch receptor expressed on the Schwann cell. Autotypic binding between Jagged and Notch, leads to Notch activation, resulting in the cleavage of the C-terminal Notch intracellular domain (NICD), which

translocates to the nucleus and functions to directly regulate transcription (Jessen & Mirsky, 2008b; Taveggia *et al.*, 2010; Woodhoo *et al.*, 2009). Recent work has shed new light on the complexities of Notch signalling in Schwann cell development, including lineage transition, repression of myelination and the stimulation of Schwann cell proliferation following PNS injury (Woodhoo *et al.*, 2009).

D) Transcriptional regulators

Myelination is ultimately governed by the co-ordinated action of positive and negative transcriptional regulators, where the prevailing net balance of these activities determines whether Schwann cells differentiate to myelinated Schwann cells or, in the case of adult nerve injury, dedifferentiate back to a non-myelinated state. Positive transcriptional regulators include Sox10, NFκB, Brn2, Oct-6 (also known as SCIP (suppressed cAMP inducible POU), Tst1 and Pou3f1) and Krox20 (Egr2) (Jessen & Mirsky, 2005; Quintes *et al.*, 2010). Negative transcription factors include c-Jun, Sox2, Pax3, Krox24 (Egr1) and NICD (Jessen & Mirsky, 2008b).

Positive transcriptional regulation

The first of these transcription factors to be expressed is Sox10, often described as the Schwann cell specification factor, which is expressed in NCCs and continues to be expressed throughout the Schwann cell lineage and indeed by all glial cells of the PNS (Britsch *et al.*, 2001; Schreiner *et al.*, 2007). Sox10 is an HMG (High Mobility Group)-box transcription factor and is a Class-E member of the Sox family (Svaren & Meijer, 2008). As previously discussed, the loss of Sox10 (in mouse models) results in the ablation of the Schwann cell lineage, demonstrating the importance of this transcription factor to Schwann cell biology (Britsch *et al.*, 2001). In terms of myelination, Sox10 is thought to function with NFκB to govern the initiation of myelination (Svaren & Meijer, 2008). However, progression to the pro-myelinating state, i.e. where the Schwann cell wraps the axon one and half times, is dependent on the expression of Oct-6 and the closely related Brn2 (both of which are POU domain III transcription factors) as well as Sox10 (Salzer *et al.*, 2008). Interestingly, the expression of both Oct-6 and Brn2 are increased markedly following axonal contact, which is known to elevate cAMP. Evidence has emerged to suggest that these intracellular pathways converge onto a 4.3kb conserved region that resides

downstream of the Oct-6 gene called the Schwann cell specific enhancer (SCE) (Mandemakers *et al.*, 2000; Svaren & Meijer, 2008). Deletion studies have shown that 500bp of this region are critical for Schwann cell differentiation and furthermore, numerous Sox binding sites have been identified in this sequence, highly suggestive of a role for Sox proteins in the regulation of Oct-6 (Svaren & Meijer, 2008). A distinct role for Sox10 in the generation of myelinating Schwann cells is supported by the finding that a hypomorphic allele of Sox10, in which Sox10 expression is driven at substantially lower rates than wild-type animals, was sufficient to specify Schwann cells, but was not sufficient to differentiate Schwann cells (Schreiner *et al.*, 2007).

Both Oct-6 and Brn2, in combination with Sox10, are important for initiating myelination at the correct developmental time, for instance loss of Oct-6 delays myelination by several weeks in mouse and combined loss of Oct-6 and Brn2 further delays myelination with pro-myelinating Schwann cells persisting in adult nerves (Bermingham *et al.*, 1996; Jaegle *et al.*, 2003; Svaren & Meijer, 2008). These findings suggest that Oct-6 and Brn2 can functionally compensate for one another. Oct-6 and Brn2 exert their pro-myelination activity through binding at multiple sites on the *cis*-acting Krox20 enhancer element - the myelin Schwann cell enhancer (MSE) - located 35kb downstream of the Krox20/Egr2 gene (Ghislain *et al.*, 2002). The binding of Oct-6 and Brn2 at the MSE activates Krox20 expression. Recently, it has been shown that Sox10 cooperates with Oct-6 to synergistically promote Krox20 expression and thus, myelination (Ghislain & Charnay, 2006). Interestingly, Krox20 activity depends on the down-regulation of Oct-6 and Brn2, for instance a study by Ryu *et al.* (2007) showed, using a conditional Oct-6 mouse (condPou3f1:MPZ) in which Oct-6 expression was driven by MPZ, that if Oct-6 expression persisted, then Krox20-dependent myelin gene expression was inhibited, leading to severe hypomyelination of adult nerves.

Krox20 is a member of the early-growth response (EGR) genes and is often cited as the master transcriptional regulator of myelination because of its sufficiency to induce myelination (Decker *et al.*, 2006; Parkinson *et al.*, 2004; Topilko *et al.*, 1994). Krox20 is necessary for myelination (in addition to Sox10) and controls an array of myelin specific gene expression including genes encoding the myelin specific

proteins, for example MBP, MPZ, MAG and periaxin (Pxn), as well as genes involved in lipid biogenesis, for instance HMG CoA reductase (Leblanc *et al.*, 2005). Krox20^(-/-) animals exhibit normal radial sorting and progress to the pro-myelinating state but are blocked from differentiating further (Topilko *et al.*, 1994). Expression of Krox20 is thus essential for progression past the pro-myelinating stage in the Schwann cell lineage and for the entirety of myelination including maintenance of myelin gene expression throughout adult life (Decker *et al.*, 2006). Krox20 is a zinc-finger transcription factor, where the zinc finger domain is essential for its function, i.e. loss of the domain results in the failure of the myelination programme (Topilko *et al.*, 1994). The activity of Krox20 is modulated by a number of proteins, of which the NGF1/Krox20-A-binding (Nab) proteins (Nab1 and Nab2) are best characterised. The Nab proteins share two homologous domains, NCD1 and NCD2, where NCD1 is known to interact with the R1 domain on Krox20 (Le *et al.*, 2005b) and NCD2 is important for transcriptional regulation (Swirnoff *et al.*, 1998). Importantly, the interaction of Nab with Krox20, through binding of the NCD1 domain of the former with the R1 domain of the later, is essential for Krox20 function and myelination (Le *et al.*, 2005b).

Negative transcriptional regulation

The negative transcriptional regulators of the myelination programme have historically received less attention; however, in recent years significant progress has been in understanding their role in the myelination programme and following injury. For instance, negative transcription regulators act to repress the myelination programme in development in order to regulate the initiation of myelination and to drive Schwann cell dedifferentiation following nerve injury. Importantly, they are usually associated with stimulating Schwann cell proliferation as opposed to positive transcription factors, which are associated with cell-cycle exit and differentiation.

The best characterised negative transcription factor is c-Jun, a basic leucine zipper transcription factor, which is expressed in Schwann cell prior to myelination and is down-regulated following the initiation of myelination, while being up-regulated upon nerve injury (Parkinson *et al.*, 2008; Salzer *et al.*, 2008). The activation of c-Jun is carried out by Jun N-terminal kinases (JNKs), which phosphorylates c-Jun on its N-terminal. c-Jun, together with JunB and JunD, form part of the AP-1

transcription complex, where the activated c-Jun signal exerts a dominant inhibitory affect on myelination, for instance Schwann cells with forced c-Jun expression do not myelinate even in the presence of Krox20 or cAMP signal (Parkinson *et al.*, 2008). c-Jun is down-regulated by Krox20 activity, thus, the onset of myelination is dependent on Krox20 expression (Parkinson *et al.*, 2004). Another transcription factor that closely mirrors c-Jun expression is Sox2, indeed there is some evidence to suggest that Sox2 expression is directly induced by c-Jun, although it is still unclear if both molecules interact (Parkinson *et al.*, 2008). Similar to c-Jun, Sox2 is expressed by Schwann cell progenitors (during development) prior to myelination and in nerve injury. Sox2 is also down-regulated by Krox20, which is required for progression to myelination (Le *et al.*, 2005a).

Pax3 is a member of the paired box gene family of transcription factors and is expressed by ISCs and non-myelinating Schwann cells *in vivo* (Kioussi *et al.*, 1995). Levels of Pax3 have been directly shown to decrease as cAMP levels increase *in vitro* (Kioussi *et al.*, 1995). Furthermore, enforced expression of Pax3 prevents either Krox20 or cAMP induced myelin gene expression. However, while Pax3 expression appears similar to c-Jun and Sox2, its activity is less well characterised and it remains to be determined if it is involved in Schwann cell dedifferentiation (Jessen & Mirsky, 2008b). Another less-well characterised transcription factor is Id-2, a member of the helix-loop-helix (HLH) family of transcription factors, which also inhibits myelination but its effects appear more subtle. Basal expression levels of Id-2 in Schwann cell development is relatively low; however, levels increase following the initiation of myelination and are later reduced as myelination progresses (Stewart *et al.*, 1997). Levels of Id-2 are also increased following nerve injury, in-line with other transcription factors, for example c-Jun, Sox2 and Pax3, although it is unclear how Id-2 antagonises myelination following injury (Jessen & Mirsky, 2008b).

In addition to Krox20, a number of other EGR transcription factors, for example Krox24 and EGR3 are involved in the myelination programme. These factors antagonise Krox20 activity and act to repress myelination, although their activity in the myelination programme is poorly understood (Jessen & Mirsky, 2008b). However, Krox24 is expressed in non-myelinating adult Schwann cells and furthermore, it is up-regulated (with EGR3) in denervated Schwann cells following

nerve injury, concomitant with a fall in Krox20 expression, although Krox24 null mice are still able to regenerate nerve following injury (Topilko *et al.*, 1994).

Recent work has implicated Notch and specifically, its Notch intracellular domain (NICD) cleaved subunit, which is the component responsible for its transcriptional regulatory activity, in the negative repression of myelination, as well as in lineage progression (as discussed earlier). Notch expression is down-regulated during myelination and has been shown to be repressed by Krox20 *in vitro* (Woodhoo *et al.*, 2009). In addition, enforced NICD expression blocks cAMP induced myelination *in vitro* and transient elevation of NICD at the onset of myelination has been shown to delay myelination (Woodhoo *et al.*, 2009). Furthermore, in the same paper, the authors showed that the distal stump of sciatic nerve cuts are strongly positive for NICD.

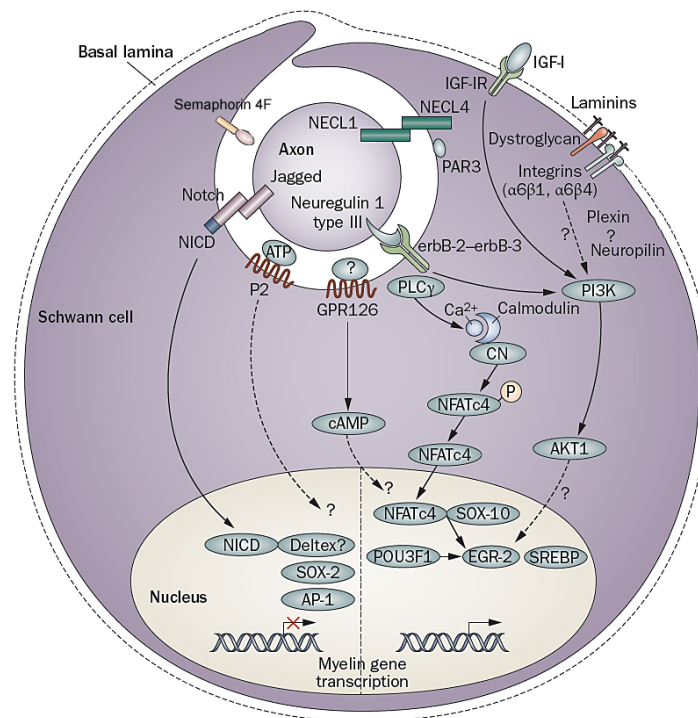


Figure 1.10 Schematic of a pro-myelinating Schwann cell, showing the balance of factors required to initiate myelination. Axon to Schwann cell signalling includes NRG1 Type III/ErbB2-B3 and Jagged/Notch, while axo-glial adhesion is mediated through Necl1/Necl4 interaction. Other extrinsic factors include signalling via GPR-126 (adaxonal face) and ECM signalling through laminins. Progression to the myelinated state is dependent on a shift in the balance between positive and negative factors (adapted from Taveggia *et al.*, 2010).

1.4.2 Nerve homeostasis and myelination

The evolution and function of myelin

The evolution of myelin is thought to have occurred in placoderms (hinge-jawed fish) at a similar time to neural crest evolution (Hartline & Colman, 2007; Zalc *et al.*, 2008), some 300 million years ago (Nave, 2010b). Myelin is a common feature of all vertebrate nervous systems, although other non-vertebrate species have separately evolved their own form of electrical insulation (Zalc *et al.*, 2008). Myelin is thought to have evolved following selective pressure to achieve rapid and reliable transmission of action potentials without the need for excessively large calibre axons, which would be unacceptable in bony organisms where cranial space is a premium (Nave, 2010b; Poliak & Peles, 2003; Zalc *et al.*, 2008). In fact, it is thought that the advent of myelination allowed the placoderm oculomotor nerve to achieve a length ten-fold greater than that of their immediate ancestors, while maintaining the same nerve diameter (Zalc *et al.*, 2008).

The primary function of myelin, which can be observed in electron micrographs (EM) as electron-dense concentric rings around the axon, is to electrically insulate the axon by reducing the capacitance of the axolemma (axonal plasma-membrane) and increasing transverse resistance (Hartline & Colman, 2007; Poliak & Peles, 2003). This provides two major benefits over equivalent non-myelinating fibres. First, myelinated fibres are more energy efficient, using less ATP, which is required by Na⁺ and K⁺ ATPase ion pumps, by reducing the area of ion exchange to a fraction (0.5%) of the surface area of the axolemma (Nave, 2010b). Second, the insulating properties of myelin coupled with regularly-spaced interruptions in the sheath at the Node of Ranvier, allow for saltatory (*Latin for saltair or 'leaping/jumping'*) conduction of action potentials down the fibre. This method of nerve conduction provides for up to 100-fold increases in the conduction velocity of the myelinated fibre compared to non-myelinating equivalents (Nave, 2010b; Zalc *et al.*, 2008). Thus, while a relatively large non-myelinated fibre of 10µm diameter could achieve an nerve conduction velocity (NCV) of 1ms/s, the equivalent myelinated fibre could theoretically achieve an NCV of 100ms/s. In addition, while

the signal along non-myelinated fibres is subject to cable properties, i.e. the original electrical signal decays at a rate equal to the inverse square of the length, the action potentials propagated by saltatory conduction along myelinated fibres, is continually regenerated at each Node of Ranvier, in a chain of membrane depolarisation and re-polarisations events (Hartline & Colman, 2007).

The NCV in myelinating fibres is determined by two main parameters. The first parameter is determined by the axonal diameter and myelin sheath thickness, represented by the 'g-ratio'. The g-ratio is calculated by dividing the axonal diameter by the diameter of the myelinated fibre as a whole, where 0.68 is an optimal value (Court *et al.*, 2004; Nave & Salzer, 2006; Quintes *et al.*, 2010; Sherman & Brophy, 2005). In healthy nerves, the ratio is maintained between 0.6 and 0.7, thus myelin sheath thickness is proportional to axonal diameter (Nave & Salzer, 2006; Sherman & Brophy, 2005). A reduction in the thickness of the myelin sheath, for example, as observed in nerves of NRG1^(+/-) mice, causes a proportional reduction in NCV (Nave & Salzer, 2006). Additionally, injured nerves, in which Schwann cells have dedifferentiated and then re-myelinated, often have larger g-ratios indicative of a reduced sheath thickness. This suggests that the NRG1 dose response is no longer perfectly coupled to myelin biosynthesis following nerve injury (Sherman & Brophy, 2005). The second parameter is the internode length, which dictates the frequency of Nodes of Ranvier along the axon. Although largely theoretical, the importance of this parameter is apparent in the periaxin null mouse, in which the lateral growth of the Schwann cell plasma-membrane is truncated. These mice exhibit a greater frequency of Schwann cells along the axon and a reduction in the average internode length, which subsequently results in a reduction in NCV concordant with the increased frequency of Nodes of Ranvier per unit length (Court *et al.*, 2004). During development, both the g-ratio and the internode length are carefully regulated to ensure maximum efficiency of nerve impulses, i.e. to achieve the desired NCV for the least axonal diameter and least energy expenditure.

Cell adhesion molecules as mediators of Schwann cell/axonal interactions

Cell adhesion molecules (CAMs) mediate interactions between Schwann cells and axons and are a central theme to this thesis. In addition, cell-cell adhesion is fundamental to the development and maintenance of the three-dimensional architecture of the nervous system (Haney *et al.*, 1999). In this section I will first give a brief overview of cell-cell interactions and adhesion molecules. I will then discuss in more detail the role of specific CAMs that mediate Schwann cell/axonal interactions and which collectively generate and maintain the structure of myelinated peripheral nerve fibres.

General principles of cell-cell interactions

When cells contact each other they may meet the same cell type (homotypic interaction) or a different cell type (heterotypic interaction). The encounter can elicit different responses which largely depend on the repertoire of cell surface expressed signalling molecules presented by each cell. They either elicit (a) no reaction, (b) repulsion, where the cell cytoskeleton is remobilised to move the cell in the opposite direction (or is extruded if in a monolayer) or (c) adhesion, where both cells form an attachment to each other. The latter two behaviours, i.e. repulsion and attraction, are initiated following recognition of the encountered cell through surveillance of the cell's surface expressed molecules. Thus, repulsion and attraction are often utilised for the purposes of cell-sorting events. If the encounter results in attraction then the force and duration of the attraction are important, as both variables have implications for generating and maintaining cell-cell junctions. Importantly, although initial forces may be weak, the collective force of a junction may strengthen over time with recruitment of additional subunits into a larger junctional complex.

Vertebrate cell-cell junctions can be of a number of different types but these mainly fall into four functional categories: (a) anchoring junctions, for example adherens junctions (abutting the actin cytoskeleton) and desmosome (abutting with intermediate filaments); (b) occluding junctions, for instance, tight junctions that form seals between cells; (c) channel-forming junctions, for instance, gap junctions, that permit the intercellular transport of diffusible solutes; and (d) signal-relaying

junctions, with highly specialised signal transduction roles (Alberts *et al.*, 2008, p1132). Importantly, the structural role of cell-cell adhesion cannot be uncoupled from cell-cell signalling, which occurs in all of these types of adhesion junctions.

Attraction between cells is mediated by cell adhesion molecules (CAMs). Typically, the structure of a CAM incorporates a transmembrane domain, an extracellular domain (for recognition and binding to the ligand expressed on an adjacent cell), and a cytoplasmic domain, which is often tethered to the cytoskeleton (Hansen *et al.*, 2008). CAMs mediate cell-cell adhesion by *trans*-interaction either by recognising an identical CAM, referred to as a homophilic interaction, or by recognising a different CAM, referred to as a heterophilic interaction. Hansen *et al.* (2008) classifies CAMs based on structure as (i) cadherin superfamily (ii) integrin superfamily (iii) selectins and (iv) immunoglobulin superfamily of CAMs. In this review I will focus on selected members of the cadherin and immunoglobulin superfamily, as these CAM groups are most relevant to this thesis.

Cell adhesion molecules of peripheral nerve

A study by Spiegel *et al.* (2006) identified three main groups of Schwann cell expressed adhesion molecules. These are: (1) early mediators of Schwann cell/axonal interaction, for example Neural cadherin (N-cadherin), L1-cell adhesion molecule (L1-CAM), neural cell adhesion molecule (NCAM) and semaphorin-4F (Sema4F); (2) structural adhesion molecules, for example Epithelial cadherin (E-cadherin), MPZ, PMP22 and claudin-19; (3) mediators of stable interactions between myelinated Schwann cells and their ensheathed axons including those involved in the specialisation and compartmentalisation of the Schwann cell/axonal membrane, for example Tag-1/contactin-2, neurofascin (NF)-155, gliomedin and Necls. These, together with the mediators of Schwann cell/ECM attachment, orchestrate various processes of myelinating Schwann cells, including cell attachment, process extension, axon ensheathment, spiral enwrapping, compaction and the formation of the Nodes of Ranvier (Spiegel *et al.*, 2006). The adhesion molecules involved in Schwann cell/axonal interactions and myelination, discussed in the following sections, are summarised in **Table 1.1**.

Cell adhesion molecules of early Schwann cell/axonal interactions

N-cadherin

The cell adhesion molecule N-cadherin/cadherin-2 will be discussed in detail because of its central relevance to this thesis. N-cadherin is expressed early in the Schwann cell lineage at the neural crest stage but appears to be down-regulated following transition to mature Schwann cells (refer to Chapter Three for more details). The cadherin or ‘calcium-dependent adherent protein’ family are defined by their dependence on soluble calcium ions for their adhesive function (Patel *et al.*, 2003). The cadherin superfamily consists of a diverse collection of CAMs that can be subdivided into five main structural and functional groups with different ligand-binding preferences. These are the classical cadherins, desmosomal cadherins, atypical cadherins, proto-cadherins and cadherin-related signalling proteins (Gumbiner, 2005). In addition to their dependency on calcium, all cadherins share a conserved region of approximately 110 residues in their extracellular domain, which are often repeated (Patel *et al.*, 2003). Cadherins function not only in cell adhesion but are also central to processes of cell-cell recognition, cell and tissue polarity, cell migration and cell-sorting (Halbleib & Nelson, 2006).

N-cadherin is a member of the classical cadherins, which are the most studied cadherin subdivision and are best known for their structural role in forming adherens junctions that hold cells together in tissues, for example epithelial tissue. Members of this group have historically been named according to their predominant site of expression. They include E-cadherin (the founding member), N-cadherin, placental (P)-cadherin, retinal (R)-cadherin, and (type II) vascular endothelial (VE)-cadherin (Gates & Peifer, 2005; Gumbiner, 2005). However, this nomenclature is confusing as the type of cadherin expressed is not restricted to the tissues as implied in their nomenclature, moreover (as in Schwann cells) different cadherins can be expressed in the same cell at different developmental times (Crawford *et al.*, 2008). Thus, the official nomenclature now defines the cadherins by a numerical suffix so that the previous list starting with E-cadherin is thus, cadherin-1 (CDH1) through to cadherin-5 (CDH5), respectively. Historically, N-cadherin was first identified in the brain and is often cited as the predominant cadherin of the developing nervous

system (Fairless *et al.*, 2005; Ranscht, 2000). In the CNS, N-cadherin plays an important role in synaptic function, synaptogenesis and dendritic spine morphology (Bard *et al.*, 2008; Benson & Tanaka, 1998). In the PNS, N-cadherin had been shown to play a central role in growth-cone path-finding (Bard *et al.*, 2008), and furthermore, has been implicated as an early mediator of Schwann cell/axonal interactions (Wanner *et al.*, 2006a; Wanner & Wood, 2002), although its exact role has yet to be determined and is the subject of this thesis.

The structure and downstream components of N-cadherin

Similar to other members of the classical cadherins, the N-cadherin molecule is structurally composed of five extracellular domains (ECD 1-5), a single-spanning transmembrane domain and a C-terminal cytoplasmic domain (Gumbiner, 2005). The ECDs are arranged in linear tandem repeats with ECD-5 juxtaposing the plasma-membrane while ECD1 is the most outer domain and is thought to be the active domain for mediating adhesion. Each ECD is composed of 110 conserved residues that form autonomous β -pleated sheets arranged in structures that resembles a 'Greek key' design and are linked together by flexible hinges containing three calcium-binding sites (Patel *et al.*, 2003) (see **Figure 1.11**).

In addition to calcium, the core cadherin structure requires homodimerisation, while large assemblages of cadherin homodimers are required to generate the mature adherens junction. Intracellularly, the cadherin dimer interacts with the actin cytoskeleton via a number of adapters that includes β -catenin and α -catenin, although the exact relationship and dynamics of this interaction is still unclear (Gates & Peifer, 2005). Nevertheless, the internal attachment of the adherens junction to the cell cytoskeleton is important for cadherin function as it provides the necessary tensile strength and intracellular anchorage for the junction. Interestingly, previous notions of a static interface between cadherin and actin have been challenged by Drees *et al.* (2005) and Yamada *et al.* (2005) who both show that α -catenin, rather than being a static link, is more likely to function as a regulator of actin dynamics, suggesting that the link between cadherin and the cell cytoskeleton is more transient than was first thought (Gates & Peifer, 2005).

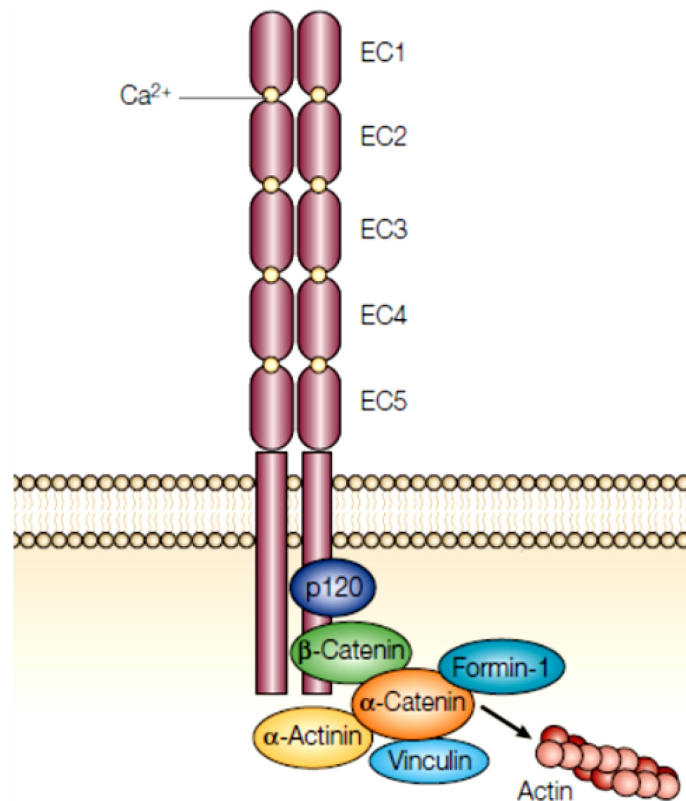


Figure 1.11 Schematic showing the classical view of cadherin structure. The molecule has five extracellular domains linked by flexible joints, a transmembrane domain and cytoplasmic domain that interacts with the actin cytoskeleton via a number of adaptors including β -catenin and α -catenin (Gumbiner, 2005).

The classical cadherins mediates cell-cell adhesion

The majority of classical cadherins, including N-cadherin and E-cadherin, mediate intercellular adhesion by binding to one another in a homophilic manner, i.e. an N-cadherin dimer present on the plasma-membrane of one cell will bind (ligate) with an N-cadherin dimer expressed on the opposing plasma-membrane of a second adjacent contacting cell. To achieve this, both cells must express the same cadherin type to allow homophilic binding, which is also important for the process of cell sorting. Homophilic N-cadherin-N-cadherin *trans*-ligation is dependent on calcium ions, which ensure the rigidity of the rod-like ECD domains and is essential for adhesive function. Many studies investigating cadherin function and cell-cell interaction exploit this central requirement by altering the calcium ion concentration of the cell media in order to functionally perturb cadherin adhesion (see **Figure 1.12**).

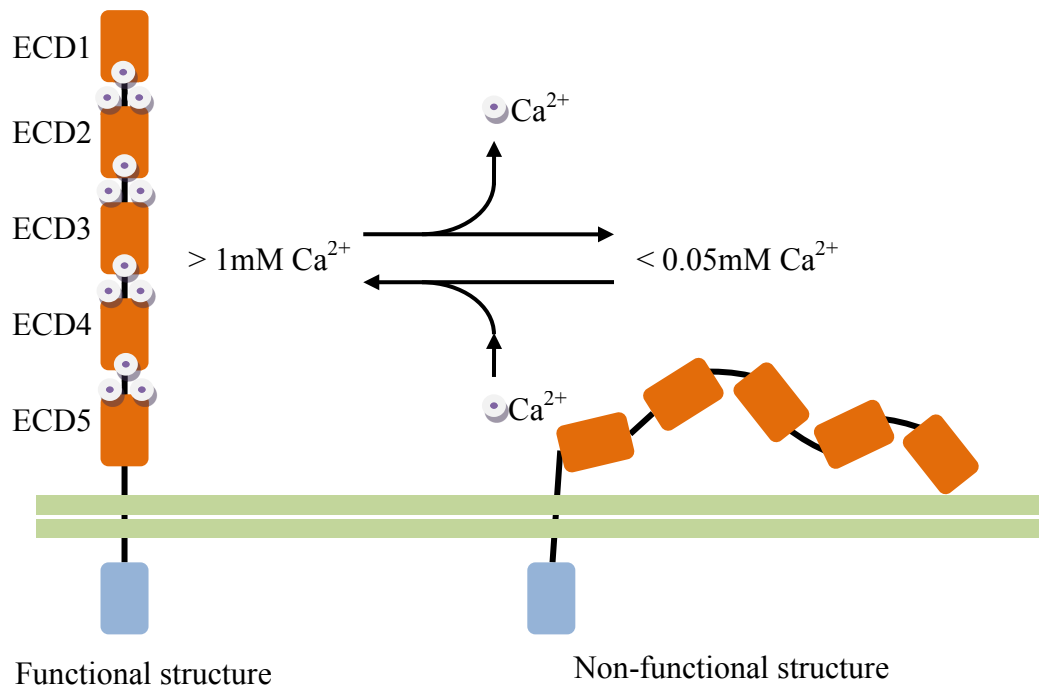


Figure 1.12 Schematic illustration showing the central role of calcium ions in generating the functional structure of the classical cadherins. Calcium ions interact with cadherin at binding sites nested within the linkage regions between the five extracellular domains (ECDs), where they generate rigidity in the molecule. Extracellular calcium ion depletion is commonly adopted as a tool to study the cadherin function and adhesion (based on Alberts *et al.*, 2008).

Despite extensive biochemical and biophysical studies, including the use of X-ray crystallography, NMR spectroscopy, electron microscopy and electron tomography, it is still unclear how the opposing cadherins sterically arrange themselves to form the adhesive bond (Gumbiner, 2005; Kiryushko *et al.*, 2004). An emerging view is that a number of different arrangements are possible - an idea which has been described as the multi-state nature of cadherin binding (Bayas *et al.*, 2006). However, the linear-zipper model is often employed to describe the molecular binding conformation of classical cadherins and was devised from the crystal structure of the ECD1 domain of N-cadherin (Shapiro *et al.*, 1995). In this model, adhesive function is reliant on both *cis* and *trans* homophilic interactions mediated by different regions of the ECD1 domain. Homophilic *cis*-interactions occur between W-moieties on ECD1, which mediate homodimerisation of N-cadherin molecules within the plane of the membrane, while homophilic *trans*-ligation occurs

at separate sites on ECD1 adjacent to the first three amino acids (conserved across all the classical cadherins) called the HAV sequence (histidine-alanine-valine) and is responsible for cell-cell ligation (Noe *et al.*, 1999). In terms of *trans*-ligation of N-cadherin at the HAV region, the molecular bond is thought to be mediated between a protruding tryptophan residue (Trp2) on the first cadherin ECD1 with the hydrophobic pocket on a second opposing cadherin ECD1 (see **Figure 1.13**).

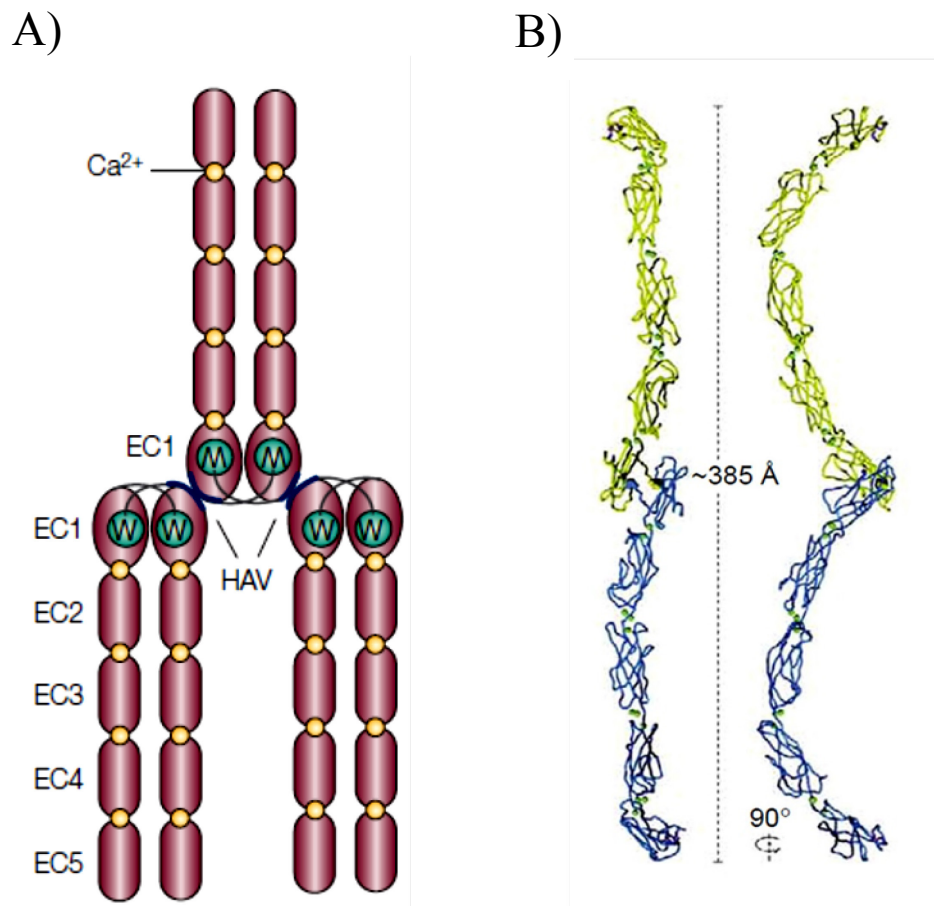


Figure 1.13 Schematic showing the proposed linear-zipper model of cadherin homophilic adhesion. (A) The ECD1 domain contains ‘W’ regions that are proposed to mediate *cis*-homodimerisation of cadherins, i.e. laterally within the membrane, and conserved histidine-alanine-valine (HAV) sequences that are thought to mediate homophilic *trans*-ligation of cadherins, i.e. between cells (Gumbiner, 2005). (B) Extracellular domain structure of non-dimerised cadherin (Patel *et al.*, 2003).

This adhesive interaction generates the ‘cadherin strand-dimer’ interface, which has been proposed to be responsible for the adhesive force in cadherin-mediated cell-cell adhesion (Patel *et al.*, 2003). Kinetic studies have revealed that the adhesive force of N-cadherin-N-cadherin *trans*-ligation is relatively weak and transient - lasting less than two seconds on average (Bayas *et al.*, 2006). Thus, the strength of adhesion mediated by cadherin interactions is only likely to be effective when multiple cadherin homodimers are combined together to form larger, multi-cadherin complexes. This process of junctional maturation is likely to explain the 'zipper-like' pattern of cadherin at cell-cell junctions, where additional cadherin homodimers are recruited to bolster the initial 'pioneer' N-cadherin-N-cadherin ligation event. In this way, the junction is thought to strengthen and mature over time as multiple cadherin dimers are recruited and *trans*-ligate across juxtaposed cell membranes to adhere cells together (Derycke & Bracke, 2004; Patel *et al.*, 2003) (**Figure 1.14**).

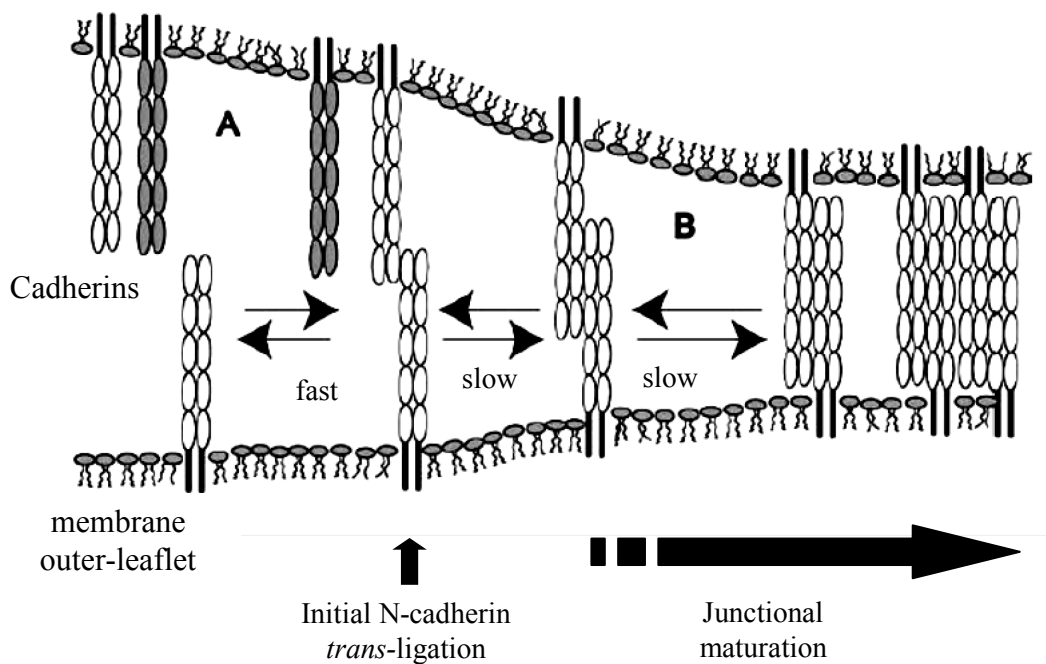


Figure 1.14 A theoretical model for adherens junction maturation. Cadherin homodimers diffuse laterally in the plane of the membrane. Following cell-cell contact, a homophilic cadherin-cadherin *trans*-ligation event occurs that weakly and transiently adhere the cells together. This interaction impedes the lateral diffusion of cadherin within the membrane of both cells, resulting in the *cis*-recruitment of further cadherin molecules to the 'junction', which gradually matures and strengthens as the number of cadherins increases (Adapted from Bayas *et al.*, 2006).

The regulation of cadherin activity

The surface expression of cadherin is tightly regulated at multiple levels including transcription, trafficking (Kawauchi, 2011) and membrane organisation (Halbleib & Nelson, 2006) as well as post-translational modification, for instance by ADAM10 and PS1/ γ -secretase, which cleave the C-terminal end of N-cadherin (Uemura *et al.*, 2006). In addition, the cadherin molecules are synthesised and transported to the membrane as inactive pro-proteins, with N-terminal pre-domains that sterically hinder the active ECD1 domain. The half-life of cell-surface expressed E-cadherin in epithelial cells is approximately 5-10 hours (Gumbiner, 2000), which suggests that post-translational modification and/or internalisation of cadherin rather than transcriptional regulation, would be preferable in order for the cell to effect dynamic responses where the speed of response was important. Another form of cadherin regulation is through alterations in catenin function. Catenins perform three main roles: they provide the physical link to the actin cytoskeleton, regulate actin dynamics and modulate the adhesive properties of the cadherin ECD (Gumbiner, 2005). Interestingly, studies have shown that cadherins interact with a number of RTK receptors (Doherty *et al.*, 2000), for example N-cadherin has been shown to interact with the EGF receptor through β -catenin (Hoschuetzky *et al.*, 1994) and directly with the fibroblast growth factor (FGF) receptor (Williams *et al.*, 1994).

Semaphorin-4F

Semaphorin-4F (Sema4F) is a member of the semaphorin family, which is broadly divided into transmembrane or secreted glycoproteins and are subdivided into eight classes, where only classes 3 to 7 are expressed by vertebrates (Kruger *et al.*, 2005). Semaphorins are expressed throughout the nervous system where they are best characterised in axonal guidance, notably through the regulation of cell migration and attachment. In addition, they are also important for immune cell regulation and heart development and are implicated in a number of cancers (Kruger *et al.*, 2005). Sema4F is a member of the class-4 semaphorins, which are the largest group of membrane-associated semaphorins (Kruger *et al.*, 2005). There are at least twenty semaphorins that all share a conserved Sema domain of approximately 400 residues, located near to the N-terminus (Kiryushko *et al.*, 2004). The structure of semaphorin

incorporates a seven-bladed, folded- β -propeller Sema domain, a PSI (plexins, semaphorins and integrins) domain, and, in the case of classes 2, 3, 4 and 7, a common immunoglobulin (Ig)-like domain (Kruger *et al.*, 2005) (**Figure 1.15**).

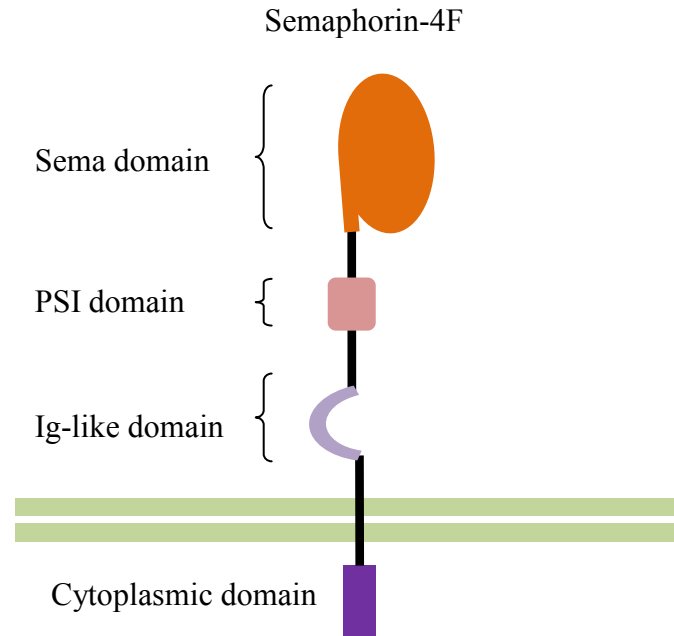


Figure 1.15 The domain structure of class-4 semaphorins. The molecular structure incorporates a cytoplasmic domain, transmembrane domain and an extracellular domain consisting of an immunoglobulin (Ig)-like stalk, abutting a small plexin/semaphorin/integrin (PSI) domain that connects to the conserved Sema domain that mediates adhesive interactions with plexins and neuropilins.

The semaphorins signal through multimeric receptors composed of neuropilins or plexins, which also incorporate the Sema domain in their structures (Kiryushko *et al.*, 2004). The binding of semaphorin with plexins is mediated between the Sema domains of both molecules. Interestingly, regions of the plexin molecule share homology with Ras GAPs, suggesting that plexin has intrinsic Ras GAP activity (Kruger *et al.*, 2005). Furthermore, Ras has since been shown to interact with plexin (Oinuma *et al.*, 2004), while plexins have been shown to interact and modulate Rho-family GTPases (Kruger *et al.*, 2005). These interactions might provide some clues as to explaining the diverse roles of semaphorin. In contrast to plexins, semaphorins have not classically been thought of as adhesion molecules, but are instead best characterised as axonal guidance molecules (Kruger *et al.*, 2005). However, a study

by our laboratory has demonstrated a novel role for Sema4F in mediating Schwann cell/axonal interaction *in vitro* (Parrinello *et al.*, 2008). Furthermore, we showed that Sema4F was required for stable Schwann cell/axonal interactions and that Sema4F was downregulated following activation of the Ras/Raf/ERK signalling pathway, which subsequently resulted in the dissociation of Schwann cells from axons. Importantly, hyperactivation of the Ras/Raf/ERK pathway is central to the aetiology of Neurofibromatosis Type I, which implicates Sema4F in the generation of neurofibromas. Furthermore, we showed that Sema4F was important for maintaining the quiescent state of associated Schwann cells, either by keeping the Schwann cell in close proximity to the inhibitory signalling milieu of the axon, or through an as yet undefined reverse signalling mechanism.

L1-CAM

L1-CAM is expressed by developing axons at growth-cones as well as by SCPs, ISCs and by mature non-myelinating Schwann cells (Haney *et al.*, 1999; Jessen & Mirsky, 2005); however, it is down-regulated in myelinating Schwann cells (Seilheimer *et al.*, 1989). L1-CAM is a member of the IgCAMs and is structurally composed of six Ig-like domains, five repeated fibronectin Type III domains, a single-spanning transmembrane region and a cytoplasmic C-terminal domain (see **Figure 1.16**) (Kiryushko *et al.*, 2004). Its structure is highly conserved in mammals with orthologs found in chick (NgCAM), zebrafish (L1.1-L1.2) and drosophila (neuroglian) (Haney *et al.*, 1999). L1-CAM can bind in a homophilic or heterophilic manner, both of which are implicated in multiple processes, for instance homophilic ligation has been implicated in neurite out-growth, axonal-axonal and Schwann cell/axonal adhesion, while heterophilic interactions have been implicated in neurite extension and migration. The binding partners for heterophilic L1-CAM interaction include Tag-1 (which is similar in structure to L1-CAM and discussed later) and integrin $\alpha_v\beta_3$, although the downstream effects of these interactions remain to be determined (Haney *et al.*, 1999). In terms of homophilic binding, the functional interaction appears to be mediated by a trimer of L1-CAM molecules on the plasma-membrane of both contacting cells. The extracellular Ig-like domains of all three L1-CAM molecules bend to form an active 'horse-shoe' configuration (Hall *et al.*, 2000). At its cytoplasmic domain, L1-CAM interacts with axonal ankyrin, which is

important for the functionality of L1-CAM (Crossin & Krushel, 2000). L1-CAM deficient mice myelinate normally, suggesting that L1-CAM is not essential for myelination (Carenini *et al.*, 1997). However, these mice exhibit malformed Remak bundles, resulting from the loss of axonal ensheathment, leading to progressive cell-death of non-myelinated sensory axons in the adult (Haney *et al.*, 1999). It has been suggested that the requirement for L1-CAM in non-myelinating Schwann cell/axonal interactions, stems from its binding with axonal ankyrin, which might be required to stabilise axonal microfilaments (Haney *et al.*, 1999).

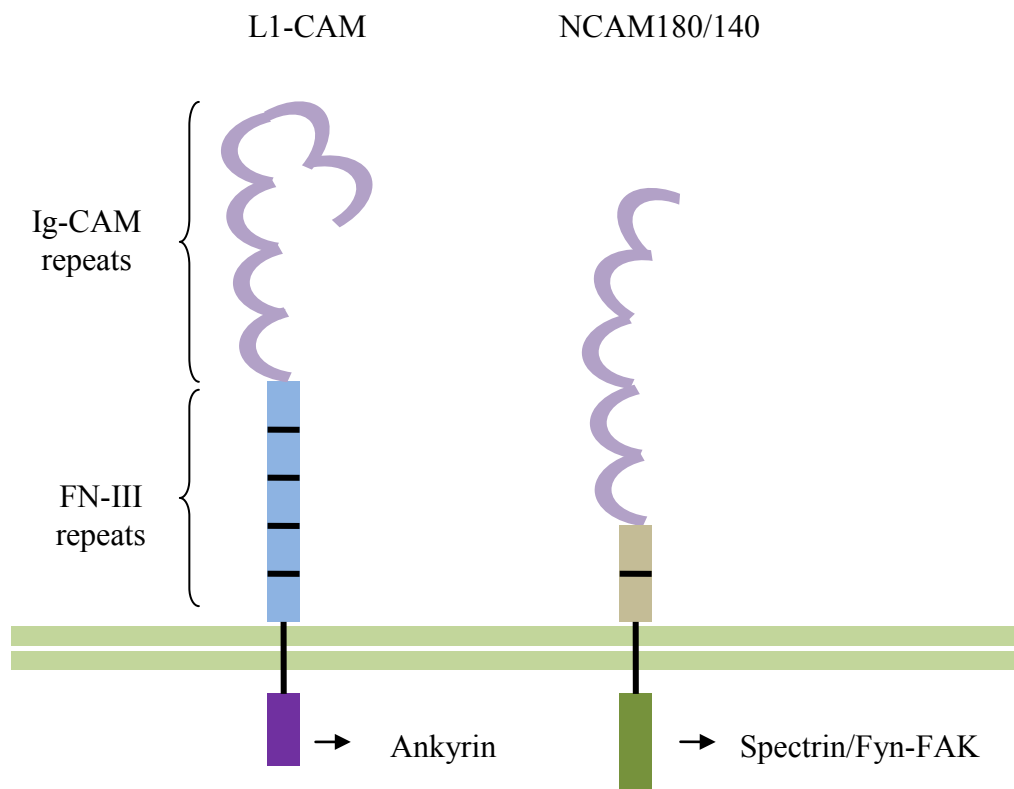


Figure 1.16 Domain structure of L1-CAM and NCAM. Both adhesion molecules are transmembrane proteins structurally composed of repeating fibronectin (FN) domains (comprising the stalk) and a repeating number of immunoglobulin (Ig)-like domains, in which the two most distal Ig-domains are linked to the rest of the molecule by a flexible hinge. Adhesion is mediated through the Ig domains; although, the exact binding conformation of both CAMs is not known. L1-CAM and NCAM interact intracellularly, via their cytoplasmic domains, with Ankyrin and Spectrin respectively.

Neural Cell Adhesion Molecule (NCAM)

NCAM is expressed by Schwann cells during development but later down-regulated along with L1-CAM and N-cadherin at myelination (Kiryushko *et al.*, 2004). NCAM is a member of the immunoglobulin superfamily of CAMs (IgCAMs) and is structurally composed of five Ig-like domains and two fibronectin (FN-III) binding domains (**Figure 1.16**). NCAM binds heterophilically with a number of binding partners including L1-CAM and Tag-1 (Brummendorf & Rathjen, 1995) as well as the FGF receptor (Kiselyov *et al.*, 1997). In terms of L1-CAM binding, NCAM appears to assist homophilic *trans*-binding of L1-CAM-L1-CAM (Kiryushko *et al.*, 2004). The adhesive interactions exhibited by NCAM is typically weaker than that mediated by calcium-dependent cadherins (Alberts *et al.*, 2008, p1146). Interestingly, alternative splicing from the NCAM gene results in NCAM isoforms that exhibit variable levels of sialic acid. This greatly affects the ability of NCAM to mediate adhesion, where high concentrations of sialic acid can switch NCAM from adhesion to repulsion. Interestingly, N-cadherin, L1-CAM and NCAM have all been shown to interact with the FGF receptor and moreover, they have all separately been implicated with activating the MAPK signalling pathway through association with RTKs (Perron & Bixby, 1999; Schmid *et al.*, 1999; Schmid *et al.*, 2000).

Structural cell adhesion molecules of myelinated nerve

Both the Schwann cell and the axon are specialised into distinct domains. The myelin sheath of the Schwann cell is specialised into two major compartments, compact myelin and non-compact myelin, which have distinct structural and functional properties (Garbay *et al.*, 2000; Kursula, 2008). For example, the extracellular space between opposing membranes in compact myelin is typically less than 2nm, while for non-compact myelin this can be as much as 12-14nm (Kursula, 2008). Thus, while the former can present an impenetrable barrier to ion flux, the latter permits sufficient space for metabolic exchange between the interior and exterior of the Schwann cell. Axonal specialisation was first alluded to by Ranvier (1871), who observed, in longitudinal sections of teased myelinated nerve fibres, the presence of regularly spaced regions (intervals) that were devoid of myelin, which have subsequently been termed Nodes of Ranvier (Rosenbluth, 1999). Thus, the two

major compartments of the axon comprise the region between Nodes of Ranvier, termed the internode and the Node of Ranvier itself. The axonal internode comprises the majority of the myelinated axon and is surrounded by compact myelin, while the Node of Ranvier and the paranode are surrounded by non-compact myelin (Poliak & Peles, 2003) (**Figure 1.17**).

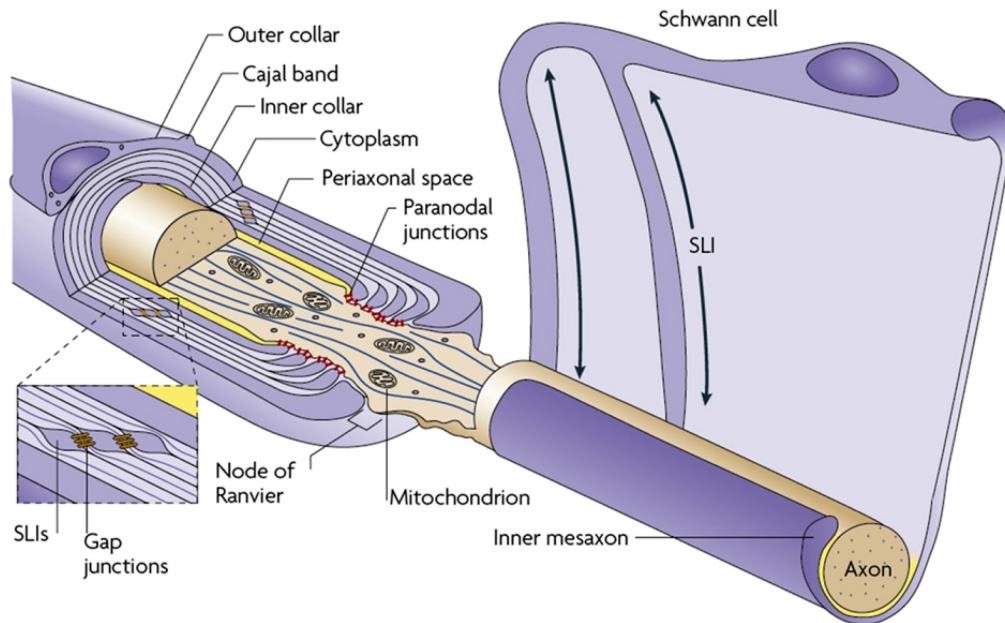


Figure 1.17 Schematic showing the structure and domains of a myelinated nerve fibre. The Schwann cell sheath is composed of compact and non-compact myelin. Compact myelin surrounds the internode and is punctuated by non-compact cytoplasmic channels called Schmidt-Lanterman Incisures (SLI), which descend radially through the sheath, and Cajal bands, which run longitudinally within the outer-collar. In addition, non-compact myelin surrounds the Node of Ranvier and its associated domains (the paranode and juxtaparanode), which allows ion-exchange essential for saltatory impulse conduction (Nave, 2010a).

In the following sections, I will discuss the internode by first considering the glial components that form the sheath and also the glial and axonal CAMs that mediate interactions at the Schwann cell/axonal interface. I will then describe the Node of Ranvier and associated domains and discuss the CAMs involved in their formation, stabilisation and function before lastly addressing the non-compact regions of the

Schwann cell, extra to the nodal domains, which form the cytoplasmic channels responsible for metabolic transport within the myelinated Schwann cell and between the Schwann cell and its ensheathed axon (Nave, 2010a; Tricaud *et al.*, 2005).

The Internode

The axonal internode is the longest domain compartment of the axon residing between two consecutive Nodes of Ranvier, and has the greatest internal cross-sectional area of all the domains. With the exception of the inner-most, axonal-facing (adaxonal) membrane of the Schwann cell and various cytoplasmic channels (discussed later), the majority of the myelin sheath that surrounds the axonal internode is composed of compact myelin.

The compact myelin sheath

Compact myelin is characterised by multiple, concentrically-wrapped tight layers of Schwann cell plasma-membrane, which excludes cytoplasm and forms a dielectric insulating barrier, or sheath, around the axonal internode. The major non-protein component of compact myelin is cholesterol, whose availability is generally considered the rate-limiting step for myelin biosynthesis (Nave, 2010b; Saher *et al.*, 2005). The major protein components of compact myelin are MPZ, MBP and PMP22 (see **Figure 1.18**).

MPZ is a member of the Ig-CAM superfamily of proteins and is structurally composed of a large glycosylated extracellular domain, a single helical transmembrane domain and a small basic cytoplasmic domain (Kursula, 2008; Lemke *et al.*, 1988). MPZ is a 30 kilodalton (kDa) protein and is the most abundant myelin protein accounting for over 50% of proteins found in peripheral myelin; furthermore, it is considered to be the predominant CAM involved in the compaction of the myelin sheath (Kursula, 2008). MPZ forms a tetramer, in which the extracellular domains (ECDs) of one tetramer binds homophillically with the juxtaposed ECDs of an adjacent MPZ tetramer, to form autotypic junctions between opposing sheets of myelin membrane (Kursula, 2008; Martini & Schachner, 1997; Menichella *et al.*, 2001) (**Figure 1.18**).

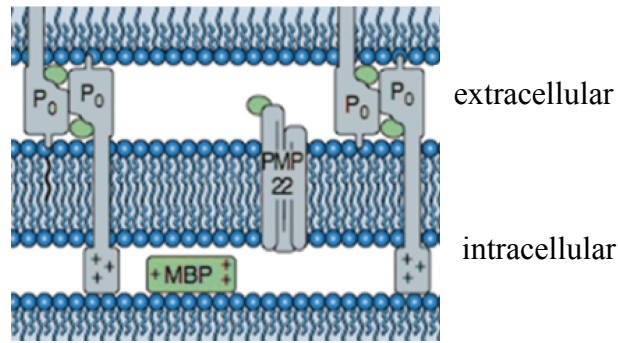


Figure 1.18 The structural components of compact myelin sheath. Molecules involved in compaction include myelin protein zero (MPZ/P0), myelin basic protein (MBP) and peripheral myelin protein-22 (PMP22) (printed with permission from Sara Ribeiro).

MPZ not only facilitates compaction across the extracellular space, but also compacts the intracellular cytosolic space via its cytoplasmic domain, which interacts with phospholipids on the internal opposing plasma-membrane of the Schwann cell (Wong & Filbin, 1996). MPZ is the largest component by mass of the sheath, accounting for 50-60% of peripheral myelin proteins (Kursula, 2008). MPZ null mouse models have hypomyelinated nerves with poor myelin compaction (Giese *et al.*, 1992). Interestingly, MPZ appears to be required for the correct localisation of E-cadherin (discussed later), with MPZ null mice displaying severely disrupted autotypic junctions (Menichella *et al.*, 2001).

MBP is expressed in both CNS and PNS myelin in a variety of different isoforms, which are generated through post-translational modification and alternative splicing of the MBP gene (Kursula, 2008). MBP is a small, highly basic protein which is localised to the cytosolic leaflet of the membrane where it assumes a curved conformation. While MBP is not strictly a CAM it is nonetheless thought to aid compaction and mediate adhesion by offsetting the negative charge of the phospholipid-rich outer leaflet, and thus neutralise electrostatic repulsion that would otherwise prevent compaction (Min *et al.*, 2009).

PMP22 is a small 22 kDa molecule, which is highly hydrophobic and is thought to be structurally composed of four transmembrane domains and an HNK-1 epitope (Martini & Schachner, 1997). The core PMP22 molecule is thought to dimerise to

generate a multimeric complex (Adlkofer *et al.*, 1995), which binds the cytosolic face of the inner-membrane leaflet and contains important lipid binding sites suggestive of a role in specialising the lipid composition of the myelin membrane (Kursula, 2008).

Schwann cell/axonal cell adhesion molecules of the internode

The region of the Schwann cell that interfaces with the axon along the internode is called the adaxonal membrane and is composed of non-compact myelin. The internode is characterised by a number of glial expressed CAMs including MAG and Necl (nectin-like)-4, while Necl-1 is expressed on the axonal membrane (axolemma) (Perlin & Talbot, 2007; Yin *et al.*, 1998) (**Figure 1.19**).

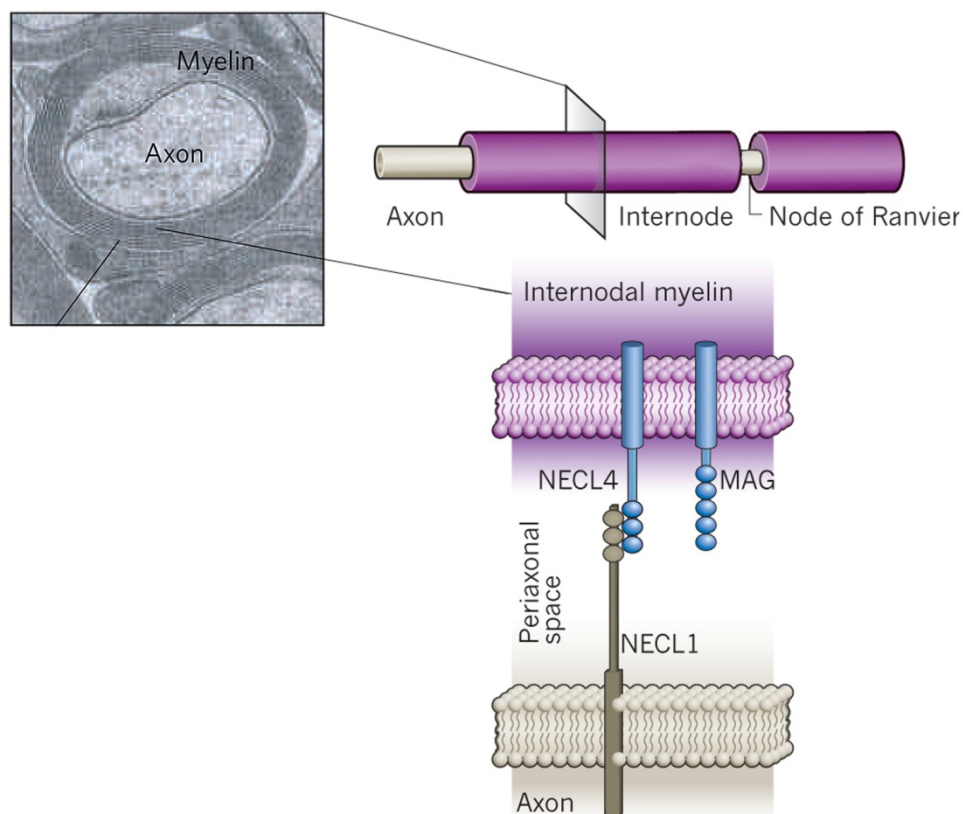


Figure 1.19 The cell adhesion molecules of the internode. Glial cell adhesion molecules (CAMs) include nectin-like (Necl)-4 and myelin-associated glycoprotein (MAG). The internode is stabilised by autotypic Necl4-Necl1 interactions, while MAG has been implicated in the stabilisation of axonal actin filaments (adapted from Nave, 2010b).

MAG is expressed in both CNS and PNS myelin. It is a transmembrane CAM composed of five highly glycosylated immunoglobulin (Ig)-like extracellular domains, with a molecular weight of 100 kDa (Martini & Schachner, 1997). MAG is localised predominantly to the periaxonal collar as well as other non-compact myelin regions (discussed later). It is expressed as two isoforms, S-MAG and L-MAG, which differ in their C-terminal domains and putative functions as structural and signalling molecules respectively (Kursula, 2008). Research into the functional role of MAG has historically been focused on its enrichment at the periaxonal membrane, suggesting a role for MAG in axo/glial interactions (Owens *et al.*, 1990; Owens & Bunge, 1991). The functional relevance of MAG is unclear; however, Yin *et al.* (1998) suggests that homophilic binding between axonal-expressed MAG and Schwann cell expressed MAG, enhances the stability of axonal cytoskeletal filaments and thus, the viability of the myelinated axon. Interestingly, this is similar to the suggested role for L1-CAM in non-myelinated axons (discussed earlier). Despite this, MAG knockout mice exhibited normal myelination (Li *et al.*, 1994; Montag *et al.*, 1994), although this might be explained by functional compensation. For instance, Carenini *et al.* (1997) showed that NCAM was able to partially compensate for MAG function in the MAG knockout mice, at least during development.

The Necl (also known as SynCam or 'cell adhesion molecules') proteins are members of the Ig-CAM superfamily that have recently been implicated in maintaining the stability of the myelinated nerve. There are four members expressed in humans and rodents, Necl-1 (SynCAM3), Necl-2 (SynCAM1), Necl-3 (SynCAM2) and Necl-4 (SynCAM4). Necls are single-spanning CAMs with three extracellular Ig-domains and a short cytoplasmic domain that contains both a PDZ moiety and a binding site for protein 4.1 members (Spiegel *et al.*, 2007). The Necls bind both homophilically and heterophilically with other Necls or closely-related nectins. Necl-4 expression occurs exclusively in Schwann cells, and was discovered by Spiegel *et al.* (2006), who conducted a screen of cell-surface expressed and secreted molecules in myelinated Schwann cells and axons, in which Necl-1, Necl-2 and Necl-3 was also identified. In contrast to Necl-4, Necl-1 is expressed exclusively on the axonal internodal membrane (Perlin & Talbot, 2007; Yin *et al.*, 1998). Two independent studies have separately found that Schwann cell expressed Necl-4 and axonal expressed Necl-1 bind in a heterophilic manner, which appears to be critical for

myelination (Maurel *et al.*, 2007; Spiegel *et al.*, 2007). Spiegel *et al.* (2007) showed this using a dominant-negative Necl-4, which blocked myelination *in vitro*, while Maurel *et al.* (2007) used an siRNA approach to knockdown Necl-4, which prevented Schwann cell differentiation and myelination in DRG/Schwann cell cocultures.

The Node of Ranvier and associated domains

Since its discovery, the Node of Ranvier has been intensely studied. Previous notions that Schwann cells were multi-nucleated cells stretching the length of the axon have long been dispelled in favour of autonomous cells with definite cellular boundaries between one Schwann cell and the next all encased within a protective and continuous basal lamina (Bunge *et al.*, 1986). Apart from forming the interface between two ensheathed Schwann cells, the function of the Node of Ranvier and its associated domains is to generate and propagate action potentials from Node to Node along the nerve fibre by fast saltatory conduction (Hartline & Colman, 2007). In normal physiology, the spacing of the Node of Ranvier, and thus the internode distance, is tightly coupled with the diameter of the fibre; a parameter that impacts upon nerve conduction efficiency and optimal NCVs (as discussed previously) (Hartline & Colman, 2007). Thus, as a rule-of-thumb, the inter-nodal distance is generally regarded as being 100 times the diameter of the myelinated fibre (Corfas *et al.*, 2004; Poliak & Peles, 2003). The formation of the Node of Ranvier and the specification of associated domains is critically dependent on Schwann cell/axonal interactions. Importantly, in contrast to the axonal NRG1 signal, the Schwann cell appears to dictate the underlining domain specialisation of the axon (Poliak & Peles, 2003; Salzer, 2003; Sherman & Brophy, 2005). The Node of Ranvier is flanked by the Paranode and Juxtaparanode (**Figure 1.20**).

The Node of Ranvier

The Node of Ranvier is approximately 1µm in length and is the first axonal domain to be specified. It is located at the interface between two adjacent ensheathing Schwann cells (Poliak & Peles, 2003). The overlying glial component of the Node is highly-ruffled, forming a so-called microvilli fringe. Importantly, homotypic

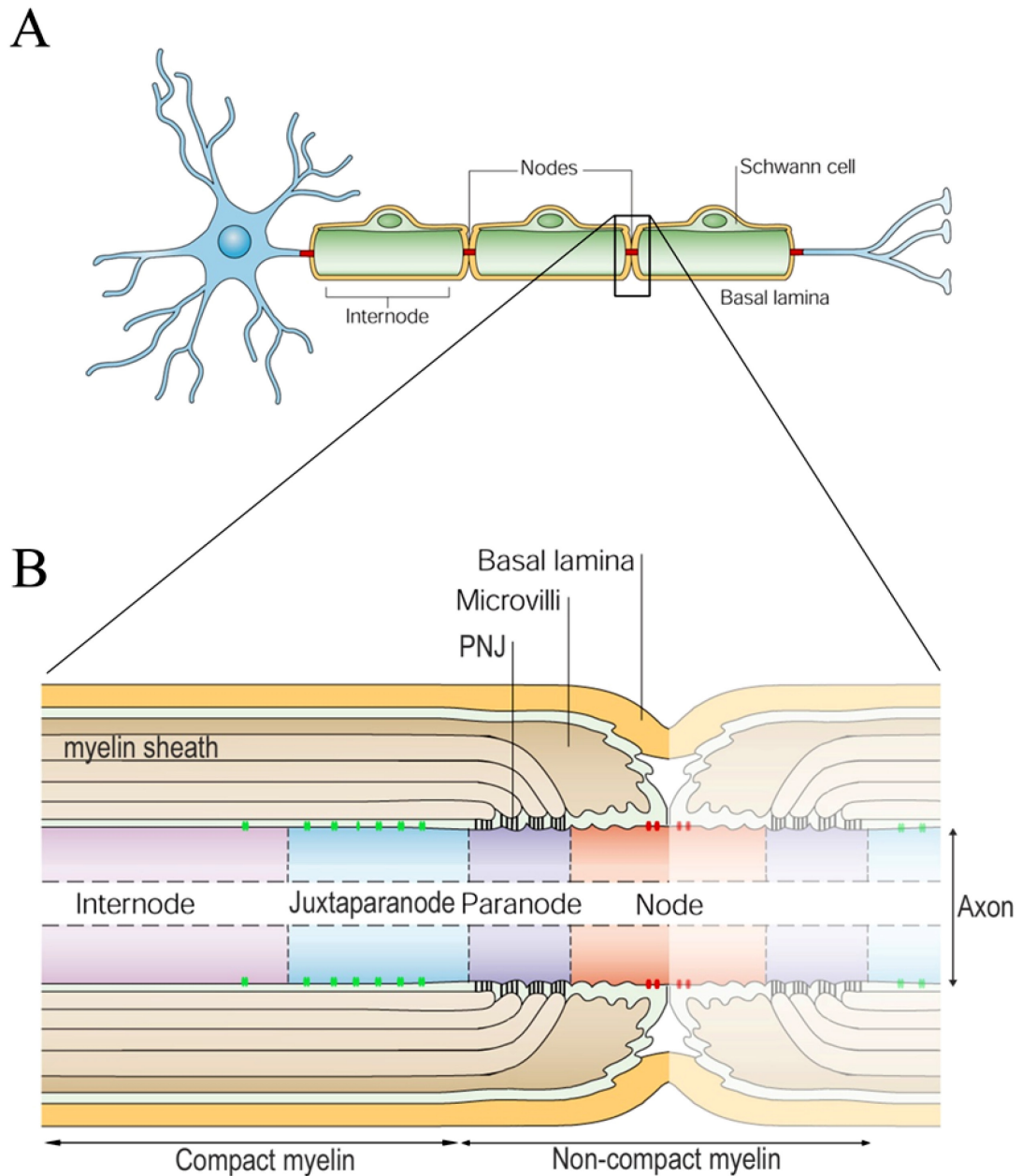


Figure 1.20 The structure of the Node of Ranvier and its associated domains in a myelinated nerve fibre. (A) The myelinated nerve fibre is enwrapped by multiple Schwann cells, which cover the length of the axon, and is protected by an outer and continuous basal lamina. (B) The Node of Ranvier is flanked by the Paranode and Juxtaparanode, where paranodal junctions (PNJs) at the Paranode, seal the axolemma to the Schwann cell. The PNJ prevents lateral diffusion of ion-channels between the Node (containing sodium ion channels - shown in red) and the Juxtaparanode (containing potassium ion channels - shown in green). Non-compact myelin surrounds the Node of Ranvier and the Paranode, while compact myelin surrounds the internode and juxtaparanode. Adapted from Poliak & Peles, 2003.

Schwann cell-cell interactions are not observed in this region. In support of this, neither E-cadherin or tight junctional components, for example claudin-1, claudin-2, claudin-3 and ZO-1 have been detected between adjacent Schwann cells at the Node of Ranvier (Alanne *et al.*, 2009). However, unlike the equivalent CNS Node, the basal lamina is continuous from one Schwann cell to the next (Alanne *et al.*, 2009; Bunge *et al.*, 1986; Schafer & Rasband, 2006). The overlying myelin sheath is composed of non-compact myelin and is characterised by an expanded extracellular space which is in contrast to the periaxonal space where the opposition between Schwann cells and axons is significantly tighter. The axolemma at the Node is highly enriched in sodium ion channels, with concentrations typically 25-fold that of the internode (Salzer *et al.*, 2008). The enrichment of sodium ion channels in the axolemma of the Node, together with a reduction in the transverse resistance of the Schwann cell plasma-membrane and the expansion in extracellular space, are all essentially important for generating and propagating impulses by saltatory conduction (Hartline & Colman, 2007; Sherman & Brophy, 2005).

In addition to sodium channels, the axolemma at the Node also expresses a number of CAMs and associated adaptors including neurofascin (NF)-186, neuronal cell adhesion molecule (nrCAM), ankyrin G and β IV-spectrin (Salzer, 2003; Sherman *et al.*, 2001; Sherman *et al.*, 2005). Interestingly, Lustig *et al.* (2001) showed that both NF-186 and nrCAM directly interact in *cis* with sodium ion channels, suggesting a role for these CAMs in the regulation of sodium ion channel localisation. A study by Eshed *et al.* (2005) later identified gliomedin as a Schwann cell expressed single-spanning, transmembrane CAM, which binds axonal-expressed neurofascin-186 and NrCAM. The gliomedin protein incorporates an extracellular olfactomedin and collagen domain, which permits binding with ECM components, notably proteoglycans via its collagen domain. Importantly, gliomedin is asymmetrically localised to the region of the plasma-membrane that forms the microvilli fringe, i.e. the outer flanks of the Schwann cell (Eshed *et al.*, 2005); thus, providing a plausible mechanism for the Schwann cell directed recruitment of axonal sodium ion channels to the prospective site of the Node of Ranvier (Eshed *et al.*, 2005) (**Figure 1.21**).

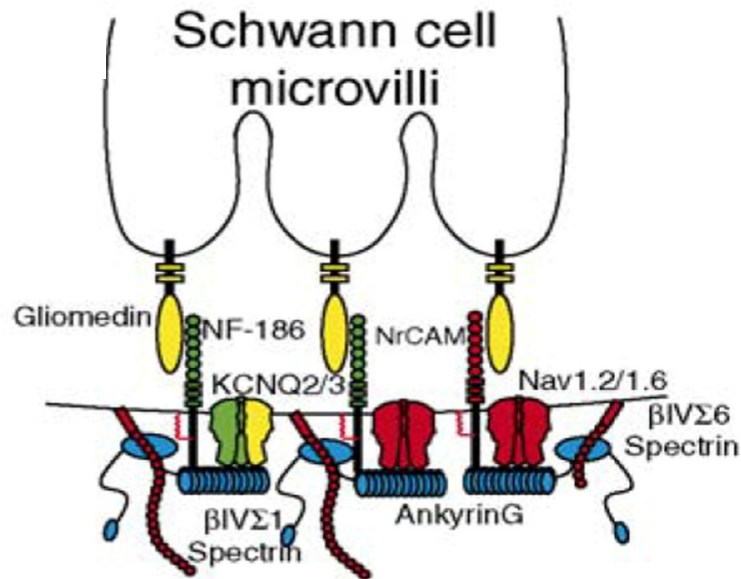


Figure 1.21 Schwann cell/axonal CAM interactions at the Node of Ranvier. Positioning of the Node of Ranvier appears to be determined by the asymmetric localisation of Schwann cell expressed gliomedin to the microvilli (extremity of the Schwann cell). The axonal expressed binding partner of gliomedin is neurofascin (NF)-186 and neuronal cell adhesion molecule (nrCAM), whose cytoplasmic domains interact in *cis* with Node specific sodium ion channels via ankyrin-G to specialise the underlying axonal domain (Schafer & Rasband, 2006).

In support of this, the gliomedin gene is under the regulatory control of Oct-6 and Krox20, in which expression is induced at the onset of myelination (Eshed *et al.*, 2005). Moreover, functional blocking of both NF-186 and nrCAM in myelinating DRG cocultures resulted in the disruption of sodium ion channels and the malformation of the Node of Ranvier (Lustig *et al.*, 2001). However, there is evidence that the positioning of the Node of Ranvier occurs prior to sodium ion clustering. A study by Melendez-Vasquez *et al.* (2001) has suggested that the location of the Node of Ranvier is specified prior to gliomedin-mediated sodium ion clustering. In this work, they show that ezrin, an ezrin-radixin-moesin (ERM) family member, is asymmetrically localised to the adaxonal Schwann cell plasma-membrane at the Schwann cell's outer-flanks, i.e. at prospective microvilli regions. Ezrin is known to interact with ankyrin-G and βV-IV spectrin, both of which are expressed by the axon, therefore this axo/glial interaction could provide a mechanism, preceding sodium ion clustering, responsible for the initial specification of the Node of Ranvier.

The Paranode

The paranode is characterised by a tight ring of Schwann cell/axonal paranodal junctions (PNJs), which bridge the gap between the axolemma and the paranodal loops (helical wraps of non-compact Schwann cell membrane). The PNJ borders the Node of Ranvier and is a large multimeric junction that is often considered to be orthologous to the insect septate junction (Salzer, 2003). It has been described as one of the largest intercellular adhesion complexes in vertebrate biology (Schafer & Rasband, 2006; Sherman & Brophy, 2005). The PNJ appears to perform two main functions. First, it provides structural support, anchoring the flanks of Schwann cell plasma-membrane to the axon and second, it functions as a diffusion barrier. In terms of the latter, the PNJ seals the extracellular space at the Node of Ranvier from the periaxonal space surrounding the internode and juxtaparanode - reducing the gap between Schwann cell sheath and the axon from ca. 15nm (at the internode) to less than 5nm (Salzer, 2003; Salzer *et al.*, 2008). This is important, as the PNJ restricts ion-flux between compartments, thereby ensuring the integrity of the charge separation required for efficient saltatory conduction. Second, the PNJ prevents lateral diffusion of domain-specific membrane proteins, notably ion channels, between the internode/juxtaparanode and the Node of Ranvier (Poliak & Peles, 2003). Thus, in mouse models where the PNJ is defective, potassium ion channels that are normally restricted to the internode/juxtaparanode, are found aberrantly mixed with Nodal sodium ion channels. Interestingly, sodium ion channels are still specifically retained at the Node of Ranvier despite the absence of the PNJ (Dupree *et al.*, 1999), presumably because these channels are anchored by interactions between gliomedin, NF-186 and nrCAM (as previously discussed).

The PNJ is formed between Schwann cell-expressed neurofascin (NF)-155 and an axonal expressed heterodimer composed of Caspr (contactin associated protein) (also known as paranodin) bound to contactin (**Figure 1.22**) (Schafer & Rasband, 2006) (Charles *et al.* 2002). Contactin lacks a transmembrane domain and is tethered to the axonal membrane via a glycosylphosphatidylinositol (GPI) moiety, where it interacts with Caspr and NF-155 via its Ig-domain. Schwann cell expressed NF-155 is a member of the IgCAM G superfamily and is one of two NF isoforms encoded by alternative splicing of the NF gene. NF-155 has been implicated in neurite out-

growth, axonal fasciculation and axon-axon adhesion (Tait *et al.*, 2000). Both isoforms are single transmembrane proteins structurally similar to L1-CAM and like L1-CAM (and NrCAM), they are able to bind ankyrin via their cytoplasmic domains. Their extracellular domains are structurally composed of six tandem Ig-domains and three or four fibronectin (FN) Type III domains. The main difference between them is that the NF-155 isoform contains an additional FN-III domain while lacking the mucin-like domain of NF-186 (Davis *et al.*, 1996).

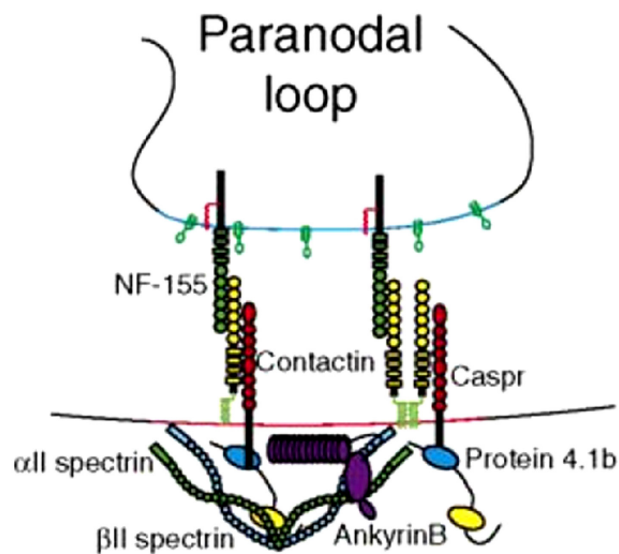


Figure 1.22 Cell adhesion molecules of the paranodal junction. The paranodal junction is composed of Schwann cell expressed Neurofascin (NF)-155 bound to axonal expressed Caspr and contactin. Caspr is anchored to the axonal actin cytoskeleton by protein 4.1b/ankyrinB interactions (Schafer & Rasband, 2006).

All three CAMs (NF-155, contactin and caspr) are essential components of the PNJ, with loss of any one component resulting in the failure of the PNJ (Bhat *et al.*, 2001; Boyle *et al.*, 2001; Sherman *et al.*, 2005). Interestingly, despite the absence of the PNJ, Schwann cell/axonal interactions were often maintained at the paranode, although the space between the axon and the Schwann cell was markedly increased. This suggested that other CAMs were able to partially compensate for the loss of the PNJ in order to ensure the continuity of stable axo/glia interactions (Poliak & Peles, 2003).

Cell adhesion molecules of the paranodal loops

The paranodal loops (PNLs) are held together by autotypic adherens junctions between multilamella sheets of non-compact myelin membrane, which collectively act to stabilise the extremities of the sheath. The principal mediator of these interactions, as well as in other non-compact myelin regions, for example the outer-mesaxon and SLIs (discussed later), is E-cadherin (Fannon *et al.*, 1995; Hasegawa *et al.*, 1996). E-cadherin is a classical cadherin, whose homophilic *trans*-ligation mediates greater adhesive strength than equivalent N-cadherin and thus mediates long-term stable interactions in tissues (Gumbiner, 2005). Consistent with this, E-cadherin, which is best characterised for generating tissue sheets in epithelial cells, predominates over N-cadherin expression in adult myelinating Schwann cells, while N-cadherin is down-regulated during differentiation concomitant with the generation of an increasingly stable nerve architecture during development (Crawford *et al.*, 2008). Importantly, E-cadherin function in myelinated Schwann cells appears to be dependent on the interaction between E-cadherin and p120-catenin (discussed in detail later). Cadherin-switching is a recurring theme in Schwann cell development, and occurs during neural crest delamination and following Schwann cell/axonal association, where Schwann cells and their progenitors need to modulate the adhesive strength of their interactions in order to generate tissues. Importantly, cadherin switching also occurs following nerve injury concomitant with Schwann cell dedifferentiation (Zelano *et al.*, 2006), where N-cadherin mediates transient interactions, which are important for repair.

The Juxtaparanode

The juxtaparanode is the most distal of the associated domains of the Node of Ranvier and interfaces with the internode. This domain is characterised by the enrichment of *shaker*-like (delayed-rectifier) potassium ion channels (Kv1.1 & Kv1.2) on the axolemma (Poliak & Peles, 2003) (**Figure 1.23**).

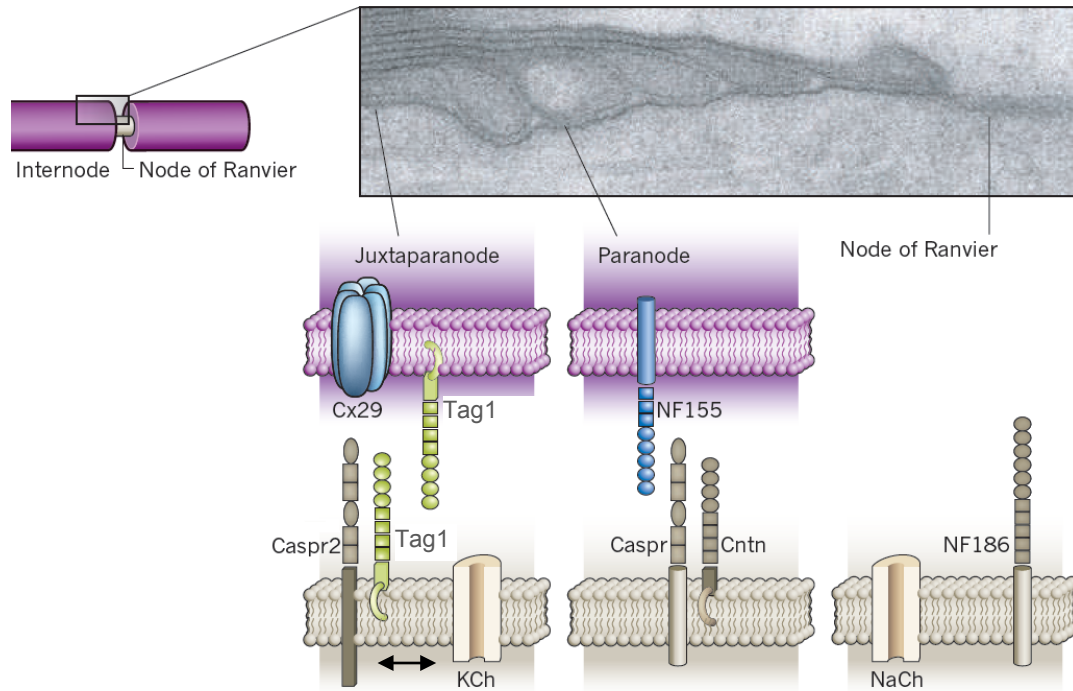


Figure 1.23 The cell adhesion molecules of the Node of Ranvier and associated domains of myelinated fibres. The juxtaparanode is stabilised by homotypic Tag1 - Tag1 interactions assisted by axonal Caspr2. The paranode is stabilised by the interaction between glial neurofascin (NF)-155 and axonal Caspr/contactin heterodimer, while the Node of Ranvier is stabilised by interactions between gliomedin and axonal NF-186, which clusters axonal sodium ion channels (adapted from Nave 2010).

Importantly (as previously discussed), the PNJ acts to prevent potassium ion channels from laterally diffusing into the Node of Ranvier and thus, mixing with sodium ion channels (Schafer & Rasband, 2006). The exact function of potassium ion channels in this compartment is still unclear; however, they are thought to be required for stabilising the internode resting potential (Poliak & Peles, 2003). A major CAM of the juxtaparanode is Tag-1/contactin-2, which is specifically expressed in this compartment by both myelinating Schwann cells and the axon (Traka *et al.*, 2002). Tag-1 is a member of the IgCAM superfamily and is a GPI membrane-tethered protein, although it can be expressed in a secreted form (Traka *et al.*, 2002). Tag-1 binds homophillically in *trans* to mediate Schwann cell/axonal interaction and has been shown to recruit Caspr2, which is a member of the neurexin superfamily (Poliak *et al.*, 1999; Poliak *et al.*, 2003). Interestingly, Caspr2 is found colocalised with potassium ion channels (Kv1.1), in which a direct interaction has

been shown; thus, a Tag-1-Caspr2-Potassium ion channel complex provides a plausible mechanism for Schwann cell-directed potassium ion channel clustering at the juxtaparanode (Poliak *et al.*, 2003). Furthermore, Tag-1 deficient mice have indistinct juxtaparanodal regions, with mis-localised Caspr2 and potassium ion channels (Traka *et al.*, 2002).

Non-compact myelin extra to the Node of Ranvier

In addition to aforementioned non-compact myelin regions surrounding the Node of Ranvier, the myelinated Schwann cell and, indirectly, the underlying axon, is 'serviced' by an elaborate system of interconnected cytoplasmic channels, which form non-compact myelin conduits through otherwise intractable regions of compact myelin (Nave, 2010b; Sherman & Brophy, 2005). The importance of these aqueous corridors have only come to light in the last twenty years or so, and are reinforcing the notion that Schwann cells and axons are not only physically integrated but are also metabolically coupled (Nave, 2010a). For instance, the ensheathed glia are thought to provide regions of the axon far from the neuronal cell body (in some cases greater than 1m), with metabolites and trophic support (Nave, 2010a). The two main types of cytoplasmic channel that exist in myelinated Schwann cells, are Cajal bands and SLIs, which permit the flow of metabolites in a longitudinal and radial direction respectively.

Schmidt-Lanterman Incisures (SLIs)

SLIs are aqueous channels of non-compact myelin that penetrate radially through successive sheets of enwrapped Schwann cell plasma-membrane to connect regions of non-compact myelin in the outer-collar (containing the nucleus) with regions of non-compact myelin of the inner-collar (interfacing the periaxonal space) (Denisenko *et al.*, 2008; Nave, 2010b) (see **Figure 1.17**). Thus, SLI channels permit the translocation of metabolites between the inner and outer layers of the Schwann cell sheath, which is necessary for myelin maintenance, and between the Schwann cell and the axon via diffusion over the adaxonal membrane. In terms of the latter, the SLI channels effectively reduce the distance for metabolites to translocate, from the nucleus to the axon, by approximately 1000-fold (Nave, 2010a).

The formation and structural stability of SLI channels is dependent on the assembly of a number of interconnecting gap-junctions, predominantly composed of connexin-32 (Cx32) and stabilised with E-cadherin/p120-catenin (Perrin-Tricaud *et al.*, 2007). Cx32 is a tetraspan transmembrane protein, which also forms channels between paranodal loops (Suter & Scherer, 2003). The SLI channel spans between two layers of myelin sheath in order to form a funnel-shaped aqueous-filled lumen, which is continuous with the cytoplasm on either side. They are composed of six connexin molecules, which interact to form a connexon, where two connexons interact in *trans* to form the SLI channel (Suter & Scherer, 2003). While Cx32 is the predominant connexin responsible for generating SLIs, diffusion experiments using aqueous dyes have shown that functional SLI channels are still present in the Cx32 null mouse (Gjb1^{-/-}) (Balice-Gordon *et al.*, 1998). One explanation for this, is that the connexin family is numerous, with at least twenty mammalian members, which are highly homologous; thus, functional redundancy between this group is likely to compensate for loss of Cx32 in the formation of SLIs in these mice (Suter & Scherer, 2003). Interestingly, loss of Cx32 appears only to be tolerated during development and not during later maintenance of the sheath (Martini & Schachner, 1997).

In addition to connexins, the assembly of SLI channels is also dependent on E-cadherin and, critically, the interaction between E-cadherin and its intracellular modulator p120-catenin; for instance, Perrin-Tricaud *et al.* (2007) used mutant E-cadherin proteins that lacked p120-catenin binding-sites, and found that SLI channel formation was ablated by the failure of this interaction *in vivo*. It is not fully understood how p120-catenin functions in this regard, although Davis *et al.* (2003) show that this interaction is important in the regulation of E-cadherin turnover. The study by Perrin-Tricaud *et al.* (2007), also found that the thickness of the myelin sheath was reduced following E-cadherin-p120-catenin disruption. This finding appears contradictory to an earlier study by Young *et al.* (2002), who questioned the essential importance of E-cadherin in myelinated nerve. The authors used an E-cadherin knockout mouse and found that E-cadherin ablation had no effect on myelination in terms of the generation, integrity and function of the myelinated nerve nor did it affect the post-injury regeneration and function recovery of re-myelinated nerve. However, they did find some disruption to nerve architecture shown by a measurable loss of compaction in the perinodal outer mesaxon.

Cajal bands

Cajal bands run in parallel with the axon (longitudinally), along the outer-collar of the myelin sheath (see **Figure 1.24**). They were first described by Cajal in 1933 as ‘longitudinal bands embedded in a meshwork of protoplasmic trabeculae’. Cajal postulated that these channels were likely to be important for the ‘nutritional requirements’ of the Schwann cell by allowing Schwann cells to elongate to cover relatively large distances between neighbouring myelinating Schwann cells on the axon (cited in Sherman & Brophy, 2005). Since then, there has been much interest in elucidating the structure and function of Cajal bands.

The formation of Cajal bands is dependent on the non-compact myelin protein periaxin (Pxn), which is expressed in Schwann cells as two isoforms, L-periaxin and S-periaxin, generated as alternative splice variants from the Pxn gene. While both isoforms share a PDZ domain for generic protein interactions, L-periaxin contains additional non-PDZ domains in the form of a basic domain and an acidic domain (Kursula, 2008) and is the active isoform required for Cajal band formation. The channel is formed following the assembly of a heterotrimeric complex composed of L-periaxin, Dystrophin-related protein 2 (DRP2) and the transmembrane laminin receptor Dystroglycan, which is localised to the abaxonal (outer) membrane of the myelinated Schwann cell (Sherman & Brophy, 2005) (see **Figure 1.24**). The heterotrimeric complex mediates interactions with the Schwann cell basal lamina and ECM, for example laminin, which is important for Cajal band formation (Sherman *et al.*, 2001).

A study by Court *et al.* (2004) using a Pxn^{-/-} mouse has demonstrated the importance of Pxn in the formation of Cajal bands, which were absent from these mice. In addition, myelinating Schwann cells from Pxn^{-/-} mice were longitudinally truncated relative to controls and displayed a greater frequency of Nodes (Court *et al.*, 2004). Intriguingly, these findings support Cajal’s original assertion that the channels were required as a means to transport nutrients to the growing extremities of the cell

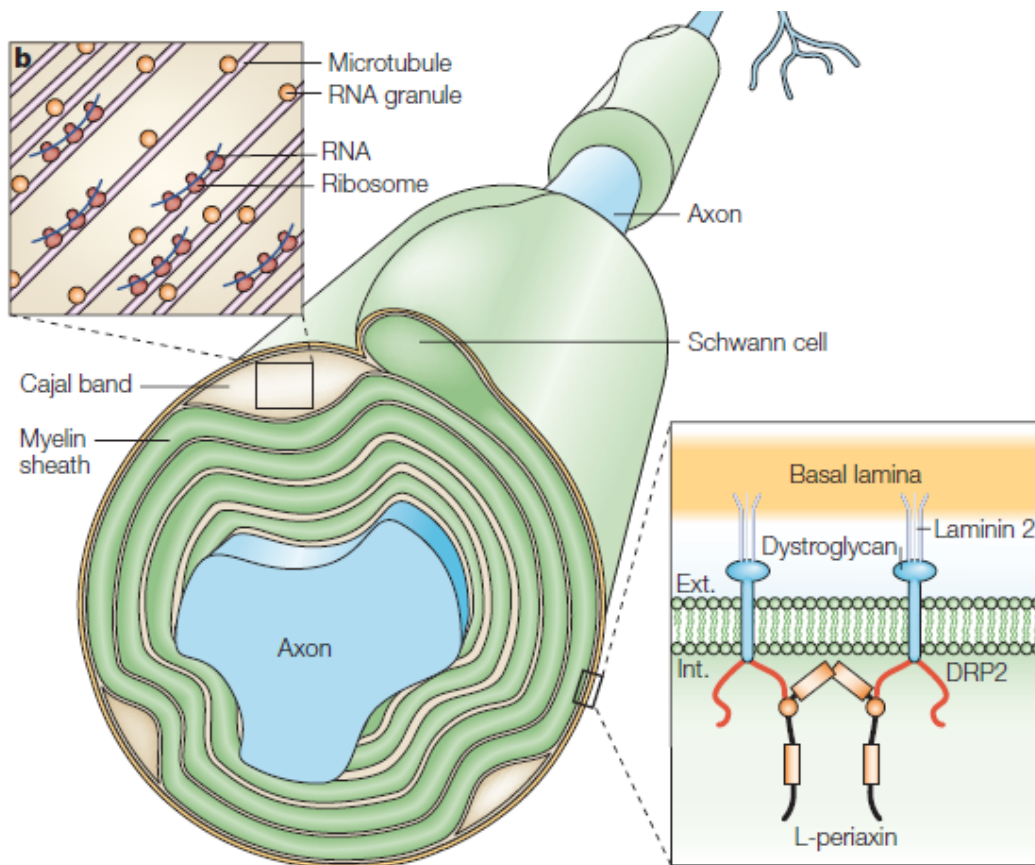


Figure 1.24 Schematic depicting the Cajal bands in myelinated fibre. The Cajal bands are cytoplasmic corridors of non-compact myelin, which extend longitudinally along the outer-collar of the Schwann cell to connect the outer-flanks with the cell nucleus. Cajal bands are dependent on the assembly of the L-periaxin-Dystrophin-related protein 2 (DPR2)-dystrophinglycan complex. Cajal bands are important for transporting mRNA, e.g. myelin basic protein (MBP), from the nucleus to the outer-flanks of the Schwann cell for localised translation (adapted from Sherman & Brophy, 2005).

(Sherman & Brophy, 2005). However, Pxn does not appear to be required for myelination as Schwann cells from $Pxn^{-/-}$ mice still enwrap axons and myelinate normally with g-ratios indistinguishable from controls (Gillespie *et al.*, 2000); although, the efficiency of conduction and the NCV are likely to be affected by the reduction in internode length. These findings show how myelin sheath thickness and longitudinal hypertrophy are regulated by distinct mechanisms and do not appear to be coupled. For instance, myelin sheath thickness is determined by trophic factors expressed by the axon, e.g. NRG1 Type III (as previously discussed), while the

supply of nutrients to the growing edge of the Schwann cell (via Cajal bands), appears to be limiting in terms of longitudinal hypertrophy (Sherman & Brophy, 2005). However, in terms of the latter, it is still unclear how longitudinal hypertrophy is regulated and whether, for instance Node formation is involved in the cessation of growth.

In addition to their role in transporting metabolites and proteins, Cajal bands have also been implicated in the translocation of mRNA transcripts encoding myelin genes from the nucleus to the outer-flanks of the Schwann cell (Court *et al.*, 2004). This remarkable discovery in 1982 (unprecedented at the time), showed that MBP was being synthesised at the growing edge of the Schwann cell from mRNA that had been transported from the nucleus (Sherman & Brophy, 2005). In support of this, Court *et al.* (2004) showed in *Pxn^{-/-}* mice, in which Schwann cells are devoid of Cajal bands, that anterograde microtubule transport was disrupted in these cells and moreover, MBP mRNA and MBP protein were absent from the leading (growing) edge of the Schwann cell.

Table 1.1 Adhesion molecules relevant to this thesis

Molecule	Symbol	Function/proposed function
Contactin	Cntn	A Component of the paranodal junction. Binds heterotypically to glial NF-155 and <i>in cis</i> with Caspr.
Contactin associated protein	Caspr	A Component of the paranodal junction. Stabilises interactions between Contactin and NF-155.
Contactin associated protein-2	Caspr-2	A Component of the juxtapanode. Stabilises Tag1-Tag1 interactions.
Contactin-2	Tag1	B Component of the juxtapanode. Tag1 binds homotypically to mediate axo/glial adhesion and is stabilised by axonal Caspr-2.
Dystroglycan	Dag-1	S Expressed in the outer-collar of the Schwann cell, where it binds extracellularly to laminins in the ECM and intracellularly to periaxin via dystrophin-related protein-2. Required for Cajal band formation.
Epithelial cadherin	E-cad	S Component of non-compact myelin. Required with p120-catenin to form autotypic junctions between sheets of Schwann cell lamella at the paranodal loop.
Gliomedin	Gliomedin	S Expressed in the region of the Schwann cell microvilli. Interacts with NF-186 and nrCAM - it is important for positioning the prospective Node of Ranvier.

L1-cell adhesion molecule	L1-CAM	B Implicated in Schwann cell/axonal interactions; thought to be required for structural stability of non-myelinated fibres.
Myelin protein zero	MPZ/P0	S Facilitates compaction of myelin. MPZ exists as a tetramer; binding homotypically with MPZ on juxtaposed membrane. It also facilitates intracellular compaction and is the most abundant myelin protein.
Myelin-associated glycoprotein	MAG	S Expressed on the adaxonal membrane. MAG has been implicated in Schwann cell/axonal interactions and has also been implicated in the stabilisation of axonal actin filaments.
Nectin-like protein-1	Necl-1	A Binds to Necl-4 to stabilise Schwann cell/axonal interactions at myelination. Required for myelination.
Nectin-like protein-4	Necl-4	S Binds Necl-1 to stabilise Schwann cell/axonal interactions at myelination. Required for myelination.
Neural Cadherin	N-cad	B Implicated in Schwann cell/axonal interactions.
Neural cell adhesion molecule	NCAM	B Facilitates homotypic L1-CAM binding. May functionally compensate for L1-CAM loss.
Neurofascin-155	NF-155	S Component of the paranodal junction; forms an adhesive bond with contactin.
Neurofascin-186	NF-186	A Expressed at the Node of Ranvier. Interacts <i>in trans</i> with gliomedin and <i>in cis</i> with sodium ion channels.
Neuronal cell adhesion molecule	nrCAM	A Expressed at the Node of Ranvier. Interacts with gliomedin and binds <i>in cis</i> with sodium ion channels.
Semaphorin-4F	Sema4F	S Schwann cell/axonal interactions; implicated in Ras/Raf/ERK mediated Schwann cell dissociation.

A, expressed by axons; S, expressed by Schwann cells; B, expressed by Schwann cells and axons.

1.5 Nerve injury and pathology

1.5.1 Injury

In contrast to the CNS, peripheral nerves are capable of remarkable regeneration following injury. The processes involved are complex and multifaceted. They require an extraordinary degree of tissue engineering, orchestrated predominantly by Schwann cells, but also involve a myriad of other cell-types, and are critically dependent on an environment permissive for regeneration (Chen *et al.*, 2007; McDonald *et al.*, 2006; Stoll *et al.*, 2002; Webber & Zochodne, 2010). The absence of Schwann cells or an equivalent in the CNS is often cited as being one of the most significant obstacles to CNS regeneration (Filbin, 2003). Pioneering experiments demonstrated essential differences in regenerative capacity between the two tissues. For instance, when an excised section of CNS tissue was juxtaposed to the proximal

stump of a peripheral nerve lesion, normal axonal outgrowth from the PNS tissue was inhibited by the microenvironment of the CNS tissue (Waller, cited by Stoll *et al.*, 2002). However, when transected CNS neuronal processes were juxtaposed with a section of peripheral nerve, the opposite was observed, i.e. CNS processes regenerated into PNS tissue (Benfey & Aguayo, 1982). It is now thought that myelin components, especially MAG, are the principle inhibitive factor for nerve regeneration (Chen *et al.*, 2007; Filbin, 2003).

Wallerian degeneration

The series of the events that takes place following axonal damage were first observed by Waller (1850) in the nerves of frogs where the ensuing processes of axonal degeneration, Schwann cell dedifferentiation, dissociation and proliferation as well as immune cell invasion, all of which are required for later regeneration of the nerve, have subsequently been called Wallerian degeneration (WD) (Dyck & Hopkins, 1972; Stoll *et al.*, 2002). Importantly, WD is a regulated set of processes that occur distal to the site of axonal injury and which ultimately provides the correct environment for later regeneration. Furthermore, WD is exclusive to peripheral nerve and is centrally reliant on the reversibility of the Schwann cell differentiated state, in which differentiated Schwann cells are instructed to dedifferentiate and reform a proliferative pool of Schwann cell progenitor-like cells. These Schwann cells, often referred to as ‘injury’ or ‘denervated’ Schwann cells (to distinguish these cells from their developmental progenitors), rapidly engage in the clearance of myelin debris (myeloids), promote the invasion of immune cells through the BNB (discussed in section 1.3.1) and later provide structural and trophic support for the re-growth of axons (Webber & Zochodne, 2010). In cut nerve, newly emerging axons leave the proximal nerve stump and are guided across the injury site (nerve bridge) by Schwann cells, which migrate in a coordinated wave of migration across the nerve bridge (Parrinello *et al.*, 2010). Dedifferentiated, dissociated Schwann cells in the distal (degenerated) portion of the nerve also play a central role. They are found aligned with the basal lamina to generate tracts, known as Bands of Bunge, which guide re-growing axons back to their target tissues (McDonald *et al.* 2006). Following axonal regeneration, Schwann cells re-associate with axons and re-differentiate to mature myelinating Schwann cells to complete the regeneration of the

functional nerve (Chen *et al.*, 2007; McDonald *et al.*, 2006; Stoll *et al.*, 2002; Webber & Zochodne, 2010) (see **Figure 1.25**).

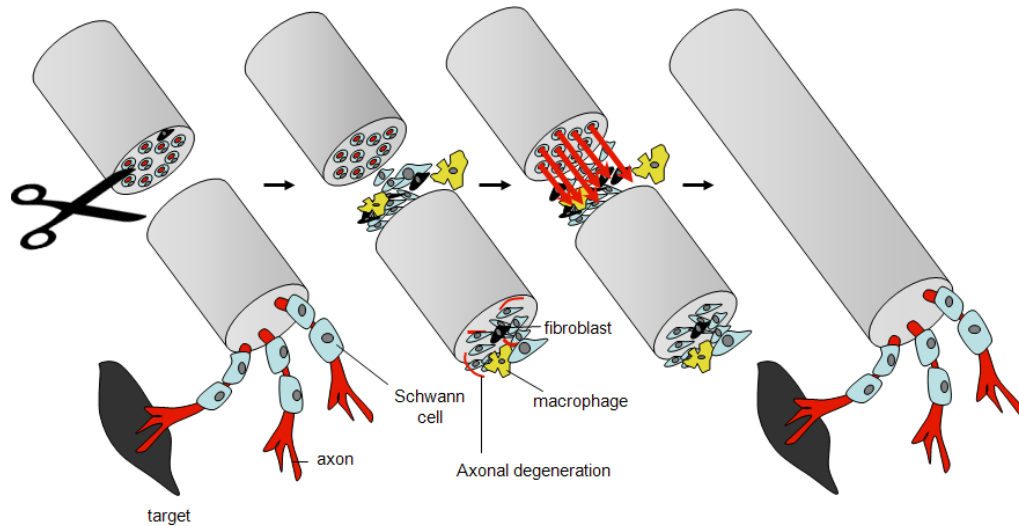


Figure 1.25 Schematic illustration of the events following nerve transection. Wallerian degeneration occurs distal to the site of injury, whereby the axon undergoes controlled disintegration concomitant with Schwann cell dedifferentiation, proliferation and myelin debris clearance. Denervated Schwann cells attract inflammatory cells, e.g. macrophages to the distal stump. This process creates a permissive environment for axonal re-growth into distal tissue for re-innervation. The repair process is completed following Schwann cell/axonal reassociation and recommencement of the myelination programme.

The axonal response

The events of WD are triggered by axonal damage; however, the exact ‘damage signal’ from the distal section of the injured axon to the surrounding Schwann cells remains to be determined (Chen *et al.*, 2007; Hall, 2005). The controlled process of axonal degeneration begins rapidly in the section of the axon that is distal to the site of injury, with the cytoskeletal disintegration of small and large calibre axons usually completed within 24-hours and 48-hours respectively (Stoll *et al.*, 2002). The emergence of the ‘Wallerian degeneration slow’ (Wld^s) mouse model, in which axonal disintegration is delayed by up to three weeks following nerve crush, has provided valuable insights into the mechanism of WD (Hall, 2005; Lunn *et al.*, 1989). This work confirmed that axonal disintegration after injury was not a passive

decay of the severed axon, i.e. occurring through lack of metabolites and contact with the nucleus, but rather, axonal disintegration during WD was an active, regulated process. Recent work to elucidate the mechanism for WD has focused on characterising the *Wld^s* mutant protein responsible for delaying the normal process of axonal degradation. The *Wld^s* protein has been identified as a mutant chimeric protein composed of full-length nicotinamide mononucleotide adenylyl transferase 1 (*Nmnat-1*) fused with 18 amino acids derived during the fusion event (termed W18) and the first 70 amino acid residues of Ubiquitination factor e4b (*Ube4b*) (termed N70) (Avery *et al.*, 2009; Mack *et al.*, 2001). It was initially thought that the active component of the *Ube4b/Nmnat* chimeric responsible for the delayed response was *Nmnat-1*, as this protein appeared to be sufficient alone to suppress axonal degradation *in vitro* (Araki *et al.*, 2004). However, it has since been reported that both components are probably required to protect the axons of *Wld^s* mice from disintegration during WD (Coleman & Freeman, 2010).

The Schwann cell response

Upon nerve injury, Schwann cells initiate a programme of dedifferentiation that results in the ‘shedding’ of the myelin sheath and the dissociation of Schwann cells from axons. The first detectable cellular response following injury in myelinating Schwann cells, is the activation of the ErbB2/B3 receptor, which occurs at the Node of Ranvier within 10 minutes following injury (Guertin *et al.*, 2005). This is followed by robust and sustained ERK1/2 activation (Harrisingh *et al.*, 2004), which precedes the down-regulation of *Krox20* and up-regulation of *c-Jun* and *Sox2*, and is followed, within 48-hours, by the down-regulation of myelin specific genes including *MPZ*, *MBP*, *Pxn* and *PMP-22* (Chandross *et al.*, 1996; Gupta *et al.*, 1988; Kuhn *et al.*, 1993) and the up-regulation of ISC-surface expressed markers, *L1-CAM*, *p75^{NTR}* and *GFAP* (Hall, 2005; Jessen & Mirsky, 2008b), as well as *N-cadherin*, *NCAM*, *Necl-1* and *Necl-3* (Shibuya *et al.*, 1995; Thornton *et al.*, 2005; Zelano *et al.*, 2006). In addition, dedifferentiated Schwann cells up-regulate *cyclin-D1* and re-enter the cell cycle (Jessen & Mirsky, 2008b). As previously discussed, the nature and/or identity of the axonal damage signal is unknown (Lunn *et al.*, 1989). Proliferating denervated Schwann cells become phagocytic and, in addition

to resident and infiltrating immune cells, for example macrophages and neutrophils, are highly active in clearing myelin debris from the site of injury and distal regions.

The repaired nerve

Nerve regeneration is remarkably effective, for instance we have shown that in rodent sciatic nerve, the majority of transected nerves had spontaneously re-established connections with distal targets by 48-hours following transection (Parrinello *et al.*, 2010). Nevertheless, clinical outcomes do vary according to the type of the injury, for example nerve transection is more severe than crush injuries, and between species, for example PNS regeneration in rodents is superior to that in humans. In addition, although functionality often returns following nerve regeneration, the structure of the repaired nerve can differ, which is most often evident by the presence of so-called mini-fascicles. Another difference is an increase in the frequency of the Nodes of Ranvier and decrease in internode length along myelinated fibres distal to the site of injury. This is because Schwann cells re-enter the cell-cycle following dissociation from axons and thus, during later re-association, the number of Schwann cells is greater than before (Poliak & Peles, 2003). These differences in nerve architecture underline the fact that the processes involved in PNS regeneration, which involve *de novo* post-developmental tissue reformation, are distinctly different from the equivalent development stages (Parrinello *et al.*, 2010).

1.5.2 Demyelinating neuropathies

In the previous section, I discussed the reversible nature of the Schwann cell differentiation programme. However, a number of disorders result in a more permanent impairment of Schwann cell/axonal interactions and/or myelin composition, structure and function. In this section, I briefly outline the various types of human PNS neuropathy and show that underpinning all these disorders is a common breakdown in Schwann cell/axonal communications (Juarez & Palau, 2012). Heritable mutations occur in genes of all major components of the myelination programme, from structural components to transcription factors, and together account for the majority of inherited neurological diseases (Suter & Scherer,

2003), accounting for dysregulation in some 40 genes (Juarez & Palau, 2012). The inherited neuropathies predominantly affect myelinated nerves of the PNS and were extensively studied and characterised by the 19th century pioneers in the field; Charcot, Marie, Tooth and Herringham. Thus, these disorders are often collectively known as Charcot-Marie-Tooth (CMT) diseases, but may also be known as hereditary motor and sensory neuropathies (HMSN) (Suter & Scherer, 2003).

CMT Type-1 disorders are the most common form of neuropathy and are caused by autosomal or X-linked dominant mutations. Additional clinical symptoms include swellings in trunk nerves that resemble 'onion bulbs', which are caused by multiple cycles of Schwann cell de-myelination and re-myelination. They often manifest at an early age and result in axonal length-dependent muscle weakness (Suter & Scherer, 2003). CMT Type-1 is subdivided according to the genes affected. These include mutations or duplications in PMP22 (CMT1A), MPZ (CMT1B) in which 80 mutations have been identified, Cx32 (GjB1) (CMTX or X-Linked CMT), in which 240 mutations have been identified (Nave, 2010b; Nave & Salzer, 2006; Suter & Scherer, 2003). By far the largest contribution of all PNS neuropathies occurs following duplication of the PMP22 allele (Suter & Scherer, 2003). Interestingly, this disorder highlights the importance of maintaining the correct stoichiometric ratios of myelin genes, for instance the ratios between PMP22 and MPZ are finely balanced; thus, duplication of PMP22 significantly destabilises the myelin sheath resulting in the de-myelinating phenotype.

The other types of CMT are less common and include Type-2 disorders, caused by dominant autosomal inheritance of mutations in axonal genes, which cause axonal degeneration followed by de-myelination - usually by the second decade of life. CMT Type-3 disorders, which are severe de-myelinating disorders inherited in a dominant or recessive manner and fall into two main groups referred to as Congenital Hypomyelinating Neuropathy (CHN) and Dejerine-Sottas (DSS), where the latter manifests in later infancy. And CMT Type-4 disorders, which encompass a number of rare autosomal recessive neuropathies (Suter & Scherer, 2003).

The de-myelinating neuropathies rarely manifest total loss of myelin but rather, they exhibit varying degrees of de-myelination or Schwann cell dysfunction, all of which

impact negatively on the efficiency of the nerve to carry impulses. However, this inefficiency does not appear to generate significant clinical symptoms; moreover, the most debilitating aspects of these disorders, result from axonal degeneration, often affecting the longest axons first, which causes progressive length-dependent muscle weakness (Nave, 2010b; Suter & Scherer, 2003). This further underlines the importance of tight, stable Schwann cell/axonal interactions for the viability of axons.

1.5.3 Neurofibromatosis type I

Neurofibromatosis type 1 (NF1) is an autosomal-dominant disorder, with an incidence of 1 in 3500 live births, which predominantly effects neural crest-derived tissues (Brannan *et al.*, 1994; Parrinello & Lloyd, 2009). NF1 is 100% penetrant, i.e. affected individuals are always symptomatic, although the disorder is complex and the age of onset and symptoms varies from patient to patient (Carroll & Ratner, 2008; Riccardi & Lewis, 1988). NF1 patients manifestations a range of symptoms including pigmentation disorders of the skin (*café-au-lait* macules and freckling) and the eye (Lisch nodules), but it is most characterised by the life-long propensity of these patients to develop sporadic benign tumours called neurofibromas (Bader, 1986; Evans *et al.*, 2002). Neurofibromas are heterogeneous tumours composed of dissociated Schwann cells, neural processes, perineural cells, fibroblasts and infiltrating mast cells all encased within an enlarged collagenous matrix (Corfas *et al.*, 2004; Zhu & Parada, 2002) (**Figure 1.26**).

Neurofibromas occur as two main types, defined according to their location and the types of nerves affected, which are either dermal neurofibromas (DNFs) or plexiform neurofibromas (PNFs). DNFs, which are the most common form, are superficial cutaneous or subcutaneous tumours with defined edges that derive from small dermal peripheral nerves and normally manifest during adolescence. Although they can cause significant disfigurement, these tumours are benign and typically, do not progress to malignancy (Zhu & Parada, 2002). In contrast, PNFs reside deep within tissues, forming irregularly defined tumours that derive from spinal and cranial nerve trunks. Although benign, PNFs are World Health Organisation (WHO) grade-1 tumours with a 5-10% lifetime risk of progression to malignant peripheral nerve

sheath tumours (MPNST), which are WHO grade-4 highly-malignant tumours with very poor clinical outcomes (Evans *et al.*, 2002; Reilly, 2009; Zhu & Parada, 2002).

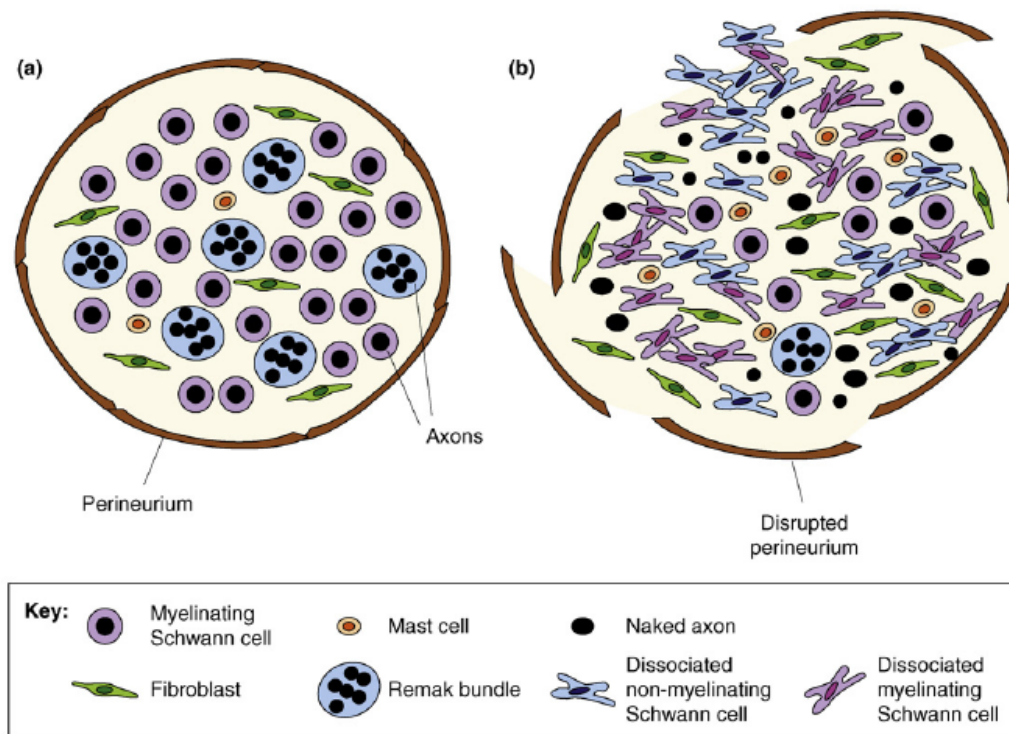


Figure 1.26 Schematic showing a cross-section through a normal nerve fascicle compared to a nerve fascicle in the early stages of neurofibroma formation. (A) The normal fascicle, in which Schwann cells are tightly associated with axons. (B) The neurofibroma fascicle, as found in NF1 patients, in which Schwann cells have dissociated from axons and proliferated along with fibroblasts. The perineurium is also disrupted, which permits immune cells to invade the epineurium and enhance the hyper-proliferative state of cells in the milieu (Parrinello & Lloyd, 2009).

Neurofibomin function and Ras signalling

For some time the cell of origin responsible for generating neurofibromas was unknown, which was largely due to the heterogeneity and complexity of neurofibromas and the Neurofibromatosis type 1 disorder as a whole (Riccardi & Lewis, 1988). However, it is now well-established that the neoplastic cell-of-origin of neurofibroma is the Schwann cell (Zhu *et al.*, 2002), while the lesion responsible occurs in the NF1 gene, which encodes the neurofibromin tumour suppressor protein.

Individuals with NF1 syndrome are NF1 heterozygotes, where neurofibromas are initiated in Schwann cells that have undergone loss of heterozygosity (LOH) in their remaining second NF1 allele. Importantly, the correct microenvironment appears to be important, for instance tumours do not tend to form when NF1 is specifically ablated in Schwann cells and the surrounded tissue is NF1^{+/+}; however, they are able to arise from NF1^{+/-}-tissue environments (Yang *et al.*, 2008).

Neurofibromin encodes a GTPase activating protein (GAP) domain, which acts to negatively regulate Ras-signalling by favouring the hydrolysis of active Ras-GTP to inactive Ras-GDP (Ballester *et al.*, 1990). Ras is a small GTPase, localised to the inner-face of the plasma-membrane, which functions as a molecular binary switch and is important for many cellular processes and additionally, is implicated in a number of cancer aetiologies. The best characterised route for Ras-activation is via RTK receptor activation following ligand-binding of extracellular growth-factors (Ogata *et al.*, 2004). Growth-factor binding to RTK receptors results in RTK dimerisation and autophosphorylation, which activates the receptor. Cytoplasmic adaptor molecules, for example Src Homology-2 (SHC) and growth factor receptor-bound protein-2 (GRB2), bind to active RTKs and further recruit guanine nucleotide exchange factors (GEFs), for example Son of Sevenless (SOS), which, in contrast to GAPs, act to promote the conversion of inactive Ras-GDP to active Ras-GTP. Activated Ras-GTP lies at the apex of a number of intracellular signalling cascades including the MAPK pathway comprising of Raf, MEK and ERK1/2, the PI3K pathway (PI3K and AKT1), which is important for cell growth and the Cdc42-RAC-RHO pathway, which is important for cytoskeletal mobilisation (Zhu & Parada, 2002) (See **Figure 1.27**).

NF1: Ras activation and tumour formation

Dysregulation of Ras signaling has been implicated in a number of different cancers including neurofibromas in patients with Neurofibromatosis type 1 (Harrisingh & Lloyd, 2004). We previously showed that oncogenic Ras signaling, that occurs following loss of neurofibromin function, acts through the Raf/MEK/ERK pathway to drive Schwann cell dedifferentiation (Harrisingh *et al.*, 2004). However, an important early stage in the aetiology of neurofibroma formation is the irreversible

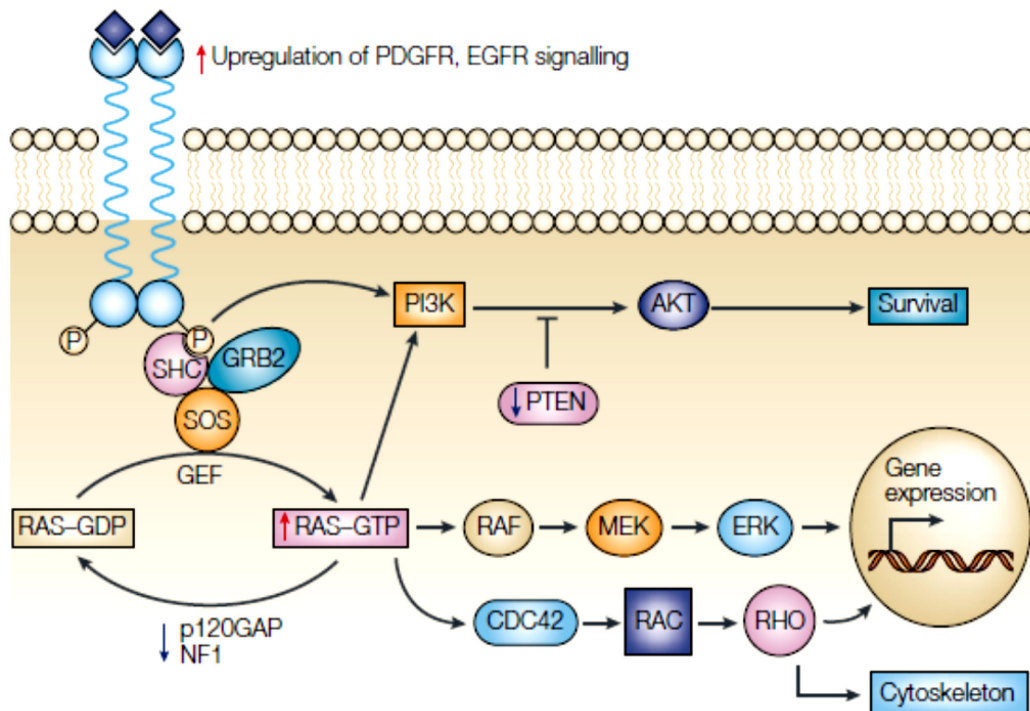


Figure 1.27 Receptor tyrosine kinase (RTK) activation of Ras and its downstream affects. Activation of RTKs, for example platelet-derived growth factor receptor (PDGF-R) and epidermal growth factor receptor (EGF-R), leads to RTK dimerisation and autophosphorylation, which in turn permits SHC and GBR2 to bind the cytoplasmic domain of the activated RTK. These adaptors recruit the guanine nucleotide exchange factor (GEF) son of sevenless (SOS), which activates Ras by favouring the conversion of Ras-GDP to Ras-GTP. Neurofibromin (NF1) is a GTPase activating protein (GAP) that inactivates Ras by hydrolysing Ras-GTP to Ras-GDP. Ras activates a number of downstream signalling cascades including the Raf/Mek/Erk (mitogen activated protein kinase, MAPK) pathway, implicated in Schwann cell dedifferentiation as well as the phosphatidylinositol 3-kinase (PI3K) pathway, implicated in growth and survival, and the Cdc42-Rac-Rho pathway, known to regulate the cytoskeleton as well as gene expression (Zhu & Parada, 2002).

dissociation of Schwann cells from axons, which must be effected via alterations in Schwann cell/axonal adhesion (Joseph *et al.*, 2008; Wu *et al.*, 2008; Zheng *et al.*, 2008). Indeed, we later identified the Schwann cell expressed axonal guidance molecule, semaphorin-4F (Sema4F), which is downregulated by oncogenic Ras/Raf/ERK signalling, as the Schwann cell/axonal mediator responsible for maintaing stable interactions (Parrinello *et al.*, 2008) (**Figure 1.28**).

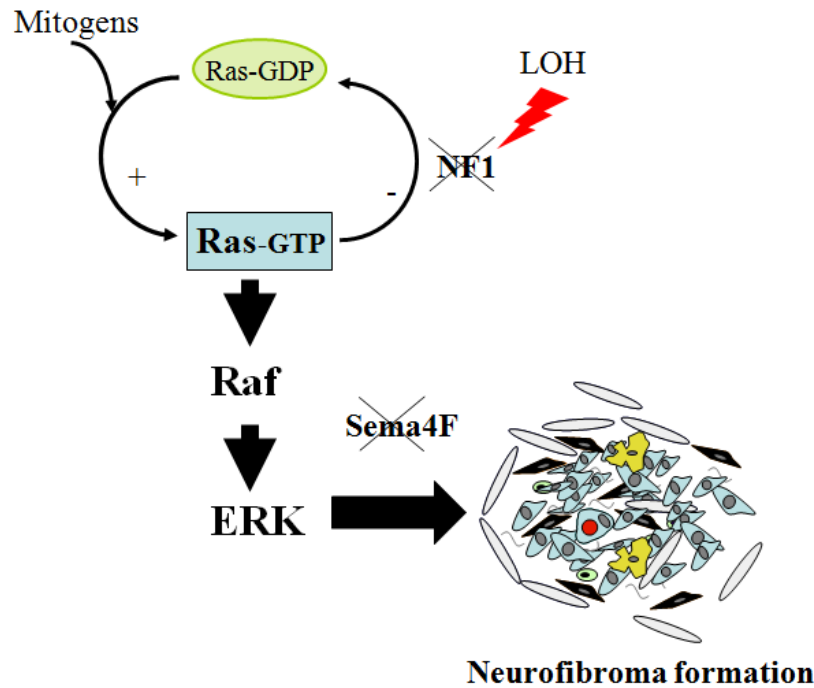


Figure 1.28 Ras function and dysregulation in Neurofibromatosis type I (NF1). Ras is a small GTPase that acts as a molecular switch between an inactive (Ras-GDP) and active (Ras-GTP) state. Ras signalling is inactivated by GTPase activating proteins (GAPs), for example neurofibromin (NF1), which favour the conversion of Ras-GTP to inactive Ras-GDP, and is activated by guanine nucleotide exchange factors (GEFs), for example son of sevenless (SOS), which favour the conversion of Ras-GDP to active Ras-GTP. Loss of NF1 in the presence of mitogens, results in oncogenic hyper-activation of the Ras/Raf/ERK pathway, which leads to the down-regulation of Semaphorin-4F (Sema4F) and subsequent loss of Schwann cell/axonal interactions, i.e. the first stages in the generation of neurofibromas.

1.5.4 Neurofibromatosis type II

Neurofibromatosis type II (NF2) is an autosomal dominant disorder with an incidence of 1:33,000-40,000 live births (Baser *et al.*, 2002). The disease clinically manifests as sporadic schwannomas, which are homogeneous tumours, composed exclusively of Schwann cells, which bulge out from the nerve sheath. These slow-growing, benign tumours are generated following an inactivating mutation in the NF2 gene, in which affected individuals are already heterozygous for NF2, resulting in the functional loss of the tumour suppressor Merlin/schwannomin (the NF2 gene

product) in affected Schwann cells. Schwannomas are thus, large clonal expansions of Schwann cells that are all NF2^{-/-} and are derived from the same founding neoplastic Schwann cell. Various mouse models have been developed in an attempt to understand the aetiology of NF2, including the NF2 null homozygous mouse (NF2^{-/-}), which was found to be embryonic lethal and the heterozygous mouse (NF2^{+/-}), which failed to develop Schwannomas, although surprisingly, these mice did develop osteosarcoma and fibrosarcoma (Ramesh, 2004). Interestingly, conditional loss of NF2 in Schwann cells (NF2^{-/-}) does cause hyperplasia and generates Schwannomas in cranial nerves, suggesting that the loss of the second allele is the limiting event in mouse models (Giovannini *et al.*, 2000).

Merlin, is highly related to the ERM (Ezrin-radixin-moesin) family of proteins which share a Four-point-one (F)-ERM domain known to mediate membrane-cytoskeletal interactions (Ramesh, 2004). Consistent with other ERM proteins, Merlin activity is critically dependent on its membrane localisation (Curto & McClatchey, 2008), where it has been implicated, both physically and functionally, in the regulation of contact-dependent inhibition of proliferation (CIP) and as a suppressor of mitogenic signals (Curto & McClatchey, 2008). However, the downstream action of Merlin is complex and multi-faceted. For instance, Merlin-dependent CIP is thought to be directed by a number of pathways including negative regulation of the Ras and Rac GTPase signalling pathways (Morrison *et al.*, 2007; Shaw *et al.*, 2001) and by modulation of growth factors, receptors and their pathways, for example growth-factor receptor degradation (Fraenzer *et al.*, 2003), receptor internalisation (Maitra *et al.*, 2006), receptor re-localisation (Fernandez-Valle *et al.*, 2002) and in the disruption of downstream components of growth factor receptor signalling (Curto *et al.*, 2007) (see **Figure 1.29**).

1.6 Conclusions and thesis goals

In this review, I have outlined the function, cellular components and structure of the peripheral nervous system, and I have described the biology of Schwann cells in terms of their development, tissue homeostasis, injury and nerve pathology. The central theme in all these processes, which underpin the behaviour of Schwann cells

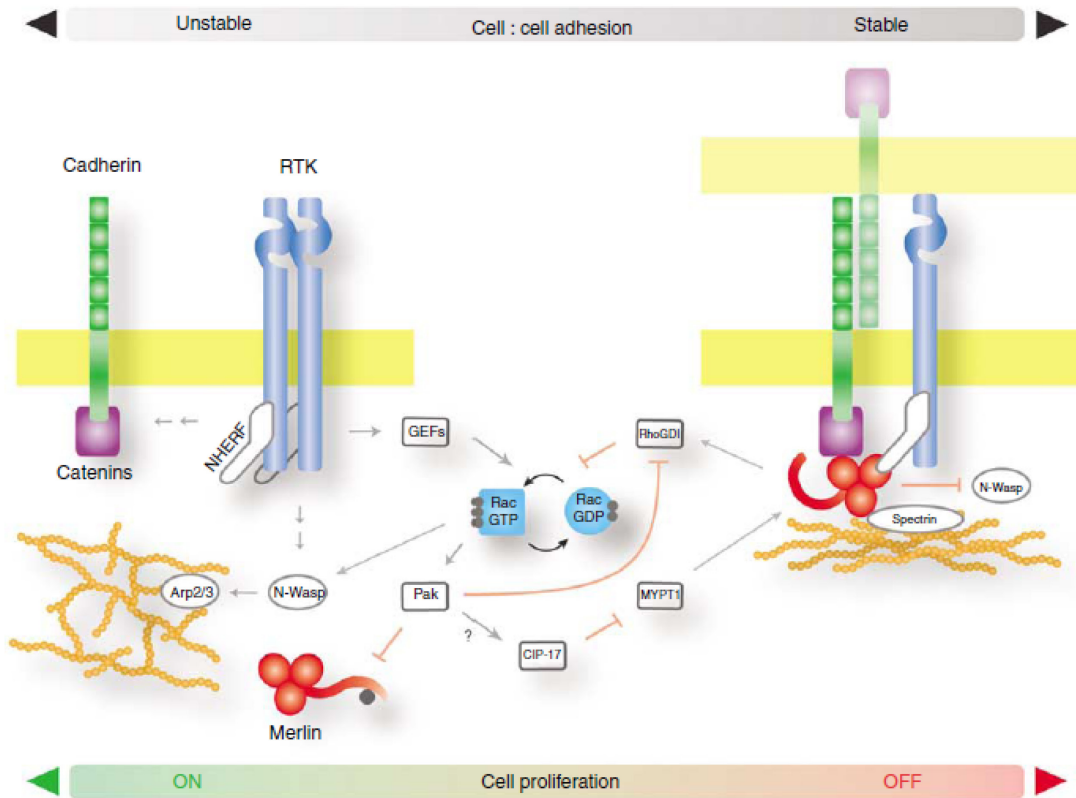


Figure 1.29 A model for the activity of Merlin in the regulation of cell-contact dependent inhibition of proliferation. Merlin coordinates and links intercellular adhesion with downstream receptor signalling. The schematic shows the interactions between Merlin/NF2, cadherin and the mitogenic receptor tyrosine kinase (RTK) epidermal growth factor receptor (EGF-R). At low cell-density (minimal cell-cell contacts), proliferation signals from activated RTKs are dominant, Rac activity is increased, the actin cytoskeleton is highly dynamic and Merlin is inactive. As cell-density increases, the number of cell-cell contacts increases, mediated through cadherin *trans*-ligation events. Cadherins interact with EGF-R *in cis* and Merlin binds their cytoplasmic domains to stabilises this interaction, while in addition, Merlin inhibits Rac activity and stabilises the actin cytoskeleton. As a result, mitogenic RTKs are increasingly restricted to non-signalling adhesion domains, cemented by stabilised actin, and prevented from further signalling resulting in an attenuation of cell proliferation (Curto & McClatchey, 2008).

and axons, is the absolute requirement for contact-dependent, bidirectional signalling. This signalling regime is supported by a plethora of cell adhesion molecules, which play pivotal roles in mediating physical interactions between Schwann cells and axons. For instance, they are required for creating and maintaining the well-ordered heterotypic and radially symmetrical nerve fibre. This

relationship allows for an optimally adapted functional nerve; both in terms of the nerve impulse, i.e. the efficiency at which electrical impulses are conveyed, and in terms of the readiness of the nerve to respond favourably to injury.

I also discussed two very different outcomes epitomised by the loss of Schwann cell/axonal contact. Firstly, in the case of nerve injury, where loss of Schwann cell/axonal contact is reversible; and secondly, in the case of tumourgenesis, where Schwann cell/axonal dissociation is considered an irreversible progression of the disease. The interaction state is important for both outcomes. In terms of nerve injury, Schwann cell dissociation from the damaged axon is essential for the repair and regeneration process. In terms of tumourgenesis, loss of contact between Schwann cells and the axon, allows for neoplastic Schwann cells (in a pro-tumourgenic environment) to proliferate free from the inhibitive environment of the axon.

Identifying and characterising the key molecular mediators governing heterotypic Schwann cell/axonal interactions will be important, if we are to fully understand the processes involved in the regulation of Schwann cell/axonal dissociation and re-association. In this thesis, I aim to identify and define a role for key adhesional mediators of Schwann cell/axonal interactions.

Chapter Two: Materials & Methods

2.1 Reference tables

2.1.1 Cell culture media

Table 2.1 Cell-culture media

Media	Component	Source	Cells
3% NS growth media	DMEM (with phenol red, Glucose 1g/L)	Cambrex	NS
	3% Charcoal-stripped Foetal calf serum (FCS)	Sigma	LTNS LTD
	4mM Glutamine	Gibco	
	100µg/ml Kanomycin	Sigma	
	2µg/ml Gentamycin	Sigma	
	1µM Forskolin	Calbiochem	
	~1000x Glial Growth Factor (GGF)*	in-house	
3% NR growth media	DMEM (without phenol red, Glucose 1g/L) Supplements as for 3% NS growth media (above)	Gibco	Raf1:ER
	400µg/ml <i>G418 (optional selection drug)</i>	Calbiochem	
10% growth media	DMEM (without phenol red, Glucose 4.5g/L)	Gibco	Fibroblast Phoenix AD293
	10% Foetal Bovine Serum (FBS)	Sigma	
	4mM Glutamine	Gibco	
	100µg/ml Kanomycin	Sigma	
	2µg/ml Gentamycin	Sigma	
Basal media	F-12:DMEM 1:1 (without phenol red)	Gibco	DRG
	100ng/ml Nerve Growth Factor (NGF)	Alamone	
	20µg/ml Insulin (human)	Lonza	
	Penicillin/Streptomycin	Gibco	
	100µg/ml Transferrin	Calbiochem	
	100µg/ml Bovine serum albumin (BSA) Fraction V	Invitrogen	
	60ng/ml Progesterone	Sigma	
	16µg/ml Putrescine	Sigma	
	40ng/ml Selenium	Sigma	
	50ng/ml Thyroxine	Sigma	
	50ng/ml Tri-Iodo-thyrine	Sigma	

Differ-entiation media**	1:100	Basal media	BD Biosciences
	50µg/ml	Matrigel (growth Factor reduced)	
	10%	Ascorbic acid	
		Charcoal-stripped Foetal calf serum (FCS)	Sigma

* Concentration of GGF is titred on a batch-by-batch basis. ** media stored in the dark (Ascorbic acid is light- sensitive)

2.1.2 siRNA oligonucleotides

Table 2.2 siRNA oligonucleotides

Gene	Entrez	Oligo	Target sequence	NS	RafER
				[]	[]
Scram			AATTCTCCGAACGTGTCACGT	1nM	3nM
Ncad	83501	#1 #3* #4	AACGGGCATCTTCATCATCAA TCCCAACATGTTTACAATCAA CAGTATACGTTAATAATTCAA	1nM	3nM
Sema4F	29745	#5 #6*	AGCGTCTCATAACGTACAATTA CCGCGGGATGGTTCAAGATAT	1nM	
Sox2	84046	#1 #2	AACAGTTACGTTTCCA ACTTA AACCGTGATGCCGACTAGAAA	1nM	

* Double transfections: 0.75nM + 0.75nM

2.1.3 shRNA oligonucleotides

Table 2.3 shRNA oligonucleotides

Construct	Target Sequence
shScram*	TGCGTTGCTAGTACCAACT
shNcad-1	CGGGCATCTTCATCATCAA

5' -atccCGGGGCATCTTCATCATCAAATTCAAGAGATTGATGATGAAGATGCCCGTTTTTTACGGGTg-
5' -aattcACGCGTAAAAAACGGGCATCTTCATCATCAATCTCTTGAAATTGATGATGAAGATGCCCGcg-

shNcad-3 CCCAACATGTTTACAATCA

5' -gatccG**CCCAACATGTTTACAATCA**ATTCAAGAGATGATTGTAAACATGTTGGGTTTTTTACGCGTg-
 5' -aattcACGCGTAAAAAACCCAACATGTTTACAATCATCTCTTGA**ATGATTGTAAACATGTTGGGC**g-

shNcad-10 TCTGCACCAGGTTTGGAAAT

5' -gatccG**TCTGCACCAGGTTTGGAAAT**TTCAAGAGAATTCCAAACCTGGTGCAGATTTTTTACGCGTg-
 5' -aattcACGCGTAAAAAATCTGCACCAGGTTTGGAAATCTCTTGAA**ATTCAAACCTGGTGCAGAC**g-

*Shown, is the 19bp target sequence and the upper and lower strands of the 66bp oligos that form the hairpin. *Negative control shRNA (Clontech)*

2.1.4 Primers for qRT-PCR

Table 2.4 Primers for qRT-PCR

Gene	Sequence	Product
GAPDH	Fwd: TGCACCACCAACTGCTTAG Rev: GGATGCAGGGATGATGTTC	177 bp
N-cadherin	Fwd: CAGAGAGTCGCCAAATGTCA Rev: TTCACAAGTCTCGGCCTCTT	163 bp
Sema3B	Fwd: GCTGTCTTCTCCACCTCCAG Rev: ACATGCCAGGTCTTGGGTAG	166 bp
Sema4F	Fwd: CTCCTATCTCACCCGGTTTG Rev: TTGACAATGGCGAGAATCTG	246 bp
MBP	Fwd: CACAAGAACTACCCACTACGG Rev: GGGTGTACGAGGTGTCACAA	106 bp
MPZ	Fwd: CTGGTCCAGTGAATGGGTCT Rev: CATGTGAAAGTGCCGTTGTC	225 bp
Ephrin-R 4A	Fwd: CACCATCATCCATTGCTTTG Rev: AAAGGGTTCAGGCCTTTGAT	199 bp

Sema, semaphorin; MBP, myelin basic protein, MPZ, myelin protein zero, GAPDH, glyceraldehyde-3-phosphate dehydrogenase; Fwd, forward; Rev, reverse, bp, base-pair

2.1.5 Antibodies and fluorescent dyes

Table 2.5 Antibodies and fluorescent markers

Primary antibody	Species	[]	Conditions	Source
Immunofluorescence				
BrdU	Mouse	1:300	0.5% Triton X-100 and 2M HCL	Roche (BMC 9318)
Fibronectin	Mouse	1:500		Sigma

GFP	Rabbit	1:6000	0.5% Triton X-100	AbCam (ab290-50)
GFP	Mouse	1:100	0.5% Triton X-100	Sigma (G6589)
Myelin Protein Zero	Mouse	1:1000	Methanol	Astex clone 18
N-cadherin	Mouse	1:400	0.5% Triton X-100	BD Transduction Labs (#610920)
Neurofilament	Rabbit	1:6000	0.1% Triton X-100	Millipore (ab1987)
p75 ^{NGFR}	Rabbit	1:350	No permeabilisation	Millipore (07-476)
RT97	Mouse	1:500	Triton X-100	Gift of J. Woods
S100 β	Rabbit		0.1% Triton X-100	DAKO (Z0311)
SV40	Mouse	1:50	0.5% Triton X-100	Fitzgerald Industries Int. (pAb4190)
Thy1.1	Mouse	1:50	No Permeabilisation	

Western blotting

N-cadherin	Mouse	1:10,000	TBST, milk	BD Transduction Labs
E-cadherin	Mouse	1:10,000	TBST, milk	BD Transduction Labs
B-Tubulin	Mouse	1:20,000	TBST, milk	Sigma (V9131)

Secondary antibody	Target	[]	Conditions
Immunofluorescence			
Alexa-Fluro 594	Mouse	1:400	Invitrogen-Molecular probes (A11032)
Alexa-Fluro 594	Rabbit	1:400	Invitrogen-Molecular probes (A11012)
Alexa-Fluro 488	Mouse	1:400	Invitrogen-Molecular probes (A1029)
Alexa-Fluro 488	Rabbit	1:400	Invitrogen-Molecular probes (A11034)
Biotin	Rabbit	1:250	Sigma
Streptavidin-FITC	Biotin	1:500	Invitrogen-Molecular probes (S32354)
Western blotting			
Anti-horse radish peroxidase (HRP)	Mouse	1:5000	TBST Milk GE Healthcare (NA9310)
Anti-horse radish peroxidase (HRP)	Rabbit	1:5000	TBST Milk GE Healthcare (NA9340)
Fluorescent dyes			
Phalloidin-FITC	F-Actin	1:1000	Sigma
Hoechst	DNA	1:6000	

2.1.6 Solutions used for molecular techniques

Table 2.6 Solutions used for molecular techniques

Solutions	Components
L-Broth agar	10g tryptone, 5g yeast extract, 5g NaCl, 1ml 1N NaOH, 15g agar or agarose, to a final volume of 1 liter in water
L-Broth	10g tryptone, 5g yeast extract, 5g NaCl, 1ml 1N NaOH, to a final volume of 1 litre in water
TE Buffer	10mM Tris-Cl (pH 7.5-8), 1mM EDTA (pH8)
TAE Buffer	40mM Tris, 20mM glacial acetic acid, and 1mM EDTA (pH 8.0)

2.1.7 Solutions and buffers for Western blotting

Table 2.7 Solutions and buffers for Western blotting

Solutions	Components
RIPA lysis buffer	1% Triton X-100, 0.5% sodium deoxycholate, 50mM Tris pH7.5, 100mM NaCl, 1mM EGTA pH8, 20mM NaF, 100µg/ml PMSF, 15µg/ml aprotinin, 1mM Na3VO4.
Discontinuous polyacrylamide gel	<p>Resolving gel (Acrylamide/Bis 30%/0.8% solution to required final polyacrylamide concentration (5-15%):</p> <p>373mM Tris (pH 8.8), 0.1% sodium dodecyl sulphate (SDS), 0.04% tetramethylethylenediamine (TEMED), 0.04% ammonium persulphate (APS).</p> <p>Stacking gel (5% acrylamide/bis):</p> <p>125mM Tris (pH 6.8), 0.5% SDS, 0.12% TEMED, 0.06% APS</p>
4x Sample buffer	200mM Tris pH 6.8, 8% SDS (BioRad), 40% glycerol, 400mM DTT, 0.25% bromophenol blue.
10x Running buffer	2.5M glycine (BDH), 250mM Tris, 1% SDS.
10x Transfer buffer	200mM Tris, 1.5M glycine, 20% methanol (BDH)
Blocking solution	5% milk, 0.05% Tween-20 (BioRad) in PBSA
Stripping buffer	200mM glycine, pH2.5, 0.4% SDS.
1x PBSA Tween	0.05% Tween-20 in PBSA
20x TBS Tween	200mM Tris pH8, 3M NaCl, 1% Tween-20

PBSA	137mM NaCL, 2.7mM KCL, 1.47mM KH ₂ PO ₄ , 8.1mM NA ₂ HPO ₄
20X TBS	200mM Tris pH8, 3M NaCl

2.2 Cell culture

Cell culture was conducted on plastic dishes and multi-well plates, which were pre-treated for adherent cell culture (Nunc/Thermo-Scientific). Culture-ware and glass coverslips were coated with 2.4µg/ml poly-L-lysine (PLL, Sigma) for at least one hour, washed twice in purified water and allowed to dry before use. PLL-coated glass coverslips were further coated with 20µg/ml laminin (Engelbreth-Holm-Swarm (EHS), Sigma) in minimal essential media (MEM)-4-(2-hydroxyethyl)-1-piperazineethanesulfonic acid (HEPES) (Gibco) for at least one hour, which was removed immediately prior to seeding cells. Adherent cells were re-suspended as follows; culture plates were washed twice with PBS to remove traces of serum and pre-warmed (37°C) Trypsin-EDTA was added to plates in order to degrade cell-substratum contacts. Cell rounding was observed using an Olympus inverted light-microscope, and further trypsinisation was inhibited by the addition of DMEM supplemented with 10% foetal-calf serum (FCS). Schwann cell suspensions were counted using a Beckman Coulter counter with cell size limits of between 9 to 27µm diameter.

2.2.1 Schwann cells

Primary rat Schwann cells were obtained from the sciatic nerves of postnatal day-7 Sprague-Dawley rats, as described by Cheng *et al.* (1995) and subjected to sequential immunopanning with Thy1.1 antibody, in order to removed fibroblasts and other contaminating cells. Following purification, 99.9% homogenous Schwann cell cultures - referred to as NS cells in this thesis - were obtained. NS cells were seeded onto 10cm PLL-coated dishes (5.8×10^5 cells) and incubated at 37°C, 95% humidity and 10% CO₂ in 3% serum growth medium (refer to **Table 2.1**). After three days, when the cells were approximately 80% confluent, the plates were trypsinised and 5.8×10^5 cells were seeded onto new 10cm culture plates. NS cells were maintained

in a continual state of proliferation and expanded by serial passages, which we previously showed, could be achieved indefinitely and without adverse culture affects (Mathon *et al.*, 2001).

2.2.2 Fibroblasts

Primary fibroblast were obtained from sciatic nerve preps as described for Schwann cells by immunopanning. Purified fibroblasts were seeded onto non-PLL coated plates and incubated in 10% CO₂, 3% (low) oxygen at 37°C and 95% humidity in 10% serum growth media (see **Table 2.1**).

2.2.3 Raf-1:ER Schwann cells

The inducible (estrodial-dependent) Raf-1/estrogen-receptor fusion protein (Raf-1:ER) (Samuels *et al.*, 1993) was stably integrated into Schwann cells by retroviral infection of the Raf-1:ER construct. Schwann cells were cocultured (1:2) with retroviral producer cells during the infection phase and then drug-selected with 400µg/ml of G418 (Lloyd *et al.*, 1997). Surviving homogenous Raf-1:ER Schwann cells were pooled and expanded under incubation conditions of 37°C, 95% humidity and 10% CO₂. The estrogen analogue 5-hydroxy-tamoxifen (Tmx) was used at 100nM in order to bind the estrogen receptor (ER) domain permitting reversible activation of Raf1 kinase (Harrisingh *et al.*, 2004).

2.2.4 SV40 Large-T antigen (LT) expressing Schwann cells (LTNS & LTD)

LTNS cells, which stably express the Large-T antigen, were generated by retroviral infection of NS cells with the pBabe-puro-SV40 vector (James DeCaprio, Dana-Farber Cancer Institute, Boston) (**Figure 2.1**).

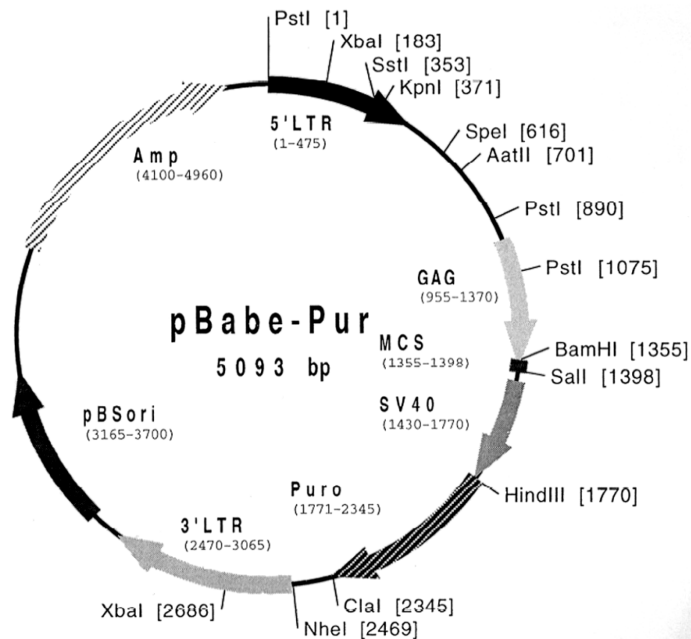


Figure 2.1 Vector map of the pBabe-puromycin vector. The vector incorporates the coding sequence for SV40, which inactivates signalling from P53 and Rb family members.

SV40 Large-T antigen positive Normal Schwann (LTNS) cells were expanded on PLL-coated plates under puromycin selection (0.5µg/ml). LT cells were seeded onto PLL-coated plates and incubated at 37°C, 95% humidity, 10% CO₂ in 3% serum NS growth media (**Table 2.1**). LT derived (LTD) cells were isolated from a population of LTNS cells and maintained under identical culture conditions.

2.2.5 Viral Packaging/Producer Cells

Adenovirus was produced using Ad293 cells (Stratagene, #240085), while retrovirus was produced using the packaging cell-line, 393T Phoenix cells (Nolan Labs, Stanford University). For both cell-types, the cells were seeded at high-density onto non-PLL coated 15cm plates (5×10^6 cells) and incubated at 37°C, 95% humidity and 5% CO₂ in 10% serum growth media (see **Table 2.1**). The cells were media-changed on the first day and passaged every 3 days for expansion and were syringed through an 18G needle to reduce cell clumping and ensure an even distribution of cells in successive plates.

2.2.6 Rat dorsal-root ganglion (DRG) explants

DRGs were obtained from the vertebrae of postnatal day 0/1 Sprague Dawley rats. The vertebrae was opened, in an anterior-to-posterior direction, using surgical scissors and the spinal cord was removed to expose DRG capsules, which are paired either side of the vertebra. DRGs were extracted using fine forceps, transferred to ice cold L-15 media (Gibco, #21041-025) and further manipulated to remove contaminating tissue. DRG capsules were then explanted onto the centre of either PLL, laminin-coated (25µg/ml) 13mm glass coverslips in 4-well plates (for analysis by immunohistochemistry) or onto the central six wells of PLL, laminin-coated (25µg/ml) 12-well plates (for analysis by time-lapse microscopy). The DRG explants were incubated at 37°C at 95% humidity and 5% CO₂ in basal media (see **Table 2.1**), where 200µl of basal media/well was added to 4-well plates and 400µl of basal media/well was added for 12-well plates. After 18 hours, the media was supplemented with the S-phase inhibitor cytosine β-D-arabino-furanoside (AraC) at a concentration of 10⁻⁵M for a 24 hour period in order to remove endogenous mitotic Schwann cells and fibroblasts. The cell media was then changed with fresh basal media and subjected to further media changes every two to three days for a minimum of 6 days up until the cultures were used in experiments. Invariably, after 6 to 7 days, the DRG explants have extended neural processes to form extensive radial networks, free from contaminating cells, that widely cover the coverslips. *In vivo*, DRG neurones are known to project a single axon that diverges into two branches, the peripheral and central branches, and are marked by the absence of dendrites (Chen et al., 2007) (refer to page 24 of the introduction for further details). Thus, for the purposes of this thesis, I shall assume and describe these neural processes are axons.

2.3 Cell culture assays

2.3.1 siRNA transfection

Schwann cells or Raf-1:ER cells were seeded onto 6-well plates (1x10⁵ cells per well) 24-hours prior to transfection so that cells were 70-80% confluent prior to transfection. The cell medium was then changed with 2.3ml of fresh 3% NS growth

media at least one hour prior to transfection. HP Genome-wide rat siRNAs oligo duplexes (Qiagen) were re-suspended to generate 20 μ M stock aliquots (see **Table 2.2** for a list of siRNAs used). Stock aliquots were diluted to form 0.2 μ M working stocks, of which 12 μ l of siRNA (36 μ l of siRNA for Raf-1:ER transfections) was made up in 100 μ l of DMEM with glutamine and mixed before addition of 6 μ l HiPerfect reagent. The transfectant was further mixed and incubated at room temperature for 15 minutes after which it was administered drop-wise to cells for a final concentration of 1nM (for NS cells) and 3nM (for Raf-1:ER cells). Plates were incubated for 18-hours with transfectant (overnight), after which they were washed twice with 3% growth media (to remove transfectant) and returned for a further 24-hours incubation. Assays were performed 48-hours after initial transfection where possible.

2.3.2 Adenovirus

Production

Batch production of adenovirus was achieved by infection and viral amplification within Ad293 producer cells. Ad293 cells were seeded 2-3 days prior to infection and allowed to reach 80% confluence. The cell media was then changed with fresh 10% serum growth media and between 5 to 10 μ l of adenovirus was added to plates, which were gently swirled to ensure even distribution of virus. The green fluorescent protein (GFP)-only expressing adenovirus (AdGFP) and the Sox2-GFP expressing adenovirus (AdSox2) were a gift from David Parkinson (University of Plymouth), while the N-cadherin expressing adenovirus (AdNcad) was a gift from Mark Rosenthal (Wistar Institute, USA). Plates were incubated (as previously described) for 3 to 4 days, and continually monitored for signs of cell-rounding (indicative of viral lytic activity). Adenovirus was obtained from the cell-suspension (from 'rounded' plates) following successive freeze-thaw cycles as follows: the cell suspension was collected and centrifuged at 2000rpm for 5 minutes. The supernatant was then discarded and the pellet re-suspended in 1ml PBS and subjected to three rounds of freeze-thaw-vortex cycles to release virus from cells. The resulting suspension was then centrifuged at 1200rpm for 5 minutes and the supernatant was passed through 0.45 μ m filters, with aliquots stored at -80 $^{\circ}$ C and discarded after each thaw. The first aliquot was thawed and used to derive an

optimal infection concentration for the batch. Briefly, NS cells were infected using serial dilutions 1:100, 1:200, 1:400, 1:800 of virus and infection rate was gauged by GFP fluorescence to achieve 90-100% infection, with minimal cytotoxic effects.

Adenoviral infection for over-expression studies

Schwann cells or fibroblasts were seeded onto 6-well plates the day before infection and maintained in culture until cells were 80% confluent, after which the cell media was changed to ensure a total plate volume of 3ml. Adenovirus was added directly to media in wells and gently mixed by swirling to ensure even distribution of virus. The plates were then returned to the incubator for 18-hours, after which the plates were washed twice with either 3% serum NS growth media or 10% serum growth media in order to remove excess virus from Schwann cells and fibroblasts respectively.

2.3.3 Retrovirus and the generation of shRNA Schwann cells

Production

The pSIREN-RetroQ-ZsGreen RNAi system (Clontech, #631526) was used to generate retrovirus in order to introduce shRNA constructs into Schwann cells to generate stable shRNA cell lines, which express the shRNA under the human U6 Promoter and coexpress the *Zoanthus sp.* GFP marker. Three independent, non-overlapping short hairpin (sh)RNA oligonucleotides were algorithmically designed using the on-line Clontech RNAi designer², which identifies a 19bp sequence that targets the gene of interest. This is then incorporated into a longer 66bp oligo, which contains BamHI and EcoRI overhangs that allows directional insertion of the oligo into the pSIREN vector. In addition, an MluI restriction site was also included so that the insert could be identified. The target sequences and the shRNA duplexes generated are shown in **Table 2.3**. ShRNA duplexes were obtained from Sigma and cloned into the RNAi-Ready pSIREN-RetroQ retroviral expression Vector (Clontech 631526). These steps are covered in detail in the Knockout RNAi Systems User Manual (Clontech Laboratories, protocol #PT3739-1) and are summarised here:

² <http://bioinfo.clontech.com/rnaidesigner/sirnaSequenceDesign.do>

(1) shRNA duplexes were annealed by mixing 100 μ M of each shRNA oligo (reverse and forward) in a 1:1 ratio and heating to 95°C for 30 seconds, followed by gradual cooling over 6 minutes. (2) Annealed shRNAs were diluted to 0.5 μ M concentration (1:100 dilution) in TE buffer and then ligated to the linearized vector by incubating the following mixture (**Table 2.8**) at room temperature for 3 hours:

Table 2.8 Reaction mixture for shRNA insert / vector ligation

Vol	[]	Component
2 μ l	25ng/ μ L	pSIREN-RetroZ Vector
1 μ l	0.5 μ M	shRNA oligos
1.5 μ l	10x	T4 DNA ligase buffer
0.5 μ l	10 mg/ml	BSA
9.5 μ l		nuclease-free water
0.5 μ l	400 U/ml	T4 DNA ligase enzyme

A ligation reaction was set up as above for each of the N-cadherin target oligonucleotides (shNcad-1, shNcad-3 and shNcad-10), scrambled shRNA and a vector-only control. (3) Each ligation reaction was transformed into competent JM109 bacteria (Progmega) by adding 2 μ L ligation mixture to 50 μ L of bacterial cell suspension, incubating on ice for 5 minutes and then heat shocking at 42°C for 30 seconds in a water bath before replacing on ice. (4) Transformed bacteria were grown in 250 μ L of Super Optimal Broth (SOC) medium, shaking for 1 hour at 37°C. 30 μ L of each transformation was then spread onto agar plates containing the selection antibiotic ampicilin and incubated at 37°C over-night. (5) Eight separated colonies were picked from each plate and grown up in small starter cultures of LB medium supplemented with ampicilin for 8 hours. (6) Plasmids were then isolated and purified from the bacteria using the Mini-Prep kit (Qiagen) and digested with the Mlu1 restriction endonuclease to check for the presence of the Mlu1-containing shRNA insert (see restriction digestion and analytic gels). (7) 0.5mls of starter culture from positive clones was inoculated into 250mL of LB medium and supplemented with ampicilin. Cultures were incubated overnight at 37°C and subjected to vigorous shacking. Plasmids were purified from these bacterial cultures by Maxi-Prep (Qiagen) and kept as a stock dissolved in TE and frozen at -20°C. The

shRNA plasmids were also verified by sequencing (MWG-Biotech), in which all three shRNA plasmids had 100% homology for their intended sequence.

Phoenix transfection and retroviral infection of cells

The Phoenix retroviral packaging cell line was used to generate viral supernatant in order to infect low-passage Schwann cells. The protocol was as follows: (1) 5×10^6 Phoenix cells were seeded onto 10cm plates (one plate for each transfection) and left to settle overnight. (2) 5 μ g of plasmid DNA was mixed with 500 μ l of serum free medium (DMEM + Glutamine), followed by 17.5 μ l of PLUSTM reagent (Invitrogen 18324-012), and incubated at room temperature for 15 minutes. A separate tube was prepared for each of the constructs. (3) In new tubes, 25 μ l of LipofectamineTM reagent (Invitrogen, 11514-015) was mixed with 500 μ l of serum free medium for each transfection, and the DNA/PLUSTM mix from step 2 added. The transfection mixture was incubated for a further 15 minutes at room temperature to allow DNA/lipid complexes to form. (4) The cell medium on Phoenix cells was replaced with 4mls of serum-free medium per plate and washed once with serum-free medium. (5) The DNA/lipid complexes from step 3 were carefully added drop-wise to the Phoenix plates, rocked gently to mix, and incubated under standard culture conditions for 3-4 hours in order to transfect the shRNA encoding DNA into Schwann cells. (6) The transfection medium was removed and replaced by fresh 10% serum media. The cell media was replaced after 24 hours with 6ml fresh medium and the cells were left overnight to produce virus. (7) 4ml of viral supernatant was collected from each plate and Polybrene (hexadimethrine bromide, Sigma H9268) was added at a final concentration of 8 μ g/ml. The solution was filtered to remove cell debris before been added to subconfluent Schwann cells. Phoenix plates were topped up with an extra 4ml medium to continue virus production. (8) Schwann cells were incubated for 2 hours with the viral supernatant, then left to recover for 2 hours in normal medium and left to recover overnight. The following day, Schwann cells were subjected to a second round of infection for 2 hours, before final recovery in normal 3% serum growth medium. (9) Infected Schwann cells were left to recover for two days in normal 3% growth medium, passaged and analysed by immunofluorescence for N-cadherin knockdown.

2.3.4 DRG cocultures for association assays

Cells were trypsinised and immediately centrifuged (Sorvall TC) at 1500rpm for 5 minutes. The cell pellets were re-suspended in basal media and cell counts were determined using a Beckman Coulter Counter. The corresponding seeding concentrations for each cell-type in 4-well plate format (as adopted for fixed cocultures) and 12-well plate format (as adopted for time-lapse microscopy) are listed in **Table 2.9**. Cells were seeded onto day-6 or 7 DRG explants. The well-volume was topped-up to 500 μ l per well (for 4-well plates used for fixed cultures) and 700 μ l per well (for 12-well plates used for time-lapse microscopy). DRG cocultures were either fixed after 8-hours or time-lapse microscopy was performed over 20 hours.

Table 2.9 Cell plating densities for DRG cocultures

Cell Type	4-well plate	12-well plate
NS	1.5x10 ⁴	2.0x10 ⁴
Fbs	1.1x10 ⁴	1.5x10 ⁴
LTNS	1.2x10 ⁴	1.6x10 ⁴
LTD	1.0x10 ⁴	1.3x10 ⁴

Cell densities determined by titration

2.3.5 Myelination assay

Scrambled and N-cadherin shRNA Schwann cell lines were generated for each myelination assay and expanded to healthy mitotic plates. shRNA cells were trypsinised, re-suspended in basal media and counted using a Beckman Coulter Counter. 4x10⁴ cells were seeded per DRG explant and cocultures were incubated in basal media for one week, during which time Schwann cells were allowed to proliferate. Myelination was then induced using differentiation media (see **Table 2.1**). The media contains matrigel (to mimic ECM signals) and Ascorbic acid (a potent differentiator). Cocultures were incubated in the dark for approximately two weeks, with cell media changes every two days. The extent of myelination was gauged by the presence of thick translucent 'myelin tubes' observed by phase-contrast microscopy in live-cells.

2.3.6 Proliferation assays

BrdU incorporation

Schwann cells were seeded at low density (2×10^4 cells) and high density (3.5×10^4 cells) in 4-well plates and transfected with siRNA 24-hours later for 16 hours. The cell media was then changed and four hours later, the media was supplemented with 5-bromo-2-deoxyuridine (BrdU) for 7 hours. The plates were fixed with 4% PFA and immunostained for BrdU, which labels cells in S-phase nuclei. Quantification of Schwann cell proliferation was achieved by blind-counting immunostained glass coverslips (by epifluorescence) to determine the proportion of BrdU positive cells.

Growth-curve assay

Schwann cells were seeded onto 10cm plates and transfected 24-hours later with scrambled and N-cadherin siRNA for 16-hours. The cell media was then changed and 8-hours later, the knockdown cells were seeded onto 6-well plates as 4 sets of triplicates, i.e. each siRNA condition was conducted in 12 well format (2x6 WP), allowing for 4 time-points at approximate 24-hour intervals (0, 24, 48, 72 and 96hrs). At each time-point, cell counts were obtained in triplicate, by analysing the cell-suspension (following trypsinisation) using a Beckman Coulter Counter, and the average count was plotted against time in culture.

2.4 Molecular techniques

2.4.1 Bacterial transformation

Agar plates were prepared by melting L-broth agar and once cooled sufficiently, adding the correct antibiotic selection prior to pouring. Ampicillin was used at a final concentration of 0.1 mg/ml, while Kanamycin was used at a final concentration of 30 μ g/ml. To transform bacteria, 10 μ l of ligation mixture or 20ng of purified plasmid was added to 100 μ l of competent bacteria (DH5 α) and incubated on ice for 45 minutes prior to 2 minutes heat-shock at 42°C. After less than 5 minutes on ice, 1ml of L-broth without antibiotics was added to each reaction and incubated at 37°C for 45 minutes. The bacteria mixture was subsequently collected by centrifugation at 6000rpm for 2 minutes in a microfuge (sigma) and about 75% of the supernatant

removed. The bacteria was then re-suspended in the remaining L-broth and spread over agar plates containing the relevant antibiotic selection. Plates were incubated at 37°C overnight and single colonies were extracted from the agar and used to inoculate L-broth (with antibiotics) to obtain cultures for plasmid extraction.

2.4.2 Plasmid DNA extraction

Either 4mls (mini) or 100mls (maxi) of L-broth containing 5µg/ml ampicillin was inoculated with a single colony of transformed bacteria and grown overnight, shaking at 37°C. The culture was centrifuged at 4000rpm for 20 minutes to pellet the bacteria and plasmid DNA was extracted by alkaline lysis using the Qiagen mini- and endotoxin free maxi-prep kits according to the manufacturers guidelines. Briefly, the bacterial pellet was re-suspended and lysed in the lysis buffer supplied. The lysates were then passed through columns containing Qiagen Anion-Exchange Resin in a low salt buffer. After a series of washes the bound plasmid was eluted and pelleted by centrifugation. DNA pellets were re-suspended in TE buffer or water.

2.4.3 Determination of quantity and quality of nucleotide

Duplex DNA and RNA was quantified using either spectrophotometry (Nanodrop-1000) or agarose gel electrophoresis. For spectrophotometry, in addition to quantification, an absorbance A_{260}/A_{280} ratio was calculated to determine purity of the product - where a value of 1.8 were desirable for dsDNA and a value of 2 was desirable for RNA.

2.4.4 Restriction digestion & analytic gels

Restriction endonucleases and buffers were sourced from Promega and correct enzyme/buffer combinations and conditions were determined using the on-line guide at the Promega website³. Restriction digests were used for plasmid diagnostics, in which NEB cutter V2⁴ was used to discover unique restriction sites and determine corresponding band-signatures.

³ http://www.promega.com/guides/re_guide

⁴ <http://tools.neb.com/NEBcutter2>

Table 2.10 Standard reaction mixture for restriction digests

Vol	[]	Component
16.3µl		Water
0.2µl		Bovine serum albumin
2µl	10x	Restriction buffer
0.5µl	5U	Enzyme
0.5µl		DNA template

*0.5µl for double enzyme combinations

The mixture was incubated at 37°C for 2 hours as per manufactures protocol. The restriction pattern was analysed following agarose gels electrophoresis to resolve DNA by size. Agarose gels (typically 0.8%) were set in 50ml tris-acetate-EDTA (TAE) supplemented with 0.5µl ethidium bromide (EtBr) in TAE and 1µl of DNA digest was run and developed using a Flash Gene UV illuminator (Syngene Bio-Imaging).

2.4.5 Polymerase chain reaction (PCR)

Table 2.11 Standard PCR reaction mix and thermal-cycler programme

Vol	[]	Component	#	Program
2.0µl	25mM	MgCl ₂	1	95°C 3'
0.5µl	10mM	dNTP	2	95°C 30s Denaturation
5.0µl		5xFlexibuffer	3	55°C 30s Annealing
0.5µl	10mM	Forward Primer	4	72°C 30s
0.5µl	10mM	Reverse Primer	5	Goto # 2 29x
15.37µl		Water	6	72°C 5' Elongation
0.125µl		GoTaq Polymerase	7	4°C End
1µl		DNA Template		

Reactions were conducted on the PTC-200 (Peltier) thermos cycler and used 1-2 µl cDNA as template in a final volume of 25µl. Primers amplified fragments ranging in size from 200–400bp and PCR conditions were determined empirically for the different primer pairs.

2.4.6 RNA extraction & purification

Standard RNA extraction protocol: Confluent cell cultures in 6-well plates were aspirated to remove the cell media, after which the cells were lysed (in wells) with 400µl of Tri-reagent (Ambion) for 5 minutes at room temperature. The lysate was then transferred to tubes and vigorously shaken with 80µl of chloroform and left to phase-partition at room temperature for 15 minutes. RNA was then isolated from the aqueous upper phase and precipitated with 200µl Isopropanol and vortexed. The mixture was centrifuged and washed in 75% ethanol, and then centrifuged after which the pellet was re-suspended in 10µl RNase-free water.

RNA extraction for sensitive assays (microarray): Total RNA was extracted from cultured cells using the RNAeasy Plus Minikit (Qiagen). Briefly, the cell media was removed, the plates were washed twice with Ice-cold PBS and the cells were lysed and homogenized in a highly denaturing guanidine-isothiocyanate-containing buffer (Buffer RLT). The lysate was then transferred to a Qias shredder homogeniser column (Qiagen) and homogenised lysates were subsequently passed through a gDNA eliminator spin column to remove genomic DNA. Ethanol was added to the flow-through to provide appropriate conditions for RNA binding to the RNAeasy spin column. Following centrifugation of the sample through the RNAeasy column, salts and contaminants were washed away with 70% ethanol and RNA was eluted in 20µl RNase free H₂O.

2.4.7 First-strand cDNA synthesis

The SuperScriptTM II Reverse First-Strand Synthesis System (Invitrogen) was used with random hexamers to reverse transcribe 500ng-1µg of RNA to produce cDNA for quantitative RT-PCR reactions. Template RNA was mixed with 1µl of random hexamers [50ng/µl] and 1µl dNTP [10mM] up to a final volume of 10µl with DEPC treated RNase-free water (RNA template mix). This mixture was incubated at 65°C for 5 minutes prior to addition to the reaction mixture (**Table 2.12**, part A) to make a final volume of 20µl and thermo-cycled (**Table 2.12**, part B):

Table 2.12 First-strand cDNA synthesis

(A) Reaction mixture			(B) Program		
Vol	[]	Component	#	Temp	
2µl	10x	RT Buffer	1	25°C	10 min
4µl	25mM	Magnesium chloride	2	42°C	50 min
2µl	0.1mM	DTT	3	70°C	15 min
1µl	40u/µl	RNase Out	4	4°C	ICE
1µl	50u/µl	Super-Script II			
10 µl		RNA template mix			

Finally, 1µl of RNase H [2U/µl] was added to the mixture, which was then at 37°C for 20 minutes in order to degrade residual RNA.

2.4.8 Quantitative RT-PCR (qRT-PCR)

Quantitative PCR was performed using the DyNAmo SYBR Green qPCR Kit (Finnzymes, NEB) and the Opticon 2 DNA engine (MJ Research). PCR reactions (25µl) contained 12.5µl of PCR Sybr Green mix and 0.3 mM primers. All reactions were performed in duplicate and each experiment included a standard curve and a no-template control. Standard templates consisted of gel purified PCR product and each standard curve consisted of 5 serial dilutions of template. The threshold cycle for each standard sample was plotted against an arbitrary number to obtain a standard curve. This was then used to extrapolate the amount of template in the unknown “test” samples. Relative expression was calculated by normalizing to GAPDH (glyceraldehyde-3-phosphate dehydrogenase). Intron-spanning gene-specific primer pairs were designed using the Primer3 algorithm (Rozen & Skaletsky, 2000). Conditions for each primer pair and template were determined empirically. At the end of 40 cycles of amplification a dissociation curve analysis was performed in which SYBR green fluorescence was measured at 1°C intervals between 55°C and 95°C.

2.4.9 Microarray

RNA was extracted from confluent, duplicate 10cm culture plates as described in section 2.4.7 and subjected to enhanced purification using an QIA RNA purified kit (Qiagen). Purified RNA was quantified by spectrophotometry and a test sample run through a 1% agarose electrophoretic gel using RNase-free TAE, in order to assess RNA quality. Five micrograms per duplicate plate for both test and reference conditions, was submitted to the Cancer Research UK Gene chip service (Paterson Institute) for gene expression analysis using Affymetrix GeneChip Rat 230_2 expression arrays (cDNA). The microarray experiment was performed according to MBCF protocols:- labelling: PICR one-cycle target labelling v1; reaction mixture: PICR cocktail v2.0 (DMSO); hybridisation: PICR one-cycle 11µM feature; scanning: PICR Scanner 3000. The experiment was controlled using Affymetrix GeneChip Operating Software (GCOS) ver 1.1.1. The data output was held in compliance with the Minimum Information About a Microarray Experiment (MIAME) database standard.

Data analysis: data pre-processing was conducted using using Bioconductor⁵, which is a set of life-science specific packages that work within the statistical programming language "R"⁶. Differential gene expression was assessed between replicate groups using an empirical Bayes' t-test as implemented in the 'limma' package.

Quality control: The Rat 230-2 GeneChip incorporates a number of internal controls. These include the hybridisation controls: bioB [1.5pM], bioC [5pM], bioD [25pM] and cre [100pM] (GeneChip Eukaryotic Poly-A RNA); (2) poly-A controls: dap, lys, phe and thr; (3) normalisation controls: 100 test probes and (4) house-keeping/control genes: GAPDH, β -actin, hexokinase-1.

⁵ <http://www.bioconductor.org/>

⁶ <http://www.r-project.org/>

2.5 Biochemistry

2.5.1 Protein extraction & quantification

The cell media was aspirated from plates, which were washed twice with ice cold PBS. The culture plates were then scraped to detach cells and the resulting cell debris was transferred to tubes and centrifuged at 8000rpm for 5 minutes at 4°C. The pellet was re-suspended with 80-100µl of lysis RIPA buffer and vortexed in order to lyse cells and the mixture further centrifuged at 13,000rpm for 15 minutes. The cell debris (pellet) was discarded and protein quantified against a BSA standard-curve using the colorimetric bicinchoninic acid assay (BCA, Thermo-Scientific), with extra RIPA added as needed to equalise protein concentration across samples. Samples were then emulsified in 4x sample buffer, heated to 95°C for 5 minutes to facilitate denaturation.

2.5.2 Western blotting

Western blotting was performed using the Bio-Rad Laboratories Western blot running kit. The apparatus was setup using a discontinuous polyacrylamide gel (see **Table 2.7** for gel recipe), where 10 to 15µg of protein was loaded per well and 5µl of Rainbow RPN756v (GE Health Care) was used as a size reference. Samples were resolved by sodium dodecyl sulfate - polyacrylamide gel electrophoresis (SDS-PAGE), and transferred to nitrocellulose membranes (Millipore Immobilon-P). Membranes were blocked for 1 hour at room-temperature in 5% milk powder/TBST. Blocked membranes were incubated overnight in primary antibody diluted in block solution, with rolling agitation, before washing in TBST and incubating for one hour in horseradish peroxidase-conjugated secondary antibody diluted in block. Membranes were then washed 4 times in TBST and once in TBS before chemiluminescent detection using ECL Plus™ reagent (GE Healthcare). Blots were developed following exposure to light sensitive film (Kodak).

2.6 Microscopy & image processing

2.6.1 Live-cell images

Phase-contrast images of live cells were routinely captured using a QICAM camera connected to an inverted Olympus CK40 microscope. Images were processed using OpenLab software and encoded using TIFF (loss-less) format.

2.6.2 Immunofluorescence

Immunohistochemistry was routinely carried out on adherent cells fixed onto 13mm glass coverslips. The incubation steps were conducted in the dark using within sealed humidity chambers. Cell monocultures were fixed in 4% Paraformaldehyde (PFA) for 10 minutes and washed 4 times by serial PBS washing. DRG cocultures were fixed in 4% PFA for 15-20 minutes and washed 4 times in serial PBS washes. In most cases, cells were first permeabilised using either detergent (Triton X-100 (BDH) in PBS) or Methanol (Refer to **Table 2.5** for the list of primary and secondary antibodies and their conditions). Detergent permeabilisation was achieved following immersion in the reagent for 10-15 minutes, following by a series of 4 PBS washed. Coverslips were transferred to droplets of 3% BSA in PBS (non-specific block) and incubated for at least 1 hour at room-temperature. Methanol permeabilisation was achieved by immersion of the coverslips in ice-cold methanol for 10 minutes at minus 20°C. Cells were then rehydrated by washing 6 times by serial PBS washing and blocked in 10% goat serum (Sigma) for at least 1 hour at room-temperature. Cells were incubated with primary antibody for 1-hour at room-temperature (or overnight at 4°C) and afterwards washed 6 times by serial PBS washing. Cells were incubated with secondary antibody (including fluorescent dyes, e.g. Hoechst, where appropriate) for a further 1 hour at room-temperature, after which the coverslips were washed 6 times and PBS, once in purified water prior to mounting on glass slides using ProLong Gold (Invitrogen) and cured for 18-24 hours before being sealed with nail varnish. Slides were viewed by epifluorescence using an Axioplan (Zeiss) fluorescence microscope and images taken with a Hamamatsu (C4742-95) camera, processed in Openlab software and encoded into TIFF format.

S100 β immunostaining: the primary signal was amplified using anti-rabbit biotin step, in which cells were incubated for 1hr at room temperature, washed (as previously) and then subjected to a final 1hr incubation with fluorescent tagged streptavidin, which has a high affinity for biotin.

BrdU immunostaining: fixed cells were permeabilised for 30 minutes at room temperature in 0.5% TritonX100 + 2M HCl, in order to denature DNA prior to blocking with 3% BSA and antibody staining as previously described.

2.6.3 Time-lapse microscopy

Time-lapse videos of DRG cocultures were performed using the central six wells of 12-well plates. The cells were seeded (in duplicate or triplicate) onto DRG explants cultured within 12-well plates (see **Table 2.9**) and allowed to settle for 15 minutes on a flat-surface. The plate was transferred to the time-lapse apparatus and installed on an automatic microscope stage within a controlled humidity chamber (95% humidity, 37°C and 5% CO₂). The cocultures were observed using an inverted Zeiss Axiovert 200M microscope with an objective magnification of 16x. Three to four XY positions were selected for each DRG at locations where added cells (rounded at this stage) were judged to be in close proximity to axons. Multi-well time-lapse image sequences were captured using a Hamamatsu (ORCA-ER) camera at 2x binning using autofocus at intervals of 3 minutes for approximately 20 hours. Time-lapse analysis was computed using Velocity 5 software. Time-lapse videos were encoded as Sorenson Quick-time movies at 0.7 frames per second.

2.6.4 Extracellular area measurements

Schwann cell monocultures were coimmunostained for p75^{NTR} and N-cadherin, while cell-nuclei were labelled with Hoechst. Images were captured using a Hamamatsu (C4742-95) camera connected to an Axioplan (Zeiss) inverted fluorescent microscope. At least twenty independent fields of view were analysed per coverslip, from triplicate coverslips for each condition. For each field of view analysed, a greyscale TIFF encoded composite was created containing three images (1) cell nuclei (Hoechst staining), used to determine cell number; (2) N-cadherin

immunofluorescence, used to check N-cadherin knockdown and (3) p75 immunofluorescence, used to calculate extracellular area. Image analysis was conducted using Image-J software (v1.37). The p75 immunofluorescent images were imported to Image-J as 8-bit grayscale (1280x1022) and transformed as follows: The image and look-up table (LUT) was first inverted and a region of interest (ROI) of 1100 x 900 dimensions was positioned over the centre of the image where intensity is most uniform. The image was cropped in order to mitigate the edge effect (an artefact of microscopy). A background subtraction of 100 was performed, contrast was enhanced by 0.5 and thresholds were set to 0-15 limits. This creates an image in which contrast is maximal and allows for algorithmic identification of extracellular areas. The number and area of these regions were measured and outlines below a threshold area of 2.5×10^5 (arbitrary units) were discounted as they were more likely to be small intracellular regions rather than extracellular gaps.

2.6.5 Scoring Schwann cell/axonal association

Fixed DRG cocultures were quantified for Schwann cell/axonal interaction by scoring three distinct states as described in Parrinello *et al.* (2008) and out-lined in Chapter Three of this thesis. These are not associated, associated, not aligned or c) associated and aligned (see **Figure 3.2B** for examples). Cocultures were fixed and immunostained with an axonal marker (e.g. neurofilament (NF) or RT97) and a Schwann cell marker (S100 β), while cell nuclei were labelled with Hoechst. Quantification was performed on triplicate coverslips and scored blind using an red-green-blue (RGB) Triple-band pass filter on an inverted Axioskop (Zeiss) microscope at 40x magnification, in order to view all three light channels simultaneous, i.e. axons, Schwann cells and cell nuclei nucleus. Fields of view were selected from less-dense, peripheral regions of the DRG-axonal radiation. The first scoring area was selected one field-of-view in from the extremity of the axonal radiation. All visible Schwann cell/axonal interactions were scored, after which the field-of-view was adjusted in order to score sequential, adjacent fields-of-view, in a clock-wise direction around the DRG, until at least 200 interactions per coverslip had been scored.

2.7 Statistics

Statistics were computed using GraphPad (Prism) software. Unless otherwise stated, the results were analysed by the student's two-tailed T-test. Results in which p-values are below 0.05 or 5% are denoted * (significant) and below 0.01 or 1% are denoted ** (very significant).

Chapter Three: A screen for mediators of Schwann cell/axonal interactions

3.1 Chapter introduction

Schwann cells are found in close proximity to axons from an early developmental stage (Armati, 2007; Woodhoo & Sommer, 2008). This intimate relationship begins shortly after NCCs have delaminated from the dorsal horn of the neural tube, migrated to the nerve roots (Corfas *et al.*, 2004; Kuriyama & Mayor, 2008; Le Douarin & Kalcheim, 1999) and have differentiated to SCPs (Jessen & Mirsky, 2005; Woodhoo & Sommer, 2008). SCPs exist in multi-Schwann cell/axonal clusters that are dependent on close axonal contact for their survival, proliferation and later differentiation to mature Schwann cells (Corfas *et al.*, 2004; Woodhoo & Sommer, 2008). These coordinated and complex processes are not only important in early development and for maturation of the nerve, but are also integral to the regeneration process that occurs following adult peripheral nerve injury (Chen *et al.*, 2007). Additionally, the loss of Schwann cell/axonal interactions is a common feature in many glial tumours, from neurofibromas (that occur in Neurofibromatosis type 1 (NF1)) to highly malignant peripheral nerve sheath tumours (MPNSTs), and appears to be one of the earliest observable events (Carroll & Ratner, 2008; Parrinello *et al.*, 2008; Zhu *et al.*, 2002). Thus, given the importance of Schwann cells in nerve development, injury and neuropathology there is a strong case for expanding our existing knowledge of Schwann cell/axonal interactions.

3.2 Characterising Schwann cell/axonal interactions

To study Schwann cell/axonal interactions, I used an *in vitro* primary DRG/Schwann cell coculture system. Sciatic nerves were extracted from postnatal day-7 rats and Schwann cells purified to at least 98% homogenous populations by removing contaminating cells, for example fibroblasts and immune cells, through sequential immunopanning as described in Mathon *et al.* (2001). By doing this, we exploited the remarkable regenerative capacity of Schwann cells to dedifferentiate and reform a proliferative population after nerve injury (Harrisingh *et al.*, 2004). In previous work undertaken by our laboratory, we showed that Schwann cells isolated in this manner could be cultured indefinitely in 3% serum while retaining normal

checkpoints and character, and without evidence of adverse culture effects (Mathon *et al.*, 2001). Schwann cells cultured in this way - referred to in this thesis as normal Schwann (NS) cells - are amenable to expansion for a range of cell interaction assays *in vitro*. Importantly, Schwann cells derived from postnatal myelinating Schwann cells have, following extraction from the animal, dedifferentiated (de-myelinated) and dissociated from axons to form a proliferating pool of Schwann cells and as such closely resemble the post-injury Schwann cells found *in vivo*. For instance, they express a similar set of cell-surface expressed molecules to ISC cells including GFAP, p75^{NTR}, L1-CAM and NCAM (Jessen & Mirsky, 2008b; Woodhoo & Sommer, 2008). Furthermore, as *in vivo*, dedifferentiated Schwann cells continue to demonstrate notable plasticity by retaining the ability to reassociate and remyelinate axons, a process that is essential for *in vivo* peripheral nerve repair following Wallerian degeneration (Chen *et al.*, 2007; Hall, 2005; Stoll *et al.*, 2002). However, there are differences between injury Schwann cells and ISCs, for instance the former strongly express N-cadherin as well as integrin $\alpha 1\beta 1$ (Jessen & Mirsky, 2008b). It is important, therefore, to stress that cultured NS cells are used to study post-injury reassociation rather than developmental processes *per se*, although insights from the former may still provide useful clues as to the developmental program of Schwann cell/axonal interaction.

Normal Schwann cell/axonal interactions

I first wanted to examine in detail the normal processes involved in Schwann cell/axonal interactions. In particular, I wanted to understand the various stages of the interactions and how they are regulated temporally. To study this, I decided to analyse the interactions using time-lapse microscopy. DRGs from day-0 or day-1 postnatal rats were extracted and explanted separately onto the central region of multi-well plates. After 24-hours, the culture medium was supplemented with the mitotic toxin cytosine β -D-arabinofuranoside (AraC) for a period of 48 hours, in order to remove contaminating cells, for example endogenous Schwann cells and fibroblasts, while leaving axons intact. The DRG-axonal cultures were incubated for an additional three to four days, after which they were generally free of contaminating cells. At this stage, the axonal networks typically covered approximately two-thirds of the surface area of the wells. I next seeded Schwann

cells onto axons at low-density and performed multi-well time-lapse microscopy over an eight hour period (**Video 3.1**). As represented by the image sequence shown in **Figure 3.1A**, I was able to observe several key stages involved in the early interactions between Schwann cells and axons. In this sequence, a representative Schwann cell was observed as it recognised, associated and aligned with an axon (see white arrow). The first image shows the Schwann cell as it appears to search its immediate vicinity for an axonal target. This process is aided by the morphology of the Schwann cell, which forms two or three large cytoplasmic protrusions that extend out bi- or tri-laterally from the cell - morphology reminiscent of ISCs (**3.1Ai**). In this example, the Schwann cell first makes contact with an axon using the extremity of one of these cytoplasmic protrusions (**3.1Aiii**), which defines the point of Schwann cell/axonal recognition. Importantly, the axon was observed to inflect slightly at the point of contact suggesting that the Schwann cell had firmly attached itself as part of the recognition process. Remarkably, as shown in the next image, the Schwann cell then appeared to contract its cytoplasm and pull itself up onto the axon (**3.1Aiv**). Once associated, the Schwann cell was observed to extend and align its cytoplasm along the axon (**3.1Avi**) and, importantly, remained fully associated with the axon for the duration of the analysis, despite exhibiting considerable lateral movement. In a few cases (not shown), associated Schwann cells were observed to contact multiple axons, which is similar behaviour to axonal bundling seen during radial sorting (Chernousov *et al.*, 2008). These initial observations of Schwann cell/axonal interactions, drawn from the time-lapse analysis, are summarised in a schematic model (**Figure 3.1B**), in which I describe the interaction programme as occurring via a number of step-wise interactions and processes:

(1) **Recognition**: the Schwann cell extends long bipolar cytoplasmic processes, which may allow for the maximal chance of locating targets. Following an encounter, the Schwann cell positively identifies its target as an axon by a, as yet, poorly understood cell-cell contact-dependent mechanism.

(2) **Association**: the Schwann cell cytoplasm contracts, while the heterotypic Schwann cell/axonal contact region, which initially mediated recognition, is maintained, resulting in the Schwann cell being pulled up towards the axon. Finally, the Schwann cell is assembled onto the axon.

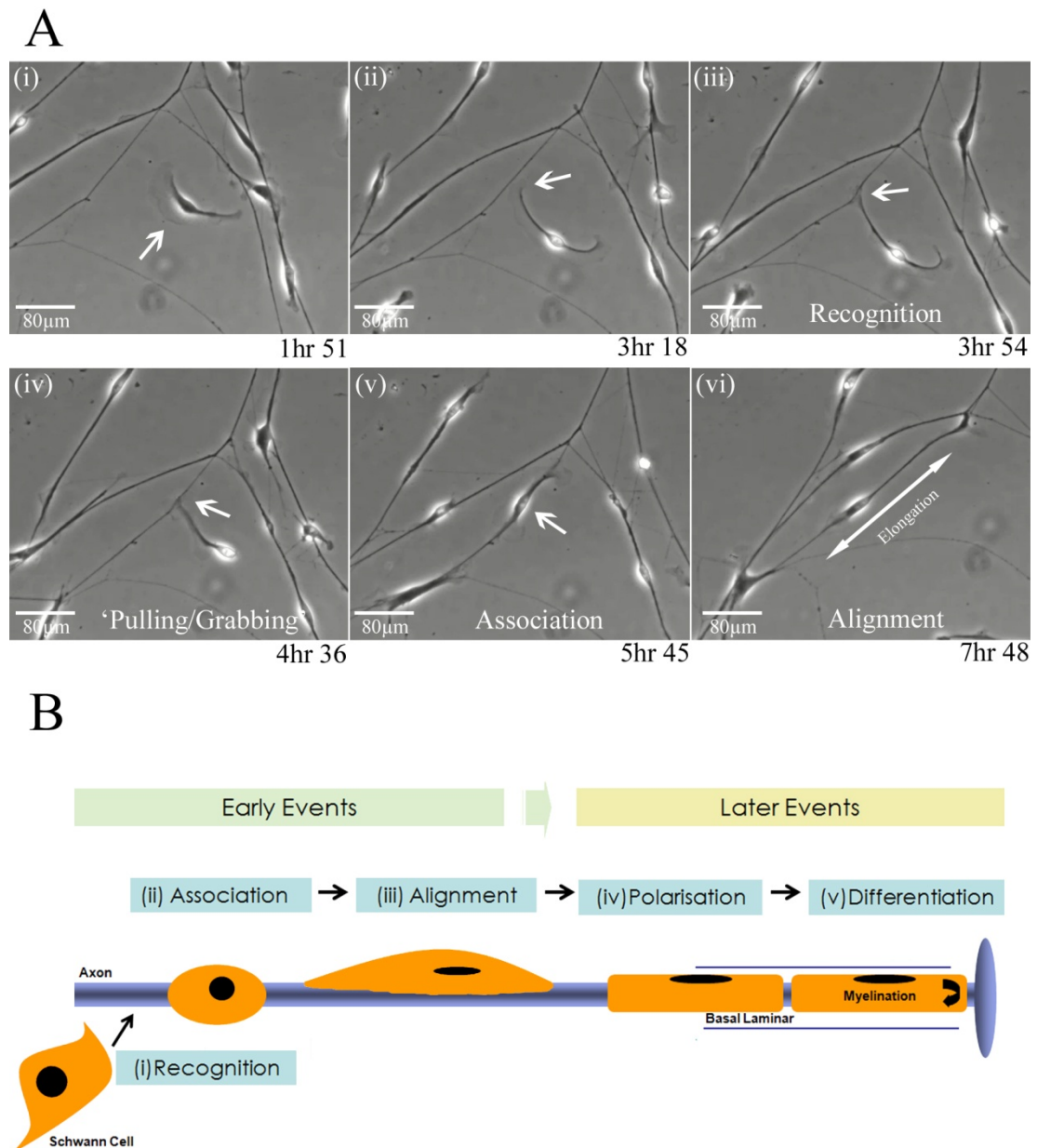


Figure 3.1 Analysis of Schwann cell/axonal interactions. (A) One-day old, rat DRGs were explanted, treated with AraC for 24hrs (to remove endogenous cells) and incubated for 6-7 days to generate axonal cultures. NS cells were seeded onto axons at 2×10^4 cells/DRG and time-lapse analysis performed over 20hrs. Shown is an image sequence from **Video 3.1**, illustrating the early interactions between Schwann cells and axons. The white arrows show a representative Schwann cell/axonal encounter, while Schwann cell alignment and elongation with axons is indicated by the white double-arrows. (B) Schematic model of NS/axonal interactions, where stages i to iii are evidenced from part A, and include: (i) axonal recognition, (ii) association, and (iii) alignment; while later processes, which become evident as the interaction matures, include (iv) polarisation (Chan *et al.*, 2006) and (v) differentiation.

(3) **Alignment:** the Schwann cell elongates its cytoplasm along the length of the axon and aligns its nucleus with the axon. The majority of the Schwann cell then remains associated with the axon, although it is free to move laterally and lamellipodia-like protrusions continue to extrude from the axon.

In addition to these early Schwann cell/axonal interactions, the model also includes later interactions, not evident from the above time-lapse analysis, but which are inferred from previous studies. These include:

(4) **Polarisation:** the cytoplasm and plasma-membrane of the Schwann cell becomes asymmetrically specialised in relation to the axonal membrane. Schwann cell/axonal polarisation was studied by (Chan *et al.*, 2006), who showed that the Schwann cell membrane contacting the axonal membrane becomes polarised through the asymmetric recruitment of partitioning defective (Par)-3. The authors showed that Par-3 mediated polarisation was important for the correct localisation of p75^{NTR} receptors at the Schwann cell/axonal interface and disruption blocked further progression to myelination.

(5) **Myelination:** the Schwann cell differentiates to its final adult phenotype by successively wrapping the axon in a lipid-rich membrane and initiating a program of protein and lipid myelin biosynthesis. In the interests of simplicity, the differentiation to non-myelinated Schwann cells is not discussed in this model. Progression to myelination is highly complex with multiple requirements, which are discussed in detail within the introductory chapter (refer to page 40).

(6) **Mature interactions:** In the absence of nerve trauma or disease, it is highly likely that once the Schwann cell has associated and myelinated an axon, that this partnership is maintained in a stable manner throughout life.

3.3 Schwann cell/axonal recognition

Encounters between cells, either between the same cell-type (homotypic) or between different cell-types (heterotypic), can elicit different responses in both contacting cells. For example, Schwann cell/fibroblast interactions result in mutual repulsion

that leads to their segregation (Dreesmann *et al.*, 2009; Parrinello *et al.*, 2010), while Schwann cell/Schwann cell encounters are typically repulsive, although they become attractive in the presence of fibroblasts (Parrinello *et al.*, 2010). In terms of the complexity of the interaction, encounters between Schwann cells and axons are unusual in that, in addition to exerting an attractive effect, the Schwann cell behaviour, morphology and differentiation are all fundamentally changed by the interaction, ultimately leading to the generation of a complex three-dimensional architecture. This programme of interactions (illustrated in **Figure 3.1B**) is only initiated when a Schwann cell encounters an axon, i.e. other cell-types, for example fibroblasts, will not elicit this response. Therefore, a key question to address is how Schwann cells recognise axons. Recognition is the theoretical first-step in the interaction program. We would expect the failure of this event to have profound consequences for further maturity of the interaction and ultimately in myelination. Despite the likely importance of this step, the mediator(s) of axonal recognition are still unclear.

Evidence from time-lapse microscopy suggests that it is the Schwann cell, rather than the axon, that initiates the interaction programme (**Video 3.1**). However, it is still unclear how Schwann cells locate axons, for instance, whether Schwann cells are directed towards axons by molecular cues/gradients (chemotaxis) or whether they locate axons in a stochastic fashion. In terms of the latter, this could either be achieved passively or by stimulation (to increase cell movement) via molecular factors in the milieu (chemokinesis). A study by Cornejo *et al.* (2010) demonstrated that both GDNF and NRG1 exhibit a chemotactic and chemokinetic effect on the migration of Spl201 cells (an SCP cell-line), while NGF was shown to mediate a chemokinetic affect. In our *in vitro* coculture assays, in which primary adult Schwann cells were seeded in close proximity to axons, the time-lapse video appeared to show non-associated Schwann cells that were migrating in a random, rather than directed, manner (**Video 3.1**). Interestingly, as previously described, Schwann cells often assumed bi- or tri-polar morphologies that resulted from the presence of multiple large cytoplasmic lamellipodia-like protrusions, projecting some distance from the Schwann cell. These structures appeared to be fairly dynamic, capable of extending and collapsing as well as making lateral 'sweeping' movements, thus it is tempting to speculate that these protrusions provide Schwann

cells with a means to maximise the chance of an axonal encounter. Together, these observations suggest that Schwann cells are likely to acquire axons stochastically, although a chemotactic component cannot be dismissed. While the Schwann cell acquires axons for association, the axon grows and elongates, making directional decisions with transient distal structures called growth-cones, in order to migrate through tissue and locate targets for innervation (Doherty *et al.*, 2000; Shi *et al.*, 2010). The directionality of the growth-cone is determined by the interplay between repulsive and attractive molecular-gradients and axonal guidance molecules (Kruger *et al.*, 2005; Rosoff *et al.*, 2004). Interestingly, a study by Seggio *et al.* (2010) showed, in the absence of secondary guidance cues, that DRG-axons would preferentially extend and orientate themselves in alignment with underlying Schwann cells *in vitro*. This is consistent with a post-injury role for Schwann cells as a cellular scaffold that is permissive for axonal regeneration (Parrinello *et al.*, 2010).

3.4 Large-T Schwann cell/axonal interactions

To understand how Schwann cells interact with axons, I initially studied axonal interaction behaviour in the context of a Schwann cell-like clone, in which normal axonal interactions have been lost. The genetic lesion in these cells - referred to as LT derived (LTD) cells – is currently unknown; although they are thought to have arisen, as a sub-population, from otherwise stably expressing LT (the large-T antigen from the SV40 virus) Schwann cells – referred to as LT normal Schwann (LTNS) cells. Furthermore, LTD cells appeared to be morphologically distinct from LTNS and to exhibit an apparent proliferative advantage over LTNS, which may explain how LTD could have become an established monoculture over successive culture passages. In contrast to LTD cells, the genetic component of LTNS cells is well defined. The expression of SV40 LT antigen has been used previously to study p53 and retinoblastoma (Rb) family signalling, as the viral protein specifically inhibits these signalling pathways (Doherty & Freund, 1997; Lloyd *et al.*, 1997). Therefore, LTNS cells are a partially transformed Schwann cell-type, which, in-line with Todaro *et al.* (1964)'s original observations show elevated proliferation compared to normal Schwann cells (Cremona & Lloyd, 2009). Importantly, in contrast to LTD cells, LTNS appeared to interact normally with axons.

In order to quantify the ability of LTD to interact with axons, I decided to compare these cells to NS and LTNS cells in an association assay. To do this, I used the primary *in vitro* Schwann cell/DRG coculture system described previously. DRG-axons were explanted, AraC treated and incubated over 7-days to generate bare axonal cultures. NS, LTNS and LTD cells were then seeded onto DRG-axons at low-density and allowed to interact for eight hours before fixation. Fixed NS/DRG, LTNS/DRG and LTD/DRG cocultures were then coimmunostained with the S100 β Schwann cell marker and the RT97 axonal marker, while nuclei were stained with Hoechst DNA dye (**Figure 3.2Ai-iii**, respectively). These images qualitatively showed that both NS and LTNS strongly interacted and associated with axons. In the NS and LTNS cocultures, the majority of Schwann cells had aligned their cytoplasm with axons and, in many cases, their nuclei were similarly aligned (**3.2Ai-ii**; see white arrows). This was in stark contrast to LTD/DRG cocultures where interaction and association was poor to non-existent even when LTD cells were in close proximity to axons (**3.2Aiii**; see white arrow-heads). Indeed, in many instances where LTD cells contacted axons, the orientation of the cell was out of alignment with the axon, and in some cases perpendicular to the axon, with the cytoplasm often extending over or under axons.

To quantify the extent of the impairment in Schwann cell/axonal interactions we devised an experimental approach and systematic scoring system referred to as a DRG association assay (Parrinello *et al.*, 2008). The assay was designed to reduce experimental bias, ensure fields-of-view were representative and allow for the range of interactions present to be quantified (refer to materials and methods for full details). Fields-of-view were chosen in a systematic manner. The scoring regions were selected one field-of-view in from the periphery of the axonal radiation and subsequent adjacent fields of view were counted, in a clockwise manner, in an arc around the coverslip until approximately 200 interactions per coverslip were scored. This method restricted scoring to regions of low axonal density, where scoring was more reliable, while also providing a high sampling coverage.

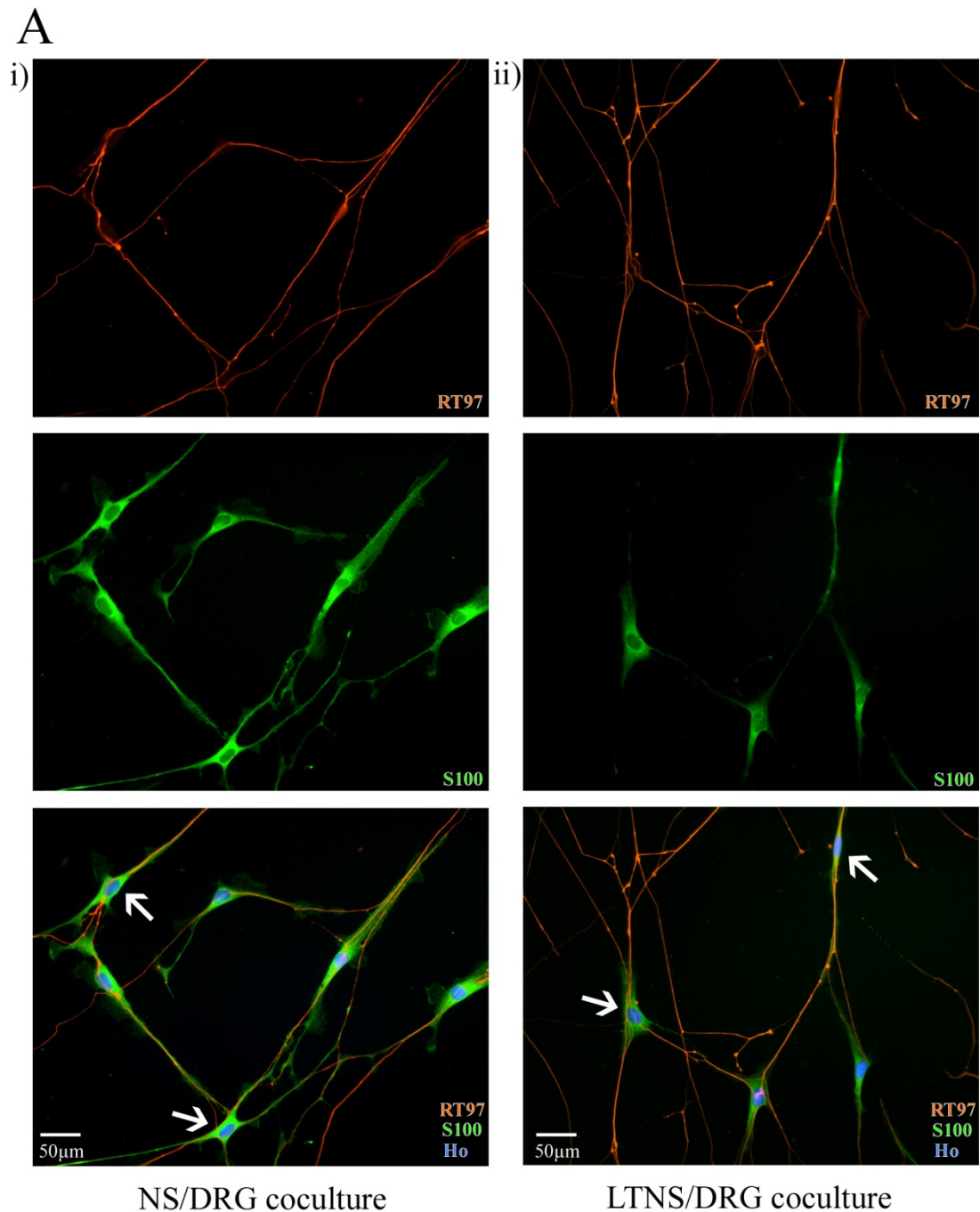
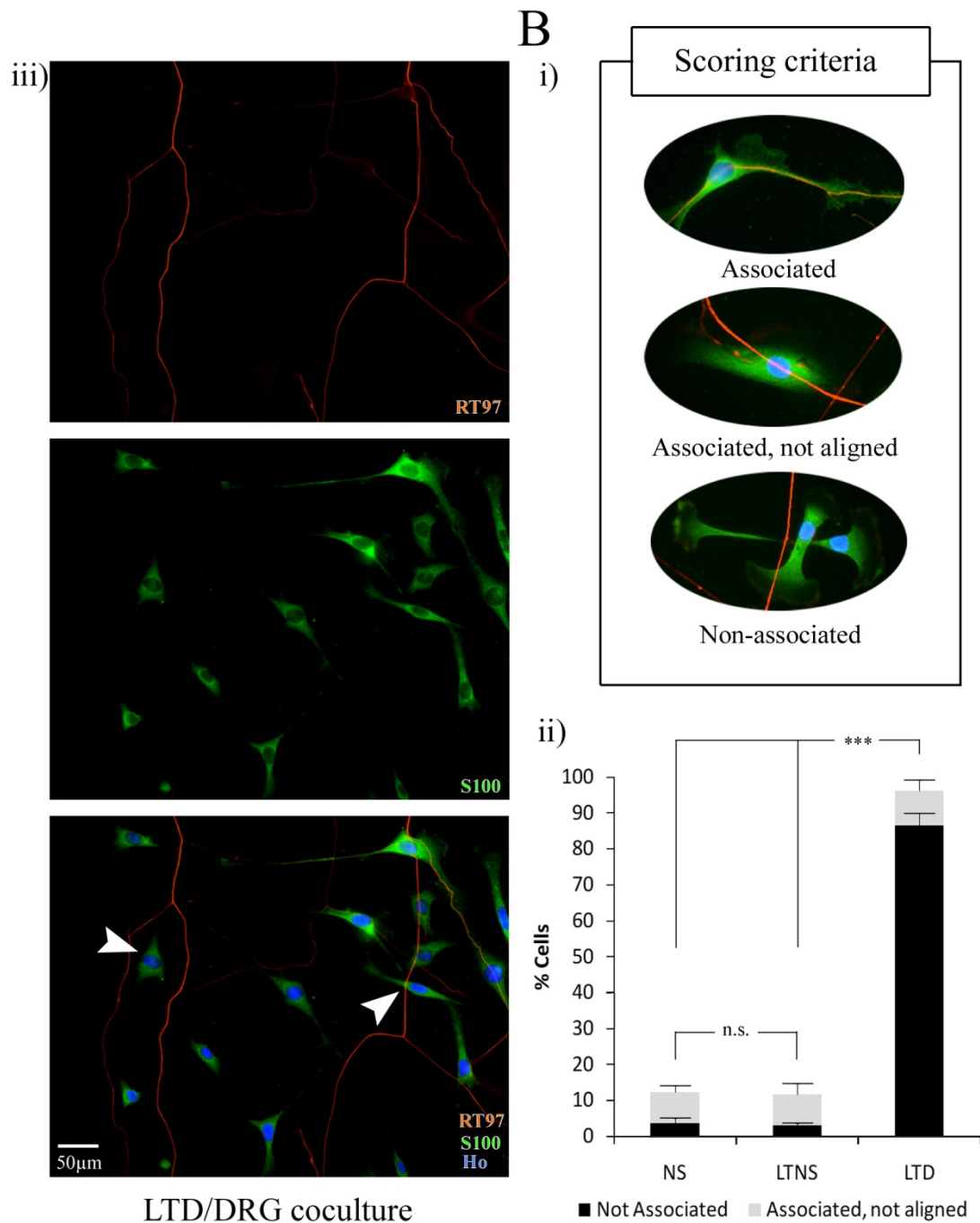


Figure 3.2 LTD/axonal interaction are severely impaired relative to NS and LTNS DRG cocultures. DRGs were incubated as previously, in order to generate axonal cultures, after which NS, LTNS or LTD cells were seeded onto axons and incubated for 8hrs before fixation. (Ai-iii) Epifluorescence of cocultures, coimmunostained for the Schwann marker S100 β (green) and the axonal marker RT97 (red), with cell nuclei labelled by Hoechst (blue). The white arrows show representative examples of tight Schwann cell/axonal interaction, while the white arrow-heads show representative examples of axonal non-interaction.



(B) Quantification of Schwann cell/axonal interactions shown in part Ai-iii. **(i)** Typical examples of three types of cell interaction found in cocultures: Associated, the Schwann cell associates and aligns with the axon; Associated, not aligned, the Schwann cell partly associates but fails to align its cytoplasm with the axon; Non-associated, the Schwann cell does not interact with the axon. **(ii)** The bar-chart shows the percentage of cells that either associated but failed to align with axons (grey), or that failed to associate entirely with axons (black), where bars show S.D. of triplicates ($n > 200$). Statistics given by the two-tailed T-test ($***P < 0.001$; n.s., not-significant). The dataset represents one of three independent experiments that gave similar results.

The scoring criteria used in the assay are illustrated in **Figure 3.2Bi**, which shows the common states of interaction observed:

- (i) **Associated and aligned:** the Schwann cell nucleus is in line with the axon and cytoplasmic protrusions are tightly aligned with the axon (or in some cases multiple axons).
- (ii) **Associated, not aligned:** Schwann cells show indications of axonal recognition with part of the cytoplasm making contact and aligning but the majority of the cell is not aligned.
- (iii) **Non-associated:** Schwann cells display no recognition and either make no axonal contact (even when an axon is in-reach) or the cytoplasm bisects the axon with no evidence of interaction.

The immunofluorescence was scored using a tri-band epifluorescent microscope so that axons (red), Schwann cell cytoplasm (green) and cell nuclei (blue) could be viewed simultaneously. The association data revealed that over 90% of NS and LTNS Schwann cells were associated and aligned with axons, with both cell-types showing comparable levels of association and alignment with axons (**Figure 3.2Bii**). This was in stark contrast to LTD cells, in which less than 10% of cells were associated with axons and of those that had associated, the majority had failed to align with axons. Two important inferences can be drawn from this data. First, LTNS and NS are similarly capable of interacting with axons, thus, the loss of p53 and Rb activity from Schwann cells does not impair Schwann cell/axonal interactions. Second, these results confirmed that LTD, a population derived from LTNS, had acquired a severe axonal interaction deficiency.

3.5 LTD cells are a non-interacting Schwann cell type

To visualise, dynamically, the encounters between LTD cells and axons, I employed time-lapse microscopy, where LTD cells were seeded onto axons at low-density and the cocultures incubated for 20 hours (**Video 3.2**). The analysis showed that LTD cells had completely lost the ability to recognise axons (**Figure 3.3**). LTD cells

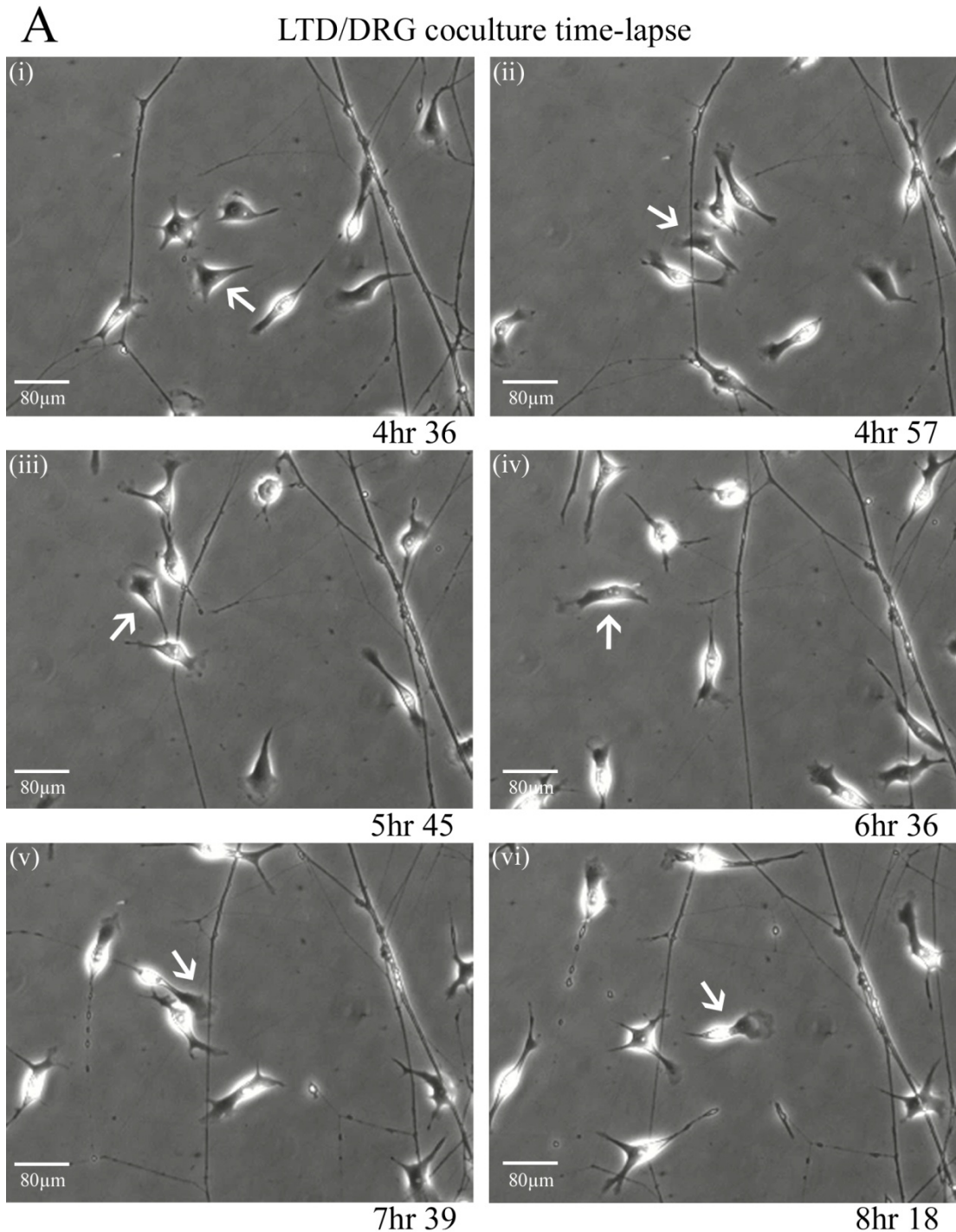


Figure 3.3 Time-lapse analysis confirmed that LTD cells were severely impaired in all aspects of axonal interaction. DRGs were explanted and incubated for 7 days, after which LTD cells were seeded onto axons and time-lapse analysis was performed for 20hrs. (A) Shown is an image sequence, selected from **Video 3.2**, which shows encounters between LTD cells and axons. The white arrows show a representative LTD cell that failed to recognise axons or to initiate classical ‘grabbing/pulling’-behaviour evident from NS/axonal cocultures (Figure 3.1A).

elicited no adhesion to axons and failed to display typical Schwann cell-like behaviours, for instance, the ‘pulling’ and ‘grabbing’ of axons, that normally follow on from an encounter with an axon. Moreover, LTD cells made multiple transgressions over axons with minimal disruption to the conformation of the axonal network. Evidence from this work strongly suggests that LTD cells are lacking either the molecules which mediate Schwann cell/axonal interactions or part of the cellular machinery that responds to this recognition signal.

As LTD cells are a non-interacting Schwann cell clone, they have the potential to provide us with a powerful tool to identify molecules that are important in mediating Schwann cell/axonal interactions. However, it was important to ensure that LTD cells were derived from LTNS and also that they shared a common Schwann cell origin, and had not originated from a rare contaminating ‘non-Schwann’ cell-type, for example, a transformed fibroblast. With this in mind, NS, LTNS and LTD cells as well as perineural fibroblasts were analysed both in terms of their gross morphology and in the expression of key cell-type specific molecular markers. I initially examined the cell-types by phase-contrast microscopy and observed that the morphology of NS, LTNS and LTD cells were all classically bipolar, which is typical of Schwann cells, while conversely, perineural fibroblasts were larger, flattened cells with a distinctly different morphology (**Figure 3.4A**). I next fixed and immunostained confluent monocultures of NS, LTNS, LTD and fibroblasts for the Schwann cell markers, S100 β and P75^{NTR} (**Figure 3.4B**), the fibroblast markers Thy1 and fibronectin (**Figure 3.4C**), and for Large-T SV40 antigen (**Figure 3.4D**). The immunofluorescence confirmed that LTD cells expressed the Schwann cell markers S100 β and p75^{NTR}, while LTD cells did not express the fibroblast markers Thy1 or fibronectin. Importantly, both LTNS and LTD cells expressed the LT SV40 antigen, supporting the assertion that LTD are derived from LTNS. Together, these results suggest that LTD cells do not originate from fibroblasts but instead, most likely originate from Schwann cells.

3.6 Expression analysis between LTNS cells and LTD cells

The evidence I have presented so far suggests firstly, that LTD cells are derived from LTNS and thus share a common Schwann cell origin, and secondly, that they have

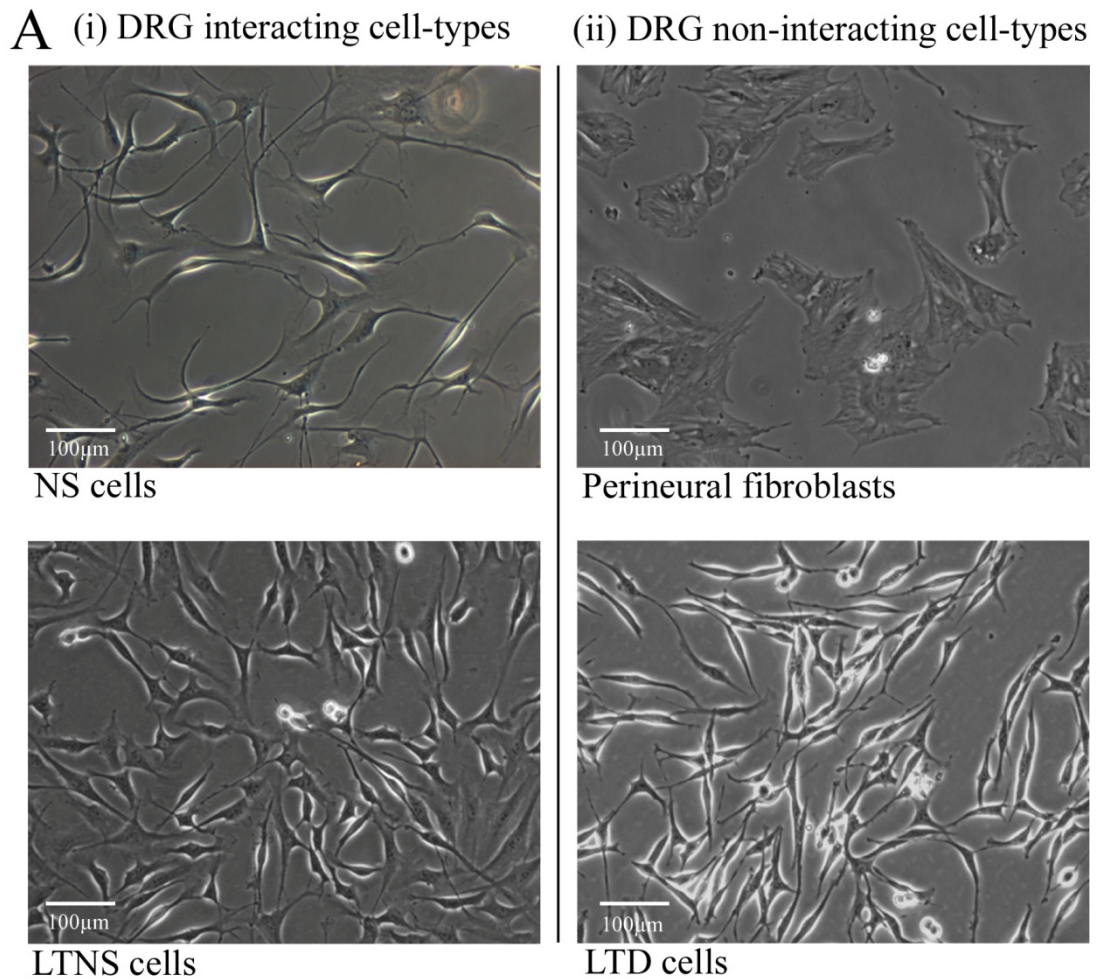
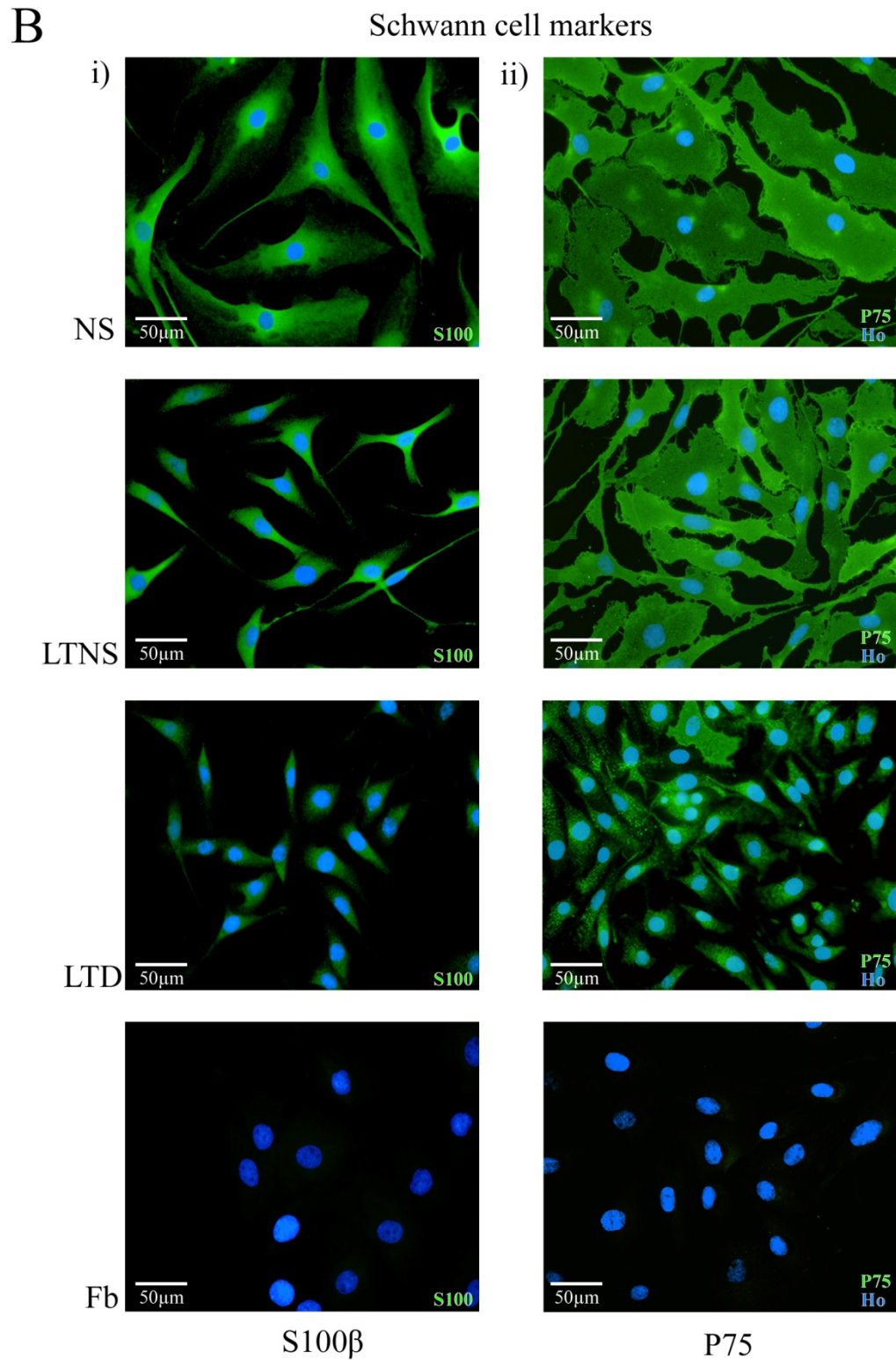
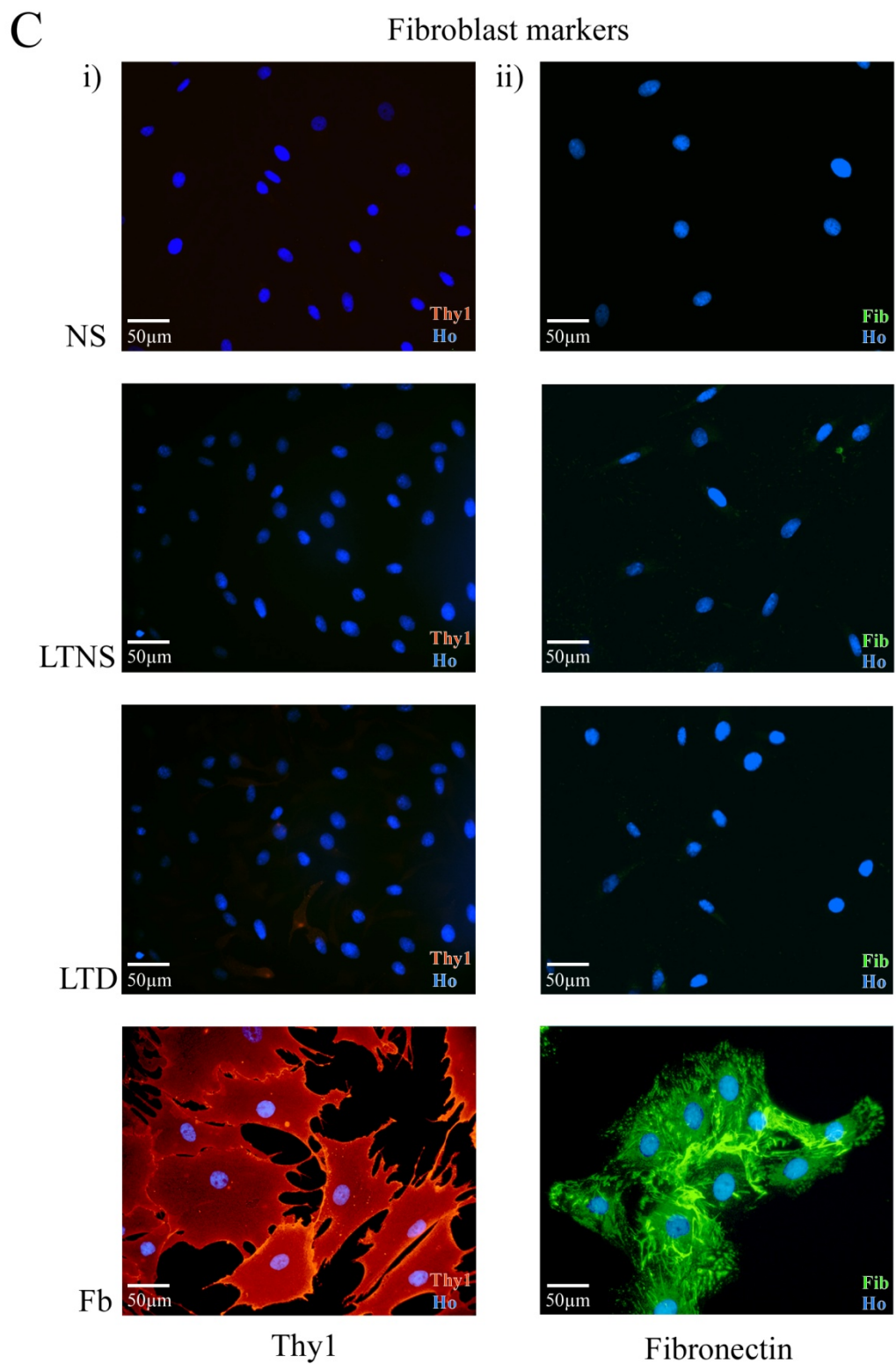


Figure 3.4 Characterisation of cell-types examined in this thesis: - NS, Normal Schwann; LTNS, Large-T Normal Schwann; LTD, Large-T derived and Perineural fibroblasts. (A) Representative phase-contrast images of live sub-confluent monocultures showing (i) axonal interacting cell-types and (ii) axonal non-interacting cell-types.



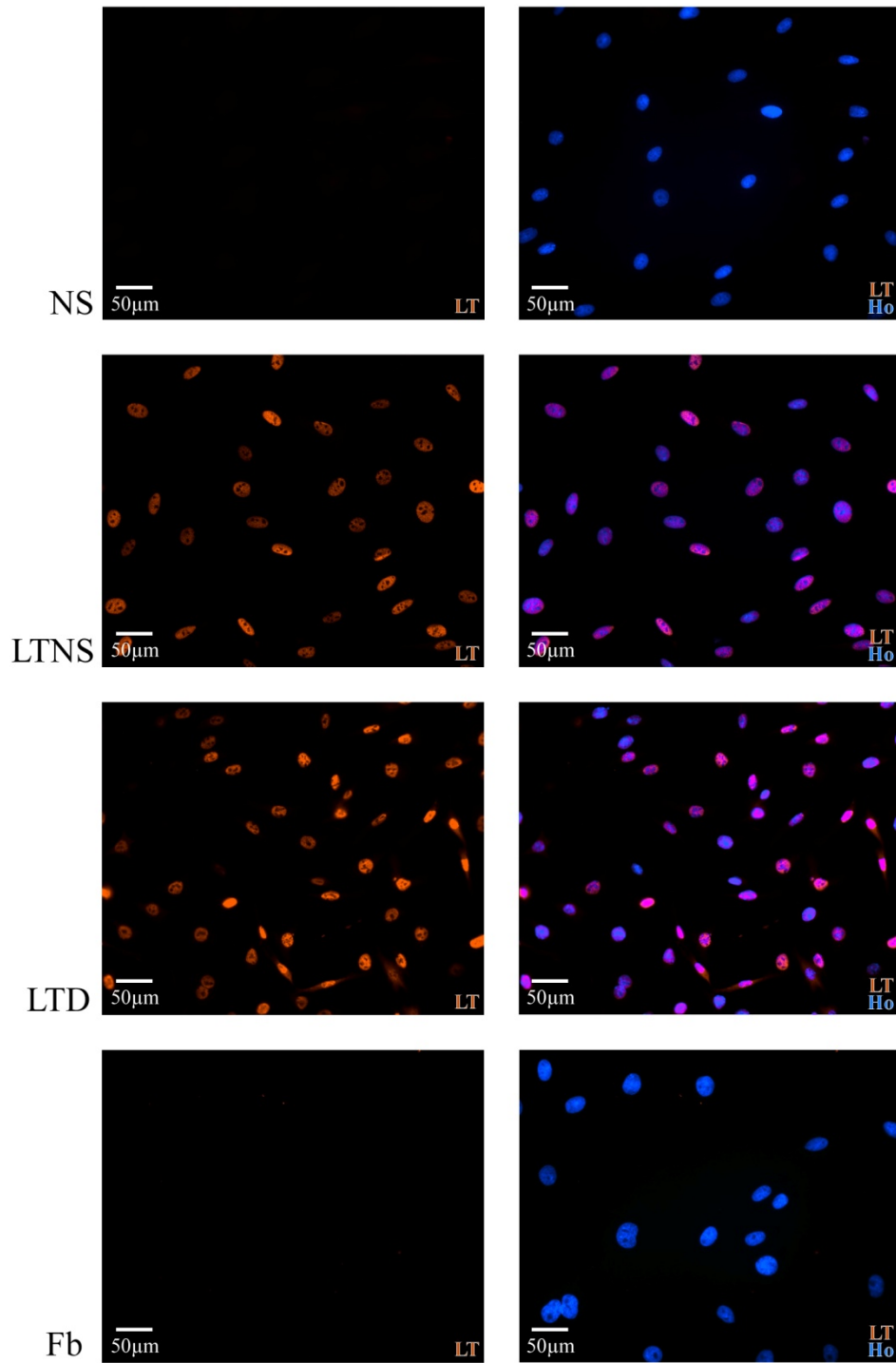
(B) Representative epifluorescence of fixed NS, LTNS, LTD and perineural Fibroblast monocultures immunostained for the Schwann cell markers (i), S100 β (green) and (ii) p75^{NTR} (green), with cell nuclei labelled by Hoechst (blue).



(C) Representative epifluorescence of fixed NS, LTNS, LTD and Fibroblast monocultures immunostained for the fibroblast markers, (i) Thy1 (red) and (ii) fibronectin (green), with cell nuclei labelled by Hoechst (blue).

D

Large-T SV40 antigen



(D) Representative epifluorescence of fixed NS, LTNS, LTD and perineural Fibroblast (Fb) monocultures immunostained for the Large-T SV40 antigen (red), with cell nuclei labelled by Hoechst (blue).

undergone a change which has resulted in their inability to recognise axons. I therefore wanted to determine the nature of the genetic change that had resulted in a loss of axonal interactions.

I reasoned that by identifying the changes in gene expression between LTNS and LTD, we could identify putative mediators of Schwann cell/axonal interactions. We envisaged two possible scenarios: (1) the loss of axonal interactions had resulted from a mutation in a single critical gene for interaction or alternatively, (2) a mutation in a key transcriptional regulator had resulted in global changes in transcription that had altered the cell state and compromised the interaction program. In order to test these two different hypothesises I conducted a cDNA differential expression microarray between LTNS cells and LTD cells. We decided to use an Affymetrix Rat 230-2 GeneChip array because this platform was considered to provide the most comprehensive coverage of the rat genome at the time⁷. In addition, we had previously used this format successfully in our laboratory (Parrinello *et al.*, 2008).

3.6.1 Array specification

The Affymetrix Rat 230-2 GeneChip is a genome-wide rat transcription (cDNA) array. It has 31,042 probesets designed against 30,000 sequences (28,000 of which were reported by the manufacture to be well-substantiated genes). According to the manufacture's protocol, probesets were designed from sequence data held by various bioinformatics depositories, which included the NIH genetic sequence database (GenBank)⁸, the Expressed Sequence Tagged database (dbEST) and the Reference Sequence (RefSeq) database. Sequences were further refined following cross-reference to the publically available draft rat genome sequence⁹ (Gibbs *et al.*, 2004). The 230-2 array combines probesets from two previous affymetrix GeneChip arrays (Rat Expression 230A and 230B) to generate a single high density oligonucleotides array with a concentration (detection) sensitivity of 1:100,000, which corresponds to approximately 1.5pM or a few transcripts per cell (Göhlmann & Talloen, 2009, p.40).

⁷ Affymetrix, Datasheet #701611 Rev. 1, 2004

⁸ National Center for Biotechnology Information ; <http://www.ncbi.nlm.nih.gov>

⁹ Baylor College of Medicine Human Genome Sequencing Center, June 2002

3.6.2 LTNS verses LTD expression microarray

The microarray analysis is summarised in **Figure 3.5A**. Total RNA was collected from sub-confluent plates of low-passage, proliferating LTNS and LTD Schwann cell monocultures and replicate samples were collected three days later. Total RNA was purified and a sample subjected to agarose electrophoretic analysis and spectrophotometry to determine the quality of RNA. As shown in **Figure 3.5B**, the presence of two distinct bands (representing the 18S and 28S ribosomal RNA) is indicative of low RNA degradation and the absence of further bands indicated that the RNA samples were free from DNA contamination, while the 260/280 absorbance was within the range of 1.8-2.0 (data not shown), indicative of low-protein contamination. Five micrograms of RNA from each condition were then sent to the Paterson Institute Microarray Service¹⁰ for GeneChip analysis in collaboration with Gill Newton. The raw data output was visualised in **Figure 3.5C**, which showed qualitative similarities between the four GeneChips analysed. This showed that there were no gross differences in the manufacturing process between the GeneChip arrays. Importantly, although vertical striations can be observed, this was mirrored across all GeneChips.

3.6.3 Analysis of quality control metrics

Prior to conducting further analysis, I examined a number of quality control metrics in order to confirm the quality of the GeneChips and quantify the variation attributed to technical rather than biological factors. The Affymetrix Rat 230-2 array structure incorporates a number of internal controls. These include: (1) hybridisation controls, (2) house-keeping/control genes, (3) poly-A controls and (4) normalisation controls. In addition, each probeset is composed of multiple probe-pairs that independently measure the same transcript. The quality control metrics were calculated automatically using Affymetrix Microarray Suite (MAS) 5.0 software, and are summarised in **Figure 3.6** (refer to Affymetrix manual¹¹ and glossary¹² for further details of these metrics).

¹⁰ The Patterson Institute for Cancer Research, Manchester

¹¹ GeneChip Expression Analysis: Data Analysis Fundamentals (www.affymetrix.com)

¹² Affymetrix report file glossary: MAS 5.0 Documentation (www.affymetrix.com)

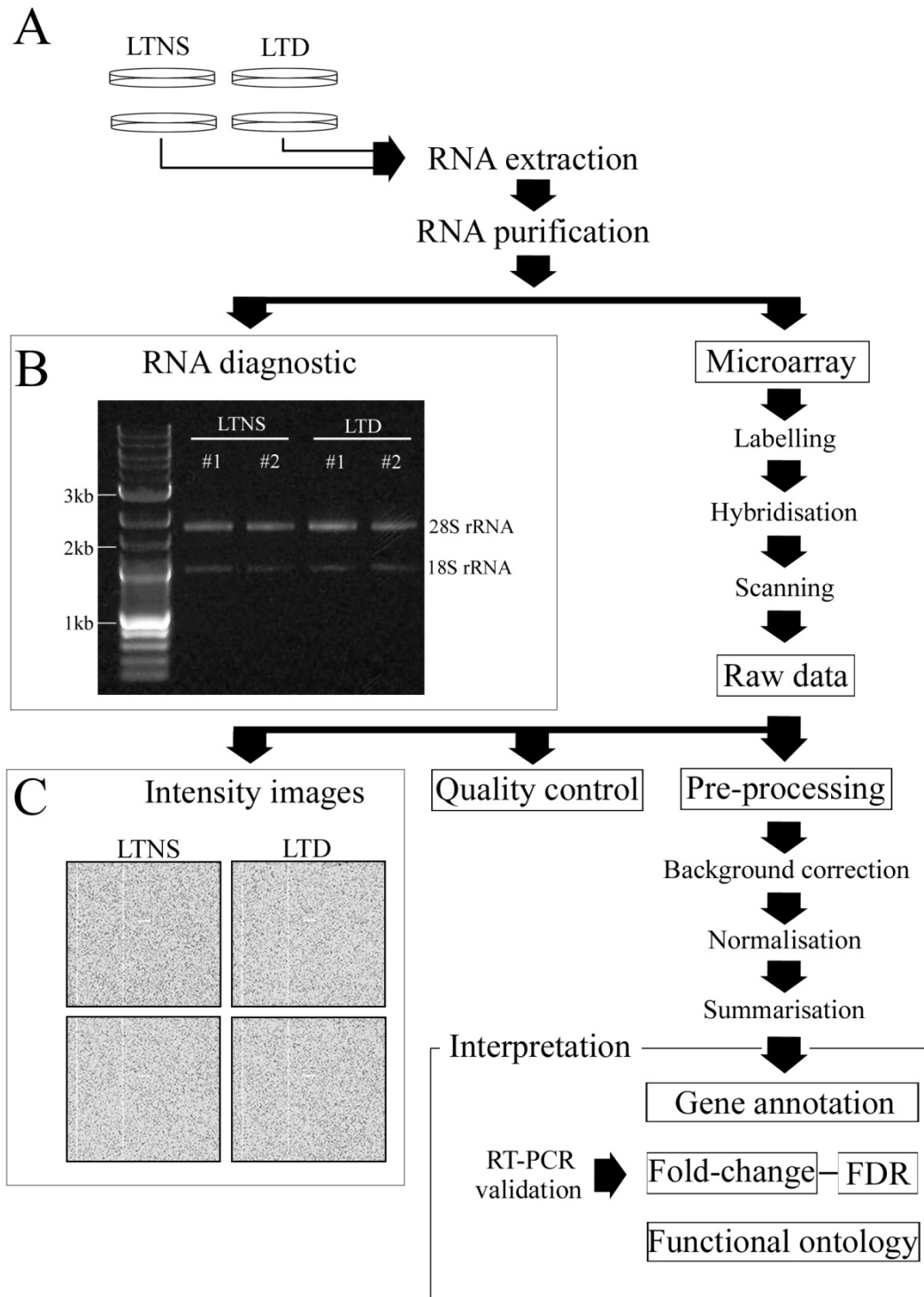


Figure 3.5 Schematic illustration showing the stages involved in microarray processing. (A) Summary of the experimental procedures of RNA processing and microarray analysis. FDR; false discovery rate (B) Electrophoretic analysis of RNA samples. (C) Graphical representations of the raw expression data from replicate GeneChips of LTNS and LTD.

The raw fluorescence intensity, as shown for each GeneChip in **Figure 3.6A**, is a measure of the background noise. It is calculated by subtracting the mean central intensity from the mean peripheral intensity for each locus (spot) on the array, giving the pixel-to-pixel variation. **Figure 3.6B** quantifies the average background intensity, which measures auto-fluorescence within the GeneChip and is derived from the mis-match (MM) probe data. Both these metrics can be heavily influenced by technical discrepancies in sample preparation and/or scanner electronics. The data showed that all four GeneChips had similar levels of auto-fluorescence and pixel variation, suggesting that they had been processed in a similar and comparable way.

The hybridisation efficiency of probes (irrespective of sample RNA) was examined using hybridisation control transcripts. **Figure 3.6C** charts the signal intensities obtained after addition, into the hybridisation mixture, of known, graduated concentrations of *BioB*, *BioC*, *BioD* and *cre* (at concentrations of 1.5pM, 5pM, 25pM and 100pM respectively). The data was plotted on a relative scale with BioB set to the array resolution (1:100,000) with the remaining controls plotted relative to this. The data, as shown in **Figure 3.6C**, accurately reflected the intensities expected given the initial concentrations of ‘spiked’ controls. Another metric used to evaluate the technical procedure (especially the efficacy of reverse transcription to generate cDNA and the process of biotin labelling to generate cRNA), are the use of control genes. The rat 230-2 array incorporates pairs of control probesets for β -actin and GAPDH that are specifically designed to independently target the 3-prime and 5-prime ends of the two ‘housekeeping’ genes. Due to an inherent three-prime bias in cDNA arrays (Cui & Loraine, 2009), the expected signal intensity ratio of the three prime probeset to the five-prime probeset should, as shown in our data (**Figure 3.6D**), be greater than one but not exceed three.

I next examined the scaling and normalisation process, which allow comparisons to be made between the four separate GeneChips. In this analysis, the data was subjected to normalisation (scaling) using the default Affymetrix MAS 5.0 algorithm. The graph shows, for each GeneChip, the scaling factor that would be required to achieve equality of total intensity means. For our data, the maximum scaling factor required to achieve normalisation was 1.5, which compares favourably against the accepted upper-limit threshold of three-fold (**Figure 3.6E**). Similarly,

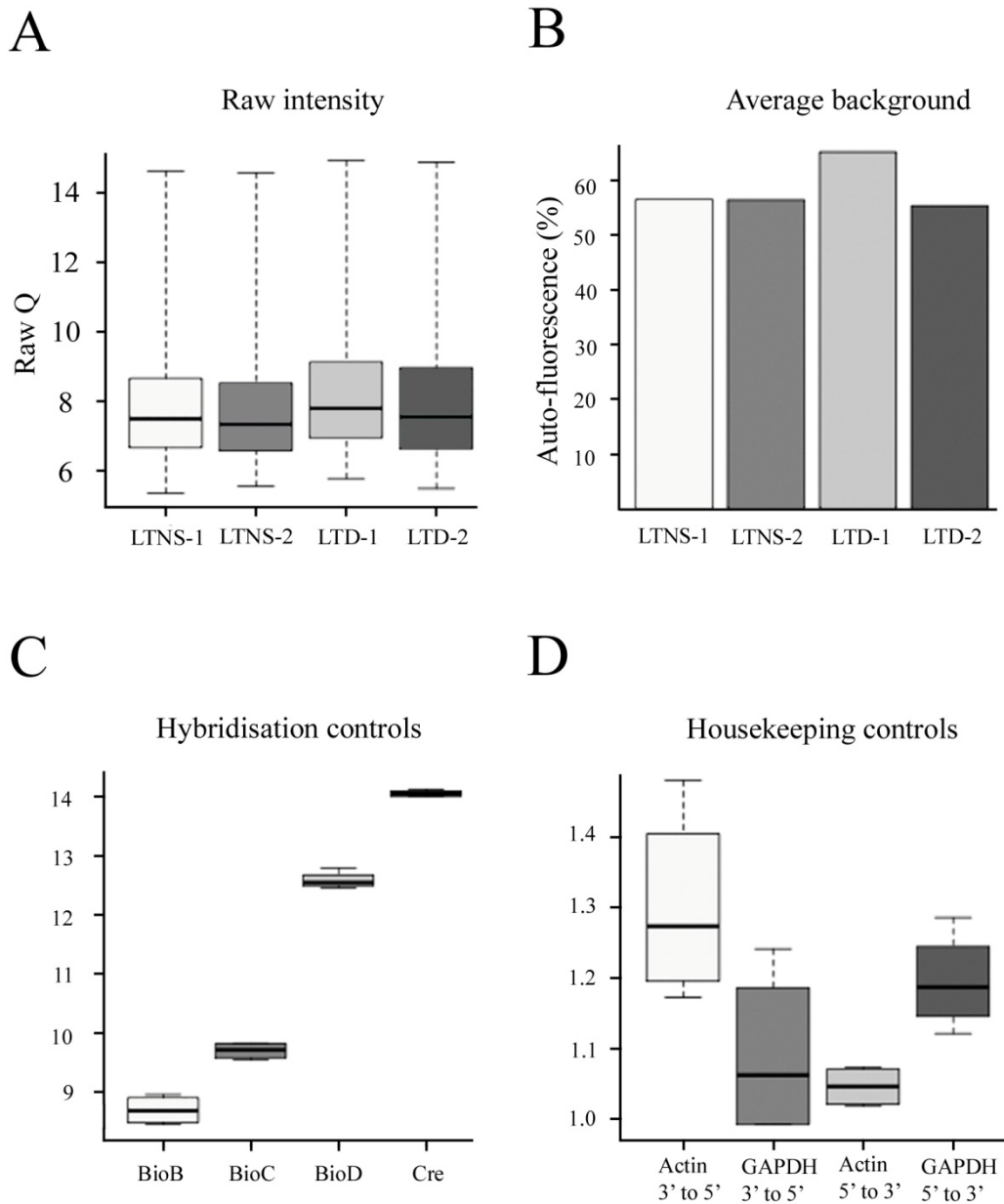
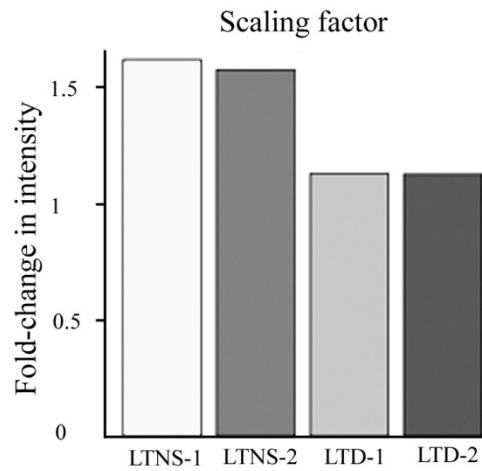
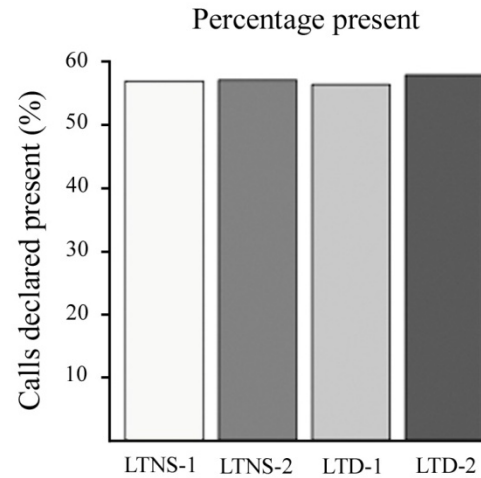
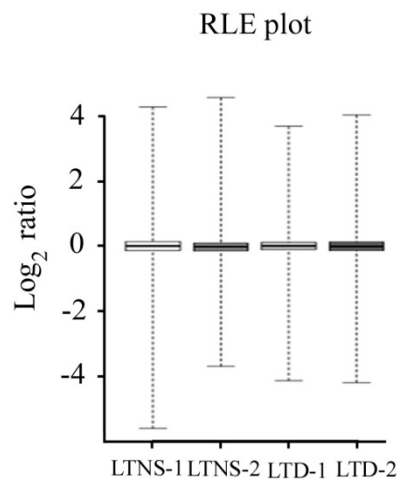
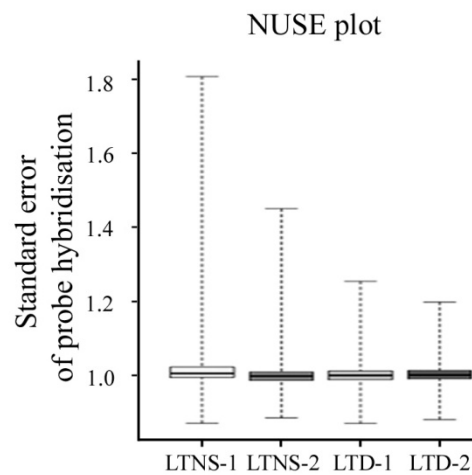
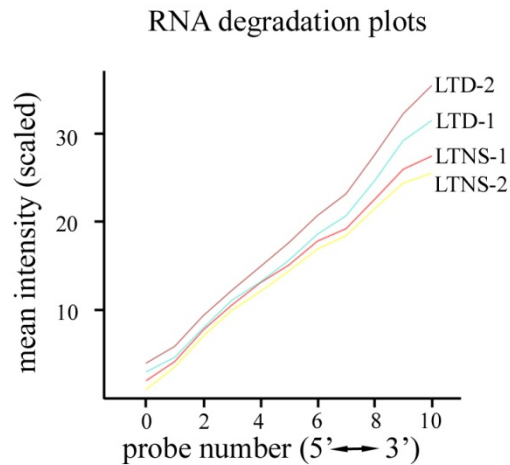


Figure 3.6 Affymetrix quality control metrics. (A) Raw intensity (RawQ); a measure of pixel-to-pixel variation used to quantify the signal attributed to ‘noise’ in the GeneChip. This is calculated by subtracting the mean central intensity from the mean peripheral intensity for each locus (spot) on the array. (B) Average background; a measure of non-specific fluorescence. This is calculated from the mismatch probes. (C) Hybridisation controls; a measure of hybridisation efficiency. Four test RNAs of known concentration (BioB, BioC, BioD and Cre) are ‘spiked’ into the hybridisation mix and their detection is analysed to determine if the ratio of intensities reflects the initial ‘spiked’ concentration. (D) Control genes; a measure of RNA and assay quality. The graph shows a ratio of intensities for two housekeeping genes (Actin and GAPDH), where the three-prime hybridisation intensity and the five-prime hybridisation intensity are plotted as a ratio.

E**F****G****H**

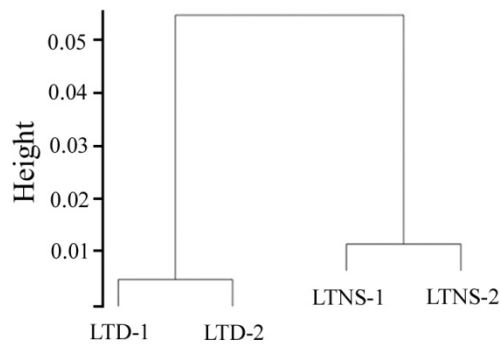
(**E**) Percentage present; a measure of the ability of the array to detect significant probe hybridisation events. (**F**) Scaling Factor; a measure of the variance in the mean intensities between GeneChips. The graph shows the magnitude of the adjustment (scaling) factor required to normalise the GeneChip data to allow direct comparisons between GeneChips. (**G**) Relative log expression (RLE) plot; a measure of the deviation in gene expression from the median expression value for all genes across all arrays. (**H**) Normalised Unscaled Standard Error (NUSE); a measure of the variance in standard error estimates from expression intensities across all arrays. The values are standardised so that the average SE estimate for a gene is one.

I



J

Hierarchical cluster dendrogram



(I) mRNA degradation plot; measures the mRNA degradation as an average across all probesets. This was calculated by plotting the signal intensity against the rank order at which the probes hybridised along the DNA, with the most five-prime probe assigned a zero rank. Because mRNA is degraded from the five-prime end first, the slope of the line at this end is used to gauge degradation rates. (J) Hierarchical cluster dendrogram; measures relatedness between samples (clusters) based on a defined similarity matrix. Clusters in the same branch are considered more similar than clusters derived nearer the root of the tree.

the ‘percentage present’ metric is a useful indicator of the specificity of probe hybridisation. The graph in **Figure 3.6F** shows the total percentage of perfect match (PM) probe hybridisations that are considered statistically significant when compared with their mis-match (MM) probe pair. This metric should be comparable across arrays, as observed in our data, in which the percentage present is about 60%.

The hybridisation quality can also be measured by the Relative Log Expression (RLE) and the Normalised Unscaled Standard Error (NUSE). The RLE plot was calculated by determining the deviation in gene expression for a gene from the median expression value for that gene across all arrays for each gene in the array. The values are shown in log scale and should, as shown by our data in **Figure 3.6G**, be approximately zero with equal chip-wise distribution. The NUSE plot is a similar metric, which shows the distribution of standard error (SE) estimates calculated for each gene across all arrays. The data is ‘standardised’ so that the median standard error of a gene across all arrays is set to one, with the box showing the mean, upper and lower quartiles and the bars showing the range. In our data, this metric was comparable across arrays, with values close to one (**Figure 3.6H**).

I next assessed the quality of sample mRNA by analysing the RNA degradation plot, which can be derived from the fact that RNA degradation preferentially occurs at the 5-prime end of mRNA transcripts. Because there are a number of probes for each target gene, the target sequences can be ranked from the five-prime end of the transcript to the three-prime end. Thus, if five-prime mRNA degradation occurs, the extent of this can be measure by plotting the relative mean intensities (on the y-axis) against the relative position of probes for a probeset (on the x-axis). The gradient of the line towards the five-prime end of the graph indicates the degree of mRNA degradation. The acceptable range is considered to be between 0.5 and 1.7. Our data showed some degree of five-prime mRNA degradation but importantly, this was comparable across all four GeneChips (**Figure 3.6I**).

Finally, **Figure 3.6J**, shows a hierarchical clustering dendrogram, which measures the relatedness of samples (clusters) based on a defined similarity matrix. Clusters in the same branch are considered more similar than clusters derived from branches nearer the root of the tree. As expected, experimental replicates of both LTNS and

LTD were observed to cluster together, while replicate pairs were delineated to different branches of the tree. As expected, this implies that the biological variation between test samples of LTD and LTNS was significantly greater than that within replicates.

In conclusion, the quality control metrics revealed no significant issues in relation to the technical procedures or RNA sample quality. I therefore proceeded to pre-process the raw intensity data so that differential expression could be determined.

3.6.4 Pre-processing of microarray data

The initial data processing was conducted in collaboration with Richard Mitter¹³. The raw Affymetrix data was first pre-processed in order to generate an expression matrix using the Robust Multi-array Average (RMA) algorithm (Irizarry *et al.*, 2003a) as implemented in the Bioconductor R package. The RMA method, which exclusively uses the perfect-match (PM) probe data, was chosen because it was shown to have an advantage over competitors, i.e. Affymetrix MAS 5.0¹⁴ or dChip (Li & Wong, 2001), in terms of specificity, consistency and sensitivity (Irizarry *et al.*, 2003b). The raw intensity values were background corrected, to remove the signal attributed to non-specific binding of fluorophore, and log₂ transformed to ensure the continuous distribution of data, which was required for later statistical steps. The data was quantile normalized in order to correct for systemic technical differences and importantly, to allow for meaningful chip-wise comparisons of expression data. A scaling factor was calculated and the global intensities were adjusted so that all GeneChips had a similar mean intensity. A linear model, derived by the ‘median polish’ algorithm (Irizarry *et al.*, 2003a), was then transposed over the normalised data in order to summarise the probe level data into a single expression measure for each probeset on each GeneChip array.

¹³ London Research Institute (LRI) Bioinformatics & Biostatistics group

¹⁴ Affymetrix (2001) Microarray Suite User Guide, V5.;
www.affymetrix.com/support/technical/manuals.affx.

3.6.5 Calculating differential gene expression

Differential gene expression was assessed between replicate groups by calculating the expression ratio, which was represented as a Log_2 fold-change. Each expression ratio was attributed a p-value, as calculated by the empirical Bayes T-test, which describes the statistical confidence in that given expression ratio. An FDR (false discovery rate) was then calculated for each expression ratio. This is an adjustment to the p-value necessary to control the family-wise error rate caused by multiple simultaneous statistical testing that would otherwise lead to unacceptably high type 1 errors (Chen *et al.*, 2010). The FDR is the proportion of false positives among all the probesets where the null-hypothesis was initially rejected, i.e. genes identified as being differentially expressed. This statistic provided a good overall compromise between false positive and false negative error rates (Cui & Churchill, 2003).

3.6.6 Gene annotation, analysis and secondary processing

The probeset-level summarisation was processed using Affymetrix NetAffx¹⁵ software in conjunction with the March 2009 Rat 230-2 Affymetrix GeneChip definition file (CDF), in order to assign the summarised intensity values for probesets to their corresponding gene targets on the rat genome. The full dataset (**Dataset A** on the CD-ROM), which contained 31,099 probesets, was then subjected to secondary processing, outlined in **Figure 3.7**, which illustrates the steps taken to refine the dataset from the full redundant probeset-level dataset to a final dataset of unique genes with significant and meaningful expression fold-change (described in detail below). As shown in **Figure 3.7**, the dataset for each stage of this process is depicted in the central column of boxes, which correspond to the datasets held on the accompanying CD-ROM. Initial analysis of the full dataset revealed that 20,220 probesets, approximately 65% of the total list, could be annotated and assigned to known rat genes, while 35% of the probes had no gene assignments (**Table 3.1**).

¹⁵ www.affymetrix.com/analysis/netaffx

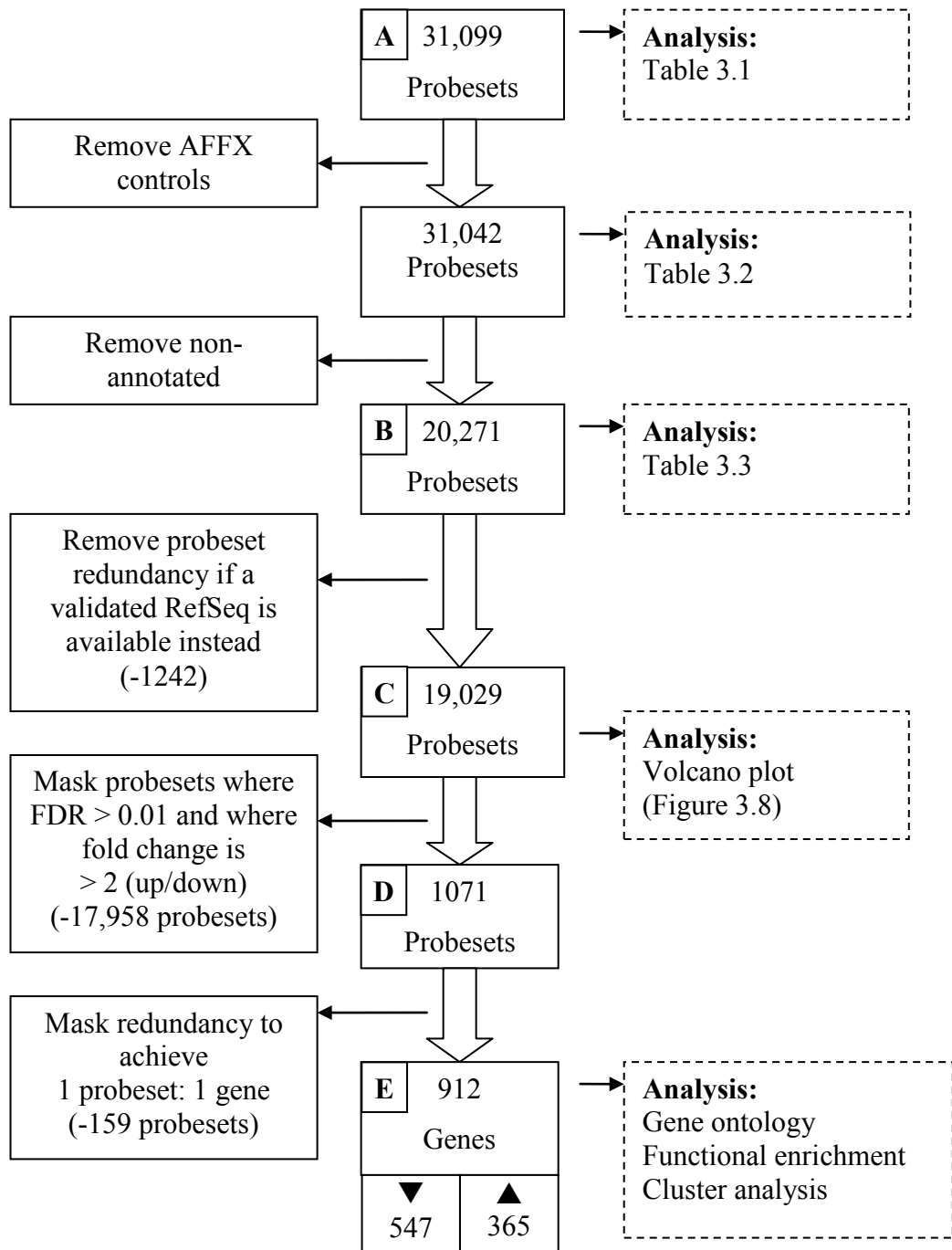


Figure 3.7 Schematic of analysis involved in secondary data processing. The left column shows processes, the middle column shows outcome and the right column shows analysis. Refer to CD-ROM for the Datasets, which are denoted by letters in the small-boxes (middle-column).

Table 3.1 Gross analysis of probesets comprising the Rat 230-2 microarray

Component	Value
Sequences with annotation	20,220 (65%)
Sequences without annotation	10,822 (35%)
AFFX- Control probesets	57
Total Probe Sets	31,099

I next examined the Rat 230-2 probesets in more detail because I wanted to fully understand the source information used by Affymetrix in their design, and also to establish the relationship between probesets and the genes they represent. As discussed previously, the Rat 230-2 probesets were designed using submissions from multiple data depositories/sources, i.e. RefSeq, GenBank, EMBL & DDBJ submissions, which, for example can include data derived from validated unique gene entries, expression-sequence tags (EST)s or journal submissions. The list is degenerate as more than one probeset (that could be designed from different sources) can target the same gene. In order to analyse this information in my data, I cross-referenced the accession numbers returned for each probeset from the annotation, with a list of accession prefix definitions published on the NCBI website¹⁶, to identify the data source used in the design of probesets (**Table 3.2**; see also **Appendix Table B** for the full list). This information shows that the design of the probesets for the Rat 230-2 array was derived predominantly from EST databases with just over 10% of probesets designed from validated RefSeq entries. Unsurprisingly, nearly 100% of the non-annotated list was derived from EST databases. The annotated portion of the dataset was composed of 16% validated RefSeq entries with 77% composed from EST databases. Although, the importance of the non-annotated list should not be underestimated, i.e. as a potential means to reveal novel but uncharacterised candidates, the constraints of this project would not allow sufficient time for the detailed investigation required. On this basis, I decided to exclusively focus all further analysis on the annotated portion of the list (**Dataset B**).

¹⁶ www.ncbi.nlm.nih.gov/Sequin/acc.html, accessed: 2011

Table 3.2 Summary of the types of source data used in the design of probesets for the Rat 230-2 GeneChip

Resource	Entire Dataset	Non-annotated dataset only		Annotated dataset only	
		%		%	%
RefSeq	3170	10.21	5*	0.05	15.61
EST	26287	84.68	10728	99.60	76.75
Direct subs	1580	5.09	37	0.34	7.61
Journal scanning	5	0.02	1	0.01	0.02
Total	31042	100	10711	100	100

*RefSeq, referenced sequences; EST, expressed sequence-tags; Direct subs, direct submissions. *ReqSeq were investigated and subsequently found to have redundant/erroneous accession numbers. (see Appendix Table B for full list).*

Table 3.3 highlights some important additional parameters for the annotated dataset. It shows that there are 6246 more probesets than unique gene targets. This redundancy is either due to multiple probesets for a single gene designed from the same source, i.e. the probeset IDs share a common accession number (310 cases), or from different sources, i.e. the probeset IDs have different accession numbers but target the same gene (5936 cases). Nearly half the genes on the array were detected with just one probeset, with just over 2000 of these detected with probesets designed using validated, reference sequences (RefSeq).

Table 3.3 Analysis of data from the annotated gene list

Parameter	Value	%
Total number of annotated probesets	20,271	
Number of probesets designed from unique sources, i.e. the number of different GenBank accession numbers)	19,961	
Number of unique gene targets	14,025	
Number of non-redundant probesets (one probeset to one gene relationships)	9,707*	47.8

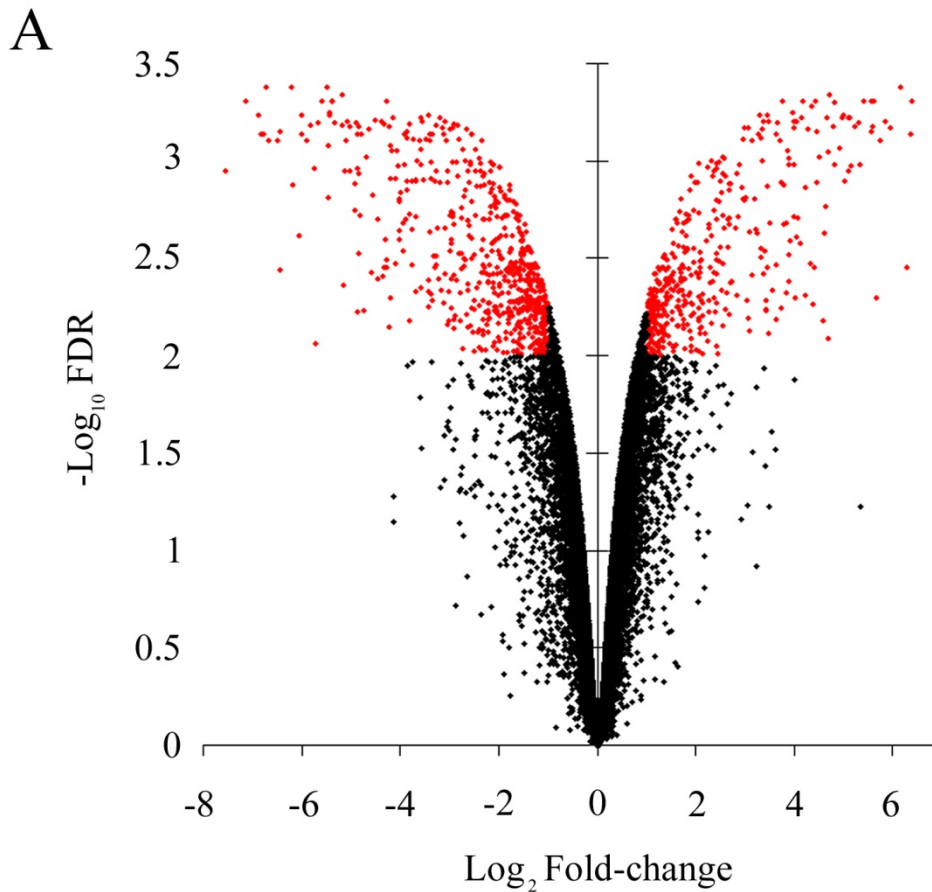
** Includes 2,212 genes represented by RefSeq designed probesets*

At this stage in the data processing, I decided to reduce redundancy from the dataset by preferentially removing duplicated probesets designed from ESTs in cases where a RefSeq designed probeset was already available. I did this because RefSeq designed probesets are derived from intact mRNA that have been validated to a unique gene, whereas ESTs are derived from mRNA fragments in which, by definition, their origin is less reliable compared to the former (Nagaraj *et al.*, 2007). Thus, in this way I gave precedence to RefSeq designed probesets over EST designed probesets. Importantly, duplicate probesets were not removed in cases where there were no RefSeq designed probesets available for a gene. Following this analysis, the refined **Dataset C** contained 19,029 probesets.

I next examined the data using a volcano plot, in order to examine the distribution and magnitude of significant expression changes. The negative Log_{10} of the FDR (on the Y-axis) was plotted against the Log_2 fold-change (on the X-axis) (**Figure 3.8**). I selected a fold-change cut-off threshold of two and a nominal FDR cut-off of less than or equal to 0.1, shown by the red markers. This graphical view of the significant expression change showed that surprisingly large numbers of genes were transcriptionally dysregulated in LTD cells, which was symmetrically distributed in terms of genes that were up or down regulated in LTD cells. I next devised a list with just the significant probesets with expression differentials that were greater than two-fold, i.e. the probesets marked in red (**Dataset D**). At this point I masked duplication by considering only probesets with the lowest FDR in order to generate a final list of uniquely dysregulated genes (**Dataset E**), of which 547 were significantly down-regulated and 365 were significantly up-regulated compared to LTNS (the top 120 dysregulated genes are summarised in **Appendix Table A**, parts i and ii respectively; refer to the accompanying CD-ROM for the full list).

3.6.7 Functional gene annotation, cluster and enrichment analysis

The final gene-list (**Dataset E**) contains 912 genes whose expression had become significantly altered (greater than two-fold) between LTNS (interacting) and LTD (non-interacting) cells. Thus, the scope of genetic change was large with no single obvious candidate identified. In order to uncover biologically meaningful trends in



- Included ($\text{FDR} < 0.01$ & $\text{FC} > 2$ up/down)
- Excluded ($\text{FDR} > 0.01$ & $\text{FC} < 2$ up/down)

Figure 3.8 LTD cells have globally dysregulated gene expression. (A) The volcano (scatter) graph shows the relationship between the negative Log_{10} of false discovery rate (FDR) and the Log_2 of the fold-change, thus illustrating the magnitude of expression differences that are significant. The red markers show the probesets where FDR is less than 0.01 and fold-change is greater than 2 (up or down), while the black markers show the non-significant and/or below 2-fold probesets that, for the purposes of further analysis, were excluded from the dataset.

this data, which might explain the overall transition from LTNS to an LTD phenotype, I conducted functional enrichment analysis. The finalised, non-redundant gene list was functionally annotated using DAVID¹⁷, a web-based tool for functional gene annotation and enrichment analysis (Huang *et al.*, 2009). Functional annotation was derived from at least 11 different gene ontology resources including the Gene Ontology (GO) project¹⁸ (specifically: biological pathway, BP; cellular component, CC & molecular function, MF) as well as KEGG¹⁹ terms (see **Appendix Table B** for the full list). The annotated gene-list contained multiple annotation terms for each gene, which reflects their multiple functions and the myriad ways in which they can be functionally classified. Enrichment analysis is a bioinformatics tool for providing statistical confidence in the discovery of functional patterns in microarray data. The gene-list (**Dataset E**) was submitted to DAVID for functional annotation enrichment analysis, which statistically highlights the most over-represented biological annotation in the dataset. The data output (**Dataset F**) from this analysis is statistically organised into clusters which are ranked by an enrichment score, reflecting the biological relevance of each cluster within the submitted gene list. The analysis was conducted using default DAVID parameters for statistical enrichment; it showed that 261 clusters of functionally related ontology terms were statistically enriched within the gene list when compared to the *Rattus norvegicus* background. The first five most enriched annotation clusters are shown in **Table 3.4** (the first 12 clusters are shown in **Appendix Table D**, while the full list is included in **Dataset F** of the CD-ROM).

Table 3.4 Functional annotation enrichment analysis (clusters 1 to 5)

Category	Term	No.	%	P-value	BG	Fold
Annotation Cluster 1	Enrichment Score: 14.5					
GOTERM_BP_FAT	GO:0022610~biological adhesion	71	7.81	3.53E-18	463	3.18
GOTERM_BP_FAT	GO:0007155~cell adhesion	71	7.81	3.53E-18	463	3.18
SP_PIR_KEYWORDS	cell adhesion	35	3.85	1.67E-09	180	3.23

¹⁷ Database for Annotation, Visualization and Integrated Discovery; <http://david.abcc.ncifcrf.gov/>

¹⁸ Gene Ontology Project; <http://www.geneontology.org/>

¹⁹ Kyoto Encyclopedia of Genes and Genomes; <http://www.genome.jp/kegg/>

Annotation Cluster 2		Enrichment Score: 13.48				
GOTERM_CC_FAT	GO:0031012~extracellular matrix	55	6.05	2.96E-20	252	4.31
GOTERM_CC_FAT	GO:0005578~proteinaeous extracellular matrix	48	5.28	1.05E-17	220	4.31
GOTERM_CC_FAT	GO:0044420~extracellular matrix part	30	3.30	2.15E-15	97	6.10
GOTERM_CC_FAT	GO:0044421~extracellular region part	83	9.13	1.76E-13	693	2.36
GOTERM_CC_FAT	GO:0005604~basement membrane	24	2.64	3.74E-13	72	6.58
GOTERM_CC_FAT	GO:0005576~extracellular region	123	13.53	9.53E-13	1281	1.90
SP_PIR_KEYWORDS	extracellular matrix	20	2.20	1.01E-06	89	3.73
Annotation Cluster 3		Enrichment Score: 7.14				
GOTERM_BP_FAT	GO:0032989~cellular component morphogenesis	49	5.39	5.00E-10	376	2.70
GOTERM_BP_FAT	GO:0048666~neuron development	45	4.95	3.32E-09	347	2.69
GOTERM_BP_FAT	GO:0030182~neuron differentiation	53	5.83	5.63E-09	457	2.41
GOTERM_BP_FAT	GO:0031175~neuron projection development	38	4.18	1.04E-08	273	2.89
GOTERM_BP_FAT	GO:0048812~neuron projection morphogenesis	33	3.63	1.09E-08	215	3.18
GOTERM_BP_FAT	GO:0030030~cell projection organization	45	4.95	1.14E-08	361	2.59
GOTERM_BP_FAT	GO:0000902~cell morphogenesis	43	4.73	1.68E-08	340	2.62
GOTERM_BP_FAT	GO:0032990~cell part morphogenesis	35	3.85	3.13E-08	248	2.93
GOTERM_BP_FAT	GO:0048858~cell projection morphogenesis	34	3.74	3.80E-08	238	2.96
GOTERM_BP_FAT	GO:0000904~cell morphogenesis involved in differentiation	32	3.52	5.92E-07	242	2.74
GOTERM_BP_FAT	GO:0048667~cell morphogenesis involved in neuron differentiation	27	2.97	6.90E-06	207	2.71
GOTERM_BP_FAT	GO:0007409~axonogenesis	25	2.75	9.78E-06	186	2.79
GOTERM_BP_FAT	GO:0007411~axon guidance	16	1.76	1.44E-04	105	3.16
Annotation Cluster 4		Enrichment Score: 6.62				
GOTERM_BP_FAT	GO:0007517~muscle organ development	28	3.08	3.43E-08	169	3.44
GOTERM_BP_FAT	GO:0060537~muscle tissue development	24	2.64	1.62E-07	138	3.61
GOTERM_BP_FAT	GO:0014706~striated muscle tissue development	23	2.53	2.62E-07	131	3.64
GOTERM_BP_FAT	GO:0060538~skeletal muscle organ development	17	1.87	7.20E-07	78	4.52
GOTERM_BP_FAT	GO:0007519~skeletal muscle tissue development	17	1.87	7.20E-07	78	4.52
Annotation Cluster 5		Enrichment Score: 5.64				
GOTERM_MF_FAT	GO:0005539~glycosaminoglycan binding	22	2.42	7.65E-09	102	4.60
GOTERM_MF_FAT	GO:0030247~polysaccharide binding	23	2.53	1.66E-08	116	4.23
GOTERM_MF_FAT	GO:0001871~pattern binding	23	2.53	1.66E-08	116	4.23
GOTERM_MF_FAT	GO:0008201~heparin binding	15	1.65	5.00E-06	72	4.44
GOTERM_MF_FAT	GO:0030246~carbohydrate binding	29	3.19	0.0023379	337	1.84
SP_PIR_KEYWORDS	heparin-binding	8	0.88	0.00581103	37	3.59

The table shows the five most enriched clusters ranked by enrichment score, where 'No.' is the number of genes involved with the term; 'p-value' is the Modified 1-tailed Fisher Exact p-value; 'BG' is the number of genes in the rat genome that map to that same term; 'Fold' is the enrichment-fold change, which is the percentage overlap of the gene list with the term over the same term in the background list (rat genome).

The first (most-enriched) cluster (14.56) contained terms exclusively related to cell-adhesion (highlighted in yellow), while the second cluster (13.48) contained terms that were either related to ECM or were more generally of a function related to extracellular localisation. This analysis showed that cell adhesion was the most statistically significant and enriched functionally altered annotation between interacting (LTNS) and non-interacting (LTD) cells. These findings are consistent with the severity of the interaction impairment shown by LTD cells, as CAMs mediate interaction between cells and so any alteration in their expression would be expected to have implications for cellular interactions. Moreover, the change in adhesion profile is indicative of a switch in Schwann cell identity, implicating the role of transcriptional master regulators in the impairment. Analysis of genes with shared functional annotation (gene functional annotation) was also conducted and is included in **Appendix Table E (Dataset G)**. This table includes an enriched cluster of adhesion genes (fifth-ranking) and an enriched cluster of transcriptional regulators (eighth-ranking). Transcription factors have the capability of regulating multiple, often related genes and therefore are possible candidates for study.

To address all these findings in more detail, I selected three functionally-related groups of genes with relevance to this thesis, for further analysis: (1) cell adhesion molecules because of their structural role in mediating cellular interactions; (2) semaphorins because we have previously showed a role for Sema4F in mediating Schwann cell/axonal interactions (Parrinello *et al.*, 2008); (3) transcription factors because of their ability to alter the expression of multiple genes, which might have implications for Schwann cell identity.

Cell adhesion molecules

As discussed, CAMs provide the physical connections for cellular interactions. Cluster one of **Table 3.4** highlighted three adhesion-related functional annotations. The genes represented by these functional groups in this cluster, together with their corresponding expression fold-change values, are listed in **Table 3.5**.

Table 3.5 List genes from functional-annotation cluster one of Table 3.4, which share common adhesion related functions

Accession ID	Gene	Fold-change
AI412746	tweety homolog 1 (Drosophila)	-117.93
BM389026	periostin, osteoblast specific factor	-87.60
NM_019153	fibulin 5	-74.16
AI599143	collagen, type XIV, alpha 1	-73.18
NM_031069	NEL-like 1 (chicken)	-36.69
AI598833	LIM domain 7	-28.81
BM389302	nidogen 2; similar to nidogen 2 protein	-25.71
AI235948	nidogen 1	-22.91
BE108345	collagen, type XII, alpha 1	-20.83
BM388456	collagen, type XI, alpha 1	-18.73
AB035507	melanoma cell adhesion molecule	-17.21
NM_021760	collagen, type V, alpha 3	-15.88
AI233246	insulin-like growth factor binding protein 7	-15.34
AF159103	tumor necrosis factor alpha induced protein 6	-15.04
BE116590	adherens junction associated protein 1	-14.57
NM_130429	lymphoid enhancer binding factor 1	-14.54
NM_017345	L1 cell adhesion molecule (L1-CAM)	-14.00
BG663483	protocadherin alpha 4	-12.80
AA943034	cell adhesion molecule 4 (Nect-4)	-10.69
AI407898	immunoglobulin superfamily, member 11	-10.52
NM_031333	cadherin 2 (N-cadherin)	-9.13
BI295776	sorbin and SH3 domain containing 1	-8.61
AI101782	collagen, type XVIII, alpha 1	-7.38
NM_134452	collagen, type V, alpha 1	-7.24
AI408064	amyloid beta (A4) precursor protein	-6.46
AF016296	neuropilin 1	-6.18
NM_013016	signal-regulatory protein alpha	-5.69
AW433901	cadherin, EGF LAG seven-pass G-type receptor 1 (flamingo homolog, Drosophila)	-5.63
NM_031521	neural cell adhesion molecule 1 (NCAM)	-5.21
BE103601	cadherin, EGF LAG seven-pass G-type receptor 2 (flamingo homolog, Drosophila)	-5.04
BE126420	AE binding protein 1	-4.98
AA956340	protocadherin 7	-4.55
NM_012974	laminin, beta 2	-3.64
AA997129	laminin, gamma 1	-3.45
NM_031977	v-src sarcoma (Schmidt-Ruppin A-2) viral oncogene homolog (avian)	-3.40
BG380309	collagen, type XVI, alpha 1	-3.33
NM_053931	glycoprotein Ib (platelet), beta polypeptide; septin 5	-3.15
NM_017338	calcitonin/calcitonin-related polypeptide, alpha	-2.98
D25290	cadherin 6	-2.91
AA891940	ras homolog gene family, member A; ras homolog gene family, member C	-2.85

AI171799	ependymin related protein 1 (zebrafish)	-2.62
AI412938	G protein-coupled receptor 56	-2.53
U72660	ninjurin 1	-2.53
BF392901	collagen, type XXVII, alpha 1	-2.38
NM_013180	integrin beta 4	-2.36
BG380566	hyaluronan and proteoglycan link protein 4	-2.30
BE115857	parvin, alpha	-2.25
AI227627	CD9 molecule	-2.23
NM_030863	Moesin	-2.19
AW527799	LIM domain containing preferred translocation partner in lipoma	-2.17
BF402765	cadherin 10	2.05
AF065438	lectin, galactoside-binding, soluble, 3 binding protein	2.11
NM_134459	CD99 molecule-like 2	2.26
BF415817	neogenin homolog 1 (chicken)	2.34
NM_053720	apoptosis antagonizing transcription factor	2.50
U69109	PTK2B protein tyrosine kinase 2 beta	3.41
NM_053481	phosphoinositide-3-kinase, catalytic, beta polypeptide	3.58
NM_057118	contactin 1	3.59
X74293	integrin alpha 7	4.19
BF412784	Fras1 related extracellular matrix 1; tetratricopeptide repeat domain 39B	4.35
BI292586	integrin alpha 3	4.64
M37394	epidermal growth factor receptor	5.22
NM_130419	discoidin, CUB and LCCL domain containing 2	5.27
NM_133298	glycoprotein (transmembrane) nmb	6.07
BI279663	desmocollin 2	6.19
AW523000	cadherin 15	8.55
NM_134455	chemokine (C-X3-C motif) ligand 1	8.92
BF419320	WNT1 inducible signaling pathway protein 1	11.30
NM_053572	protocadherin 21	24.81
NM_030856	leucine rich repeat neuronal 3	28.15
AB001382	secreted phosphoprotein 1	58.21

This table lists genes with the adhesion-related GO-Terms stated in Cluster one of Table 3.4. and may not contain all adhesion genes. The out-put was cross-referenced with the LT microarray to obtain fold-change values. Genes of interest are highlighted in yellow.

Many of the CAMs previously implicated as playing a role in Schwann cell/axonal interactions were found to be down-regulated in LTD cells, including L1-CAM (14-fold), NCAM (5.2-fold) and N-cadherin/cadherin-2 (9.1-fold). Importantly, while the majority of adhesion genes were down-regulated, a minority were up-regulated including several cadherins, for example cadherin-10, cadherin-15, and protocadherin-21. While it was not surprising that adhesion genes were dysregulated, both the number of adhesion genes affected and the magnitude of the fold-change of affected genes was surprising. These findings suggest that LTD cells

had undergone a change in cell-state that had radically altered the repertoire and levels of surface expressed CAMs, which had possibly compromised their cellular identity as Schwann cells. This could reflect an adhesion profile, expressed in Schwann cells, which was under the regulatory control of the defective molecule found in LTD cells.

Semaphorins

In addition to classical adhesion molecules, I also examined gene expression changes in the semaphorin family of genes, as we had recently shown in our laboratory, that loss of Sema4F in Schwann cells caused Schwann cell/axonal disassociation and was implicated in the aetiology of Neurofibromatosis type I (Parrinello *et al.*, 2008). **Table 3.6** lists the significantly dysregulated semaphorin family genes and their receptors from **Dataset E** (CD-ROM).

Table 3.6 Semaphorin family members and their receptors significantly changed in LTD cells

Accession ID	Gene	Fold-change
BM386525	Semaphorin 6D	-26.71
BI275485	Semaphorin 3B	-8.49
BE108859	Semaphorin 3G	-3.11
NM_019272	Semaphorin 4F	-2.92
BM387083	Semaphorin 6A	-2.61
BM390000	Semaphorin 3F	3.07*
NM_017310	Semaphorin 3A	3.37
AF016296	Neuropilin-1	-6.2
AI102248	Plexin D1	-4.61

*Genes of special interest are highlighted in yellow (FDR < 0.01, FC > 2 up/down); *(0.01 < FDR < 0.1)*

Consistent with this work, Sema4F was shown to be down-regulated nearly three-fold in LTD cells. Interestingly, four other members of the family were also down-regulated, with Sema6D levels down-regulated by nearly 27-fold. It is still unclear whether other members of the semaphorin family function as adhesion molecules because their primary function described to date has centred on axonal guidance, attraction and repulsion (Kruger *et al.*, 2005). In addition to semaphorins, a number of semaphorin receptors (plexins) and co-receptors (neuropillins) were also found to

be dysregulated, these include neuropillin-1 (down-regulated 6.2-fold) and Plexin D1 (4.6-fold down-regulated), where Plexin-D1 is the receptor for class-3 semaphorins (Kruger *et al.*, 2005).

Transcriptional regulators

Transcription factors regulate the expression of multiple genes and co-ordinate the level of expression to control many aspects of cell biology, particularly during differentiation where different programmes of gene expression are required. In addition, they are often implicated in establishing a cellular identity or 'molecular signature', which is defined by the pattern of gene expression under their regulatory control. **Table 3.7** lists the genes from **Dataset E** that share the BP GO-Term 'regulators of DNA transcription'.

Table 3.7 List of genes involved in transcription

Accession ID	Gene	Fold-change
BF388057	hairy/enhancer-of-split related with YRPW motif 2	-30.28
NM_019193	SRY (sex determining region Y)-box 10 (Sox10)	-23.76
NM_130429	lymphoid enhancer binding factor 1/LEF1	-14.54
BG671865	necdin homolog (mouse)	-10.85
AI072336	naked cuticle homolog 2 (Drosophila)	-9.24
NM_022300	brain abundant, membrane attached signal protein 1	-8.29
BI295741	homeo box A10	-7.66
AI408064	amyloid beta (A4) precursor protein	-6.46
BI284495	transcription factor AP-2, gamma	-5.35
NM_013154	CCAAT/enhancer binding protein (C/EBP), delta	-5.04
BE126420	AE binding protein 1	-4.98
AI013919	cyclin-dependent kinase inhibitor 1C (P57)	-4.96
BE107033	ecotropic viral integration site 1	-4.40
BF416474	retinoic acid induced 14	-4.28
NM_024364	Hairless	-4.26
BF415939	FBJ osteosarcoma oncogene	-3.47
NM_053369	transcription factor 4	-3.45
AI411774	B-cell CLL/lymphoma 3	-3.37
BF548737	SRY (sex determining region Y)-box 2 (Sox2)	-3.19
BM390477	cut-like homeobox 1	-3.06
BI289559	SRY (sex determining region Y)-box 6 (Sox6)	-2.98
NM_139113	nuclear receptor subfamily 2, group F, member 6	-2.96
AF140346	secreted frizzled-related protein 4	-2.93

BE120513	TAF13 RNA polymerase II, TATA box binding protein (TBP)-associated factor	-2.64
AI176779	hypothetical protein LOC654482	-2.46
BF396205	homeo box C10	-2.42
NM_053894	Jun dimerization protein 2	-2.39
BM386654	SCAN domain-containing 1	-2.33
AB062135	DnaJ (Hsp40) homolog, subfamily C, member 12	-2.32
AI228548	S100 calcium binding protein A1	-2.20
NM_031528	retinoic acid receptor, alpha	-2.18
BE113920	signal transducer and activator of transcription 3	-2.17
AJ132046	metastasis associated 1	-2.16
BE107303	homeo box A5	-2.12
AW529031	zinc finger E-box binding homeobox 2	-2.06
BG378709	ArfGAP with SH3 domain, ankyrin repeat and PH domain 1	2.00
AI176506	necdin-like 2	2.16
NM_031789	nuclear factor, erythroid derived 2, like 2	2.33
NM_053412	interleukin enhancer binding factor 3	2.35
BE102096	jumonji domain containing 1C	2.42
BE099050	nuclear factor I/B	2.48
NM_012576	nuclear receptor subfamily 3, group C, member 1	2.52
AI713965	iroquois homeobox 3	2.53
BF545627	ets variant 4	2.87
BE108745	nucleosomal binding protein 1	2.90
BF386078	eyes absent homolog 2 (Drosophila)	2.93
NM_032462	Kv channel interacting protein 3, calsenilin	3.34
NM_053349	SRY (sex determining region Y)-box 11 (Sox11)	4.36
BE117444	teashirt zinc finger homeobox 1	5.34
AF474979	cyclin-dependent kinase inhibitor 2B (p15, inhibits CDK4)	5.36
NM_053530	twist homolog 1 (Drosophila)	6.46
NM_021693	SNF1-like kinase	7.17
AI599177	teashirt zinc finger homeobox 3	10.82
AI175048	SIX homeobox 1	25.73

The main dataset was searched using GO-term "GO:0006355~regulation of cellular transcription, DNA-dependent", in order to return genes involved in transcription (FDR<0.01, FC>2 up/down). Total R. norvegicus genes in this category: 2707 (Feb 2012). Genes of special of interest are highlighted in yellow.

This analysis showed that a substantial number of transcription factors had become dysregulated in LTD cells. Importantly, this included members of the Sox/SRY family, of which, Sox2, Sox6 and Sox10 are down-regulated by 3.2-fold, 3-fold and 24-fold respectively, while Sox11 was up-regulated 4.5-fold. Both Sox2 and Sox10 are key transcription factors known to be important in Schwann cell biology. Sox10 expression begins in NCCs, continuing throughout the developmental lineage of Schwann cells and persists in mature adult Schwann cells, where it is thought to be

important for the specification of Schwann cells (Jessen & Mirsky, 2005). Sox2 is similarly expressed in early Schwann cell development, however its expression declines with differentiation and transition to mature myelinating Schwann cells (Parkinson *et al.*, 2008; Salzer *et al.*, 2008). Importantly, Sox2 expression is elevated in Schwann cells as they undergo dedifferentiation following nerve injury (Le *et al.*, 2005a). Given the importance of these transcription factors, notably Sox2 (as its expression is co-ordinated at times of early Schwann cell/axonal interaction), it is plausible that one of these master regulators are important for generating a Schwann cell adhesion profile or identity. If this were the case, then loss of a transcription factor in LTD cells, responsible for cell-surface expression of CAMs, might explain the axonal interaction failure inherent in these cells. In later experiments, I will explore the role of Sox2 as a possible candidate in this regard.

3.7 Array validation by qRT-PCR

In order to validate the expression ratios from the microarray analysis, the mRNA levels of key selected genes was analysed independently using real-time polymerase chain reaction (qRT-PCR). The following down-regulated genes of interest were selected: N-cadherin, Sema4F, Sema3B, MPZ and Sox2, while ephrin-4A was selected as an example of an up-regulated gene. Total RNA was obtained from the LTNS and LTD cells used in the original microarray, while GAPDH was selected as the normalising control because its expression levels are thought to remain constant between the two cell-types. Although this approach does not represent a systematic validation of the microarray, it nonetheless confirmed the substantial down-regulation of key genes of interest highlighted from the microarray, for example N-cadherin, Sema4F and Sox2, while also confirming the up-regulation of ephrin-4A (**Figure 3.9**). Interestingly, the magnitude of the fold-changes reported by qRT-PCR was invariably greater than that reported in the microarray, therefore it is likely that the fold-change reported in the microarray under-represents the true fold-change.

3.8 Over-expression of Sox2 in Schwann cells

Analysis from the microarray experiment showed that both N-cadherin and the transcription factor Sox2 were down-regulated in LTD cells by 9.1-fold and 3.2-fold

A

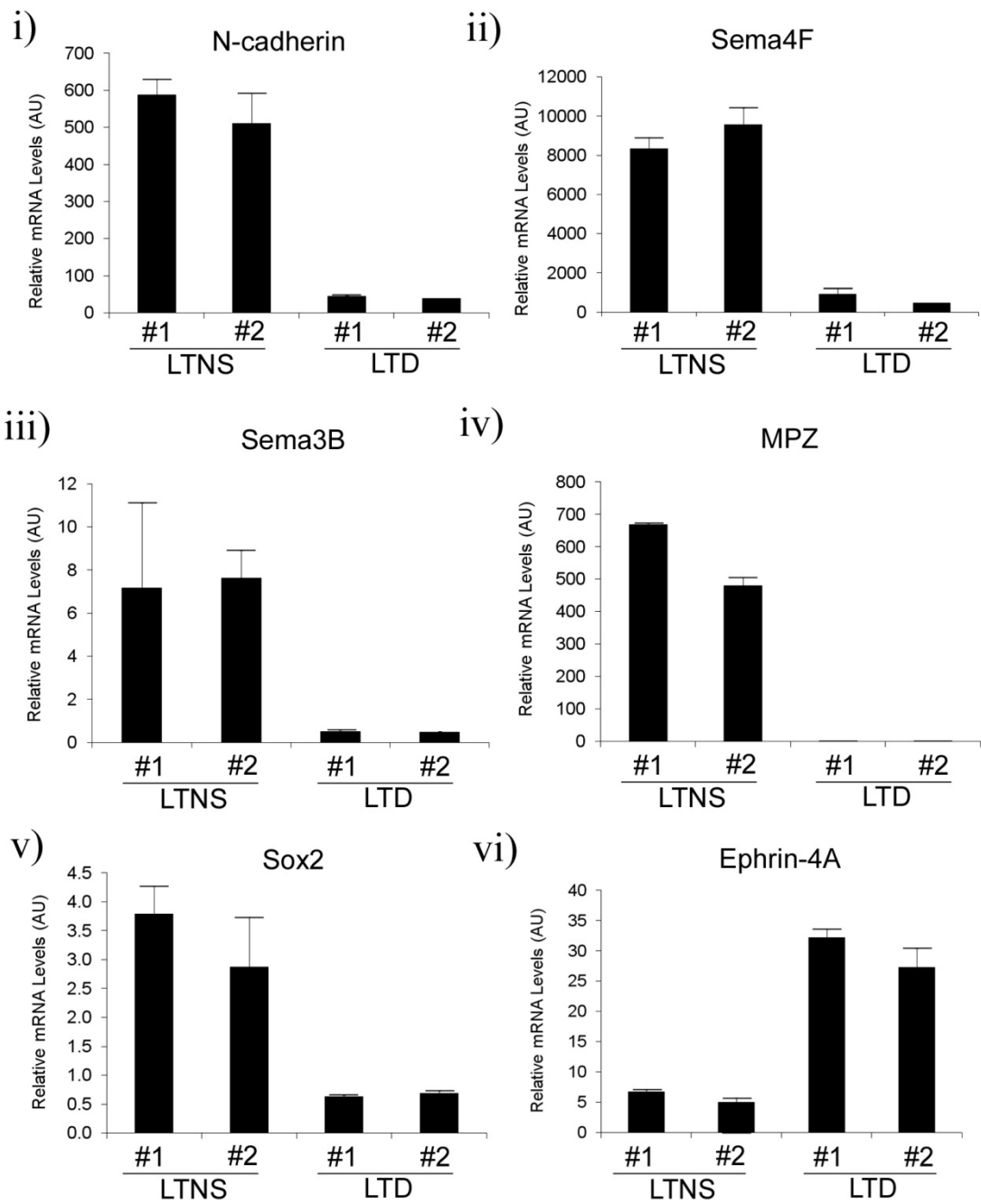


Figure 3.9 Validation of selected genes from the microarray analysis. Quantitative RT-PCR analysis, from original LTNS and LTD replicate microarray samples (#1 & #2), was performed to assay for relative levels of (i) N-cadherin; (ii) semaphorin-4F (Sema4F); (iii) semaphorin-3B (Sema3B); (iv) myelin protein zero (MPZ); (v) Sox2 and (vi) Ephrin-4A. Expression levels were normalised to GAPDH levels with bars showing S.D. of duplicates.

respectively. As previously discussed, Sox2, in addition to N-cadherin, is expressed in Schwann cells during early development and following nerve injury; both of which coincide to a time when Schwann cells are forming early interactions with axons, i.e. when they are recognising and associating with axons. While N-cadherin is a putative candidate for mediating Schwann cell/axonal interactions, Sox2 might be involved in the transcriptional regulation of N-cadherin as well as a number of other CAMs, which collectively might form part of a profile of adhesion gene expression required for normal Schwann cell/axonal interactions. I therefore wanted to determine if the loss of axonal interaction displayed by LTD cells was caused by the loss of Sox2 expression, therefore leading to dysregulation of downstream Sox2 targets. To test this, I adopted an adenoviral approach to drive Sox2 expression. I obtained a GFP adenovirus (AdGFP), a Sox2-GFP adenovirus (AdSox2) and an N-cadherin adenovirus (AdNcad) and optimised the concentration of virus by exposing NS cells to a serial-dilution of viral supernatant in order to obtain a batch titre. I then seeded NS monocultures onto culture plates and infected the cells 24-hours later with AdGFP and AdSox2-GFP for 16-hours. The medium was then changed and the infected cultures were incubated a further 24-hours before fixation. The cultures were immunostained for N-cadherin while GFP was used to determine the infection rate, which for all adenoviruses, was nearly 100% in Schwann cells (**Figure 3.10A**). Interestingly, I observed a surprising result in that the localisation of N-cadherin within Schwann cells was dramatically different between Ad-GFP controls and AdSox2-GFP infected Schwann cells. As shown by the white arrows, Sox2 expression appeared to localise N-cadherin to Schwann cell homotypic cell-cell junctions. This was striking to observe, with large strands of N-cadherin encroaching from the junction into or across the Schwann cell. However, it was not clear if this pattern of N-cadherin immunofluorescence was as a result of increased N-cadherin expression, i.e. increased protein levels - which we expected, or was caused by the relocalisation or post-translational modification of existing N-cadherin in the cell.

In order to investigate further, I infected NS cells with AdGFP, AdNcad and AdSox2-GFP and examined the expression of junctional N-cadherin (**Figure 3.10B**). This showed that the over-expression of N-cadherin (using AdNcad) only marginally increased N-cadherin levels at cell-cell junctions, while most of the additional N-

A

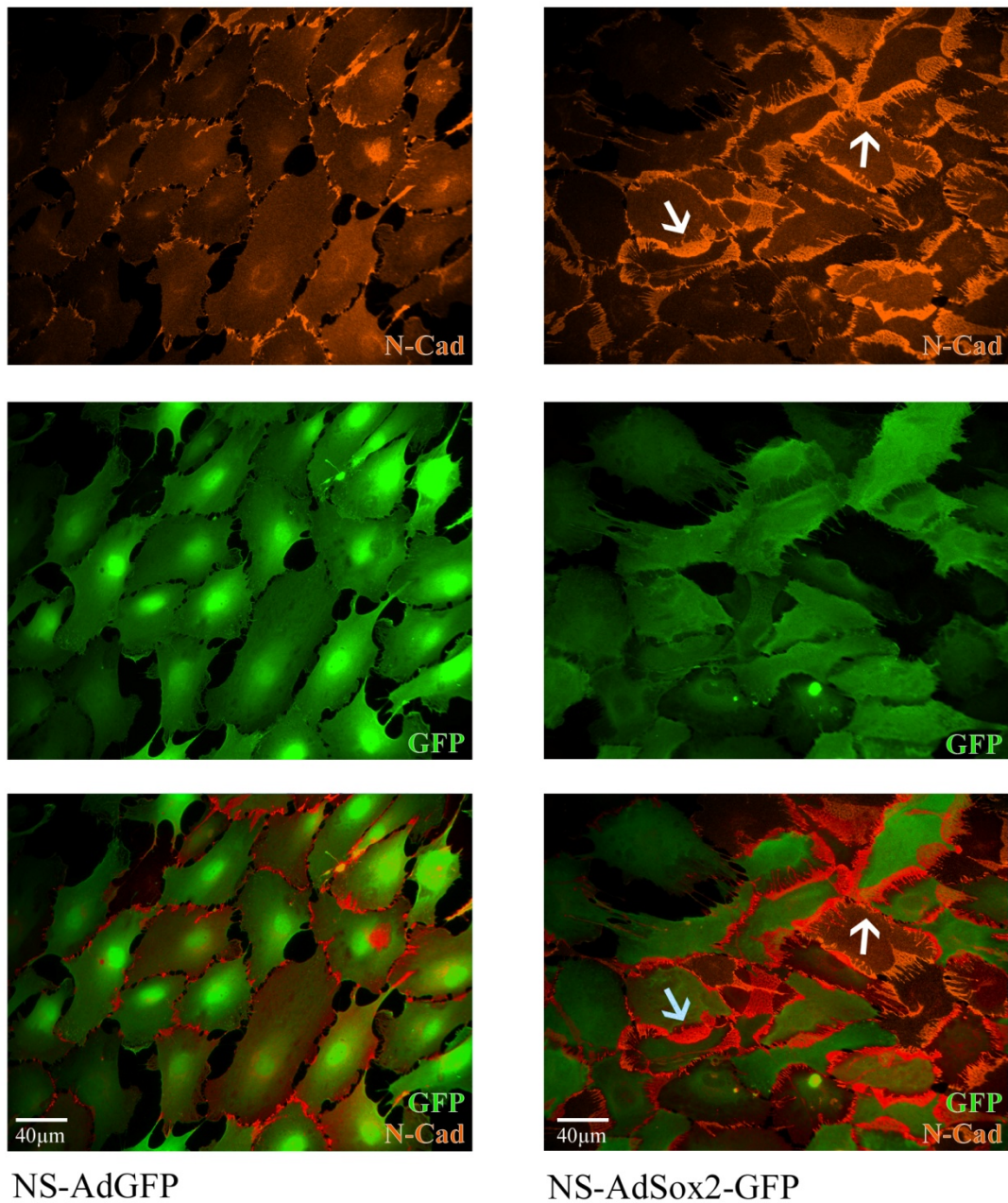
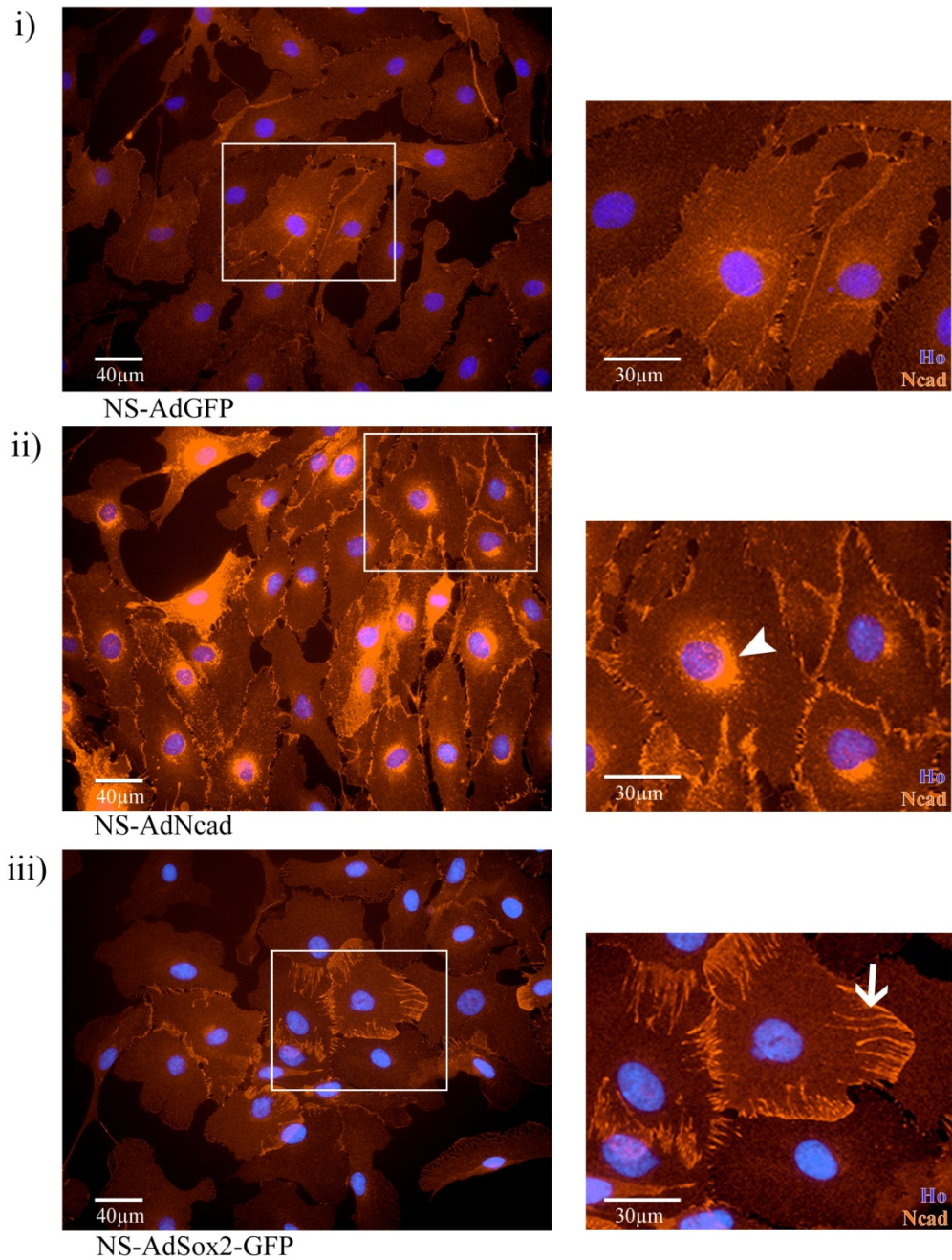


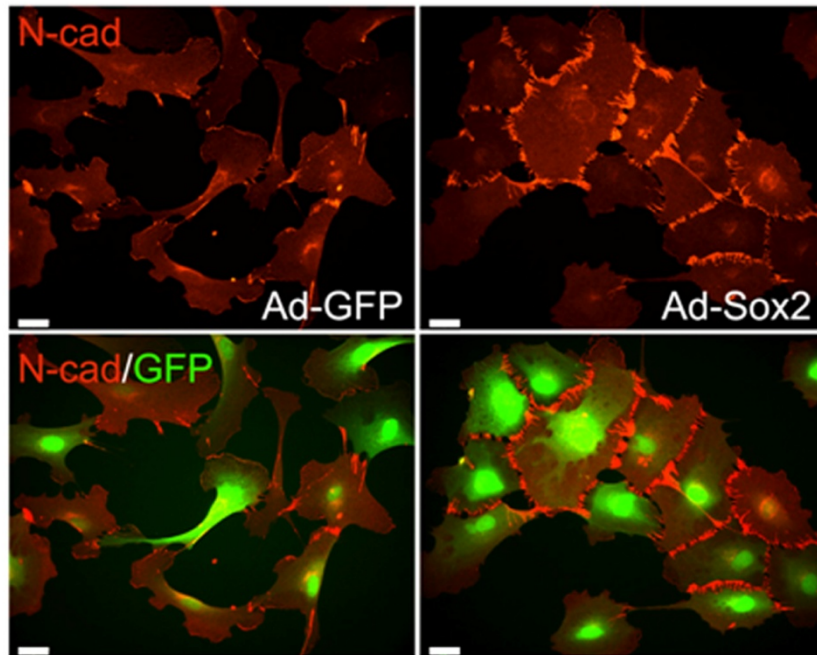
Figure 3.10 Over-expression of Sox2 in Schwann cells strengthens N-cadherin junctions and promotes homotypic Schwann cell clustering. Schwann cells were infected with either GFP or Sox2-GFP adenovirus for 16hrs, media-changed and fixed after a further 24hrs of incubation. (A) Representative epifluorescent images from Schwann cell cultures immunostained for N-cadherin (red) with infected cells marked by GFP expression (green). The white arrows show examples of extensive N-cadherin re-localisation.

B

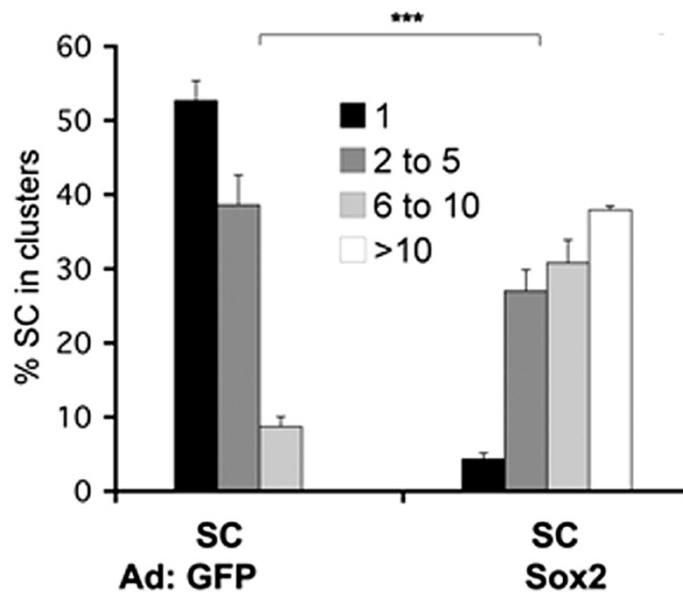


(B) Representative epifluorescence from **(i)** AdGFP, **(ii)** AdNcad and **(iii)** AdSox2-GFP Schwann cell infected monocultures that were immunostained for N-cadherin (red) with cell nuclei labelled with Hoechst (blue). **(RHS)** Enlargements from the regions outlined by the white boxes. The white arrow-head shows perinuclear deposits of N-cadherin, while the white arrow shows long N-cadherin junctional strands.

C



D



(C) Representative epifluorescence from low-density AdGFP and AdSox2-GFP monocultures that were fixed and immunostained for N-cadherin (red), with infection marked by GFP expression (green). Scale-bars are 25 μ m. (D) Quantification of the Sox2 induced clustering of Schwann cells. Clustering was scored by counting the number of Schwann cells in groups of 1, 2-5, 6-10 and greater than 10. Statistics by Fisher's exact test for rxq contingency tables ($p < 0.001$).

cadherin protein appeared to accumulate in perinuclear regions. Conversely, expression of Sox2 (using AdSox2-GFP) appeared to result in a targeted increase of N-cadherin localisation to cell-cell junctions, while non-junctional N-cadherin was comparable to AdGFP controls. The altered pattern of N-cadherin at the cell-cell junctions, in which long-strands of N-cadherin are found perpendicular to the junctions, can be clearly observed in higher magnification images (**3.10Biii**, see white arrow). The significance of longer N-cadherin strands at the junction is not clear although it may be indicative of stronger (mature) adherens junctions. In terms of understanding the relationship between Sox2 and N-cadherin, this data suggested that Sox2 expression does not substantially increase N-cadherin levels but rather, its main role is to alter the localisation of N-cadherin at cell-cell junctions.

3.8.1 Sox2 drives Schwann cell clustering by an N-cadherin-dependent mechanism

In order to investigate further, the role of Sox2-mediated N-cadherin at the cell-cell junctions, I worked collaboratively with Simona Parrinello, to determine if this observation had a functional role in Schwann cell biology. We were especially interested to discover if Sox2 had a role to play in nerve regeneration because Sox2 has been shown to be up-regulated in dedifferentiated Schwann cells upon nerve injury (Le *et al.*, 2005a). To study this, we adenovirally infected subconfluent Schwann cells with either AdGFP or AdSox2-GFP for 16-hours. After which, the medium was changed and the monocultures were incubated for a further 24 hours. At this point, we viewed the live monocultures by phase-contrast microscopy. Remarkably, we observed that low-density AdSox2 infected Schwann cells were aggregating together in clusters, which was not observed in low-density AdGFP Schwann cell cultures. We next fixed the cultures and immunostained for N-cadherin. Consistent with previous observations, Sox2 over-expressing Schwann cells, as indicated by endogenous GFP expression, were generally present in groups, with clustering mediated by robust N-cadherin at junctions between the cells (**Figure 3.10C**). We quantified this effect by scoring the frequency of Schwann cell clusters which contained either 1, 2-5, 6-10, or more than 10 Schwann cells. Our results showed that Sox2 resulted in a shift from single cells to large clusters of cells, which we showed was the result of a switch in contact-behaviour from repulsion to cell

aggregation (**Figure 3.10D**). Simona later showed that Sox2 expression, responsible for this altered response, was induced by heterotypic interactions between fibroblasts and Schwann cells mediated by contact-dependent signalling through Ephrin-B (expressed by the fibroblast) and EphB2 (expressed by the Schwann cell) (Parrinello *et al.*, 2010). Furthermore, ephrin-mediated Sox2 expression in Schwann cells was required for the coordinated migration of Schwann cells from the proximal stump in transected sciatic nerve *in vivo* (Parrinello *et al.*, 2010).

3.8.2 Re-expression of Sox2 in LTD cells

Dysfunction of a master-regulator, for instance Sox2, in LTD cells might have resulted in an aberrant expression profile of adhesion genes required for interactions with axons. To determine if establishing Sox2 expression in LTD cells could restore the ability of these cells to interact with axons, I initially examined the levels of selected CAMs, down-regulated in LTD cells, following Sox2 expression in LTD cells. LTNS and LTD cells were infected for 16-hours with either AdGFP or AdSox2 and, after changing the cell media, the cultures were incubated for a further 24-hours. The plates were then either fixed or RNA was collected for RT-PCR. In addition to Sox2, I chose to analyse the transcript levels N-cadherin and Sema3B because both CAMs were down-regulated in the LT microarray, by 9.1-fold and 8.5-fold respectively, and therefore I wanted to determine if re-expression of Sox2 could induce their expression. The RT-PCR analysis showed that Sox2 expression did not significantly affect the transcript levels of either N-cadherin or Sema3B (**Figure 3.11A**). I next examined low-density cultures of LTNS and LTD, infected with AdGFP and AdSox2, by phase-contrast microscopy in order to study the monocultures for evidence of clustering. While Sox2 expressing LTNS cells showed evidence of clustering, the Sox2 expressing LTD cells appeared not to cluster (**Figure 3.11B**). The cultures were then fixed and immunostained for N-cadherin, which showed that LTNS cells were clustering, consistent with previous Sox2 expression studies in NS cells. Interestingly, LTD cells infected with AdSox2-GFP did not restore N-cadherin levels and furthermore, these cells appeared not to cluster (**Figure 3.11C**). These observations corroborate the RT-PCR data (**Figure 3.11A**) and immunofluorescence (**Figure 3.11B**), as well as our previous work (Parrinello *et*

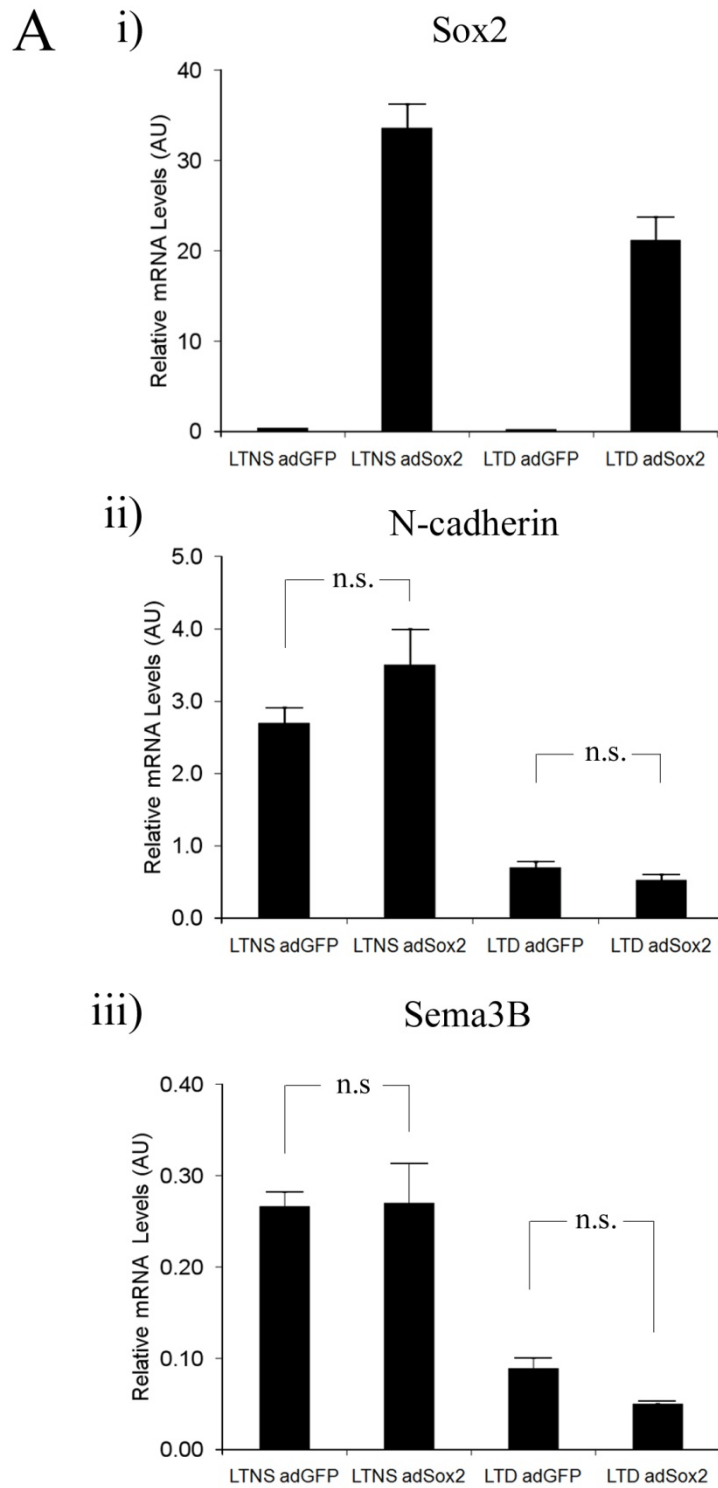
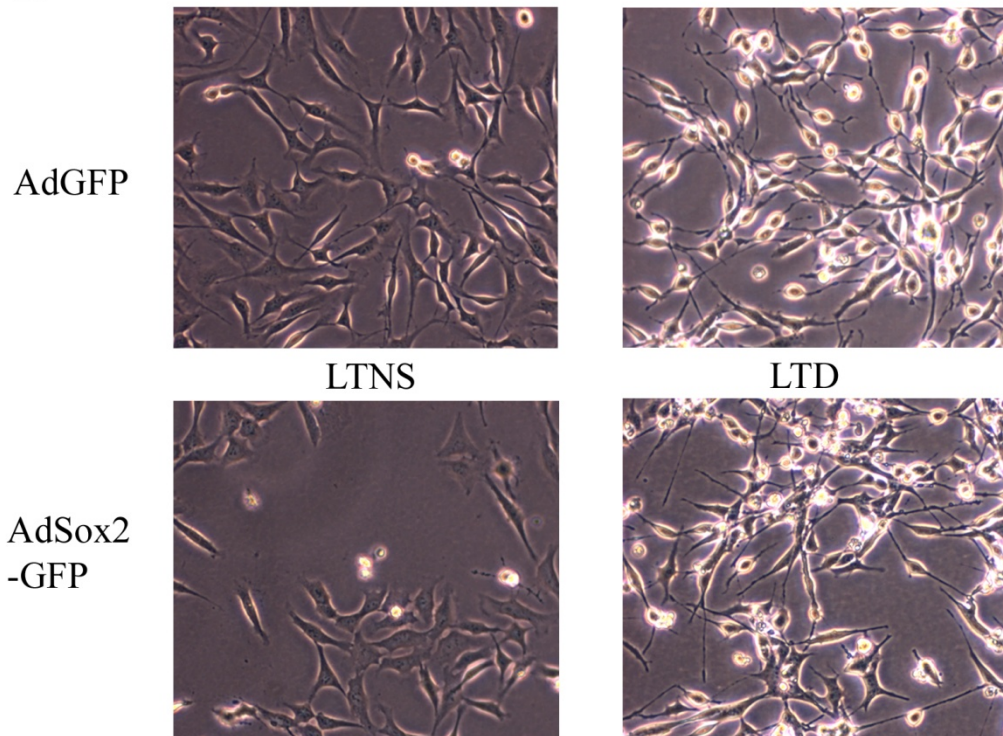
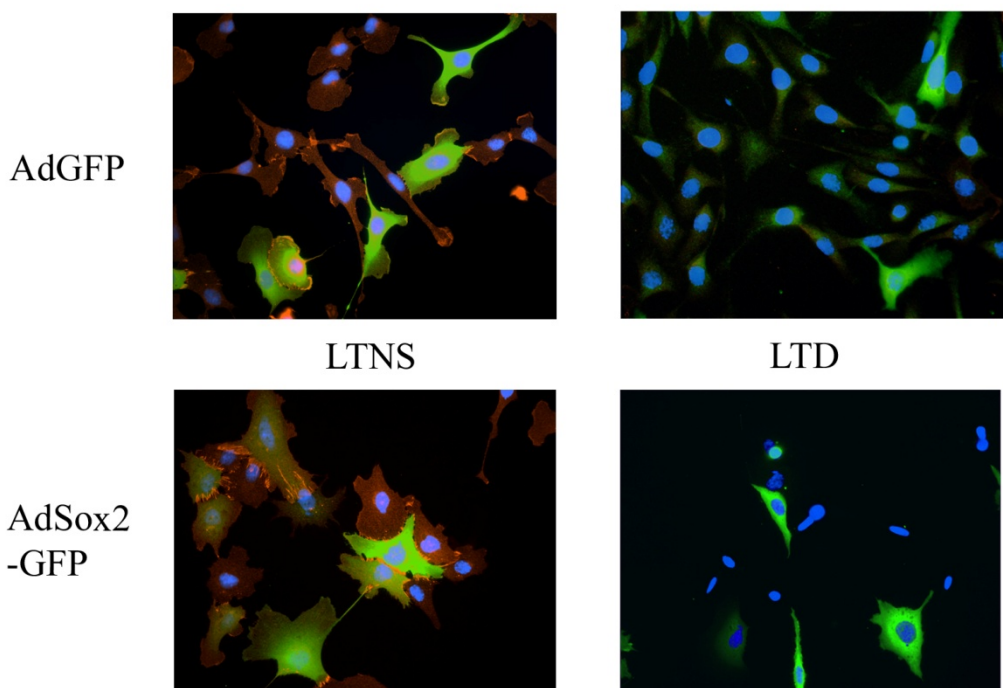


Figure 3.11 Sox2 over-expression does not affect N-cadherin levels in LTNS and LTD. LTNS and LTD cells were infected for 16hrs with either AdGFP or AdSox2 adenovirus, media-changed and incubated a further 24hrs. (A) Quantitative RT-PCR to determine levels of Sox2 and N-cadherin, with levels normalised to GAPDH levels. Statistics by Turkey-Kramer multiple comparison test ($p > 0.05$: n.s., not-significant). Bars show S.D. of duplicates.

B



C



(B) Phase-contrast images of low-density LTNS and LTD monocultures infected with GFP and Sox2-GFP adenovirus. **(C)** Representative epifluorescent images showing N-cadherin immunostaining (red) and GFP expression (green) with cell nuclei labelled with Hoechst (blue).

al., 2008), which together suggest that Sox2 does not induce N-cadherin expression but rather alters the localisation of existing N-cadherin at cell-cell junctions. Thus, LTD cells and fibroblasts, which do not express N-cadherin, do not exhibit N-cadherin re-localisation following Sox2 expression and, consequently, do not exhibit cell clustering.

3.9 Chapter summary and conclusions

In this chapter, I have shown how normal encounters between Schwann cells and axons results, via a step-wise process of interactions, in Schwann cells that are stably associated and aligned with axons. A key first step in this process is Schwann cell recognition for axons. We found that while LT expression in Schwann cells does not affect Schwann cell/axonal interactions, a derivative LT population (LTD) had, through unknown genetic changes, entirely lost the inherent ability to recognise and interact with axons. I used LTD in order to screen for possible mediators of these interactions and showed, by microarray analysis, that LTD cells had significantly altered global gene expression changes, notably in genes encoding cell adhesion molecules, for example N-cadherin, Sema4F, NCAM, L1-CAM and Necl-4 as well as in genes encoding important Schwann cell transcription factors, for example Sox2 and Sox10. I went on to confirm, by functional enrichment analysis, that cell adhesion was the most enriched functional gene ontology.

Globally dysregulated gene expression suggested that a transcription factor controlling Schwann cell identity might explain the loss of axonal interaction elicited by LTD cells. I therefore investigated Sox2, as this transcription factor is up-regulated in Schwann cells following nerve damage and prior to Schwann cell/axonal re-association. Surprisingly, I found that Sox2 had a distinct role in that it promotes Schwann cell clustering, by directing N-cadherin localisation to cell-cell junctions, but did not restore N-cadherin or Sema3B levels when expressed in LTD cells. Interestingly, Sox2 altered the morphology of the junction – generating long strands of N-cadherin that project into the cell from the cell-cell junction. This was quite distinct from Schwann cells in which N-cadherin was over-expressed, suggesting that Sox2 played a more refined role in altering the cellular localisation of N-cadherin. The functional purpose of this remains to be clarified, although it is tempting to

speculate that the long strands of N-cadherin observed in Sox2 expressing Schwann cells might be involved in strengthening and stabilising homotypic junctions, in-line with an *in vivo* function for Schwann cell clustering in nerve repair.

While the identity of the genetic lesion responsible for the LTD non-interaction phenotype still remains to be determined, a number of novel and previously identified CAMs were detected in the array. In terms of the latter, a number of down-regulated CAMs including melanoma CAM (mCAM), NCAM, N-cadherin and Necl4 were also identified from a screen conducted by Spiegel *et al.*, (2006) of Schwann cell expressed CAMs. Thus, the fact that the current microarray methodology has independently identified CAMs, which have been previously discovered in an independent screen of Schwann cell CAMs, further validates our approach. In terms of the former, a number of novel CAMs not previously implicated in Schwann cell/axonal interactions were identified, including cadherin-6, protocadherin-7, protocadherin alpha 4 and CD9, which are discussed more fully in the discussion.

Chapter Four: N-cadherin mediates homotypic and heterotypic cell-cell interactions

4.1 Chapter introduction

In Chapter Three, I set out a theoretical model to describe Schwann cell/axonal interactions, which emphasised the importance of direct, reciprocal cell-cell contact dependent communication throughout all stages of the interaction process. Although previous research has largely focused on the study of heterotypic interactions, i.e. between Schwann cells and axons, the importance of homotypic Schwann cell-cell interactions to normal nerve physiology should not be underplayed. Both homotypic and heterotypic cell interactions are important in the generation and maintenance of the mature functional architecture of the PNS. While heterotypic interactions are clearly a defining property of Schwann cells, homotypic interactions also play important roles in Schwann cell biology. For instance, they are required to generate SCP clusters during PNS development (Wanner *et al.*, 2006b) and might also play a role in the homeostatic nerve between differentiated Schwann cells at the Node of Ranvier (Poliak & Peles, 2003; Salzer, 2003). They also play central roles in the nerve repair process, where they facilitate the coordinated outgrowth of Schwann cells from the proximal stump, into and across the nerve bridge (injury site), and are important in the formation of cellular conduits in the degenerated distal nerve (known as Bands of Büngner), which create a favourable substratum for later axonal re-growth and regeneration (Chen *et al.*, 2007; McDonald *et al.*, 2006; Napoli *et al.*, 2012; Parrinello *et al.*, 2010; Ribeiro-Resende *et al.*, 2009; Webber & Zochodne, 2010). Both types of interactions are mediated through cell adhesion molecules (CAMs) which are pivotal to the ensuing interaction process (Patel *et al.*, 2003; Spiegel *et al.*, 2007), although the exact mediators involved remain poorly defined. In this chapter, I have addressed the role of N-cadherin, a calcium-dependent CAM, in the generation of homotypic Schwann cell-cell and heterotypic Schwann cell/axonal interactions.

Research spanning several decades into Schwann cell/axonal interactions has led to the identification of a number of CAMs thought to play significant roles in the interaction process, for example L1-CAM (Haney *et al.*, 1999; Seilheimer *et al.*, 1989; Wood *et al.*, 1990), NCAM (Hansen *et al.*, 2008), Necl4/cell adhesion

molecule-4 (Maurel *et al.*, 2007; Perlin & Talbot, 2007; Spiegel *et al.*, 2007) and N-cadherin/cadherin-2 (Hansen *et al.*, 2008; Letourneau *et al.*, 1991; Wanner & Wood, 2002). The importance of some of these CAMs has since been questioned. For instance, L1-CAM was thought to be an important mediator of axonal ensheathment (Seilheimer *et al.*, 1989) and myelination (Wood *et al.*, 1990). Both authors used antibodies designed to block L1-CAM function; however, later work by Dahme *et al.* (1997) and Haney *et al.* (1999), who investigated the role of L1-CAM using mouse knockout models, have since found that Schwann cells devoid of L1-CAM interacted normally with axons.

In this chapter, I investigated the role of N-cadherin, which I chose to study because N-cadherin, similar to L1-CAM, NCAM and a number of other CAMs, was down-regulated in non-interacting LTD cells when compared to interacting LTNS controls (Chapter Three), and was therefore a potential candidate for mediating Schwann cell/axonal interactions. In addition, evidence from the literature alluded to the importance of N-cadherin as a facilitator of both homotypic and heterotypic interactions. A role for N-cadherin was first suggested by Letourneau *et al.* (1991) who showed that calcium ion depletion from the cell media of chicken Schwann cell/DRG cocultures was sufficient to perturb heterotypic interactions. A later study by Wanner & Wood (2002), followed this by investigating Schwann cell-cell and Schwann cell/axonal interactions within an *in vitro* rat denervated Schwann cell culture system. Here, the authors used a number of N-cadherin ‘function-blocking’ techniques and reagents, for example, calcium depletion, ligand blocking antibodies and inhibitory cyclic pentapeptides, in order to disrupt N-cadherin ligation and therefore function in Schwann cells. Although the use of these techniques and reagents is subject to a number of caveats, for instance the risk of off-target effects, the work nonetheless suggested that N-cadherin was likely to be involved. Follow up studies by the same group investigated the developmental expression of N-cadherin in the Schwann cell lineage of the early developing PNS nerve (Wanner *et al.*, 2006a; Wanner *et al.*, 2006b). In these studies, SCPs were found to express N-cadherin; however, levels were later substantially reduced following their differentiation to mature Schwann cells, although a mechanism to explain this has yet to be defined (Wanner *et al.*, 2006a). This work also found that NRG-1 (NRG-1) was sufficient to drive the up-regulation of N-cadherin in Schwann cells *in vitro*.

The physiological relevance of this, however, is unclear because NRG-1 is present throughout development, including at times when N-cadherin is normally down-regulated. Nevertheless, it has been shown that N-cadherin is strongly up-regulated in Schwann cells following sciatic nerve injury (Parrinello *et al.*, 2010; Shibuya *et al.*, 1995; Thornton *et al.*, 2005; Zelano *et al.*, 2006), which suggests that up-regulated N-cadherin expression, in denervated ‘injury Schwann cells’ was likely to facilitate Schwann cell directed processes of nerve repair.

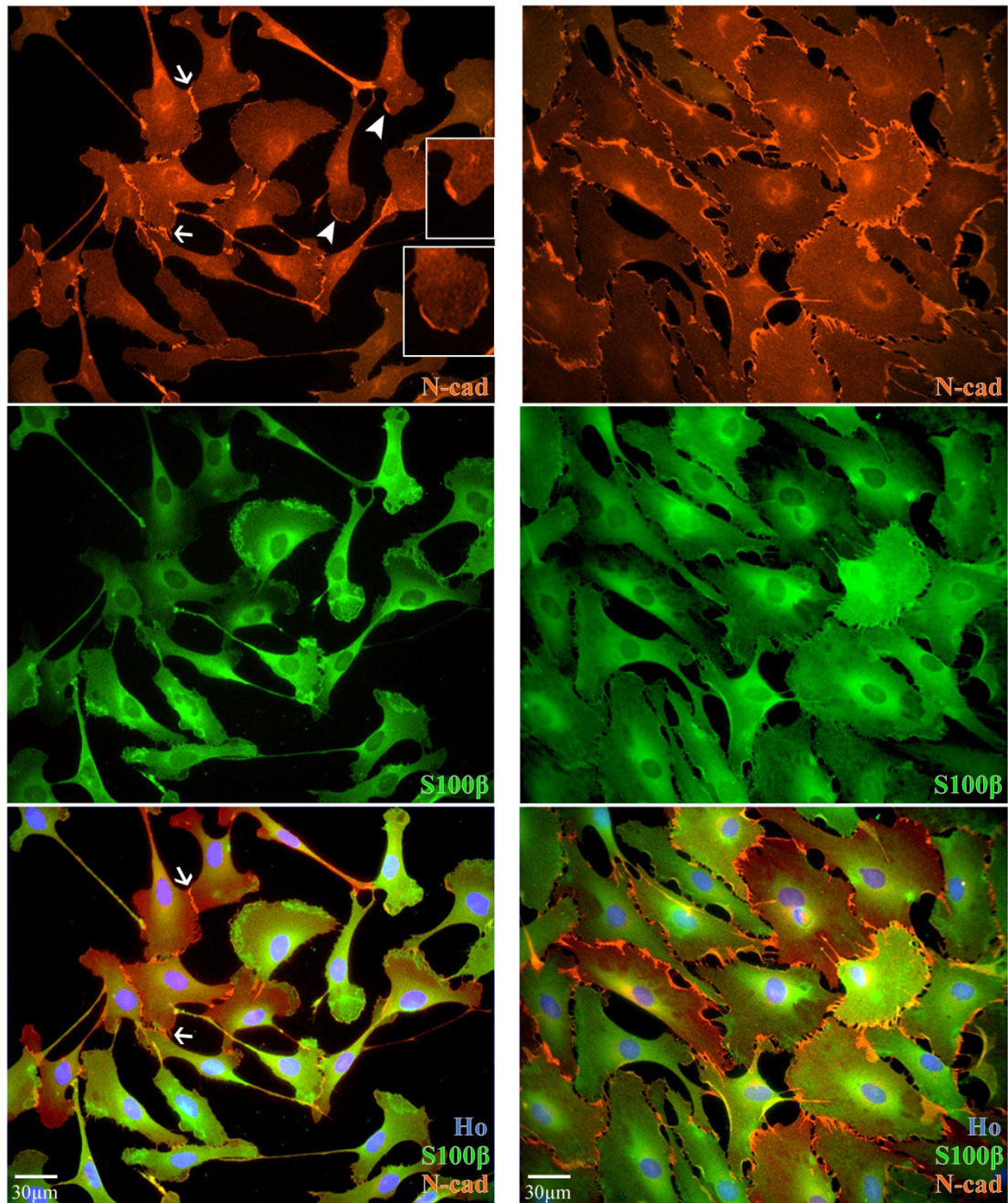
To determine the role of N-cadherin in mediating homotypic Schwann cell-cell and heterotypic Schwann cell/axonal interactions I decided to use an siRNA approach to specifically deplete N-cadherin levels in primary Schwann cells. This was done in preference to post-translational ‘functional blocking’ strategies described earlier as siRNA action is efficient and highly specific to the intended mRNA, with off-target effects further mitigated by using multiple independent and non-overlapping siRNAs for each gene targeted. In contrast, inhibitory reagents used to block cadherin function are largely problematic in these respects, for example Fairless *et al.* (2005) reported that cyclic pentapeptide inhibitors were relatively inefficient at blocking N-cadherin function in Schwann cells, while the specificity of these approaches remains unclear.

4.2 Homotypic Schwann cell-cell junctions

4.2.1 The expression and localisation of N-cadherin in Schwann cells

In order to examine the role of N-cadherin in mediating Schwann cell-cell homotypic interactions, I first determined the sub-cellular expression and localisation of N-cadherin in Schwann cell monocultures. NS cells were plated at either low or high density and fixed three days later. Immunofluorescence was then performed using an N-cadherin antibody that recognised the cytoplasmic C-terminal region of the N-cadherin protein. In addition, monocultures were coimmunostained with the Schwann cell specific, cytoplasmic marker S100 β in order to clearly demark the extent of the cell. As expected, low-density Schwann cell monocultures had fewer

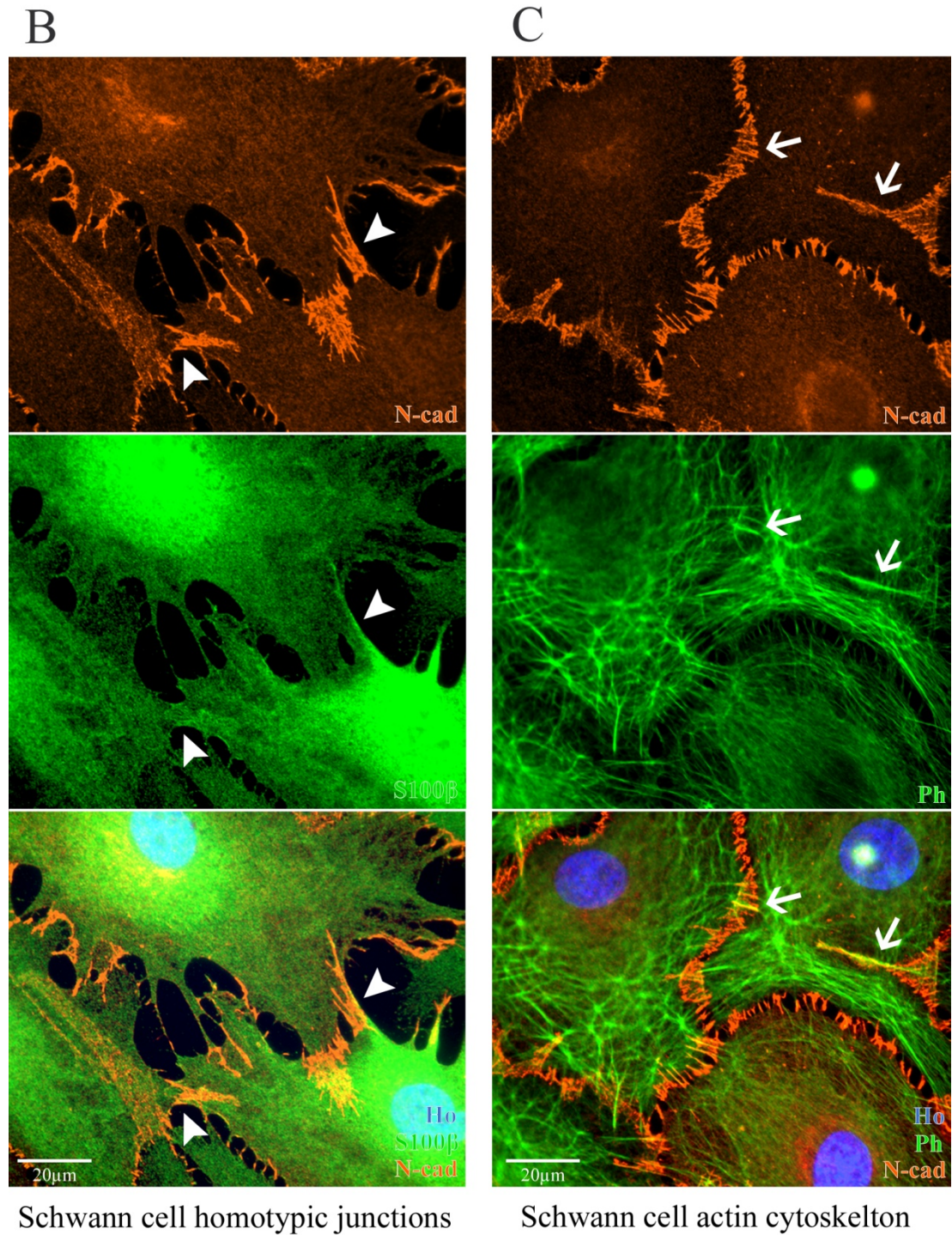
A



(i) Low-density NS monoculture

(ii) High-density NS monoculture

Figure 4.1 Schwann cells express N-cadherin which is localised to homotypic Schwann cell-cell junctions. (Ai-ii) NS cells were seeded at low (2×10^4 cells) and high (3.5×10^4 cells) density, and fixed after 72hrs. Representative epifluorescent images of NS monolayers were coimmunostained for N-cadherin (red) and S100 β (green), with cell nuclei labelled by Hoechst (blue). The white arrows illustrate examples of N-cadherin localisation at cell-cell junctions, while the white arrow-heads illustrate examples of N-cadherin localisation at ‘lamellipodia-like’ cytoplasmic processes not in contact with other cells. The white boxes show 4x enlargements of selected regions from the main image.



(B-C) Representative high-magnification epifluorescent images of Schwann cell monocultures showing Schwann cell-cell homotypic junctions. **(B)** Monocultures were coimmunostained for N-cadherin (red) and S100β (green), with white arrowheads indicating homotypic cell-cell junctions. **(C)** Monocultures were immunostained with N-cadherin (red) and counterstained with phalloidin fluorescein (green) to show the actin cytoskeleton. The white arrows indicate colocalisation of N-cadherin with F-actin filaments. The cell nuclei are labelled with Hoechst (blue).

homotypic junctions than higher-density counterparts, with homotypic junctions clearly associated with the presence of robust accumulations of N-cadherin at the cell-cell interface, as shown by the white arrows in **Figure 4.1**. Diffuse low-level N-cadherin staining was also observed throughout the cytoplasm of the cell, but was notably absent from the nucleus. Importantly, N-cadherin was also observed at the surface of cytoplasmic, lamellipodia-like protrusions (indicated by the white arrow-heads). As discussed in Chapter Three, these structures are a morphological characteristic of non-associated Schwann cells. In high-density Schwann cell monocultures (**Figure 4.1Aii**), and also more clearly defined in higher magnification images (**Figure 4.1B**; see white arrow-heads), Schwann cells were observed to form multiple N-cadherin-rich cell-cell junctions with multiple Schwann cells appearing to bind together to form a monolayer. In many cases, N-cadherin immunostaining was extensive, with large ‘zipper-like’ accumulations of N-cadherin observed between contacting cells. There were also examples of large N-cadherin assemblages at cell-cell junctions that permeated deeper into the cytoplasm of neighbouring Schwann cells (**Figure 4.1B**). These observations are consistent with the formation of mature N-cadherin junctions that strengthen overtime via the stepwise *cis*-recruitment of N-cadherin dimers. This was especially evident in high-density cultures where cell-cell encounters are more frequent and are presumably more stable.

In order to further characterise Schwann cell homotypic cell-cell junctions, I visualised the actin cell cytoskeleton in conjunction with N-cadherin immunofluorescence. This was important because cell-cell junctions require firm anchorage to the cell cytoskeleton to withstand the forces required, for example, to maintain Schwann cell clusters or facilitate association to axons. It is well established in epithelial cells that the classical cadherins interact with the actin cytoskeleton, and that this linkage is critical to generating the strength of the cadherin mediated cell-cell junction (Shewan *et al.*, 2005). Thus, alignment between peripheral actin filaments and N-cadherin junctions would indicate that N-cadherin was more likely to be a functional CAM for Schwann cell-cell homotypic interactions. Consistent with this view, Schwann cell monocultures counterstained with phalloidin fluorescein revealed that spurs from the peripheral (cortical) actin network taper towards, and appose with, N-cadherin junctions (**Figure 4.1C**; the white arrows indicate examples of colocalisation and coalignment). This observation supported

the view that the actin cytoskeleton, important for cell movement and structure, is linked and responsive to the adherens junction that maintains the homotypic interactions with neighbouring cells.

4.2.2 siRNA as a tool for N-cadherin knockdown in Schwann cells

To specifically deplete N-cadherin mRNA transcripts from Schwann cells I used small interfering (si)RNAs. I used three different siRNAs from Qiagen's HiPerfect (HP) genome-wide range (siNcad-1, siNcad-3 & siNcad-4), which were designed to recognise non-overlapping short sequences within the three-prime region of the rat N-cadherin mRNA transcript, while scrambled siRNA was included as a control for all siRNA experiments. As we had not previously used siRNA in Schwann cells – I first titrated the siRNA and lipid concentration and varied other parameters in order to determine the optimum conditions for transfection and knockdown. Schwann cell monocultures were transfected 24-hours after plating with siRNA for 16-hours using a range of siRNA concentrations from 1nM to 10nM. Following transfection, the culture plates were washed with fresh-media, in order to remove excess siRNA complexes, and further incubated for 32-hours before fixation, i.e. 48-hours post-transfection. The titration was then assessed by epifluorescence to determine the least amount of siRNA required to achieve the greatest silencing efficacy. This was important, as increasing siRNA concentration is correlated with deteriorating cell health and an increased incidence of cell death (Qiagen manual). Surprisingly, I found that a relatively low concentration of siRNA – 1nM N-cadherin siRNA – was sufficient to efficiently reduce N-cadherin levels in Schwann cells (**Figure 4.2A**). The immunofluorescence showed that while the majority of Schwann cells were depleted of N-cadherin, a small number still retained normal (control) levels of N-cadherin protein (see white arrows); reflecting instances where transfection had not been successful.

The proportion of non-transfected cells, as quantified from N-cadherin immunofluorescence, was determined for each siRNA (scrambled, siNcad-1, siNcad-3, siNcad-4), with both siNcad-3 and siNcad-4 achieving the greatest proportion of Schwann cells knocked down for N-cadherin at over 90% (**Figure 4.2B**). I next

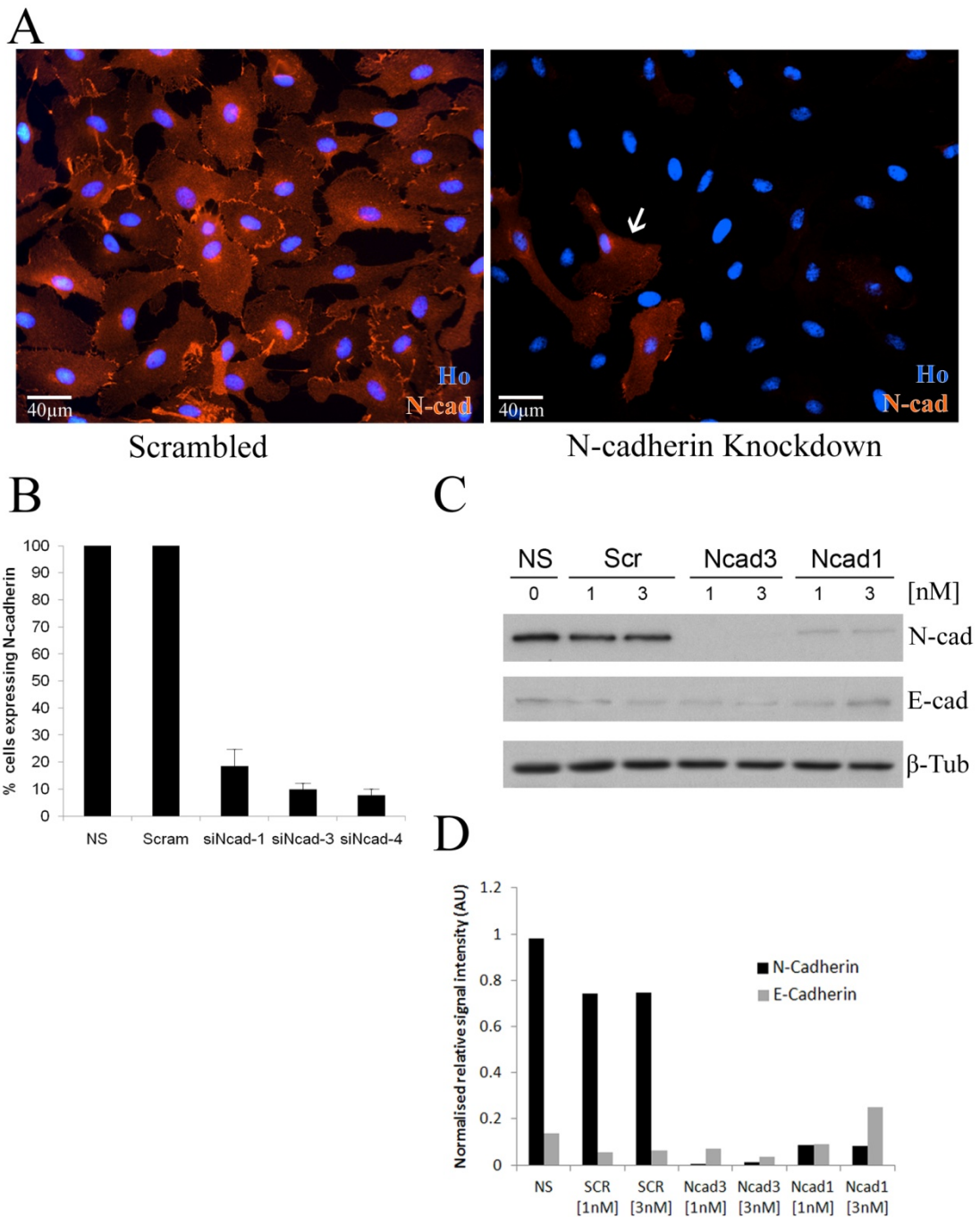
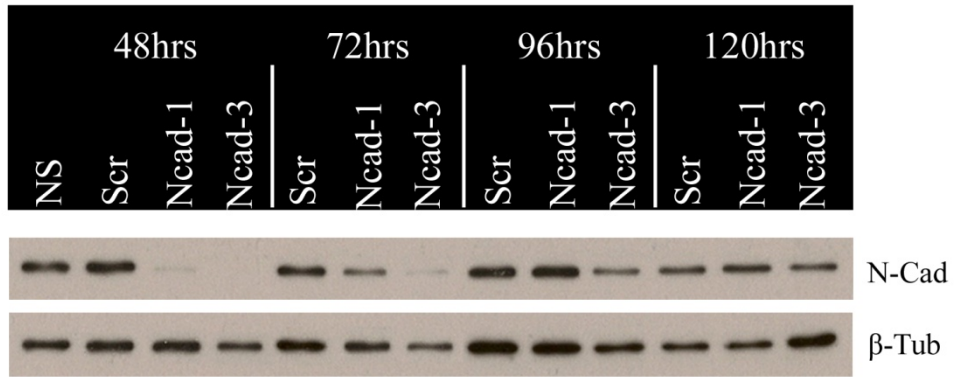
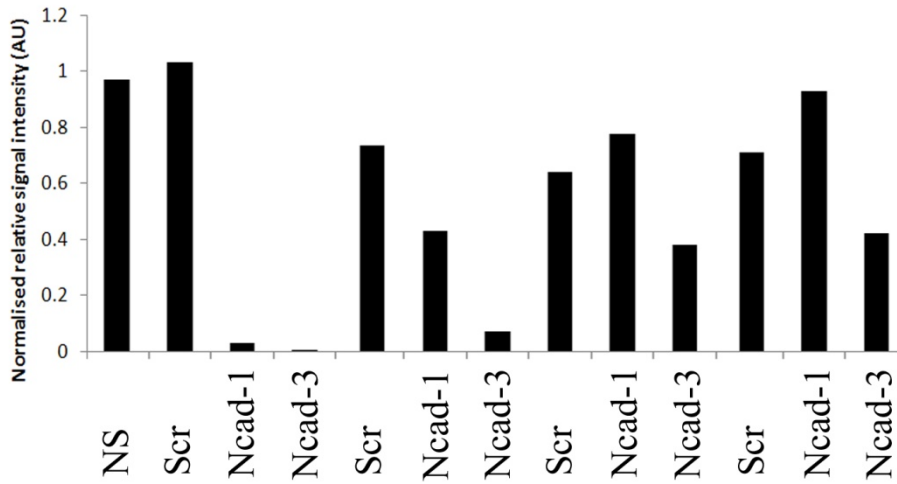


Figure 4.2 siRNA mediated N-cadherin silencing is effective, specific and transient. NS cells were transfected 24hrs after seeding for 16hrs with 1nM or 3nM siRNA of either scrambled or three N-cadherin siRNAs (siNcad-1, siNcad-3 & siNcad-4). Cells were media-changed and further incubated for 32hrs, after which cells were fixed and RNA collected. **(A)** siRNA transfected monocultures were immunostained for N-cadherin (red), and cell nuclei were labelled with Hoechst (blue). The white-arrows show examples of N-cadherin-positive, non-transfected cells. **(B)** The proportion of Schwann cells expressing N-cadherin following siRNA treatment. Counts in triplicate with 200+ cells scored per coverslip; bars represent S.D. **(C)** Western blot: relative levels of N and E cadherin following N-cadherin knockdown. **(D)** Quantification of Western analysis in part C by densitometry.

E**F**

(E) NS cells were transfected with 1nM of either scrambled, siNcad-1 or siNcad-3 siRNA 24hrs after seeding for 16hrs. Initial cell concentrations were adjusted to achieve confluent plates at respective time-points (48hrs, 72hrs, 96hrs and 120hrs following addition of transfactant), and cell lysates were obtained from plates for Western analysis to determine relative levels of N-cadherin across conditions with β -tubulin used to control lane loading. (F) Densitometric analysis of Western blot (part E) to quantify relative levels of N-Cadherin with time post-transfection. The data was normalised against β -tubulin.

analysed N-cadherin protein levels by Western blot to quantify the level of knockdown. Schwann cells were transfected with either 1nM or 3nM of scrambled, siNcad-1 or siNcad-3 and RNA was collected 48-hours after the start of transfection. Western blots were immunoprobed for N-cadherin and E-cadherin (**Figure 4.2C**) and normalised relative levels were quantified by densitometry analysis (**Figure 4.2D**). This work confirmed that 1nM of Ncad-1 siRNA was sufficient to achieve a good knockdown of N-cadherin (approximately 8-fold), while 1nM of Ncad-3 siRNA was sufficient to substantially deplete N-cadherin from Schwann cells (approximately 200-fold), which was particularly impressive. Increasing the siRNA concentration to 3nM did not reduce N-cadherin levels further for either siRNA. This is consistent with previous findings, i.e. from the siRNA titration, which showed that 1nM of siRNA was optimal for N-cadherin knockdown. The specificity of N-cadherin siRNA was confirmed by the finding that E-cadherin levels remained relatively constant. I next wanted to determine the period of N-cadherin knockdown following a single transfection as this would be an important limiting parameter for subsequent siRNA experiments. To do this, I assayed, by Western analysis, the relative change in N-cadherin protein levels over time after the start of transfection (**Figure 4.2E**); and quantified this result by densitometry in **Figure 4.2F**). This data showed that the knockdown of N-cadherin lasted at least 72-hours, after which N-cadherin levels increased and were returned to basal levels by 96-hours – consistent with the time-wise dependent degradation of siRNA. Thus, on this basis I decided to take a conservative approach to future siRNA experiments, stipulating that the experiment be concluded 72-hours after the addition of transfectant, in order to guarantee N-cadherin knockdown at the experimental endpoint.

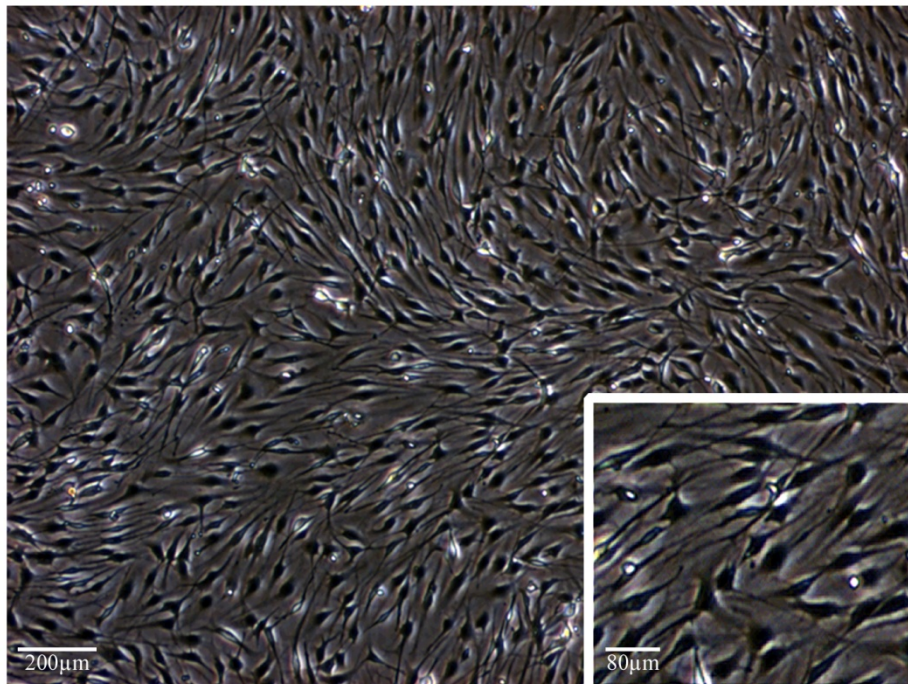
4.2.3 N-cadherin is the principal mediator of homotypic interactions

Having optimised siRNA as an effective tool to deplete N-cadherin specifically from primary Schwann cells, I next assessed whether N-cadherin was required for homotypic Schwann cell-cell interactions. NS cells were plated and transfected 24-hours later with N-cadherin siRNA for 16-hours. Culture plates were then washed with fresh medium and further incubated for 48-hours until the monocultures were confluent. In contrast to non-transfected or scrambled controls, which showed characteristic ‘swirling’ patterns of Schwann cells typical of a confluent monolayer,

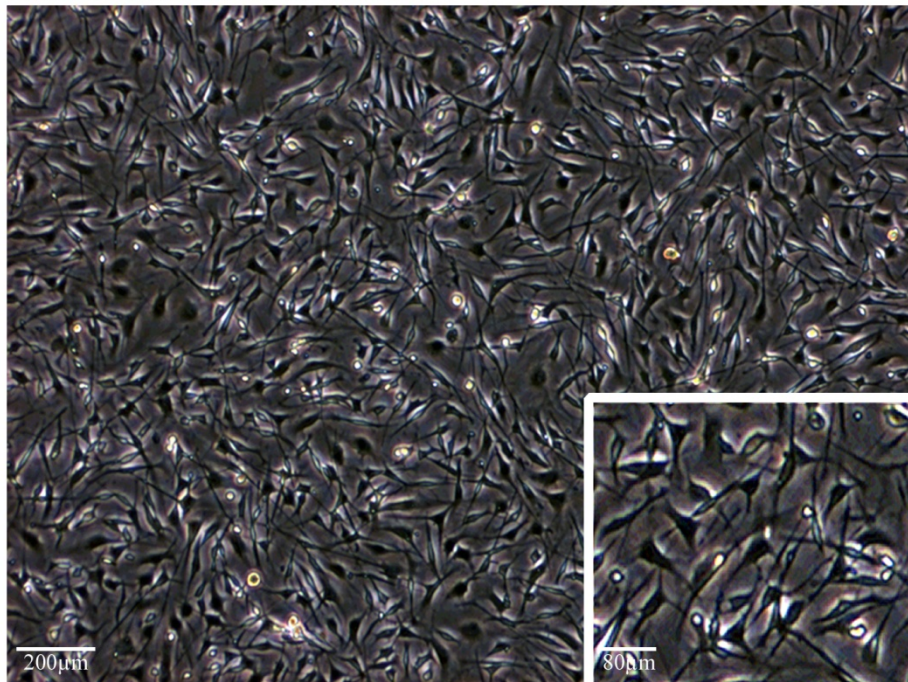
the N-cadherin-deficient monocultures were highly disorganised. These monocultures did not form Schwann cell ‘swirls’; instead, Schwann protrusions were often observed to encroach over the cytoplasm of adjacent Schwann cells (**Figure 4.3A**; also see enlargement box). These observations highlighted a general breakdown in the integrity of the Schwann cell monolayer. To examine this further, I next fixed and immunostained the monocultures for N-cadherin and counter-stained with phalloidin in order to visualise the actin cytoskeleton. While control cultures formed a tight monolayer, which was maintained by multiple homotypic interactions, monocultures depleted of N-cadherin formed very few homotypic junctions and consequently the monolayer was highly disrupted (**Figure 4.3B**). The cell morphology and actin cytoskeleton are also substantially altered in these cultures. In the scrambled (control) Schwann cells cultures, the cytoplasm of cells appeared to be stretched between neighbouring Schwann cells, while the phalloidin stain revealed large parallel and polarised arrangements of F-actin, which typically spanned the length of the cell and were often observed to link homotypic junctions from polar ends of the cell (see white arrow). In contrast, N-cadherin-depleted Schwann cells had fewer cell-cell junctions and presented a rounded, less-polarised morphology. Moreover, the phalloidin stain revealed that the actin cytoskeleton predominantly formed concentric rings about the cortex of the cell rather than parallel stress fibres observed in controls (see white arrow-head). It is highly likely that the different cellular phenotypes outlined above arise from the failure of N-cadherin mediated Schwann cell-cell interactions. This is primarily because of the loss in the combined tensile force that would otherwise have been exerted by adjacent and contacting cells. In addition, Gavard *et al.* (2004) showed, using another cell-culture system, that interactions between adherens junctions and the actin cytoskeleton was a key determinant to overall cell morphology.

In order to quantify the loss of Schwann cell-cell homotypic interactions, I developed an algorithm, using Image-J software, to determine the extent to which N-cadherin-loss affected the integrity of the Schwann cell monolayer. I designed a systematic, non-biased assay to detect differences in the extracellular area within Schwann cell monocultures in which the cells had been transfected with either scrambled or N-cadherin siRNA. We hypothesised that, for a fixed number of cells per unit area, the extracellular area comprising the gaps between cells would be inversely correlated to

A



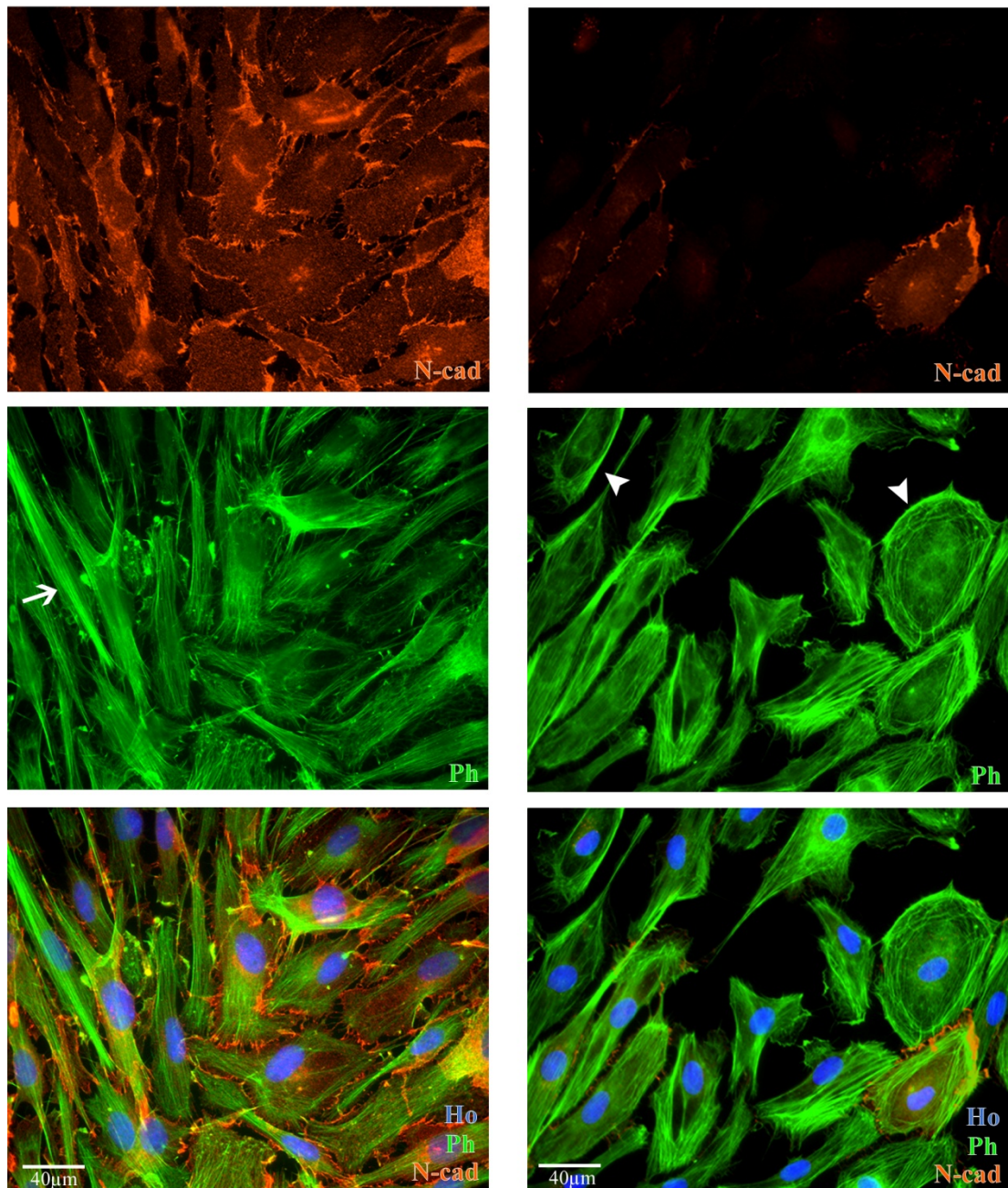
Scrambled Schwann cells



siRNA N-cadherin knockdown Schwann cells

Figure 4.3 N-cadherin knockdown disrupts homotypic interactions in NS monocultures. Schwann cells were transfected with 1nM of either scrambled or siNcad-3 siRNA. The media was then changed and monocultures were further incubated for 32hrs. (A) Phase-contrast live images of cells 48hrs after transfection. The box inserts show representative enlargements from the main image.

B



Scrambled siRNA monoculture

N-cadherin siRNA monoculture

(B) Representative epifluorescent images of Scrambled and N-cadherin-deficient Schwann cells. Schwann cells were fixed 48hrs after transfection and immunostained for N-cadherin (red) and counter-stained with phalloidin fluorescein (green) to reveal the actin-cytoskeleton, while cell nuclei were labelled with Hoechst (blue). The white arrow shows an example of stretched actin filaments observed in scrambled siRNA cultures, while the white arrow-heads show examples of cortical actin arrangements as often observed in N-cadherin depleted Schwann cells.

the density of homotypic junctions present. Thus, an increase in extracellular area would imply a decline in homotypic interaction and junctions, reflecting a loss of integrity in the Schwann cell monolayer. NS monocultures were transfected with either scrambled or N-cadherin siRNA for 16-hours and fixed 48-hours post-transfection. Monocultures were immunostained first for N-cadherin which confirmed that N-cadherin siRNA transfected cultures were depleted of N-cadherin relative to controls (**Figure 4.4Ai**), and second, for cell-surface expressed p75^{NTR}, which was used in preference to S100 β immunofluorescence, in order to highlight Schwann cells because this antibody provided improved contrast between intra- and extra- cellular regions, an essential requirement for the automation of this analysis (**Figure 4.4Aii-iv**). Greyscale-images were captured from randomly selected fields-of-view taken from p75^{NTR} immunostained Schwann cell monocultures. Images were processed using Image-J to identify the extracellular regions, shown in red (**Figure 4.4Aiii-iv**), which were then converted to an area map, depicting the boundary of the extracellular area, and overlaid against the original p75^{NTR} immunofluorescence (**Figure 4.4Aiv**). This enabled us to calculate the extracellular area in the monolayer which showed that loss of N-cadherin from Schwann cells resulted in a 2.5-fold increase in the extracellular area reflecting the loss of homotypic interactions (**Figure 4.4B**). Together, this data indicates that N-cadherin is the principle mediator that forms and maintains homotypic adhesive interactions between Schwann cells.

4.2.4 N-cadherin inhibit Schwann cell proliferation

While investigating the effect of N-cadherin depletion on homotypic interactions, we noticed that there appeared to be an increase in cell number in monocultures where N-cadherin was depleted. I decided to investigate this further by measuring the rate of proliferation in scrambled and N-cadherin knockdown monocultures. To do this I initially used a 5-bromo-2-deoxyuridine (BrdU) incorporation assay. NS monocultures were seeded at low and high density and transfected for 16-hours with either N-cadherin (siNcad-3 and siNcad-4) or scrambled siRNA, or they were left untransfected. Monocultures were further incubated for 24-hours prior to the addition of BrdU for 7-hours, and then fixed and immunostained for BrdU to label nuclei in S-phase. The proportion of cells in S-phase was used as a read-out for the

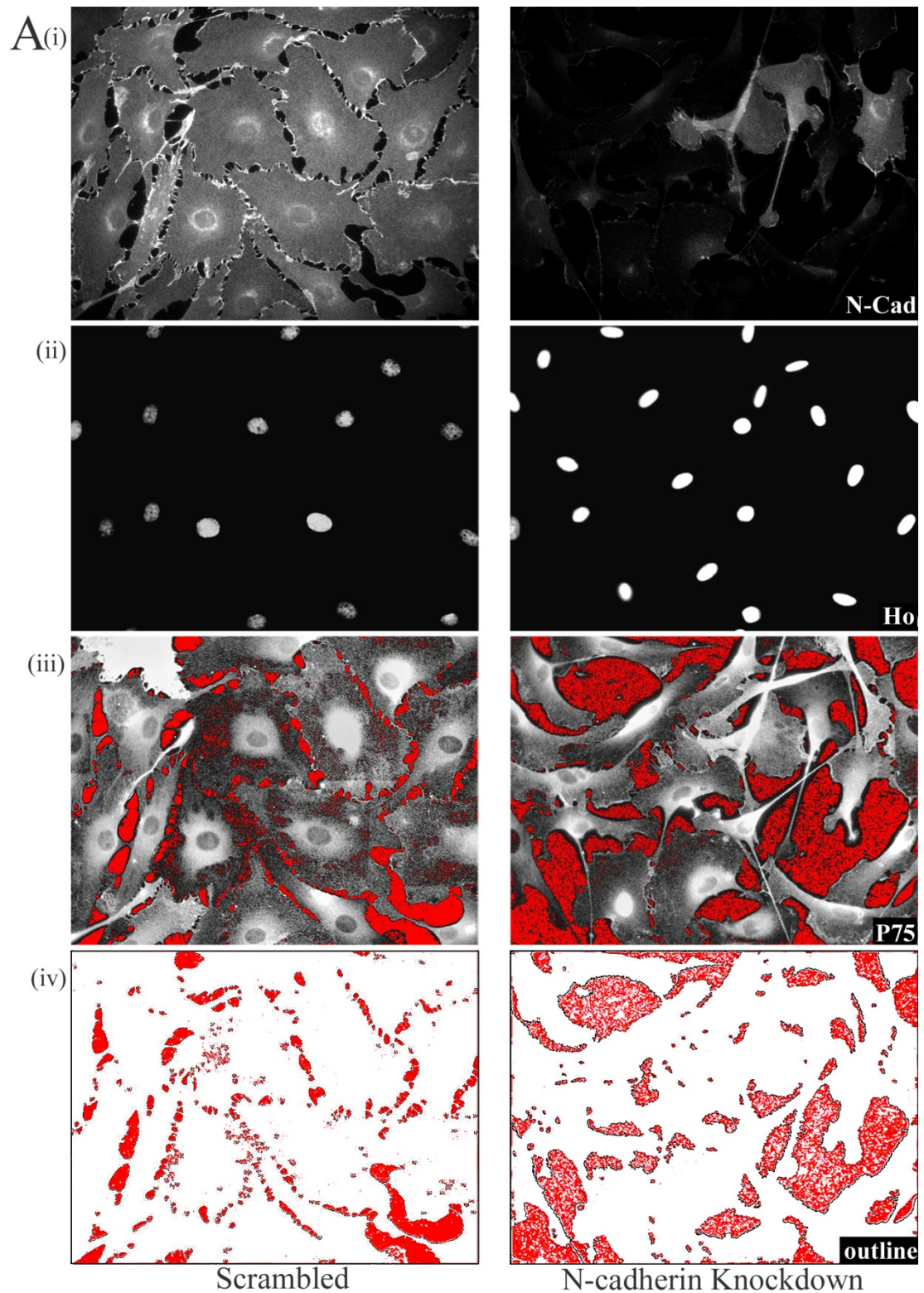
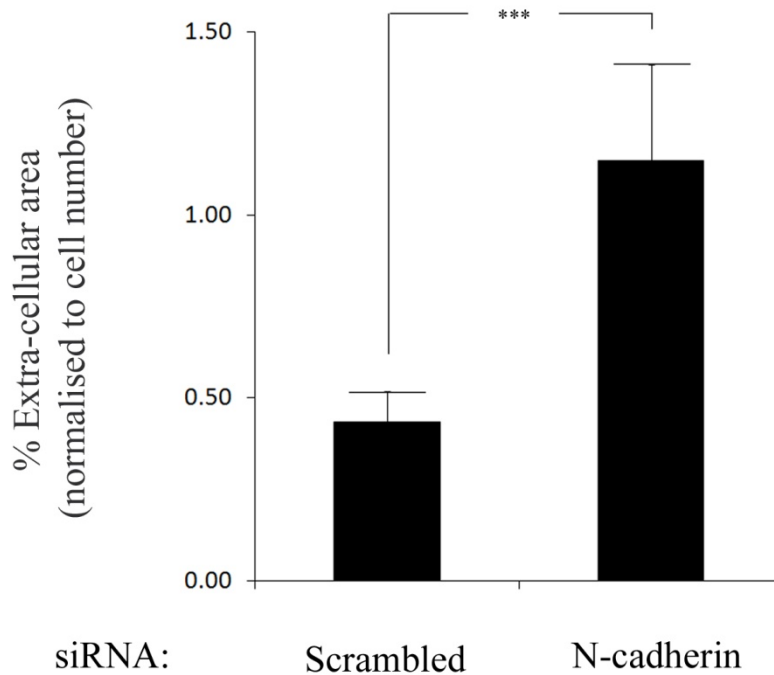


Figure 4.4 N-cadherin silencing disrupts homotypic Schwann cell-cell interactions. Scrambled or Ncad-3 siRNA transfected Schwann cells were immunostained for (i) N-cadherin and (ii) nuclei labelled with Hoechst. (iii) Cultures were immunostained for P75^{NTR}, images were cropped and extracellular area was demarked in red using Image-J. (iv) Extracellular area was calculated using a pre-optimised threshold particle area, to prevent erroneous counting of intracellular regions.

B



(B) Quantification of the extracellular area, as calculated in part A, was determined from multiple sets of immunofluorescent images captured in a randomised fashion from scrambled and N-cadherin siRNA Schwann cell monocultures with bars showing S.D. from triplicates. The data was normalised by dividing the area fraction by the total number of cells. Shown is one of three independent experiments showing similar results. Statistics: two-tailed T-test ($T=9.004$, $***p > 0.0001$).

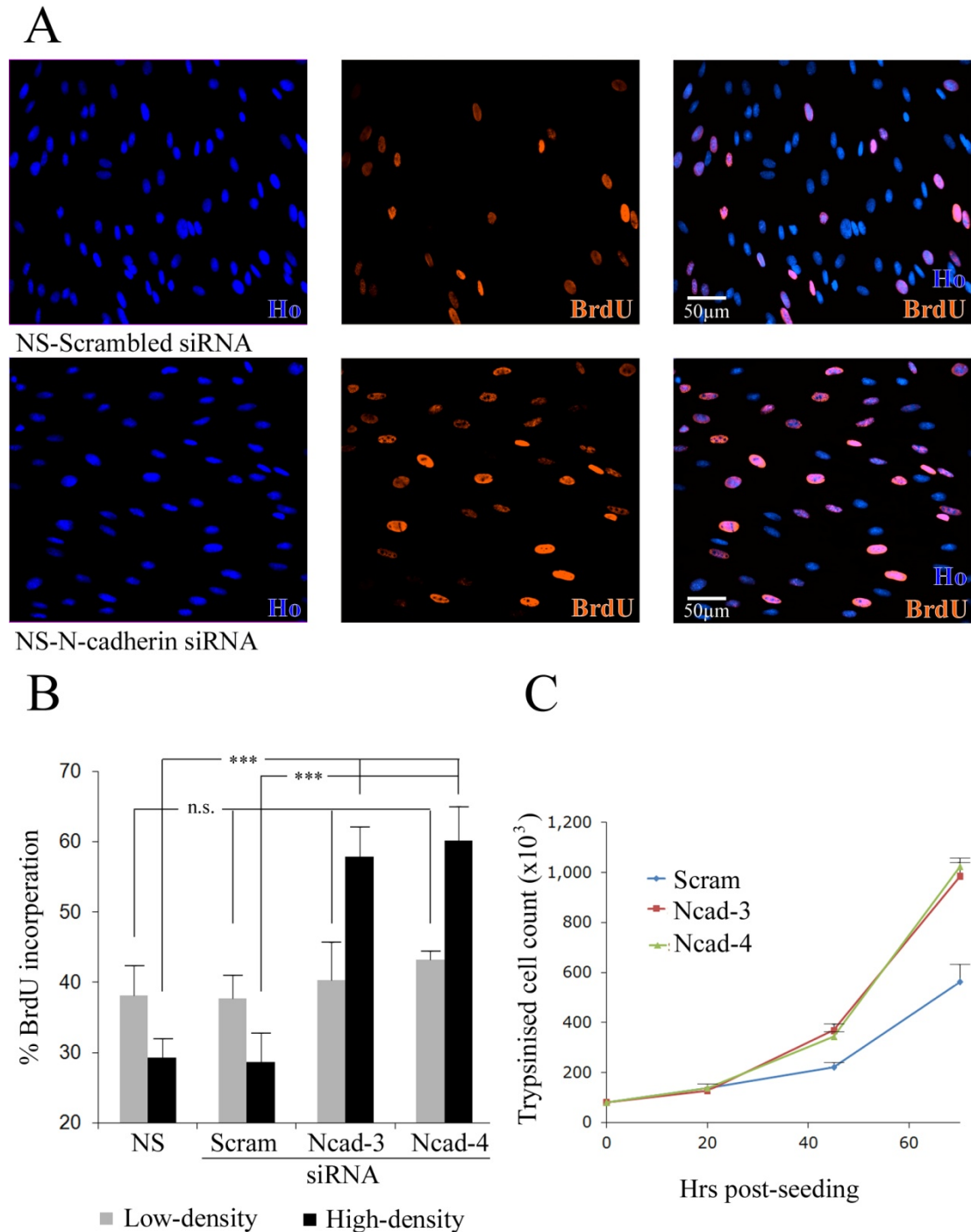


Figure 4.5 N-Cadherin reduces Schwann cell proliferation in a density dependent manner. (A) Low and high density Schwann cells were transfected with scrambled or N-cadherin siRNA for 16hrs and further incubated for 24hrs prior to addition of BrdU for an 8hr pulse. Representative epifluorescence from cultures immunostained for BrdU (red) with cell nuclei labelled with Hoechst (blue). (B) Proportion of BrdU positive cell nuclei. Counts conducted in triplicate with 200+ cells scored per coverslip; bars represent S.D. with statistics by T-test (** $p < 0.001$) (C) Transfected Schwann cells were plated and trypsinised at 20, 45 and 70hrs post-seeding in order to obtain cell counts; bars represent S.D. of triplicates. Datasets from parts B & C are representative of three independent experiments.

rate of cell proliferation. The data confirmed that N-cadherin deficient Schwann cells exhibited elevated proliferation in higher density cultures, showing a two-fold increased rate of BrdU incorporation over relevant controls (**Figure 4.5A-B**). This was consistently observed for both independent N-cadherin siRNAs (siNcad-3 and siNcad-4) confirming the specificity of the response. In contrast, N-cadherin knockdown did not significantly alter the rate of proliferation in low-density cultures in which homophilic N-cadherin *trans*-ligation occurred less frequently. Thus, the increased proliferation observed in N-cadherin depleted cells appeared to be density-dependent, implicating N-cadherin signalling in the inhibition of cell proliferation as Schwann cells reached confluency. To confirm these findings, I perfected a temporal proliferation assay by counting the total number of cells with time in culture. To do this, NS cells were transfected with either scrambled, siNcad-3 or siNcad-4 for 16-hours, the cell media was changed and the cells were trypsinised 4-hours later. Transfected cells were then seeded in triplicate onto culture plates (time 0) and incubated for 20, 45 and 70-hours after seeding. At each time-point, the plates were trypsinised and the cell-suspension counted using a Coulter Counter to obtain cell counts (**Figure 4.5C**). Consistent with previous results, the rate of cell proliferation at early time-points was not significantly different. However, as the cell density increased, N-cadherin depleted Schwann cells continued to proliferate rapidly, while control cells proliferated at a markedly slower rate. Together with the BrdU analysis, these findings suggest that N-cadherin *trans*-ligation between Schwann cells that mediate homotypic Schwann cell-cell junctions is inhibitive to proliferation and at least partially responsible for CIP observed in confluent Schwann cell monolayers.

4.3 Heterotypic Schwann cell/axonal interactions

I next wanted to determine the role of N-cadherin as a mediator of heterotypic Schwann cell/axonal interactions. I initially focussed on the early events of Schwann cell/axonal interactions as modelled in **Figure 3.1B**. In order to do this, I adapted the defined DRG/Schwann cell coculture system described in Chapter Three. DRG capsules were explanted and exposed to AraC for 48-hours and then further incubated for five days in order to generate axonal cultures free from endogenous Schwann cells. In parallel, Schwann cells were transfected with either scrambled or

N-cadherin siRNA for 16-hours and further incubated for 24-hours. Cells were then trypsinised, counted with a Coulter counter and seeded at low-density onto DRG axonal explants. Schwann cell/DRG cocultures were then incubated for 8-hours, fixed and coimmunostained for Schwann cell specific S100 β and axonal specific RT97 in order to assess the state of heterotypic interaction. As expected, when scrambled (control) Schwann cells were incubated with DRGs, the majority of the cells were found to be strongly associated and aligned with axons (**Figure 4.6A**; see white arrows). Interestingly, when N-cadherin-deficient Schwann cells were incubated with DRGs, there were many examples of deficiencies in both axonal association and alignment (see white arrow-heads). In contrast to controls, the N-cadherin-deficient Schwann cells that failed to associate properly with axons, were often observed either to fail entirely to contact an axon despite close proximity, or to extend their cytoplasmic protrusions over and/or under axons without making contact. In other cases an indeterminate interaction was evident, in which the Schwann cell made contact but the cell cytoplasm was not aligned with the axon. Quantification of the interactions using the association scoring system (association assay) described previously (**Figure 3.2D**), i.e. associated and aligned, associated, not aligned or not associated, confirmed that heterotypic Schwann cell/axonal interactions were impaired in N-cadherin-deficient Schwann cells, to the extent that 40% of cells either failed to associate with, or failed to align themselves with, axons as compared to around 10% deficiencies in relevant controls (NS, Scrambled or LTNS) (**Figure 4.6B**). However, while depletion of N-cadherin from NS cells was sufficient to disrupt heterotypic interactions with axons, it did not account fully for the impairment observed in LTD/DRG cocultures, in which the vast majority of LTD cells (in excess of 95%) failed to associate or align with axons. This implied that while N-cadherin is an important mediator of heterotypic interactions, it was not the only molecule involved, and thus, was likely to be acting in concert with other molecules to mediate these interactions.

A

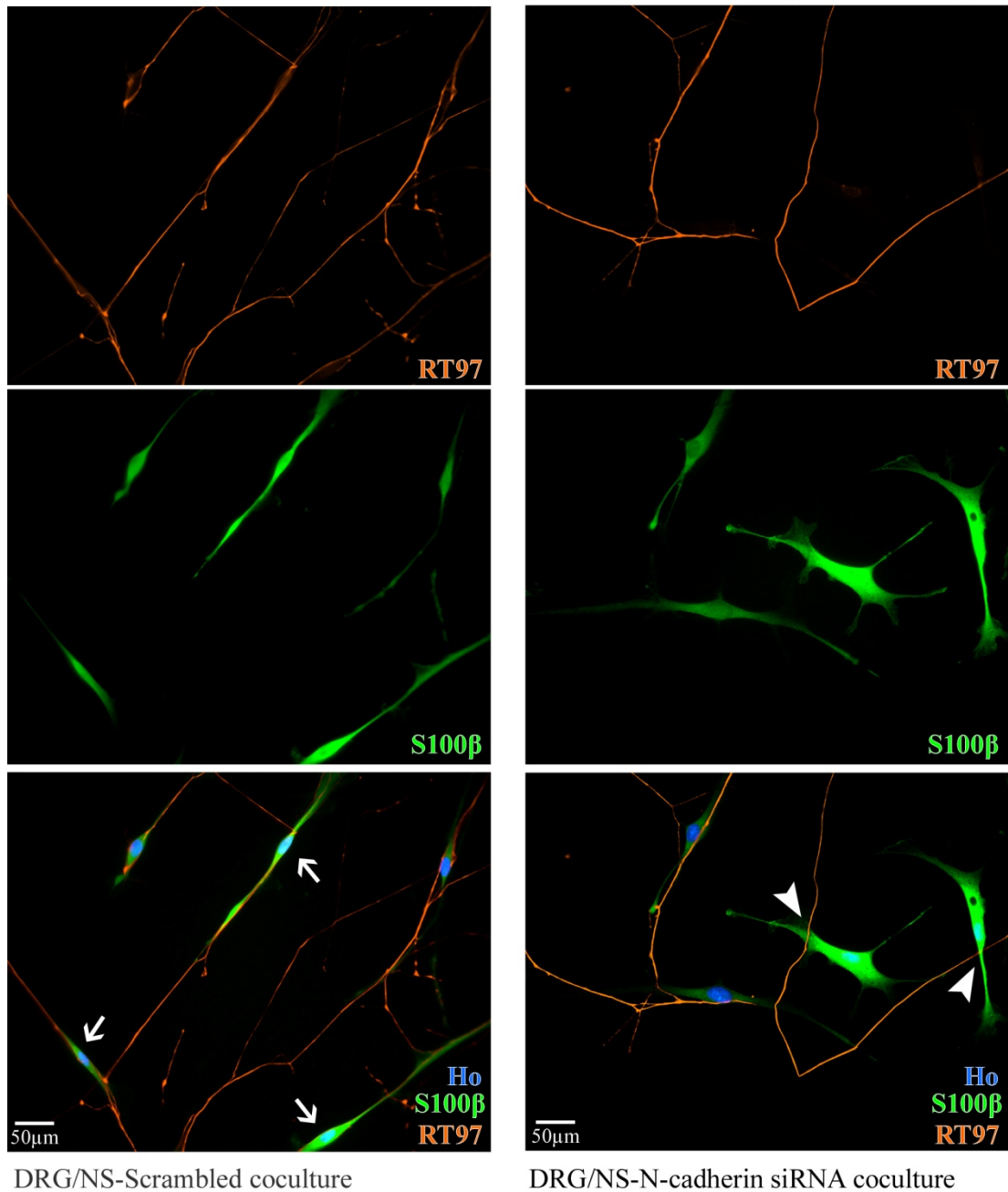
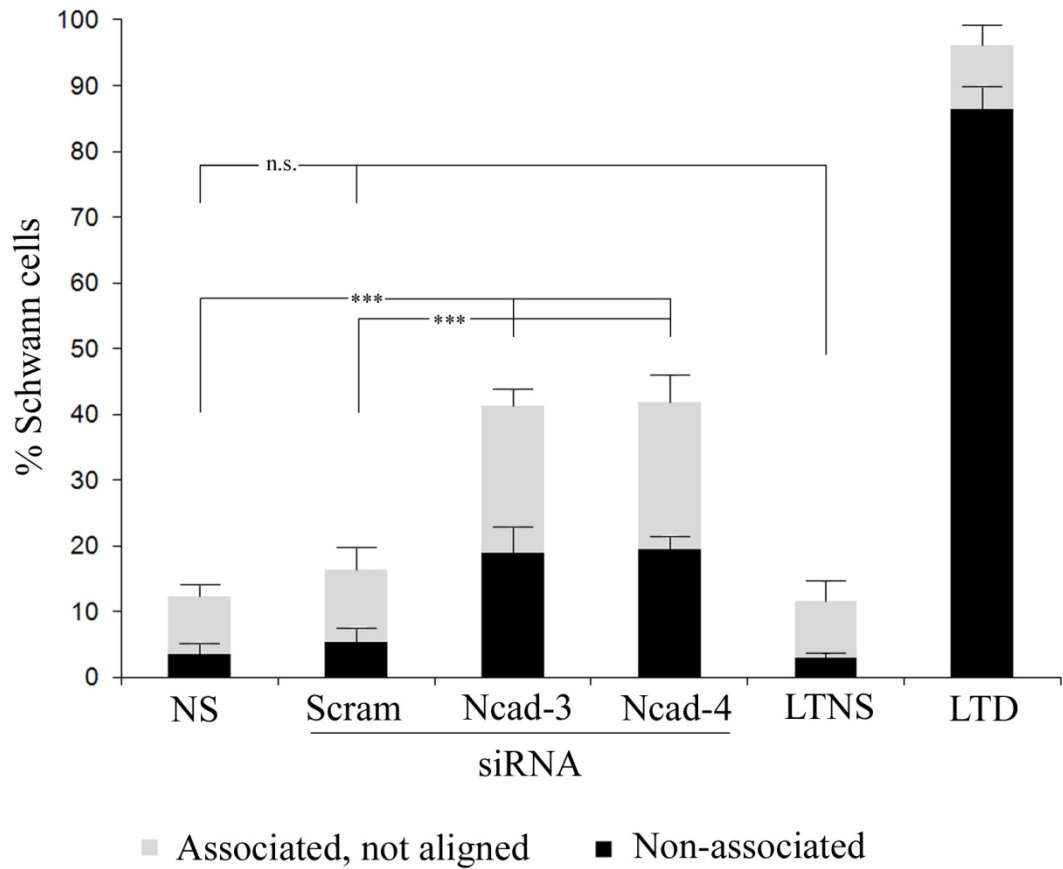


Figure 4.6 N-Cadherin knockdown disrupts heterotypic Schwann cell/axonal association & alignment. NS cells were transfected for 16hrs with either scrambled or N-cadherin siRNA, while DRG explants were incubated over 5 to 6 days to generate axonal networks. Transfected Schwann cells were media-changed and further incubated for 24hrs, after which Schwann cells were seeded onto DRG axons and cocultures fixed after 8hrs. (A) Representative epifluorescent images from cultures coimmunostained for S100 β (green) to show Schwann cells and RT97 (red) to show axons, with cell nuclei labelled with Hoechst (blue). The white arrows show examples of Schwann cell association and alignment, while the white arrow-heads show examples of non-associated Schwann cells.

B

(B) Quantification of Schwann cell/axonal interactions. Immunofluorescence from NS, scrambled (Scram), N-cadherin siRNA (siNcad-3 and siNcad-4), LTNS and LTD cell/DRG-axonal cocultures were scored. The graph shows the proportion of non-associated cells (black bars) or associated but not aligned cells (grey bars) (refer to Figure 3.2D for scoring criteria). Scoring was conducted blind from triplicate cocultures (200+ cells/DRG) with bars showing S.D. Shown is a representative dataset from three independent experiments that gave similar results. Statistical significance analysed by one-way ANOVA Tukey-Kramer Multiple Comparisons Test (***p* < 0.001, n.s. not significant).

4.3.1 N-cadherin localisation in Schwann cells, axons & heterotypic junctions

To address how N-cadherin might be mediating heterotypic interactions, I next examined the localisation of N-cadherin within Schwann cells and axons. To do this, Schwann cells were seeded onto established DRG-axonal cultures and cocultures were fixed after three, six or eight hours of incubation, after which they were coimmunostained for N-cadherin and neurofilament. The immunofluorescence showed that N-cadherin was expressed by both Schwann cells and, to a lesser extent, axons (**Figure 4.7**). Importantly, by eight hours, which was the incubation time selected as the end-point for the association assays, Schwann cells and axons were observed in close associated interactions (**Figure 4.7Aiii**). Interestingly, I found that N-cadherin was strongly localised at the extremities of Schwann cell lamellipodia-like protrusions, either robustly at sites of Schwann cell/axonal heterotypic interaction, as indicated by the white arrows, or in regions that had yet to make contact with an axon, as indicated by white arrow-heads. In the case of the latter, this is consistent with earlier findings in Schwann cell monocultures (**Figure 4.1A**), in which I observed N-cadherin concentrated at the extremity of Schwann cell protrusions. With this in mind, it is likely that N-cadherin, present in the protrusions of Schwann cells, might be functioning as an axonal sensor. Positive recognition of axons by Schwann cell ‘lamellipodia-like’ processes, through homophilic *trans*-ligation of N-cadherin, could then culminate in the later generation of N-cadherin-rich heterotypic junctions between Schwann cells and axons. These adherens junctions continue to mature so that by eight hours, strong N-cadherin staining can be observed - resulting in the stabilisation of the Schwann cell/axonal association (**Figure 4.7Aiii**).

4.3.2 Schwann cells use cytoplasmic protrusions to locate, recognise and initiate association

Immunofluorescence derived from fixed cocultures, revealed that N-cadherin was enriched in the tips of the Schwann cell cytoplasmic protrusions, which we hypothesised could be acting as an axonal sensor. I therefore wanted to examine the importance of N-cadherin enrichment in these structures, which often make first

A

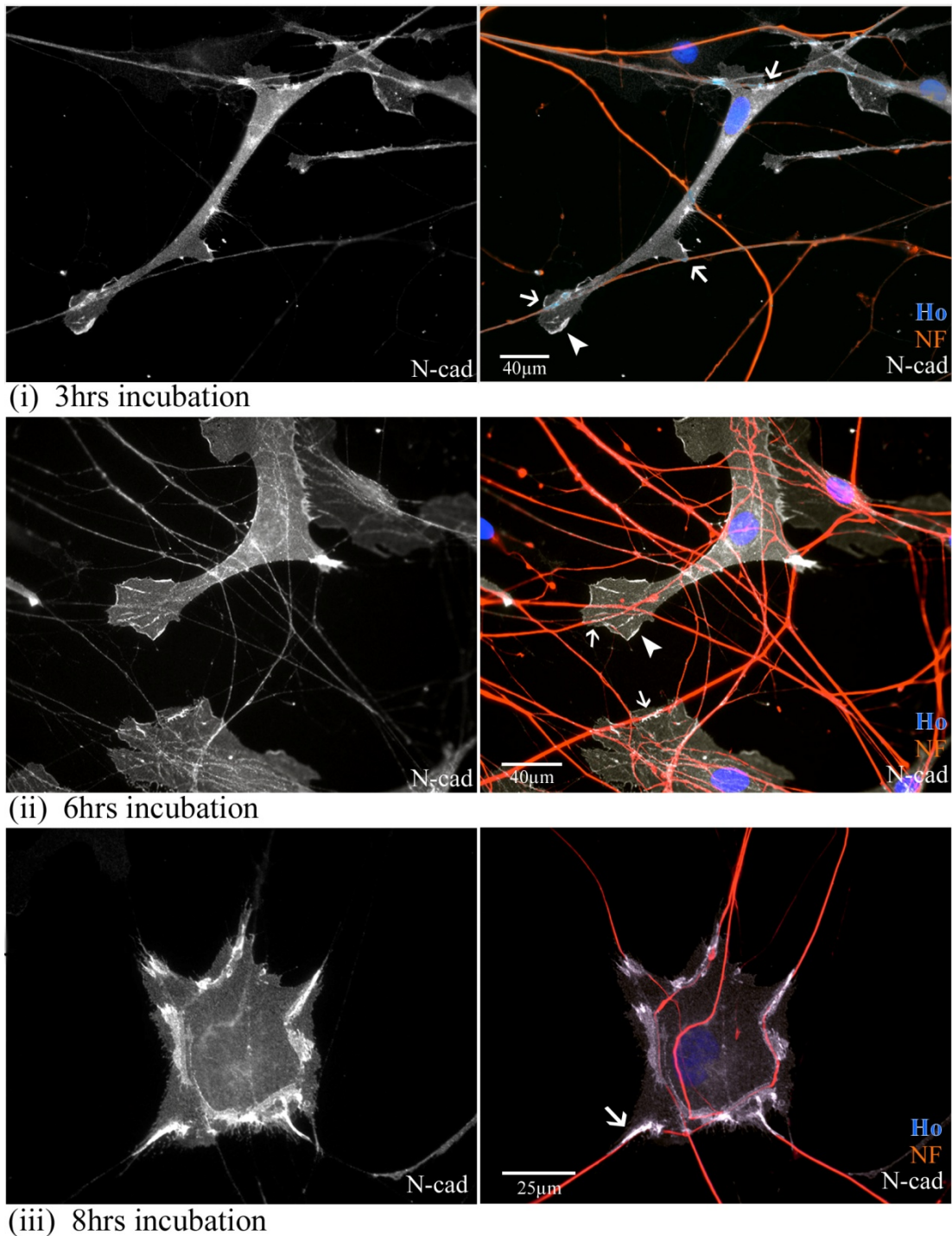


Figure 4.7 Temporal analysis of N-Cadherin localisation in Schwann cells interacting with axons. Schwann cells were seeded onto day-7 explanted DRG axons and cocultures fixed after 3hrs, 6hrs and 8hrs incubation. (A) Epifluorescence of cocultures coimmunostained for N-cadherin (white) and the axonal marker neurofilament (red), with cell nuclei labelled with Hoechst (blue). White arrows show examples of N-cadherin localisation at sites of Schwann cell/axonal interaction and white arrow-heads show examples of N-cadherin localisation at Schwann cell lamellipodia-like protrusions prior to axonal contact.

contact with axons as observed in earlier time-lapse analysis (**Figure 3.1**). To understand the role of N-cadherin in Schwann cell axonal-'grabbing'-behaviour, I performed time-lapse microscopy and analysed the behaviour of Schwann cells upon encountering axons. DRG's were explanted and axonal cultures were incubated for 7 days. Schwann cells were transfected with scrambled or N-cadherin siRNA for 16-hours and seeded onto axons 24-hours later so that multi-point time-lapse analysis could be performed over 20-hours. Three videos were captured for each condition, with fields-of-view selected so that recently seeded Schwann cells were in close proximity to axonal arbours. The behaviour of scrambled Schwann cell/axonal encounters was indistinguishable from previously analysed NS/axonal interactions (see **Figure 3.1** & **Video 3.1**), both of which exhibited classic 'grabbing-like' behaviour, making extensive use of cytoplasmic protrusions to search for and 'pull' on axons. This behaviour often resulted in substantial remodelling of the axonal network as axons were 'pulled' by, and between, different Schwann cells. In contrast, N-cadherin-deficient Schwann cells appeared to have lost the inherent ability to recognise and 'grab' axons (**Figure 4.8A**). Consequently, the axonal network remained largely static as Schwann cell protrusions failed to pull or move axonal arbours. Loss of N-cadherin, therefore, resulted in the failure of Schwann cells to elicit recognition and to trigger the process of association that would normally cause the Schwann cell to 'swing-up' onto the axon. I next quantified the observed behaviour using a simple paradigm. Each initial encounter between a cytoplasmic protrusion (from a Schwann cell) and an axon was coded as either a) grabbing or b) not grabbing. These criteria only take into account first contact events and do not measure the overall state of association and alignment as determined in fixed cultures. This quantification provided striking evidence that loss of N-cadherin, especially from Schwann cell cytoplasmic protrusions, significantly abrogated the Schwann cell's ability to 'grab' axons, to the extent that there were less than half as many 'grabbing' behaviours scored in videos of N-cadherin depleted cells as compared to scrambled siRNA controls (**Figure 4.8B**). These findings support the previous localisation studies and allowed us to propose a model of how N-cadherin functions to enable Schwann cell/axonal interactions. Intriguingly however, many Schwann cells were still able to associate in some way with axons even if their cytoplasmic protrusions appeared to pass over or under the axon. This appeared to be because the Schwann cell 'body' still makes an adhesive contact with

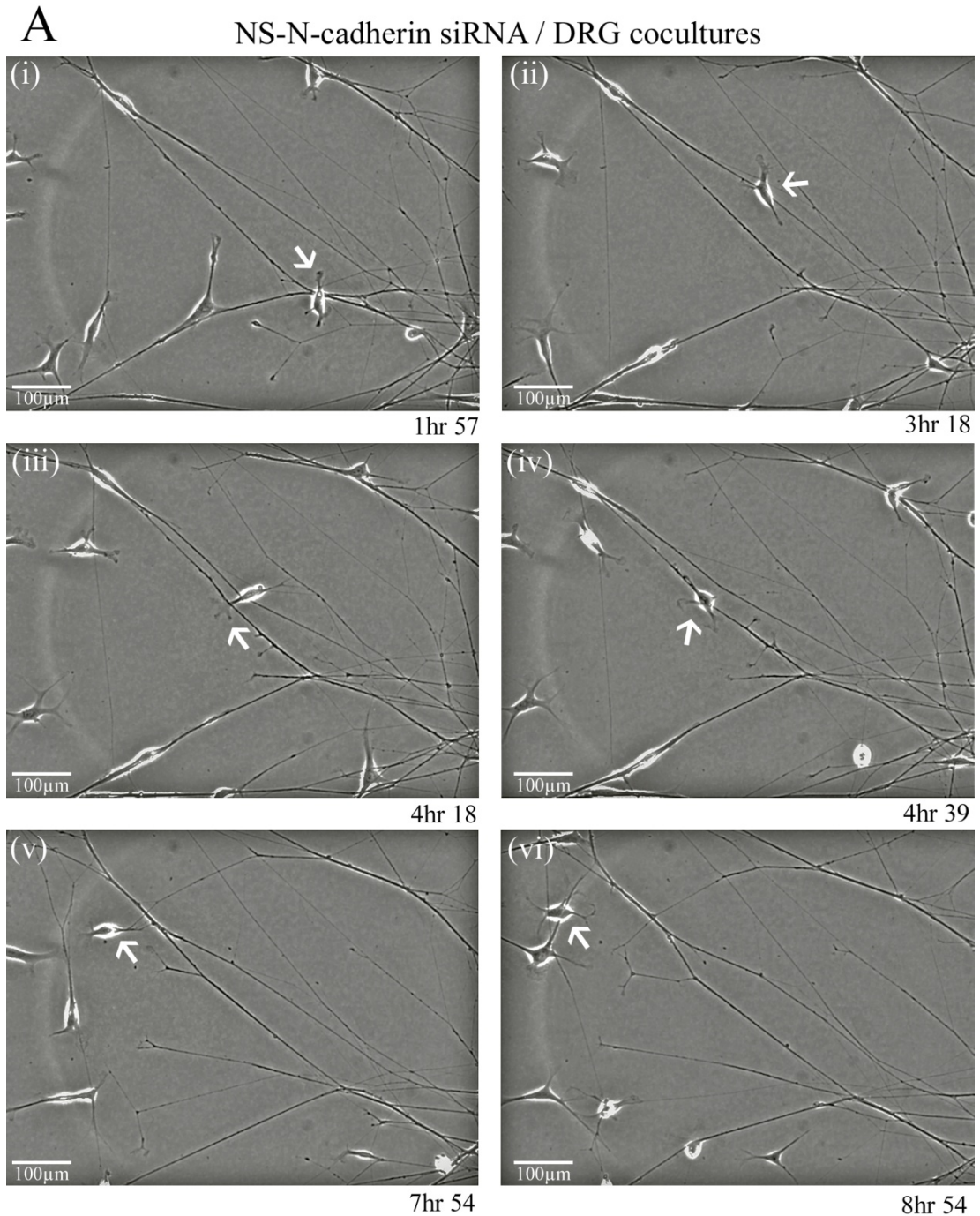
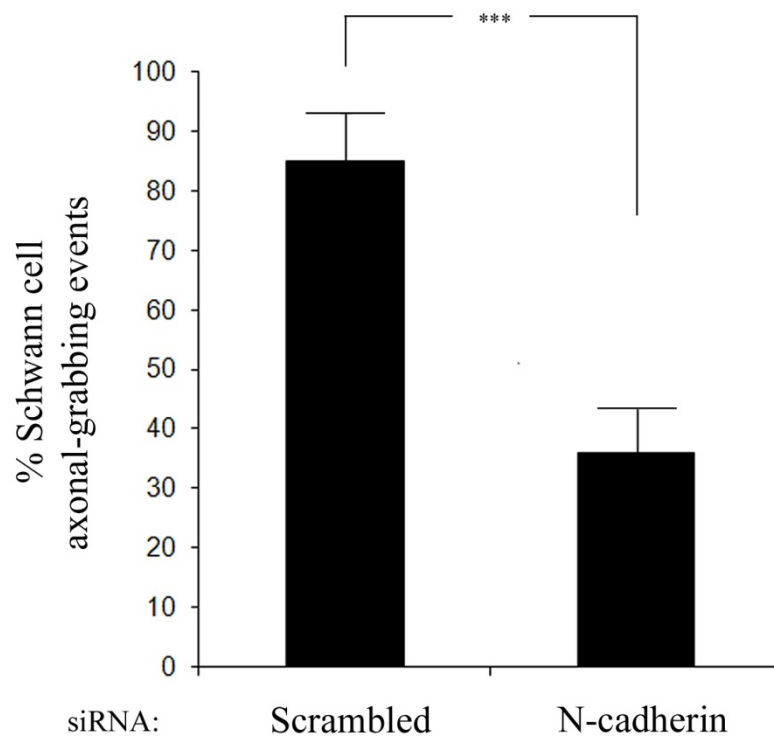


Figure 4.8 N-cadherin deficient Schwann cells showed an impaired ability to recognise and ‘grab’ axons. NS cells were transfected with either scrambled or N-cadherin siRNA, seeded onto DRG axons and incubated for 20hrs in order that time-lapse analysis could be performed (**Video 4.1**). (**A**) An image sequence from Video 4.1, where white arrows illustrate the course of a typical N-cadherin deficient Schwann cell as it encounters axons. Note that the distal tips of the lamellipodia-like protrusions pass under or over axons but will invariably fail to ‘grab’, ‘pull’ or manipulate axons.

B



(B) Quantification of Schwann cell/axonal ‘grabbing’ behaviour. The bar chart shows the percentage of Schwann cell/axonal encounters which resulted in the Schwann cells ‘grabbing’ the axon, specifically by using their ‘lamellipodia-like’ cytoplasmic projections. At least three videos were quantified per experiment with typically 15-20 Schwann cells scored per video. The dataset represents one of three independent experiments showing similar results with bars showing the S.D. of triplicates. Statistical significance analysed by two-tailed T-test ($T=7.609$, $***P<0.0016$).

the axon and suggests that another adhesion molecule may be involved after N-cadherin perhaps acting to stabilise the bulk of the cell onto the axon following association (a role for Sema4F in this regard is explored in Chapter Five).

4.4 N-cadherin expression enables fibroblast/axonal interactions

To determine if N-cadherin expression was sufficient to mediate axonal contact and recognition, I decided to express N-cadherin in a cell-type which does not normally interact with axons. I decided to use fibroblasts because they are found within all three concentric layers of the nerve, i.e. epineurium, perineurium, and endoneurium (Dreesmann *et al.*, 2009), yet these fibroblasts do not normally express N-cadherin and do not interact with axons. I used primary fibroblasts because preliminary immunofluorescence studies had indicated that immortalised fibroblasts, although more amenable to culture, occasionally expressed N-cadherin unlike primary fibroblasts. In order to express N-cadherin in primary fibroblasts, I used an adenoviral expression system, as primary fibroblasts transfected poorly. Primary fibroblasts were incubated in low-oxygen (3%) conditions in order to avoid cellular stress (Parrinello *et al.*, 2003) and were infected with either adenovirus expressing GFP (control) or adenovirus expressing N-cadherin for 16-hours, after which the cell medium was changed and the cultures were further incubated for 24-hours, prior to seeding onto established DRG axonal cultures. After 8-hours incubation, the GFP-fibroblast/DRG and N-cadherin-fibroblast/DRG cocultures were fixed and coimmunostained for N-cadherin and neurofilament (axonal marker) in order to determine the state of interaction (**Figure 4.9**). As expected, GFP-fibroblasts did not express N-cadherin, with only weak staining observed in axons. Moreover, as shown by the white arrow-heads, GFP-fibroblasts did not interact or align themselves to axons. In contrast, N-cadherin-fibroblasts were able to form multiple N-cadherin-rich homotypic fibroblast cell-cell interactions, as shown by the short white arrows, in a similar fashion to Schwann cells (**Figure 4.1**). Despite lacking the robustness of N-cadherin localisation observed in Schwann cell/axonal cocultures, there were still many examples, indicated by the long white-arrows, of N-cadherin-fibroblast/axonal alignment. This suggested that fibroblasts expressing N-cadherin behave, at least partially, in a similar manner to Schwann cells when contacting axons (**Figure 4.7A**).

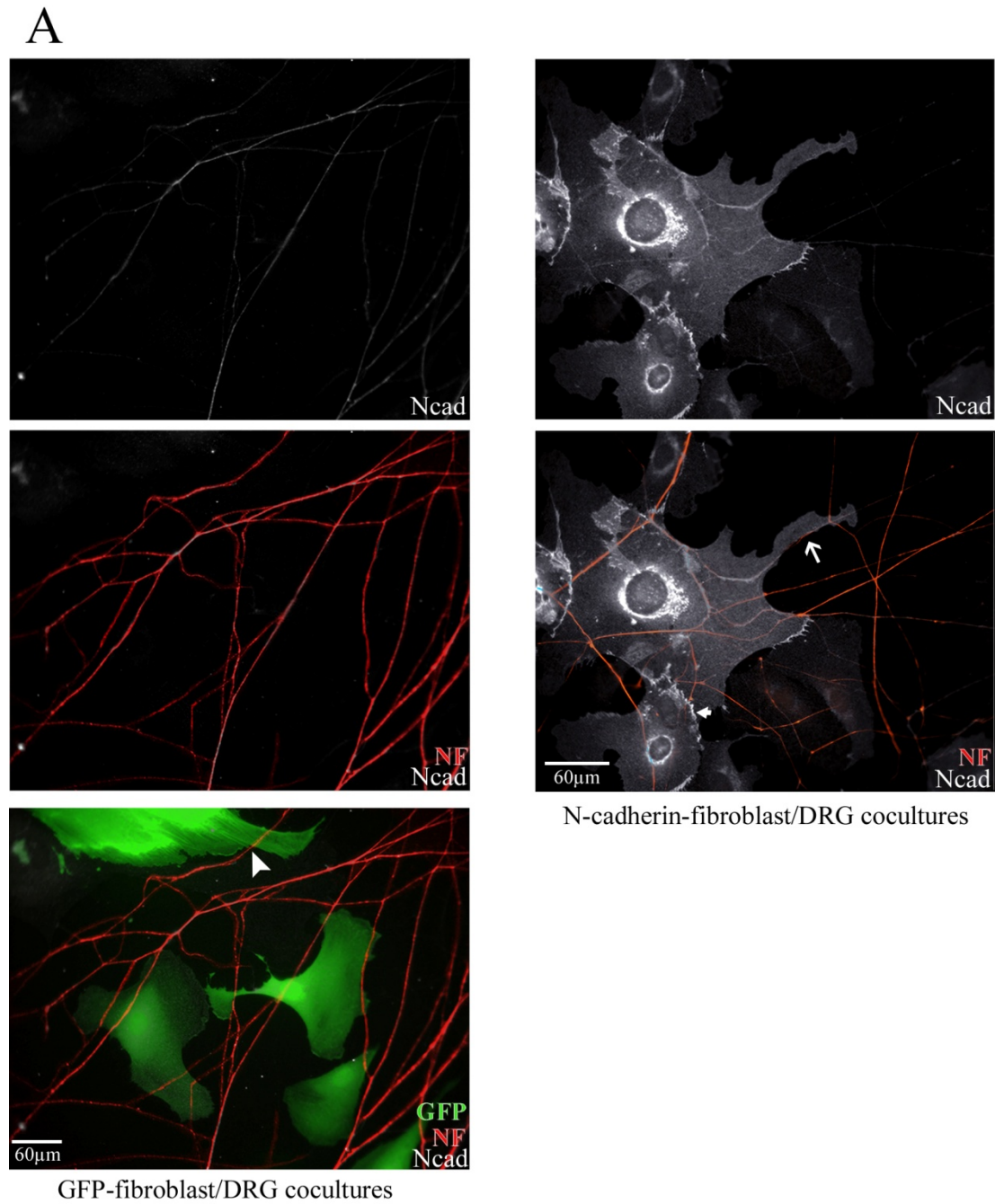


Figure 4.9 N-cadherin-expressing fibroblasts interact with axons. Fibroblasts were seeded 24hrs prior to infection with either GFP (AdGFP) or N-cadherin (AdNcad) adenovirus for 16hrs. Cells were media-changed and incubated a further 24hrs before seeding onto DRG-axons and incubated for 8hrs prior to fixation. **(LHS)** DRG/GFP-fibroblasts were coimmunostained for N-cadherin (white) and neurofilament (red), while infected cells were labelled by GFP expression (green). The white arrow-head shows an example of non-interaction with axons. **(RHS)** DRG/N-Cadherin-fibroblasts were coimmunostained for N-cadherin (white) and neurofilament (red). The short-arrow shows an example of N-cadherin at homotypic fibroblast cell-cell junctions, while the long-arrow shows an example of alignment between the fibroblast cytoplasm and the axon.

Moreover, heterologous N-cadherin expression allowed fibroblast to recognise axons and to manipulate axons for association, even if full axonal association was not achieved.

To study the dynamics of the interactions between N-cadherin expressing fibroblasts and axons, I performed time-lapse video analysis. GFP-fibroblasts and N-cadherin-fibroblasts were seeded onto established DRG-axonal cultures and videos were taken over 20-hours. As expected, GFP-fibroblasts did not interact with axons. In the majority of axonal encounters, fibroblasts protruded their cytoplasm under or over axons without interaction and without evidence of axons being ‘grabbed’ or associated with (**Figure 4.10A** and **Video 4.2**). In marked contrast to controls, and somewhat to our surprise, we found that N-cadherin-fibroblasts interacted with axons in a similar manner to Schwann cells, displaying an axonal ‘grabbing’ and ‘pulling’ behaviour, on first contact with axons, typical of Schwann cell/axonal interactions (**Figure 3.1A**), and culminating in varying degrees of axonal interaction (**Figure 4.10B** and **Video 4.3**). I quantified this behaviour by scoring fibroblast/axonal encounters as either ‘grabbing’ or ‘non-grabbing’. This analysis revealed that 60% of N-cadherin-fibroblasts interacted with axons through ‘grabbing’ events compared to less than 5% of controls (**Figure 4.10C**). Therefore, heterologous N-cadherin expression in previously non-interacting fibroblasts showed that N-cadherin alone was sufficient to alter fibroblast behaviour (on encountering axons), allowing fibroblasts to recognise and manipulate axons.

In order to confirm these findings, I analysed fibroblast/axonal interactions by a separate approach, in which the change in the axonal network was determined over the course of the video. By this method, the extent to which the axonal network was remodelled was used as a read-out for the ‘pulling’ and ‘grabbing’ activity of fibroblasts for axons. To analyse this, the shape of the axonal network, as shown in the first image of **Figure 4.10A** and **Figure 4.10B**, was represented by a green mask, while the last image was represented by a red mask. Both the initial (green) and final (red) masks were then overlaid in order to gauge the change in the overall shape of the axonal network. This qualitative analysis indicated that the axonal networks in GFP-fibroblast cocultures have minimally altered axonal networks, inferring a low incidence of interaction between fibroblasts and axons. In contrast, N-cadherin-GFP

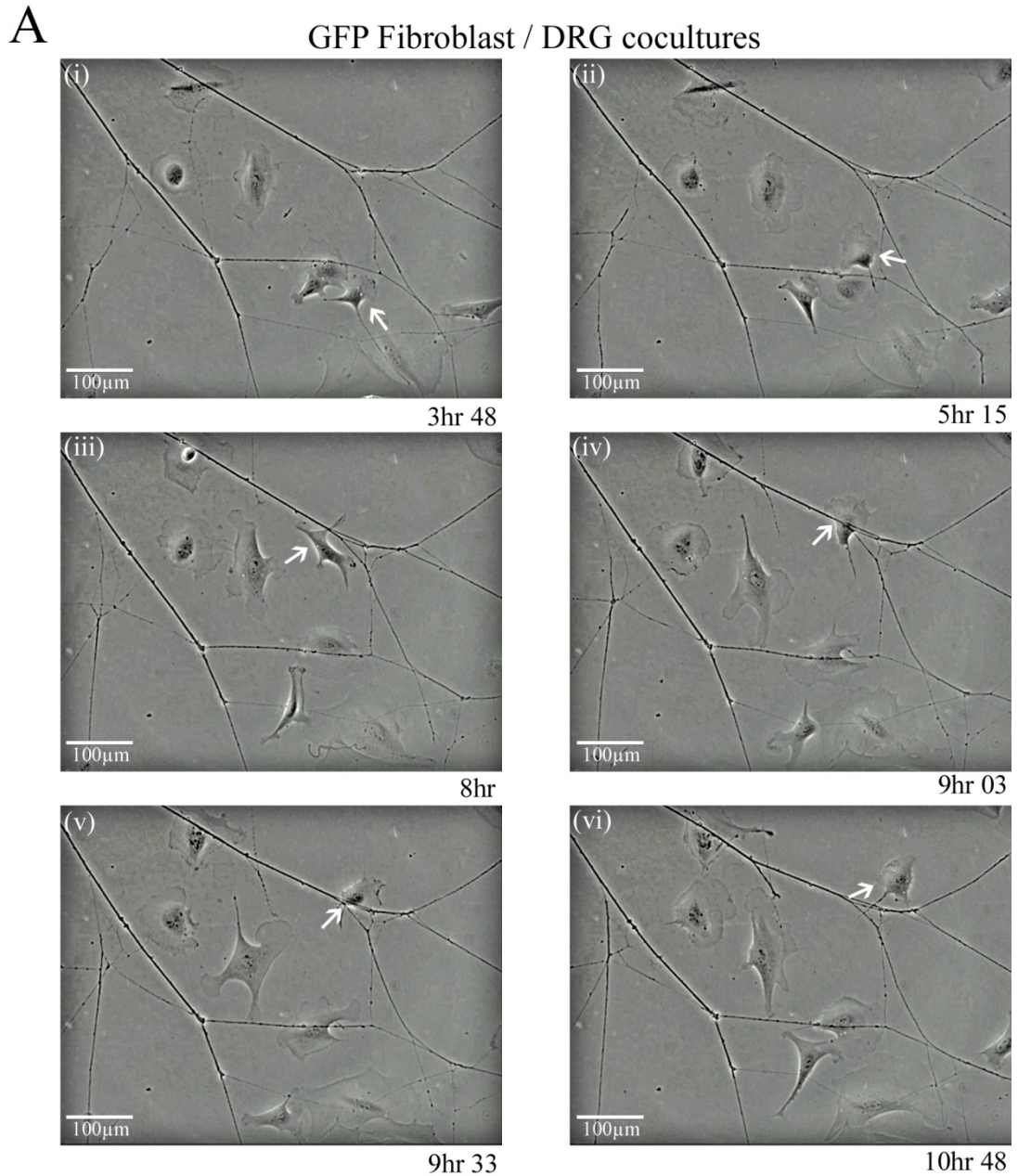
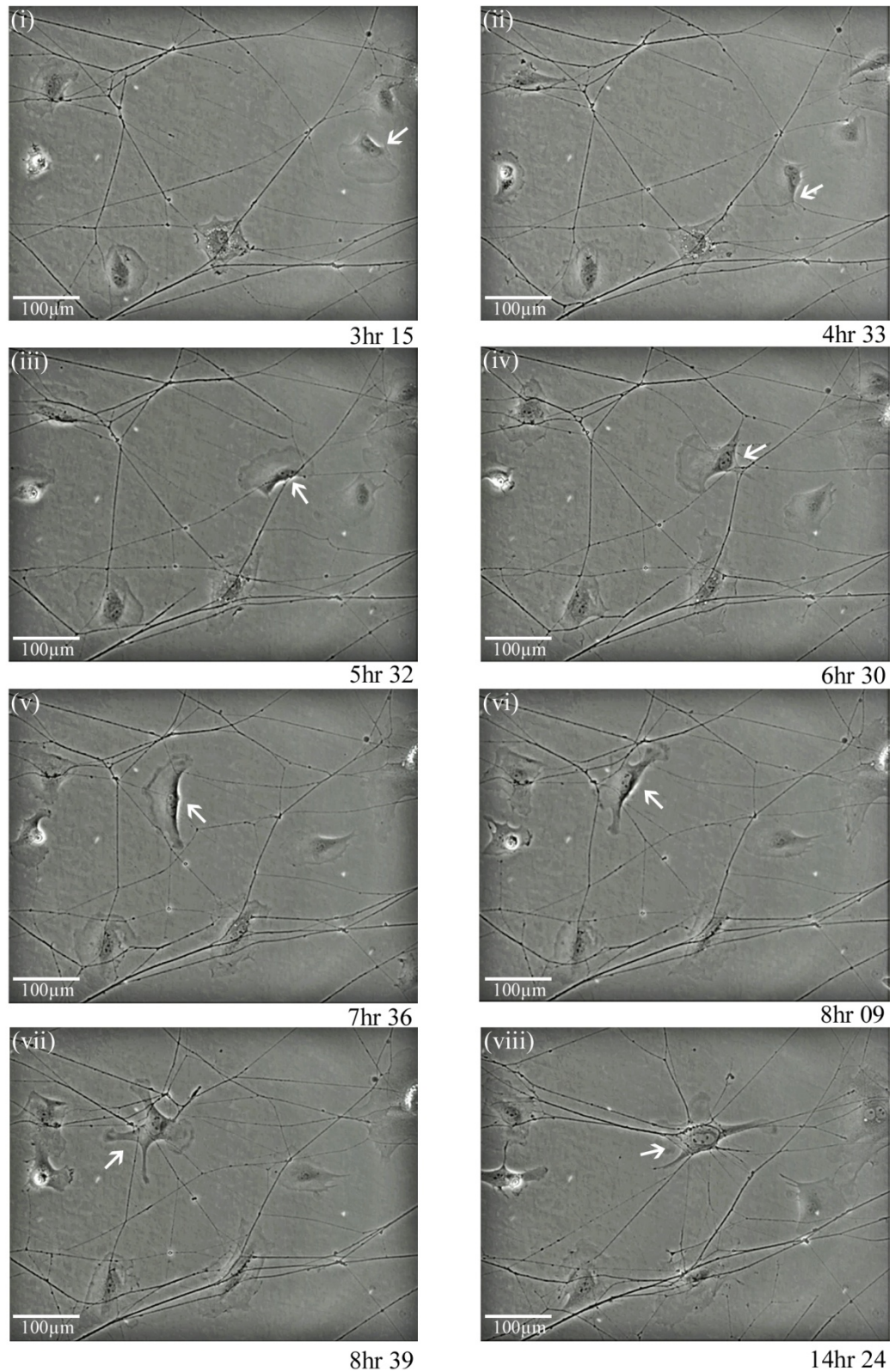
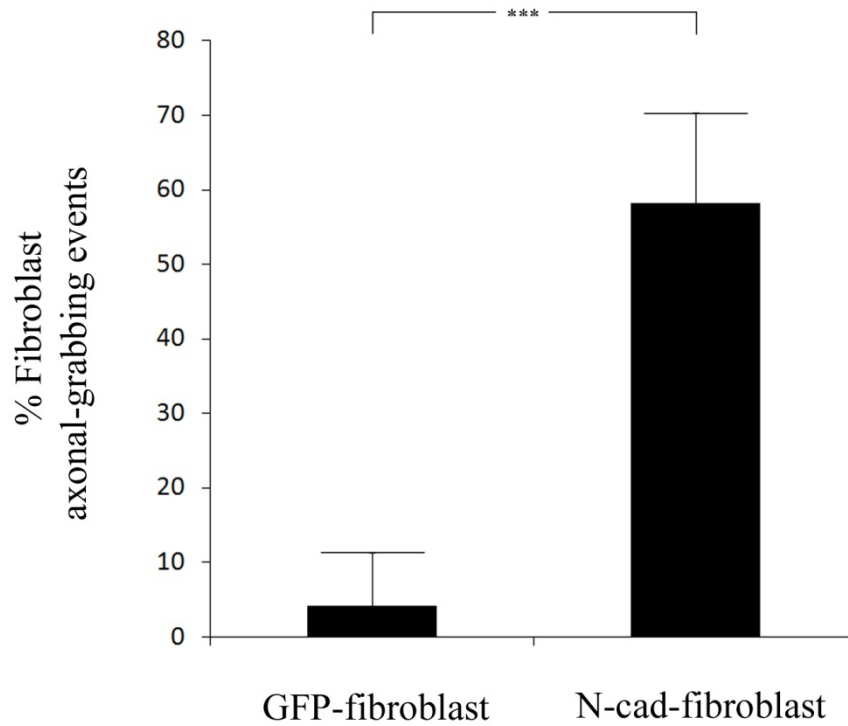


Figure 4.10 Fibroblasts that express N-cadherin can recognise, grab and partially associate with axons. DRGs were explanted and incubated over 5-6 days prior to seeding either GFP-fibroblasts or N-cadherin-fibroblasts for time-lapse analysis over 20hrs. (A) Representative phase-contrast image sequence of GFP-fibroblasts/DRG interactions (Video 4.2). The white arrows chart the progress of a typical GFP-fibroblast as it passes over or under axons but importantly, does not interact with axons.

B**N-cadherin Fibroblast / DRG cocultures**

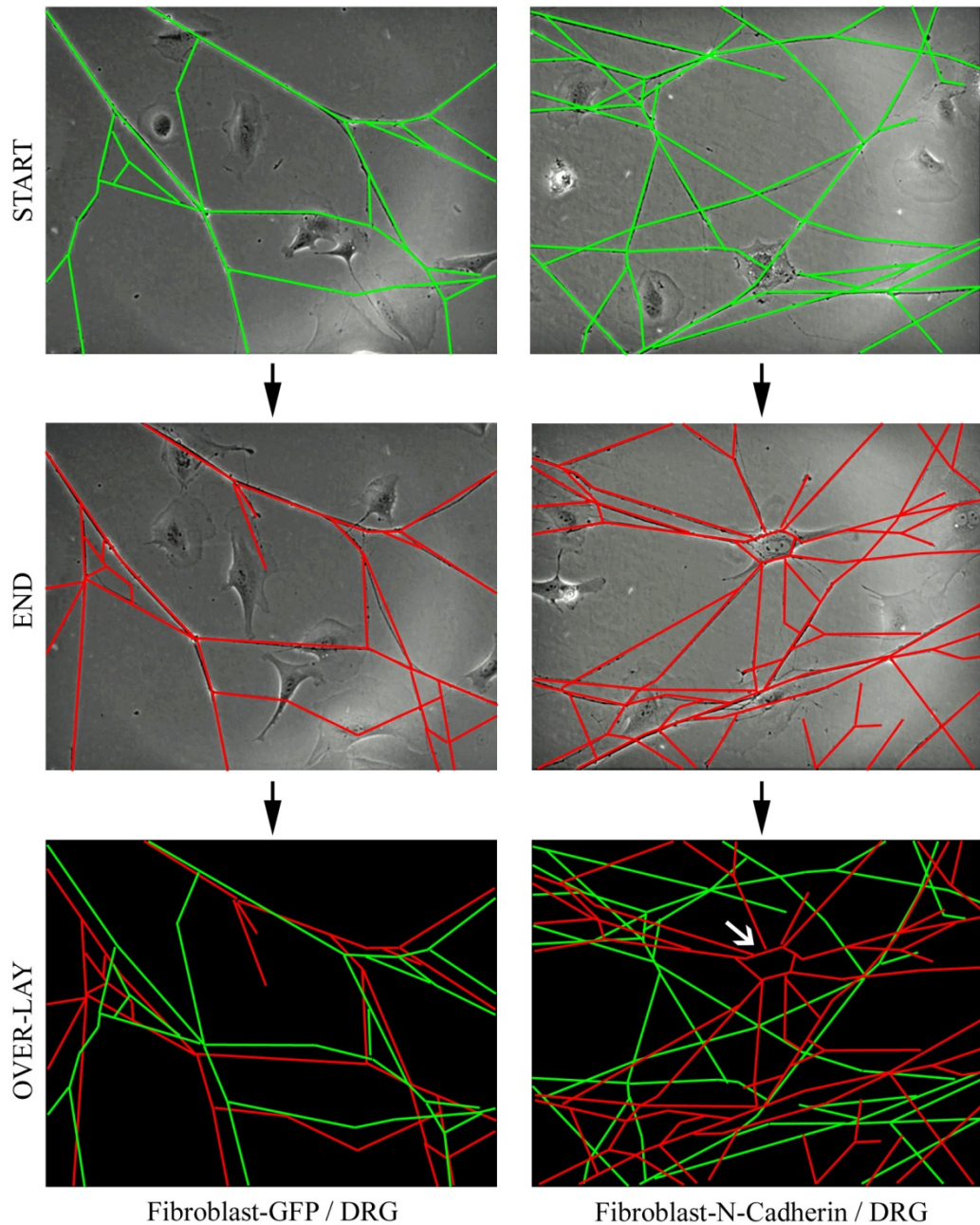
(B) Representative phase-contrast image sequence of N-cadherin-fibroblast interactions with DRG axons (**Video 4.3**). The white arrows chart the passage of a typical N-cadherin-fibroblast as it recognises, interacts and pulls on axons; a pattern that is repeatedly observed during the course of the analysis.

C



(C) Quantification of fibroblast/axonal ‘grabbing’. The bar chart shows the percentage of fibroblast/axonal encounters which resulted in ‘grabbing’ by the fibroblast for the axon. At least 3 videos were quantified per experiment with typically 10-15 fibroblasts scored per video. The dataset represents one of three independent experiments showing similar results with bars showing the S.D. of triplicates. Statistics by two-tailed T-test ($T=6.667$, $***P<0.0026$).

D



(D) The schematic illustrates the differing degrees to which the axonal network is remodelled over the course of the time-lapse analysis represented in part A (GFP-fibroblasts) & part B (N-cadherin-fibroblasts). The axonal pattern in the first image of the sequence is shown in green while the axonal pattern of the final image is shown in red. Both green and red masks were overlaid to generate a composite, which qualitatively illustrates the shift in the axonal network and reflects the degree of manipulation exerted by fibroblasts on axons. The white arrow shows an example of where axons had become twisted and pulled around an N-cadherin-fibroblast.

fibroblasts/DRG cocultures had dramatically altered axonal networks. In some cases, as shown by the white arrow, the axonal network was completely distorted, for instance, as in this example, where the axons have been physically twisted around the N-cadherin expressing fibroblast. This work is consistent with previous findings and taken together, further supports a distinct role for N-cadherin in Schwann cell/axonal 'grabbing/pulling'-behaviour and axonal recognition.

4.5 Mature Schwann cell/axonal interactions

4.5.1 N-cadherin expression in polarisation and myelination

I next wanted to determine the pattern of N-cadherin expression in Schwann cells and axons following association, i.e. in mature interactions leading up to myelination. To do this, I seeded NS cells at high density onto DRG-axonal explants and incubated the cocultures over 7 days to generate established cocultures. At this point we would expect the Schwann cells to be polarised with respect to the axons (Chan *et al.*, 2006). Cocultures were then fixed and coimmunostained for N-cadherin and neurofilament, which showed robust up-regulation of N-cadherin at the Schwann cell/axonal interface (**Figure 4.11**). This work is consistent with previous observations made by Chan *et al.* (2006), who showed, while examining the importance of p75^{NTR} in myelination, that Par-3, a well known component of the polarity machinery, was localised with N-cadherin along the axon, at the Schwann cell/axonal interface in established cocultures. It was therefore tempting to speculate that N-cadherin may be functioning to facilitate polarisation of Schwann cells prior to myelination.

4.5.2 shRNA as a tool for stable N-cadherin knockdown in Schwann cells

The evidence I have presented thus far suggests that N-cadherin is a mediator of early Schwann cell/axonal interactions and is robustly expressed along the axon in more stable interactions: but does the disruption of these initial interactions, for instance, following loss of N-cadherin in pre-associated Schwann cells, present long-term consequences for later Schwann cell function, i.e. the events of polarisation and

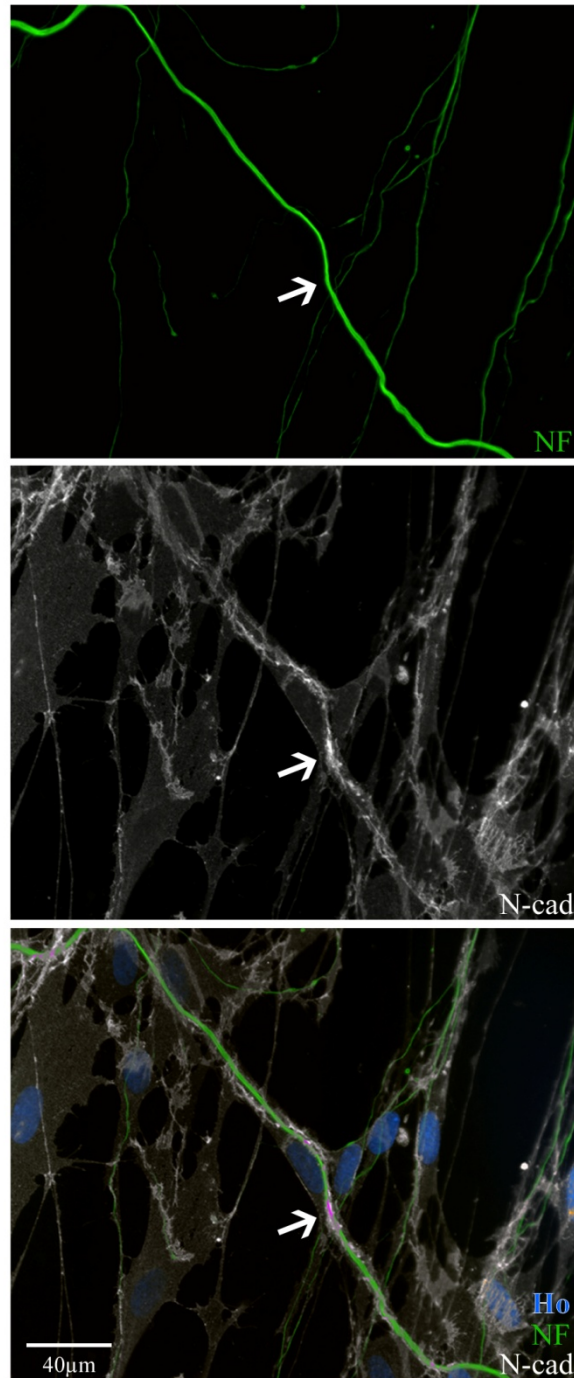
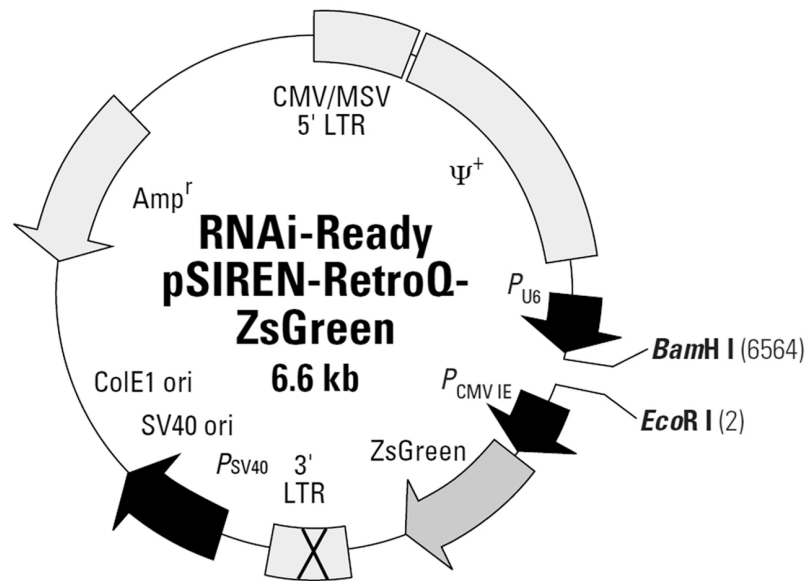


Figure 4.11 N-cadherin localises along axons in established Schwann cell/axonal cocultures. DRG explants were incubated for 6-7 days, after which Schwann cells were seeded onto DRG-axons at high-density (4×10^4 cells/DRG). Cocultures were incubated for 7 days before fixation with media-changes every 2 days. The epifluorescence shows cocultures that were coimmunostained for N-cadherin (white) and the axonal marker neurofilament (green), with cell nuclei labelled with Hoechst (blue). The white arrow indicates an associated Schwann cell in which the N-cadherin expression pattern parallels axonal NF expression. Note how the axon is forced to curve around the nucleus of the associated Schwann cell.

myelination? In order to investigate this, it was necessary to use a different system for N-cadherin silencing, and switch from transient transfection to a stable system for effecting knockdown of N-cadherin expression. This was essential because the protocol to induce myelination *in vitro* takes several weeks and therefore exceeds the time-frame for transient knockdown using siRNA. To achieve stable, long-term knockdown of N-cadherin, I used the Clontech retroviral ‘Knockout RNAi’ system to deliver and stably integrate vectors encoding short-hairpin (sh)RNAs into the Schwann cell genome. In addition to encoding shRNA, the integrated DNA also incorporated the green fluorescent protein (GFP) marker so that shRNA expressing cells can be identified. We used the Clontech ‘RNAi designer’ to select three shRNA sequences referred to in this thesis as shNcad-1, shNcad-3, shNcad-10 (these sequences are not related to aforementioned siRNA sequences). The oligonucleotides, including the manufacture's negative control (referred to as shScram), were then ligated into the pSiren (zsGreen) Retro-Q expression vector (**Figure 4.12A**). Clones positive for the insert were identified by restriction enzyme analysis (**Figure 4.12B**) and subsequently sequenced to confirm the sequence was as designed. Retroviral supernatant, from producer cells transfected with shScram, shNcad-1, shNcad-3 and shNcad-10 shRNAs, were then used to infect low-passage Schwann cells. Infected shRNA monocultures were maintained in culture for two passages, to ensure sufficient time for recovery from infection, after which cells were assessed for N-cadherin expression, while GFP expression was analysed to determine the level of infection. The immunofluorescence showed that while shScram monocultures strongly expressed N-cadherin in all cells (similarly to NS monocultures), the three shRNA N-cadherin cell-lines showed varying degrees of N-cadherin knockdown (**Figure 4.12C**). In these images, white arrows show examples of cells coexpressing N-cadherin and GFP, while white arrow-heads show examples of N-cadherin deficient cells expressing GFP. Schwann cells infected with shNcad-1 were most effective at reducing N-cadherin levels (see white arrow-heads). In contrast, shNcad-3 and shNcad-10 were less efficient, only partially reducing N-cadherin levels in some of the cells, while failing entirely to reduce N-cadherin levels in the majority of cases (see white arrow-heads). To quantify this, I scored the proportion of GFP and N-cadherin expressing cells present in shScram, shNcad-1, shNcad-3 and shNcad-10 monocultures (**Figure 4.12D**). Overall, the data showed that the rate of infection, as inferred from GFP expression, was consistently around

A



B

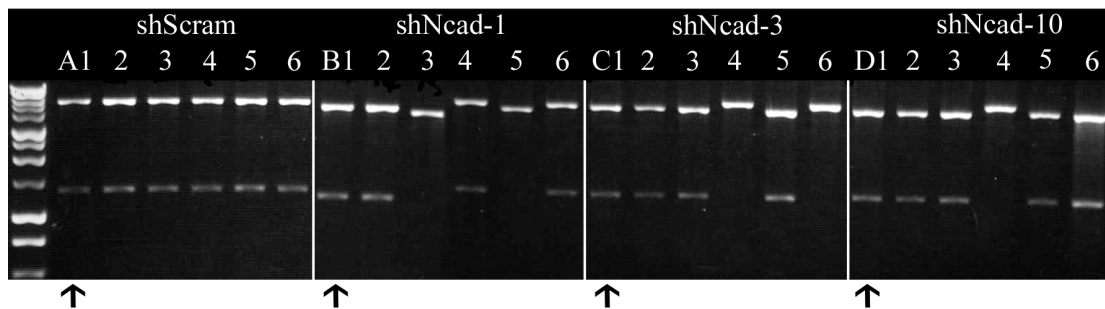
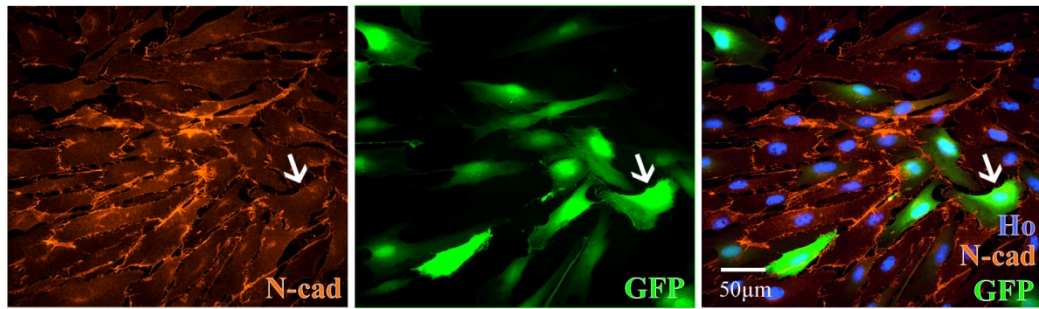
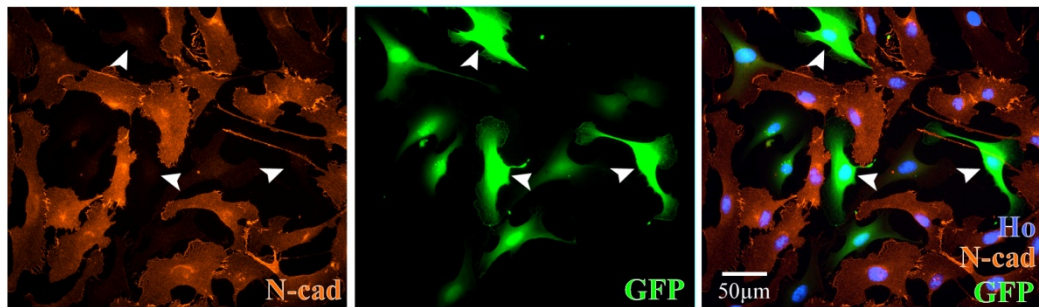


Figure 4.12 Generating stably integrated N-cadherin shRNA Schwann cells. Three shRNA sequences were designed to target N-cadherin mRNA and (A) ligated into the pSIREN-RetroQ vector. (B) Mini-prep DNA derived from 6 clones were analysed by restriction analysis to identify positive clones that were later confirmed by sequencing (not shown).

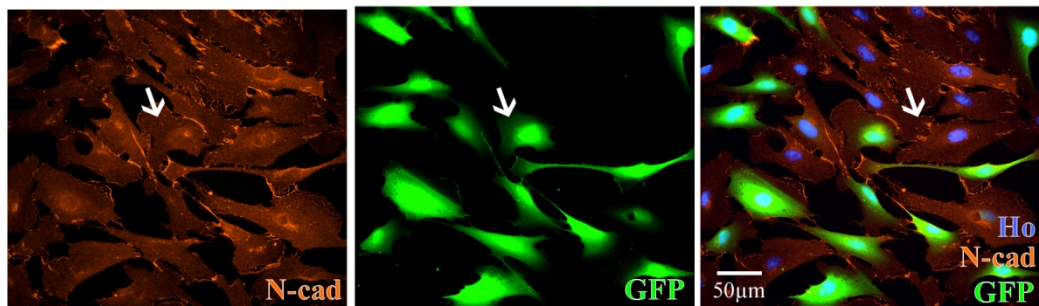
C



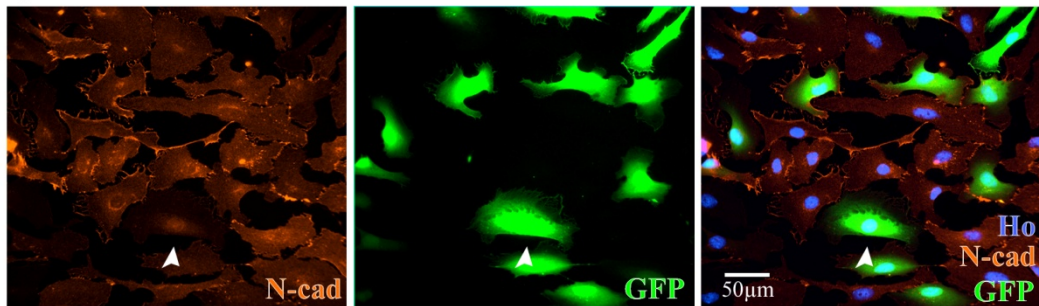
(i) shScram Schwann cells



(ii) shNcad-1 Schwann cells



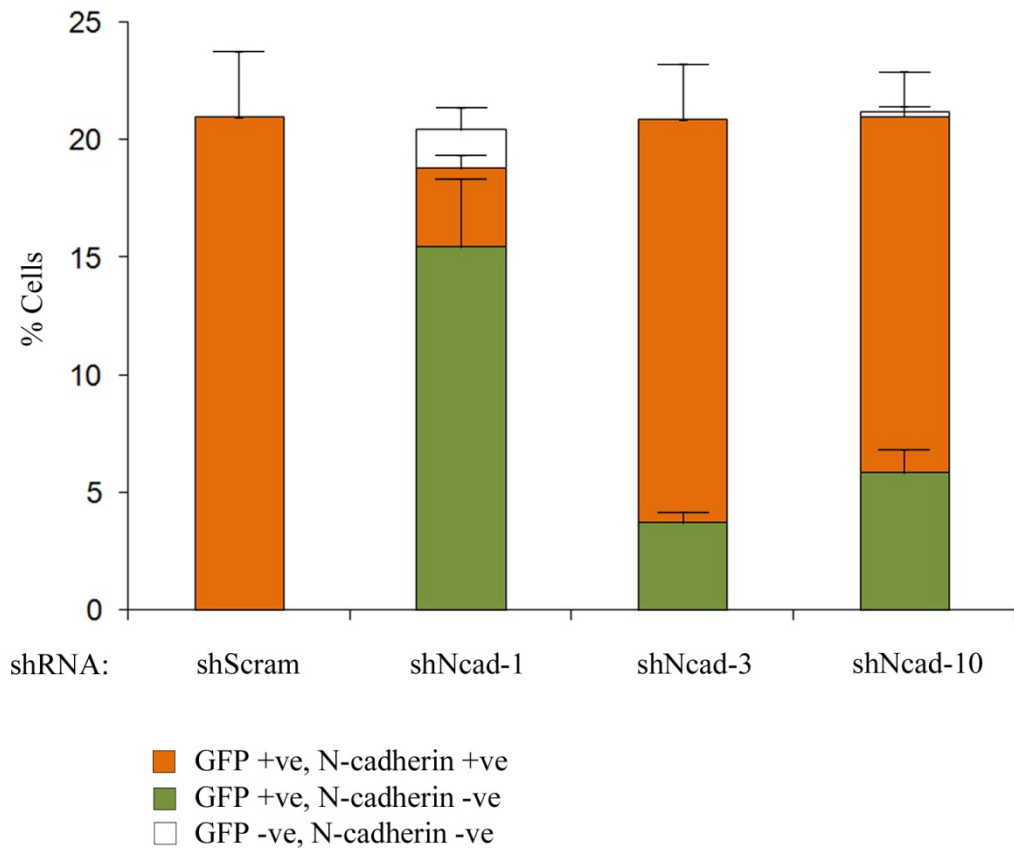
(iii) shNcad-3 Schwann cells



(iv) shNcad-10 Schwann cells

(C) shRNA-mediated N-cadherin knockdown was assayed by immunofluorescence. Low-passage Schwann cells were plated 24hrs prior to retroviral infection with shScram, shNcad-1, shNcad-3 and shNcad-10 for 2hrs. Cells were then media-changed and further incubated over several passages prior to fixation. Representative epifluorescence from cultures immunostained for N-Cadherin (red) with cell nuclei labelled by Hoechst (blue) & infected cells by GFP expression (green). The white arrows show examples of N-cadherin positive shRNA cells, while the white arrowheads show examples of N-cadherin negative shRNA cells.

D



(D) Quantification of immunofluorescence from shRNA cell-lines. The bar charts show the proportion of Schwann cells expressing N-cadherin and GFP (red), GFP alone (green) or negative for N-cadherin and GFP (white) for each of the shRNA cell types. The data quantifies the reliability of the shRNA system by matching GFP expression with N-cadherin knockdown across N-cadherin shRNA lines. Scoring was conducted in triplicate with at least 200 cells counted per DRG; bars represent S.D. Shown is one of two independent datasets of similar results that reflect the shRNA lines later used in myelination assays depicted in **Figure 4.13**.

20%, which although low was still, in our view, acceptable for myelination assays. shNcad-1 scored highest for efficacy of knockdown, with 85% of shRNA infected (GFP) cells depleted for N-cadherin, which includes 5% of shNcad-1 cells that were knocked down for N-cadherin but failed to coexpress the GFP marker. This contrasts with the findings from shNcad-3 and shNcad-10 shRNA lines, in which less than 20% and 30% of GFP-labelled cells were knocked down for N-cadherin respectively. It was therefore decided to use only the shNcad-1 cells to determine the role of Schwann cell N-cadherin expression in myelination.

4.5.3 Loss of N-cadherin from pre-associated Schwann cells impedes progression to myelination

To examine if N-cadherin deficient Schwann cells were able to myelinate axons, I used an *in vitro* myelination model to mimic the myelination process. DRGs were explanted and incubated over 5 days in order to obtain bare DRG-axonal networks. Low-passage, recently infected Schwann cells that expressed either shScram or shNcad-1 were seeded onto DRG-axonal cultures and cocultures were incubated over 7 days. After this, cocultures were incubated a further 2-3 weeks in pro-myelinating conditions, with medium supplemented with ascorbic acid and matrigel, and changed every two days. This was independently repeated two further times, staggered to separate weeks, using newly generated shRNA cells for each experiment.

Evidence of myelination was observed from phase-contrast microscopy of live cocultures, which was detected as thick semi-translucent tubes criss-crossing the cocultures. Following sufficient myelination, the cocultures were fixed and immunostained for N-cadherin, to ensure that the effectiveness of the shRNA constructs had been maintained during the experiment. As shown in **Figure 4.13A**, while GFP-shScram cells are positive for N-cadherin (see white arrows), the GFP-shNcad-1 cells are largely devoid of N-cadherin (see white arrow-heads). In both shScram and shNcad-1 myelinating cocultures, there is evidence of robust N-cadherin localisation at sites of Schwann cell/axonal contact; however, in the case of the latter, this is restricted to the non-GFP background Schwann cell population.

A

Myelinating shRNA/DRG cocultures

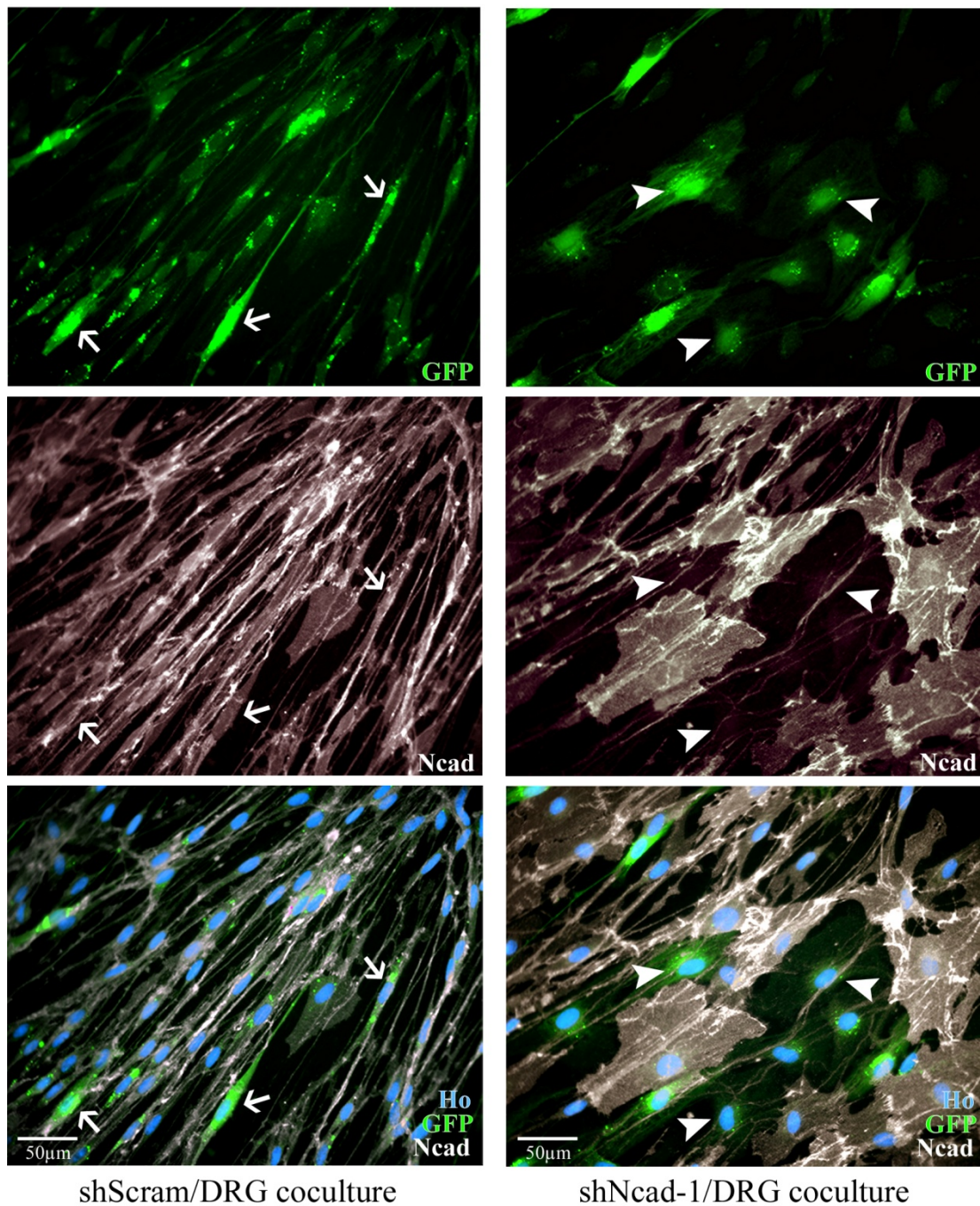
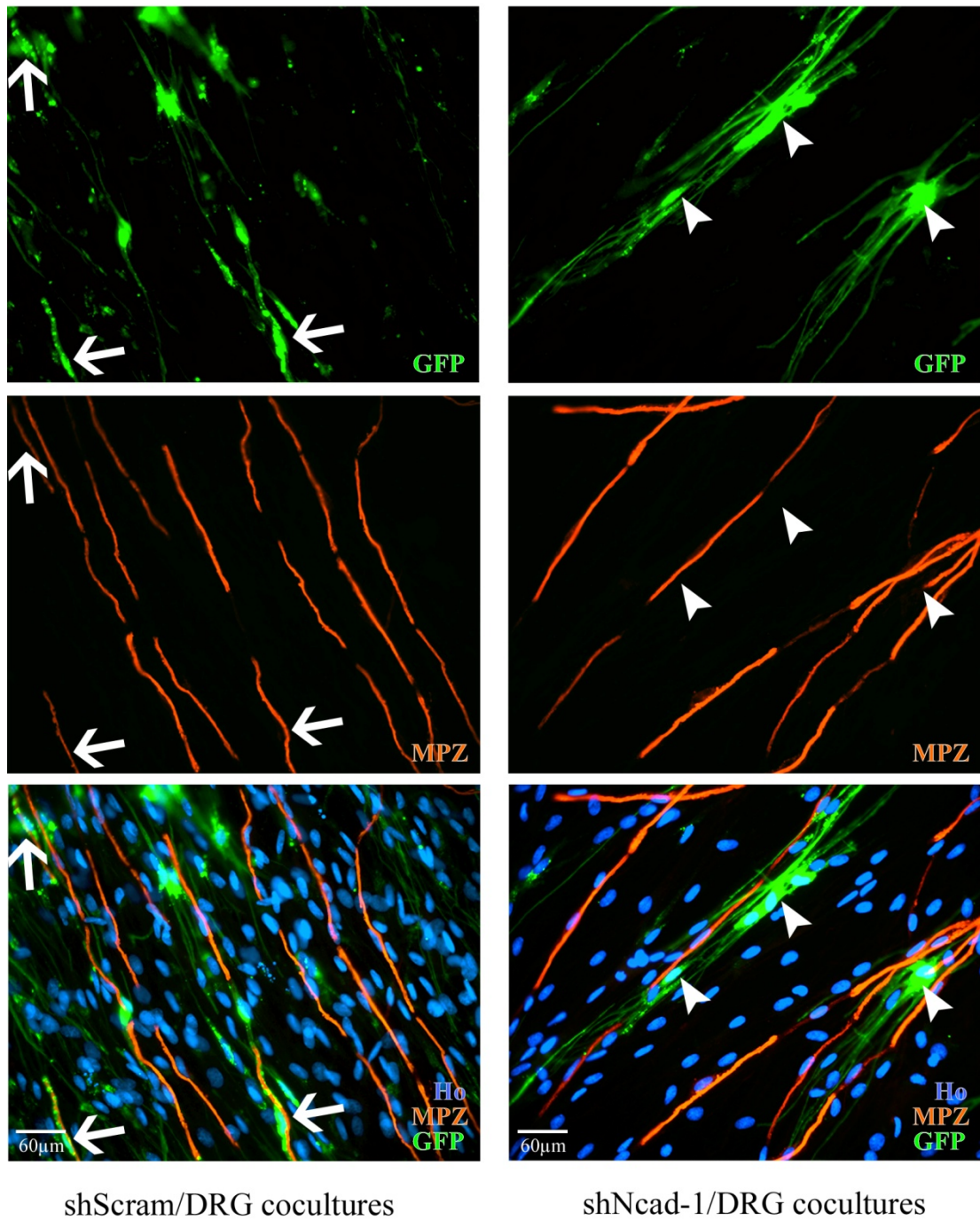


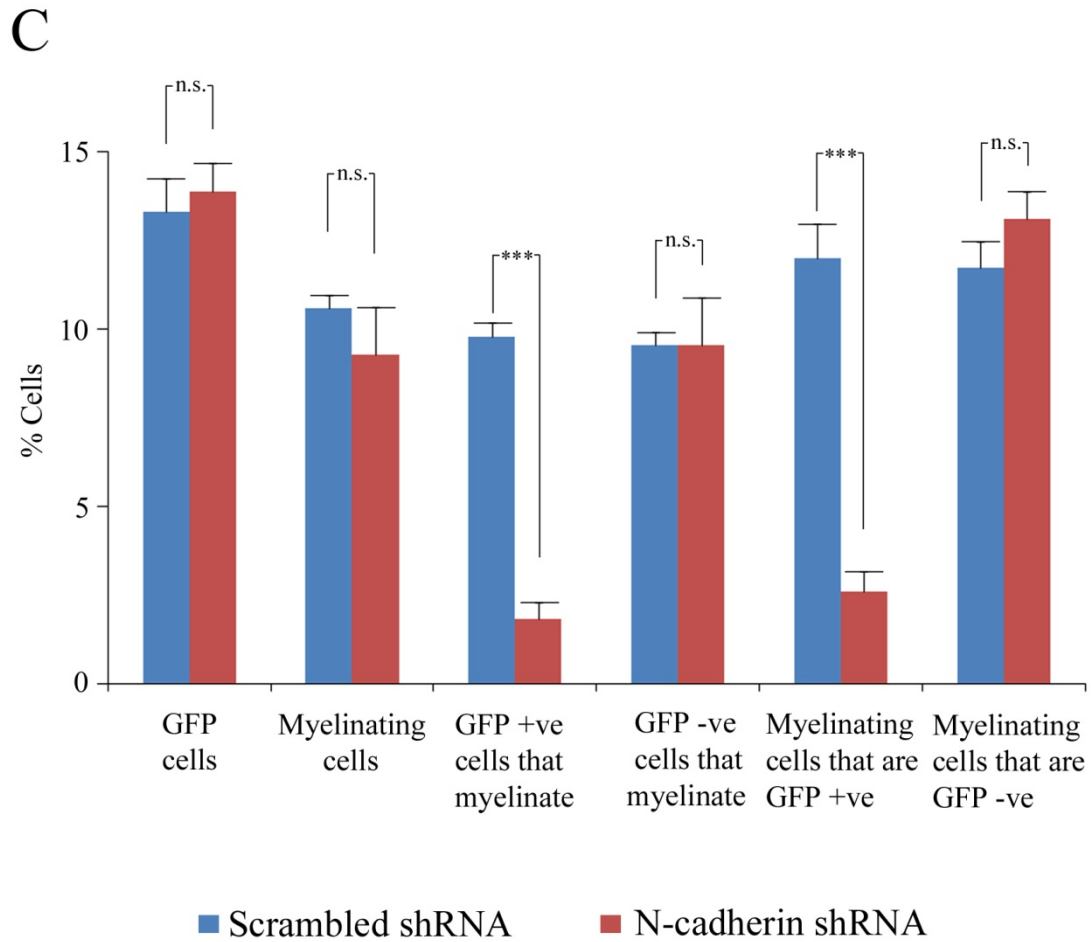
Figure 4.13 N-cadherin shRNA cells show a reduced propensity to myelinate axons. DRG explants were incubated for 5-6 days before addition of shRNA cells to DRG axons (4×10^4 cells/DRG). Cocultures were incubated for 7-days in basal media and then switched to differentiation media (with matrigel and ascorbic acid), for an additional two weeks to stimulate myelination before fixation. (A) Representative epifluorescence from cocultures immunostained for N-cadherin (white), with shRNA cells labelled by GFP (green) and cell nuclei labelled with Hoechst (blue). The white arrows show examples of GFP cells that express N-cadherin, while the white arrowheads show examples of GFP cells depleted for N-cadherins.

B

Myelinating shRNA/DRG cocultures



(B) Scrambled and N-cadherin shRNA Schwann cell/DRG cocultures were immunostained with myelin protein zero (MPZ) to label myelinating Schwann cells (red), with cell nuclei labelled with Hoechst (blue) and shRNA expressing cells were marked by GFP (green). The white arrows show representative examples of myelinating shScram-GFP cells and the white arrow-heads show representative examples of non-myelinating shNcad-1/GFP cells.



(C) Quantification of immunofluorescence as scored from myelinating shRNA/DRG cocultures (shown in Part B). Six to 7 representative fields of view were analysed with typically 2000+ cells scored per coverslip. In each field of view 100% of Schwann cells were scored in two ways. First, as either GFP-positive or GFP-negative and second, as either myelinating or non-myelinating. Counts were obtained from triplicate coverslips with bars representing the S.D. Shown is one of two independent datasets of similar results. Statistics by two-tailed T-test (***) $p < 0.0001$; n.s., not significant).

In order to determine if myelination was affected by N-cadherin depletion in Schwann cells, I next immunostained the shRNA/DRG cocultures with MPZ, which is a marker of myelination. The immunofluorescence showed that both shScram/DRG and shNcad-1/DRG cocultures had similar levels of myelination, which is was not unexpected given the high proportion of non-infected background cells present in the cultures. However, while there were many individual examples of GFP-shScram cells that had myelinated axons, i.e. where GFP expression colocalised with MPZ (see white arrows), there were few such examples in GFP-Ncad1 cultures, with most GFP cells remaining unmyelinated despite close proximity to non-GFP myelinating cells (see white arrow-heads). In order to quantify this result, I scored the proportion of GFP verses non-GFP Schwann cells that were myelinating, and then I scored the proportion of myelinating cells that either expressed GFP or did not express GFP (**Figure 4.13C**). The overall proportion of cells in the cocultures that expressed GFP was approximately 14%, which represented a slight fall in shRNA numbers relative to uninfected Schwann cells after three weeks of incubation. This may be explained in terms of a reduction in the proliferation of shRNA cells relative to the uninfected background population due to GFP related cellular stress. The overall proportion of myelinating cells was approximately 10%, with slightly less myelination observed in N-cadherin shRNA cocultures, although this result was not significant. However, when the proportion of myelinating to non-myelinating N-cadherin-shRNA cells were compared it was found that GFP-shScram (control) cells myelinated with, on average, three to four fold greater frequency then their N-cadherin-shRNA counterparts. This trend was also observed when comparing the proportion of N-cadherin-shRNA myelinated cells to uninfected (non-GFP) myelinating cells. Again, it was found that GFP-shScram cells made up a greater proportion of the myelinating population, which was found to be three to four fold higher than equivalent N-cadherin shRNA cocultures. Thus, depletion of N-cadherin in Schwann cells, prior to interaction with axons, inhibits the ability of these cells to myelinate axons.

4.6 Chapter summary and conclusions

In this chapter, I have shown that the cell adhesion molecule N-cadherin is localised at cell-cell junctions during both homotypic Schwann cell-cell and heterotypic Schwann cell/axonal interactions. N-cadherin expression was found to be essential for the formation and maintenance of Schwann cell-cell junctions, with loss of N-cadherin resulting in the disruption of CIP. The automated assay I developed to detect homotypic Schwann cell-cell interactions is currently being adapted, in our laboratory, as a quantitative assay for scoring cell interactions in a non-biased RNAi screen to detect novel mediators of Schwann cell interactions.

I have also identified an important role for N-cadherin, expressed by Schwann cells and axons, as a mediator of Schwann cell/axonal interactions. I found that N-cadherin was concentrated at the tips of Schwann cell lamellipodia-like protrusions, which was used by Schwann cells to locate axons through homophilic N-cadherin ligation with axonally expressed N-cadherin. Loss of N-cadherin from Schwann cells impaired the ability of Schwann cells to locate axons, while introduction of N-cadherin in otherwise non-interacting fibroblasts was sufficient to permit recognition and allow partial association with axons. This confirmed the importance of N-cadherin as the primary mediator of initial axonal interactions. Finally, loss of N-cadherin from Schwann cells was shown to significantly impair the ability of Schwann cells to later myelinate axons. Together these findings confirm the importance of N-cadherin as a key mediator of cellular interactions within the PNS.

Chapter Five: N-cadherin and semaphorin-4F play separate but cooperative roles in heterotypic Schwann cell/axonal interactions

5.1 Chapter introduction

In Chapter Four, I showed that N-cadherin played an important role in early heterotypic Schwann cell/axonal interactions, while loss of N-cadherin in Schwann cells prior to reassociation disrupted re-myelination *in vitro*. However, this work also showed that N-cadherin does not act alone to facilitate and maintain stable Schwann cell/axonal interactions. For instance, Schwann cell association assays revealed that while 90% of LTD cells failed to interact normally with axons (Chapter Three), N-cadherin depletion alone only caused a 40% disruption of Schwann cell/axonal association and alignment (Chapter Four). This difference in phenotypic severity suggested that loss of N-cadherin alone was unlikely to explain all of the LTD interaction defect. In addition, evidence from time-lapse microscopy showed that N-cadherin-depleted Schwann cells were still partially capable of forming associations with axons; however, importantly, this interaction did not occur at cell protrusions but rather, the interaction was mediated through adhesion of the body of the Schwann cell with the axons, i.e. distinct from the cellular protrusions that usually elicit the axonal recognition response. Together, these findings suggested that another adhesion molecule might be acting at a sub-cellular localisation distinct from cell protrusions, in concert with N-cadherin, to allow Schwann cells to establish stable heterotypic Schwann cell/axonal interactions. In our laboratory, we previously identified a novel role for semaphorin-4F (Sema4F) as a Schwann cell expressed adhesion molecule that mediates heterotypic Schwann cell/axonal interactions (Parrinello *et al.*, 2008). Interestingly, in addition to N-cadherin and a number of other cell adhesion molecules, I showed in Chapter Three that Sema4F was significantly down-regulated approximately three-fold in non-interacting LTD cells. In this chapter, I set out to investigate whether Sema4F was acting with N-cadherin as a co-mediator of heterotypic Schwann cell/axonal interactions and whether both molecules together, might account for the LTD interaction defect.

5.2 Sema4F and the Ras/Raf/ERK signaling pathway

Before directly testing a role for Sema4F, I first investigated the effect that oncogenic signalling through the Ras/Raf/ERK pathway in Schwann cells had on Schwann cell/axonal interactions. We showed that the down-regulation of Sema4F was implicated in the aetiology of neurofibromatosis type I (NF1) (Parrinello *et al.*, 2008). NF1 is an inherited cancer predisposition syndrome which manifests as multiple sporadic nerve tumours, heterogeneously composed of dissociated Schwann cells, fibroblasts and neurons (Carroll & Ratner, 2008; Evans *et al.*, 2002; Gottfried *et al.*, 2010; Parrinello & Lloyd, 2009). The initiating stage in tumour progression is thought to be the spontaneous loss of heterozygosity (LOH) of the remaining NF1^{+/-} allele in the neurofibromin gene in Schwann cells of affected individuals. Neurofibromin is a tumour suppressor and functions as a Ras-GAP that acts to attenuate the Ras signal, thus loss of NF1 results in the hyper-activation of Ras leading to oncogenic signalling through the Ras/Raf/ERK pathway. Importantly, a key step in the generation of neurofibroma tumours is the dedifferentiation and irreversible dissociation of Schwann cells from axons (Harrisingh & Lloyd, 2004; Parrinello & Lloyd, 2009; Zheng *et al.*, 2008). We showed that oncogenic Ras/Raf/ERK was driving the down-regulation of Sema4F, which subsequently led to the dissociation of Schwann cells from axons (Parrinello *et al.*, 2008).

5.3 Oncogenic Ras signal disrupts Schwann cell/axonal interactions

5.3.1 Ras activation disrupts Schwann cell/axonal interactions despite N-cadherin expression

In order to expand upon our previous findings that Ras activation disrupted Schwann cell/axonal interactions, I used Schwann cells generated in our laboratory that expressed a constitutively active form of Ras, in which the glycine at residue 12 was substituted for valine (V12). The Ras-V12 variant, referred to in this thesis as NS-RasV12 cells, are insensitive to GAPs and thus, exhibit constitutively active Ras/Raf/ERK signalling. In order to examine the affect of oncogenic Ras/Raf/ERK on Schwann cell/axonal interactions, I used our primary *in vitro* DRG coculture model described previously (Chapter Three). DRG axons were explanted and

incubated over 7-days in order to generate established DRG-axonal cultures. NS-RasV12 cells were seeded onto axons and incubated for eight hours before fixation. Cocultures were coimmunostained for S100 β and RT97, which appeared to show that Schwann cell/axonal interactions were at least partially disrupted in Ras-activated Schwann cells (**Figure 5.1A**). The immunofluorescence was scored for Schwann cell/axonal interaction, i.e. to determine the proportion of Schwann cells that were associated; associated, not aligned or non-associated. These results confirmed that Ras-activation resulted in an approximate 50% impairment in heterotypic interactions, compared to a 15% background impairment in control cocultures (**Figure 5.1B**). In order to examine whether N-cadherin was expressed in Ras-activated Schwann cells, I coimmunostained the cocultures for N-cadherin and neurofilament (to highlight axons) (**Figure 5.1C**). Interestingly, the immunofluorescence showed that N-cadherin was still expressed by NS-RasV12 cells. Moreover, as shown by the white-arrows, N-cadherin localisation was similar to that observed in NS cells, where N-cadherin was localised at lamellipodia-like protrusions (see white arrows, **Figure 5.1A**). Together, these results showed that Ras-activated (NS-RasV12) cells are impaired for axonal interaction, despite continued expression of N-cadherin and despite its correct localisation at cytoplasmic protrusions. Therefore, the axonal-interaction impairment exhibited by NS-RasV12 does not result from N-cadherin-loss but instead implicates additional co-mediators, for example Sema4F - known to be dysregulated upon Ras activation - that might function with N-cadherin to mediate interactions.

5.4 Raf-ER cells: an inducible Raf for studying Schwann cell/axonal interactions

In order to study Ras-activation and specifically the ERK pathway, I used Schwann cells generated in our laboratory, which expressed an inducible form of Raf referred, in this thesis, as Raf-ER cells. The inducible Raf kinase is a fusion protein consisting of Raf fused to the hormone binding domain of the estrogen receptor (ER), which can be reversibly activated by addition of tamoxifen (Tmx) - an estrogen analogue - to the cell media, while remaining inactive in the absence of ligand (Lloyd *et al.*, 1997). We previously showed that activation of Raf-ER and subsequent sustained

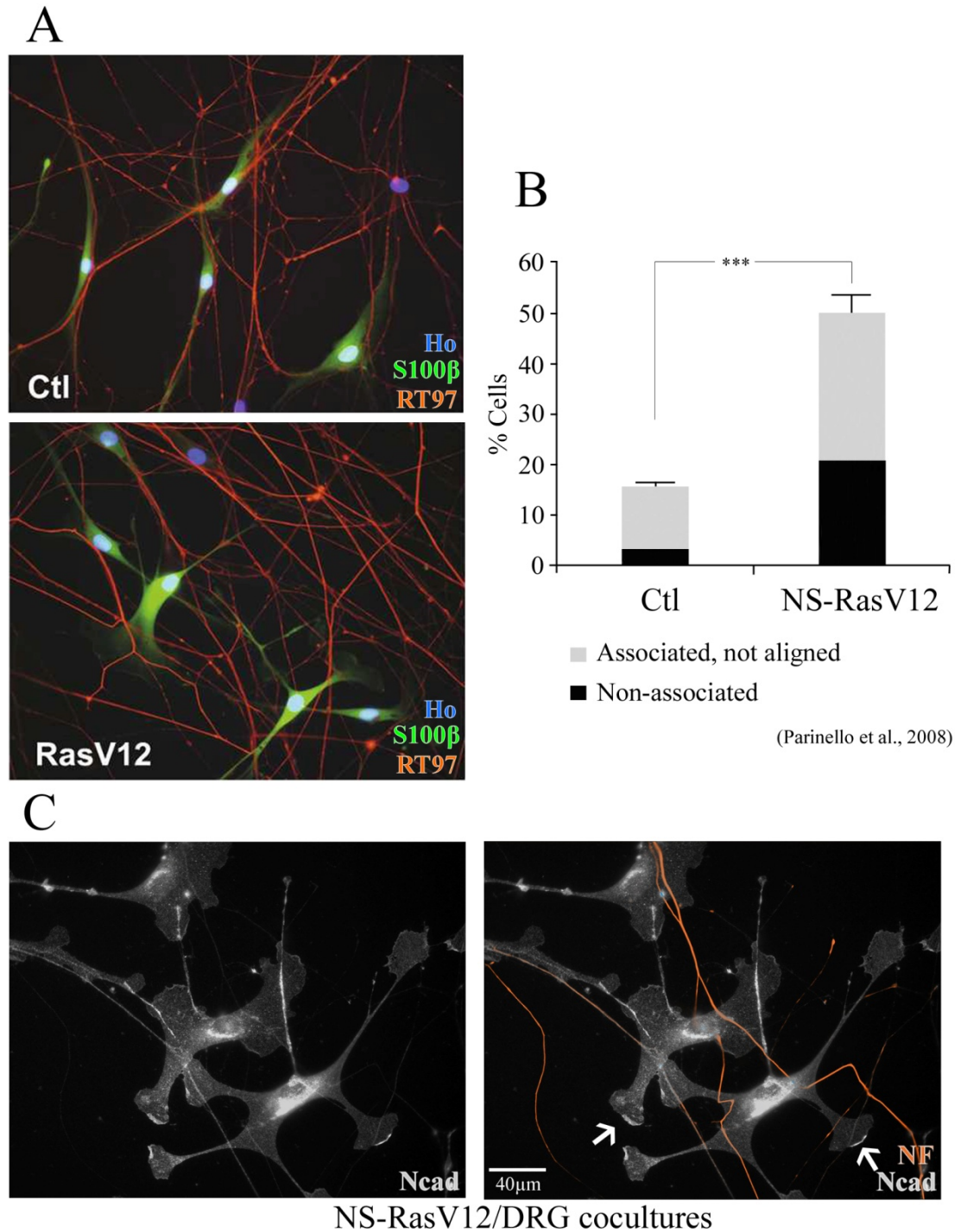


Figure 5.1 Ras Schwann cells failed to remain associated with axons despite N-cadherin expression localised to cytoplasmic protrusions. NS-RasV12 cells were seeded onto day-7 established DRG explants and fixed after 8hrs. Representative epifluorescence of cocultures coimmunostained for (A) S100 β (green) and RT97 (red), with cell nuclei labelled with Hoechst (blue). (B) Association assay: blind scoring conducted in triplicate with 200+ cells counted per DRG; bars represent S.D. Statistics by T-test (***) $p < 0.0038$. (C) Cocultures were coimmunostained for N-cadherin (grey) and neurofilament (red), where the white-arrows show examples of N-cadherin localisation at cell protrusions.

signalling through the Raf/ERK pathway, was sufficient to induce Schwann cell dedifferentiation and drive the dissociation of Schwann cells from axons (Harrisingh *et al.*, 2004; Parrinello *et al.*, 2008). This work also showed that the signalling pathway downstream of Ras activation was via the Raf/ERK cascade rather than, for example the PI3 kinase pathway. Thus, Raf-ER cells are a useful inducible model to study the effect of hyper-activation of Ras in Schwann cells in relation to Schwann cell/axonal dissociation.

5.4.1 N-cadherin expression and knockdown in Raf-ER cells

I first wanted to ensure that activated Raf-ER cells, like NS-RasV12 cells, expressed N-cadherin. I also wanted to determine if Raf-ER cells were amenable to siRNA mediated N-cadherin silencing. Low-passage Schwann cells that stably expressed the inducible Raf-ER kinase were transfected 24-hours after cell-plating with either scrambled or N-cadherin siRNA for 16-hours. The cell media was changed and the monocultures were incubated for a further 4-hours, after which the media was supplemented with either Tmx to activate Raf or ethanol (EtOH) to act as a control. Raf-ER Schwann cell monocultures were fixed 28-hours later, as in previous experiments, and immunostained for N-cadherin (**Figure 5.2A**). These results confirmed that N-cadherin is expressed by Raf-ER Schwann cells in both Raf inactive and activate states, with seemingly greater levels of N-cadherin expressed by Raf-activated cells. Furthermore, there were multiple examples of homotypic cell-cell interactions that were clearly mediated through *trans*-N-cadherin-N-cadherin ligation in either condition. The results also showed that N-cadherin expression in Raf-ER Schwann cells could be silenced effectively by siRNA to a similar degree as achieved in NS cells, which is quantified in **Figure 5.2B**. However, preliminary experiments (not shown) revealed that activated Raf-ER Schwann cells were resistant to siRNA transfection at the level previously used to knockdown N-cadherin in NS cells, i.e. 1nM. I therefore titrated the siRNA concentrations from 1nM to 10nM in order to determine the optimum concentration and discovered that 3nM was sufficient (as shown in **Figure 5.2A-B**) to achieve comparable transfection and depletion of N-cadherin in Raf-ER cells.

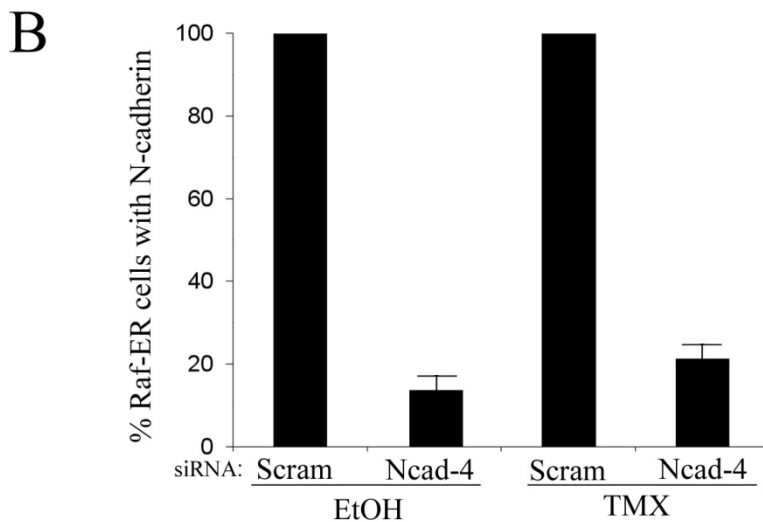
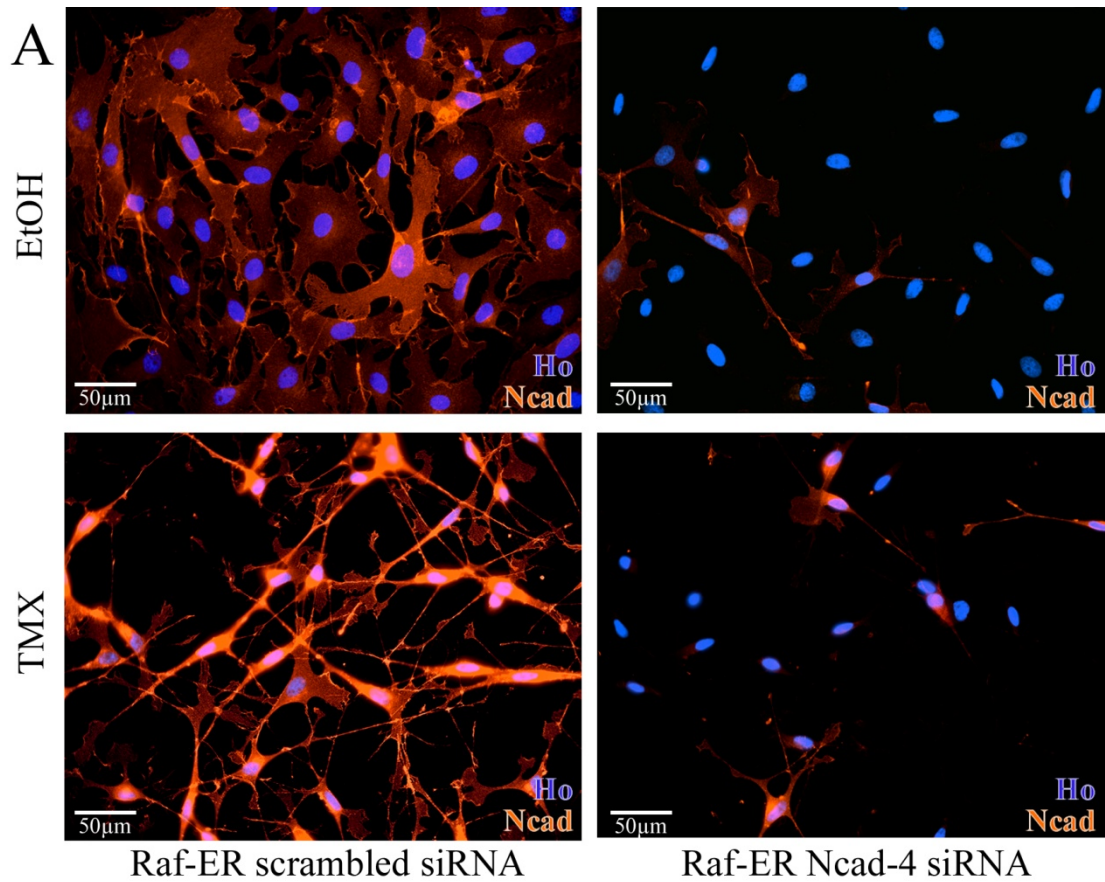


Figure 5.2 N-cadherin knockdown in Raf-ER cells is effective, but only at a higher concentration of siRNA. Raf-ER cells were transfected with 3nM of scrambled or Ncad-4 siRNA for 16hrs, after which the cell media was changed and 4hrs later, the cell media was supplemented with either tamoxifen (TMX) or ethanol (EtOH) for 28hrs prior to fixation. (A) Representative epifluorescence of monocultures immunostained for N-cadherin (red) with cell nuclei labelled with Hoechst (blue). (B) Quantification of the proportion of N-cadherin expressing cells. Counts were conducted in triplicate with 200+ cells counted per coverslips; bars represent S.D.

5.5 Loss of N-cadherin and hyper-elevated Raf/ERK signalling severely disrupted heterotypic Schwann cell/axonal interactions

I next wanted to address whether the loss of N-cadherin from Schwann cells in which Raf/ERK is constitutively activate would lead to an impairment in Schwann cell/axonal interactions that was greater than either state alone. To test this, I used our *in vitro* DRG coculture system and association assay. Raf-ER Schwann cells were transfected with either scrambled or N-cadherin siRNA for 16-hours. The transfectant was removed and the cells further incubated for four hours prior to addition of either Tmx or EtOH. Treated Raf-ER cells were then incubated for an additional 24-hours, after which they were seeded onto DRG axons and incubated for eight hours in media supplemented with Tmx or EtOH, fixed and coimmunostained for S100 β and RT97. As expected, the immunofluorescence showed that either loss of N-cadherin or activation of Raf/ERK in Schwann cells, resulted in partial impairments in Schwann cell/axonal interactions, while the majority of scrambled, EtOH-treated (control) Raf-ER cells were observed to be associated and aligned with axons (as illustrated by the white arrows). Interestingly, the depletion of N-cadherin from Raf-activated Schwann cells resulted in a substantially worse impairment of Schwann cell/axonal interactions as indicated by the white arrow-heads in **Figure 5.3A**. In order to quantify this effect, I scored Schwann cell/axonal interaction using the DRG association assay as described previously (Chapter Three) and found that Schwann cell/axonal association and alignment in N-cadherin-deficient, Raf-activated Schwann cells, was impaired by as much as 75% (**Figure 5.3B**). This accounted for a significantly greater impairment than the approximate 40% disruption to axonal interactions elicited by either N-cadherin knockdown or Raf-activation alone. Scrambled, Raf-inactive (EtOH-treated) Raf-ER cells were strongly associated and aligned with axons, and were indistinguishable from previously scored NS/DRG association scores, which typically had a 10% background impairment in interaction. These results indicated that both N-cadherin and Raf-activation were largely additive in terms of their contribution to Schwann cell/axonal interactions. This is similar in terms of severity to the interaction defect exhibited by LTD cells, although there were still cells that interacted normally with axons. In this regard, it is important to bear in mind that while all LTD cells carry the same genetic impairment for axonal-interaction, the siRNA approach does not achieve a 100%

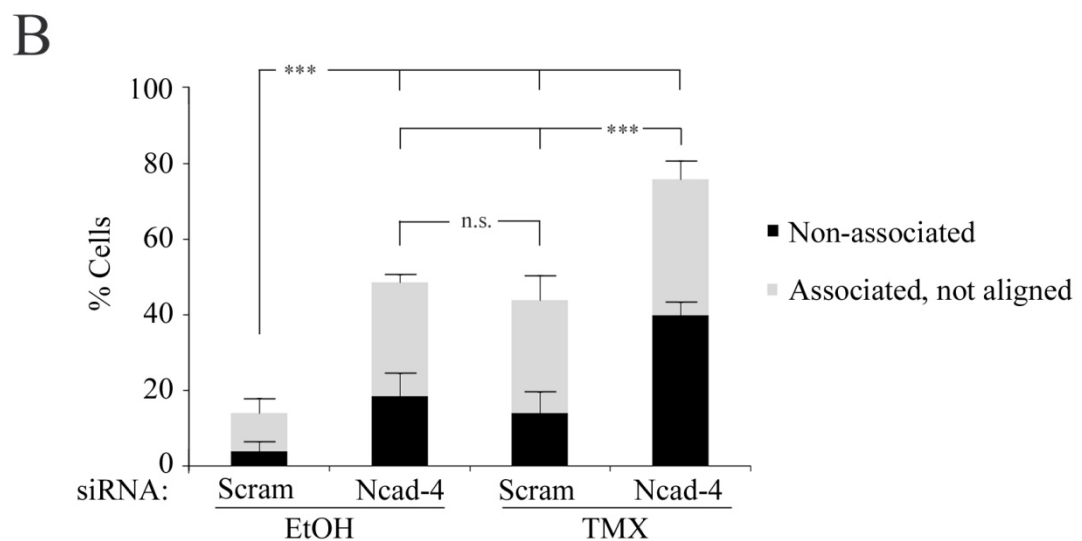
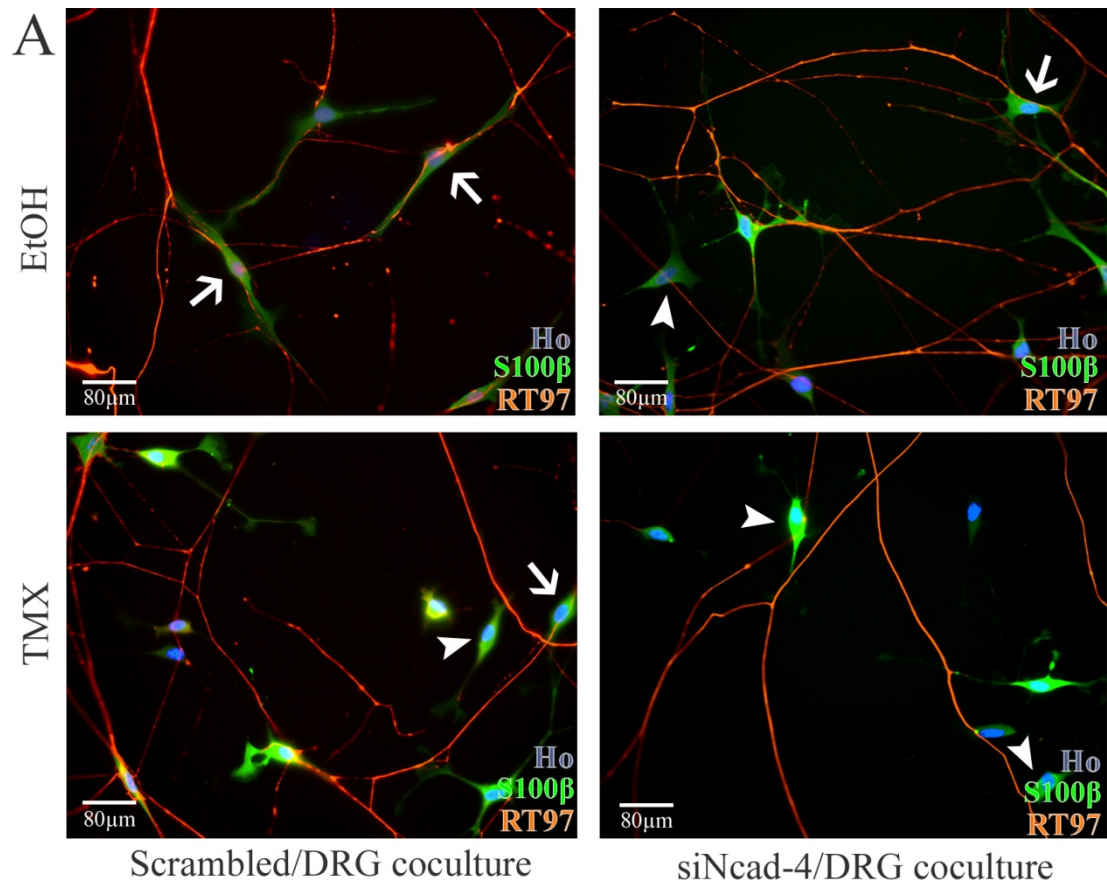


Figure 5.3 N-cadherin knockdown in Raf-activated Schwann cells severely disrupts interactions with axons. Raf-ER cells were transfected and the cell media supplemented with either EtOH or TMX. Monocultures were then incubated for 24hrs, seeding onto day-7 established DRG-axons and fixed after 8hrs. (A) Representative epifluorescence of cocultures coimmunostained for S100β (green) and RT97 (red), with nuclei labelled with Hoechst (blue). The arrows show examples of Schwann cell/axonal interaction, while the arrow-heads show examples of non-association. (B) Association assay. The bars represent S.D. of triplicates. Statistics by two-tailed T-test (** $p < 0.05$; n.s., not significant).

transfection rate, which might explain the reduced phenotypic severity exhibited by N-cadherin siRNA Raf-ER (Tmx) cells.

To study the loss of interactions dynamically, I used time-lapse microscopy. The four different Raf-ER cell types were generated as previously described, i.e. scrambled Raf-ER Schwann cells (+/- Tmx) & N-cadherin knockdown Raf-ER Schwann cells (+/- Tmx). The Raf-ER Schwann cells were then seeded separately onto axons and incubated for 20-hours so that time-lapse microscopy could be conducted. Analysis from the time-lapse data showed that the majority of scrambled Raf-ER Schwann cells that were either Raf activated (Tmx) or inactivated (EtOH), were able to grasp, pull or otherwise manipulate axons using the distal tips of their cytoplasmic protrusions. This behaviour can be observed in the image sequence shown in **Figure 5.4A (Video 5.1)**, depicting scrambled, Tmx-treated Raf-ER Schwann cell/DRG cocultures, where the white arrows show the path of a typical Schwann cell that grasps and pulls upon axons it encounters. However, while Schwann cells appeared to initially recognise and associate with axons, they often went on to form less-stable interactions when compared to Tmx-negative controls, for instance, Schwann cells would often spontaneously dissociate from axons. In stark contrast to these observations, when N-cadherin-deficient, Raf-activated (Tmx-positive) Schwann cell/DRG cocultures were studied, these cells invariably failed to recognise and grasp axons with their cytoplasmic protrusions (**Figure 5.4B; Video 5.2**). Instead, as shown by the white arrows, Schwann cells would often extend cytoplasmic protrusions across axons without a recognition response, which is similar in behaviour to NS cells transfected with the N-cadherin siRNA (Chapter Four). However, unlike the latter, the Raf-activated, N-cadherin-deficient Schwann cells would often fail entirely to interact with axons in a manner similar to LTD cells and fibroblasts. Thus, the combination of these interaction deficits, i.e. deficiencies in Schwann cell/axonal recognition at cytoplasmic protrusions (due to loss of N-cadherin) and loss of interaction stability (due to Raf-activation), may explain the increased severity of the phenotype.

In order to confirm this, I quantified the time-lapse videos to calculate the extent of Schwann cell-directed axonal grasping behaviour, where only initial axonal encounters mediated by the Schwann cell cytoplasmic protrusion were scored. These

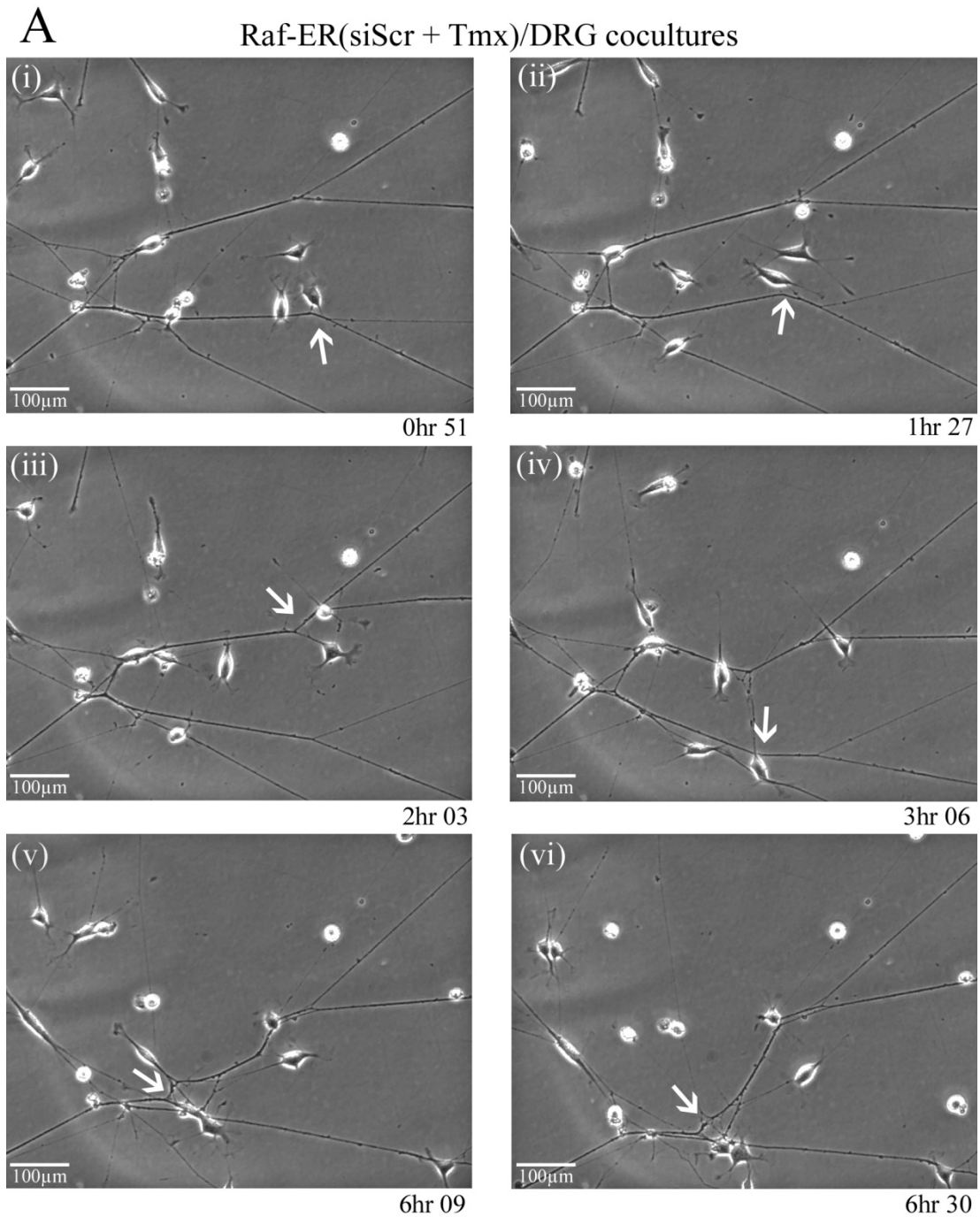
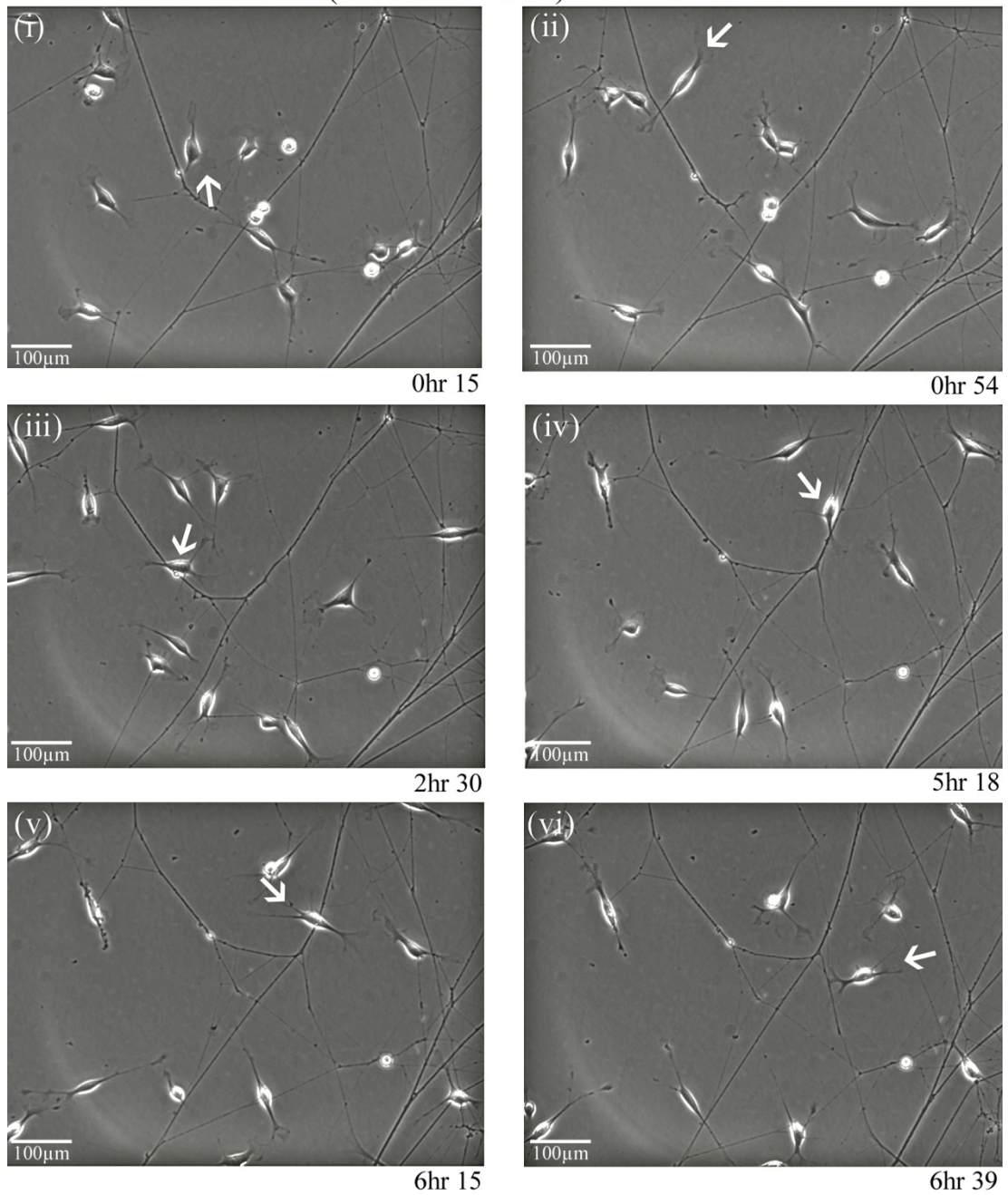


Figure 5.4 Schwann cell/axonal ‘grabbing’ behaviour is severely affected by loss of N-cadherin in a background of Raf/ERK activation. DRGs were explanted and incubated to generate axonal cultures. Inducible Raf-ER cells were transfected with scrambled or Ncad4 siRNA and subjected to treatment with EtOH or TMX (as previously described). Monocultures were then incubated for 24hrs after which cells were seeded onto axons and time-lapse analysis conducted over 20hrs. (A) Representative phase-contrast image sequence from **Video 5.1** of scrambled transfected, Raf-activated (TMX) Schwann cell/DRG cocultures. The white arrows illustrate the course of a representative Raf-ER cell as it encounters axons.

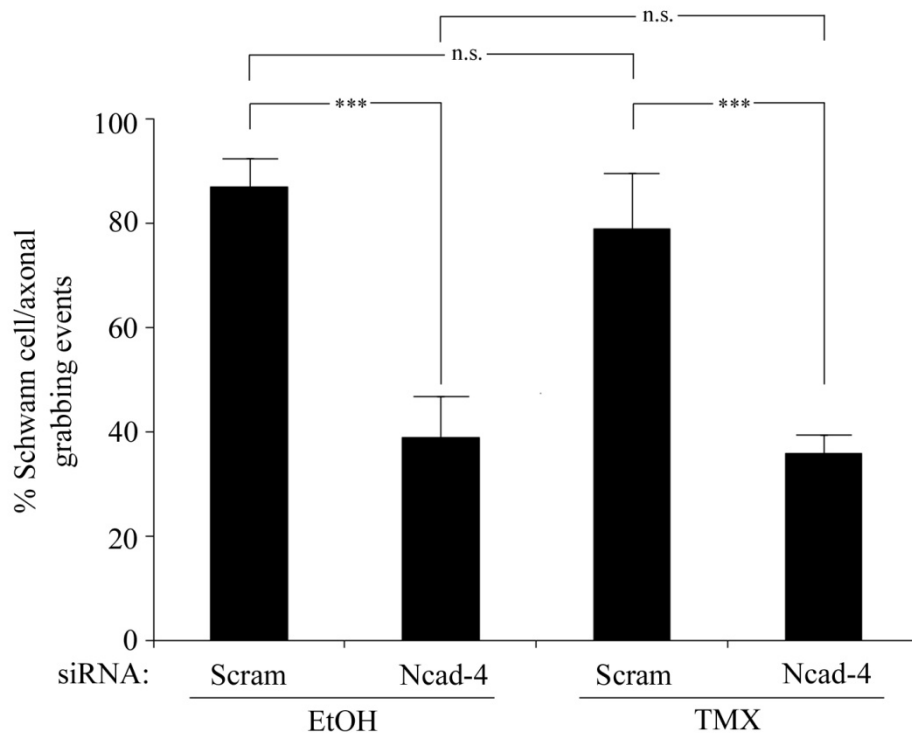
B

Raf-ER (siNcad-4 + Tmx)/DRG cocultures



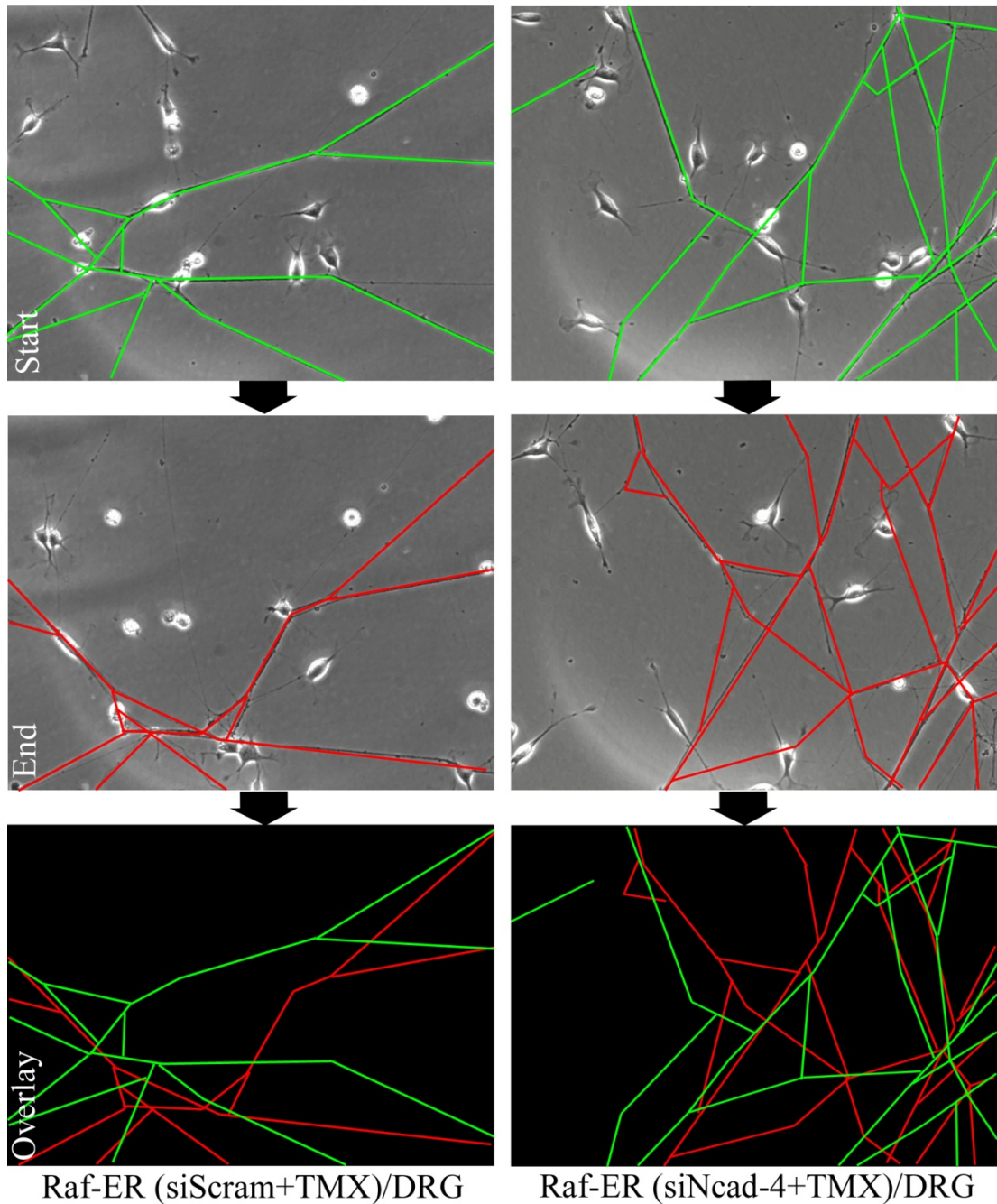
(B) Representative phase-contrast image sequence from **Video 5.2** of N-cadherin knockdown, Raf activated (TMX) Schwann cell/DRG cocultures. The white arrows illustrate the course of a typical Raf-ER cell during encounters with axons. Note the reduction in axonal ‘grabbing’ behaviour elicited by Schwann cells.

C



(C) Quantification of Schwann cell/axonal ‘grabbing’ events elicited by Schwann cells for axons at their cytoplasmic protrusions. Three videos were scored per DRG from triplicate wells with typically 20-25 Schwann cells scored per video. Bars represent S.D. with statistics by one-way ANOVA Tukey-Kramer Multiple Comparisons Test (** $p < 0.01$; n.s., not significant). Shown is one of three independent datasets of similar results.

D



(D) The schematic illustrates the differing degrees to which the axonal network is remodelled over the course of the time-lapse analysis represented in part A (Raf-ER scrambled/TMX) & Part B (Raf-ER siNcad-4/TMX). The axonal pattern in the first image of the sequence is shown in green while the axonal pattern of the final image is shown in red. Both green and red masks were overlaid to generate a composite, which qualitatively illustrates the shift in the axonal network and reflects the degree of physical manipulation exerted by Schwann cells on axons.

results showed that the loss of N-cadherin from Schwann cells resulted in a substantially less Schwann cell/axonal grasping events, which was independent of Raf activation (**Figure 5.4C**), thus, this suggested that N-cadherin, rather than Sema4F, functions primarily in cell protrusions to elicit the Schwann cell/axonal recognition response. In addition, I qualitatively examined the extent to which Schwann cells were able to manipulate and remodel the axonal network during the course of the time-lapse. The change in the axonal network was highlighted by overlaying the first frame with the last frame of the image sequence depicted in 5.4A-B. The skew in the pattern was then used to gauge the overall extent of Schwann cell/axonal interaction (**Figure 5.4D**). Consistent with previous findings, the analysis showed that in the scrambled Raf-activated cocultures, the axonal network had become skewed, which was indicative of significant manipulation of axons by Schwann cells. In contrast, the axonal network shape for the N-cadherin knockdown Raf-activated Schwann cells remained largely unchanged. In conclusion, the Raf-activated (Tmx-positive) Schwann cells retained normal ‘grabbing’ behaviour, consistent with their N-cadherin expression; however, they appear to lack the adhesive force necessary to maintain the association once the cell was ‘loaded’ onto the axon.

5.6 Double knockdown of semaphorin-4F and N-cadherin in Schwann cells

We found that the molecule downstream of the Raf signal responsible for the loss of Schwann cell/axonal interactions was Sema4F (Parrinello *et al.*, 2008). I therefore wanted to examine directly, the effect on Schwann cell/axonal interactions, of specifically depleting both N-cadherin and Sema4F from Schwann cells simultaneously. In particular, I wanted to see if these experiments corroborated previous findings from Raf-ER, N-cadherin Schwann cell knockdown experiments. In order to test this, I obtained two non-overlapping, independent siRNAs targeted against Sema4F (siSema4F-5 and siSema4F-6). The efficacy of Sema4F knockdown in Schwann cells was examined by RT-PCR because of the lack of a reliable Sema4F antibody. NS cells were transfected for 16-hours with 1nM scrambled siRNA, N-cadherin siRNA, two Sema4F siRNAs or a combination of N-cadherin and Sema4F siRNA (double knockdown). After the cell medium was changed, the monocultures

were incubated for a further 32-hours and then viewed by phase-contrast microscopy. N-cadherin-depleted monocultures were clearly identifiable in both the single N-cadherin knockdown and double N-cadherin/Sema4F knockdown by the distinctive nature of the cell monolayer, which in both cases was highly disorganised (**Figure 5.5A**). RT-PCR analysis was then performed using RNA extracted from culture plates. As expected, this analysis confirmed that N-cadherin siRNA was highly effective at depleting N-cadherin, while Sema4F siRNA was effective at reducing Sema4F levels by at least two-fold in both the single Sema4F and double N-cadherin/Sema4F siRNA knockdowns (**Figure 5.5B**). I next investigated the effect on Schwann cell/axonal interactions of directly depleting both N-cadherin and Sema4F from Schwann cells. To examine this, I repeated earlier association assays using primary DRG-axonal cultures. NS cells were transfected with scrambled, N-cadherin, Sema4F and N-cadherin/Sema4F siRNA for 16-hours. The monocultures were then further incubated for 24-hours prior to seeding onto axons. The cocultures were then incubated for eight hours, fixed and coimmunostained for S100 β and RT97. The immunofluorescence was quantified using the DRG association assay to assess the extent of Schwann cell/axonal association and alignment. Consistent with previous findings from Raf-ER association studies, the quantification showed a similar trend, in that depletion of either N-cadherin or Sema4F alone resulted in approximately 40% impaired interactions, while depletion of both adhesion molecules simultaneously, resulted in approximately 80% disruption to association and alignment (**Figure 5.6**). Similar to Raf-ER experiments, the majority (85%) of scrambled siRNA transfected Schwann cells were associated and aligned with axons.

5.7 Chapter summary and conclusions

In this chapter, I have shown that Schwann cell/axonal interactions are largely mediated by two independent cell adhesion molecules, N-cadherin and Sema4F, which both cooperate to mediate separate roles in the interaction process. I showed that N-cadherin was operating mostly at the lamellipodia-like cytoplasmic protrusions, to initiate recognition and facilitate Schwann cell-mediated grasping for axons. Sema4F is likely to have a more uniform distribution on the cell-surface, although lack of an effective antibody has hindered efforts to characterise its sub-cellular localisation. However, unlike N-cadherin, Sema4F is not required for

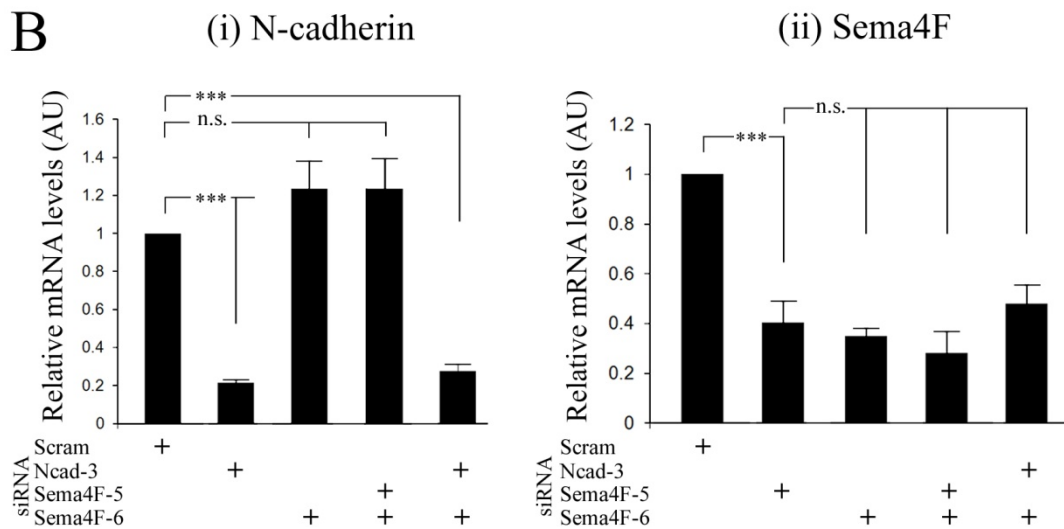
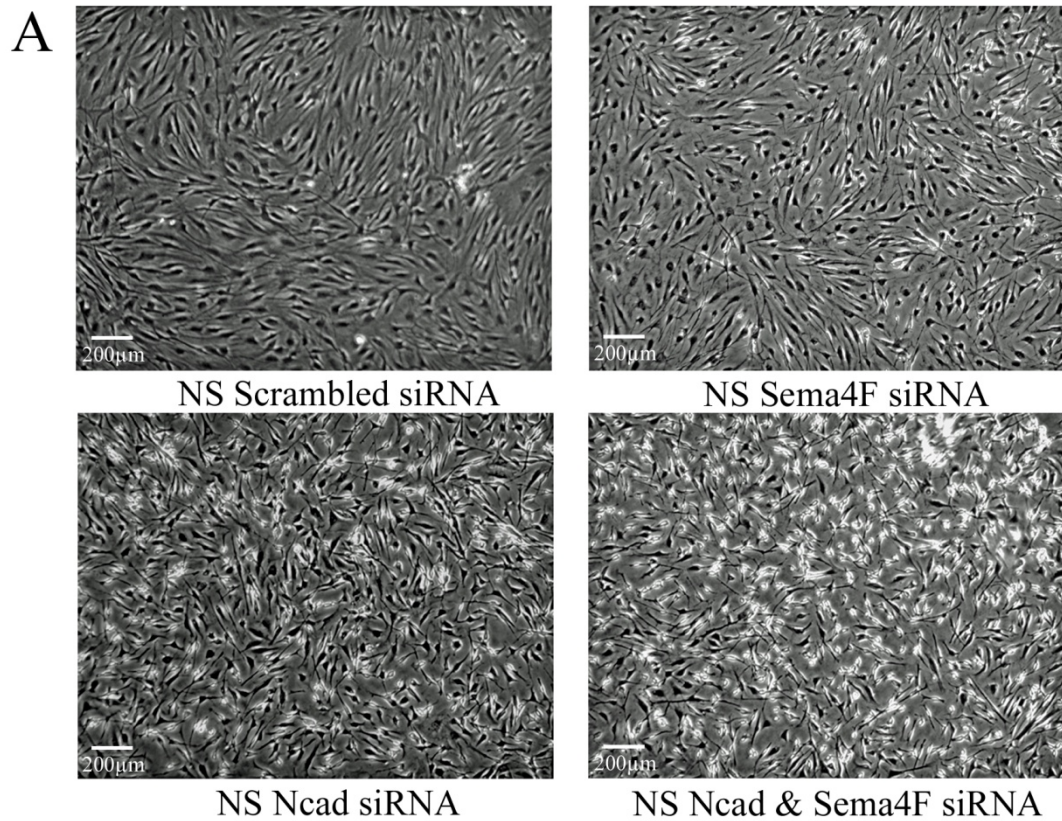


Figure 5.5 Simultaneous silencing of N-cadherin and Sema4F in NS cells after double siRNA transfection. NS cells were transfected for 16hrs with either single siRNA (scram, Ncad-3, Sema4F-5 or Sema4F-6) at a concentration of 1nM or double siRNAs (Sema4F-5 & -6, Sema4F-6 & Ncad-3) at a combined concentration of 1.5nM. Monocultures were then incubated a further 28hrs. **(A)** Representative phase-contrast images of live cells displaying classic N-cadherin-deficient refractive phenotype. **(B)** RT-PCR quantification of relative mRNA levels with GAPDH used to control lane-loading and levels standardised to scrambled. Bars represent S.D. with statistics by two-tailed T-test (***) $p < 0.001$; n.s., not significant).

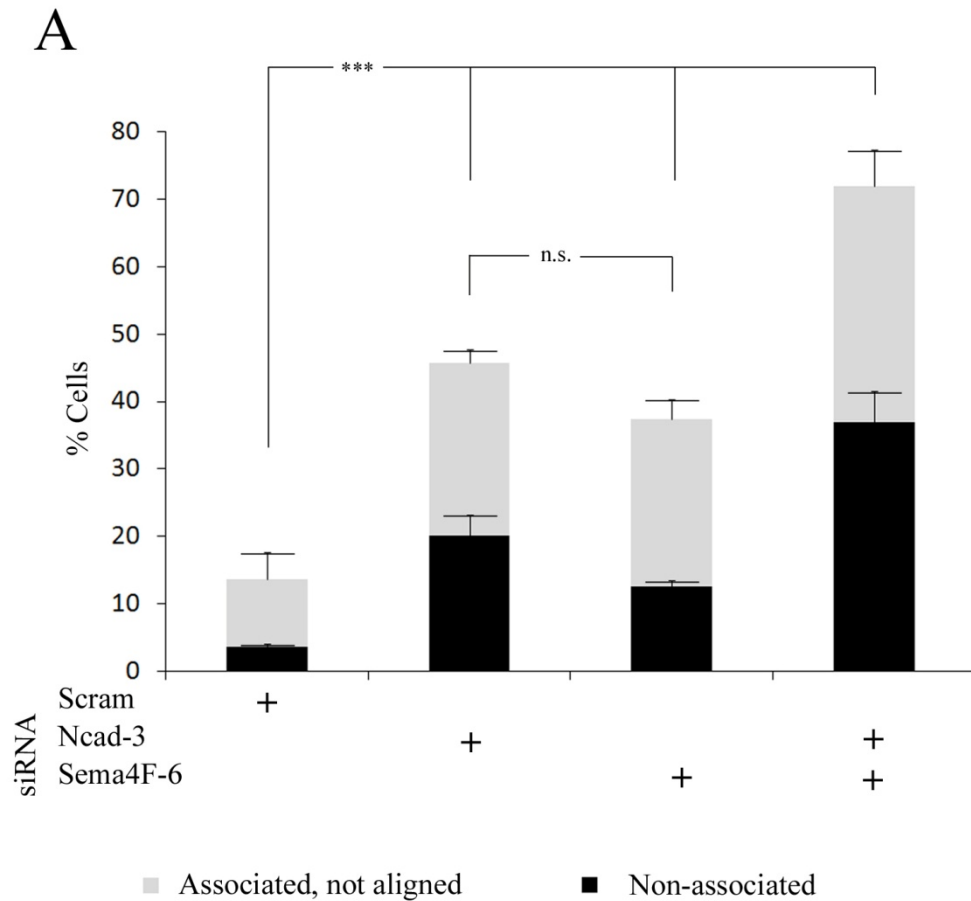


Figure 5.6 Combined loss of N-cadherin and Semaphorin-4F from Schwann cells severely impairs association and alignment. DRGs were explanted and incubated for 7 days to generate axonal networks. NS cells were transfected for 16hrs with 1nM of either scrambled, siNcad-3 or siSema4F-6 siRNA, or with a combination of siNcad-3 [0.75nM] and sema4F-6 [0.75nM]. The cell medium was changed and monocultures incubated a further 24hrs, after which cells were seeded onto axons and fixed after a further 8hrs. Cocultures were coimmunostained for S100 β and RT97. (A) Association assay: blind scoring conducted in triplicate with 200+ cells counted per DRG; Bars represent S.D. from triplicate coverslips with statistics by T-test (**p<0.01; ***p<0.001; n.s., not significant). Shown is one of three independent experiments of similar results.

Schwann cell/axonal recognition, rather its function appears to be in the stabilisation of Schwann cell/axonal associations following association. The importance of Sema4F in this regard is underlined by its down-regulation in Neurofibromatosis type 1 caused by hyper-activation of Ras, which is ultimately sufficient to cause Schwann cell/axonal disassociation as a first step in neurofibroma formation. This was particularly impressive given that the Sema4F knockdown was not complete. Thus, together N-cadherin and Sema4F cooperate at different stages of the interaction to facilitate and maintain Schwann cell/axonal interactions.

Chapter Six: Discussion

6.1 Chapter introduction

The Schwann cell is a remarkably plastic cell. It is capable of extraordinarily complex differentiation and specialisation, essential for the formation of the radial architecture and function of both myelinated and non-myelinated nerve fibres, while simultaneously remaining competent to respond to nerve injury - where the differentiation process is reversed to generate undifferentiated proliferating Schwann cells. Underlying all Schwann cell behaviour is reciprocal signalling between Schwann cells and axons that is mediated in a cell-contact dependent manner, which by definition, is reliant on a close and physical relationship mediated through cell adhesion molecules. In this thesis, I set out to investigate the interactions between Schwann cells and axons; in particular, to elucidate the molecular identity, and the localisation of action, of key mediators that facilitated these processes.

6.2 Summary of main findings

In Chapter Three, I described a model for early Schwann cell/axonal interactions which was based on time-lapse analysis. I then studied a Schwann cell clone (LTD), where the normal interaction process with axons had become severely impaired. In order to identify the genetic source of the LTD non-interaction phenotype, I conducted a differential expression microarray between axonal interacting (LTNS) and non-interacting (LTD) Schwann cells. This work revealed a global shift in gene expression, which suggested that a master regulator of the Schwann cell interaction phenotype was mutated in this clone. Interestingly, functional enrichment analysis showed that cell-adhesion was the most enriched functionally dysregulated group of genes in LTD cells. This functional cluster included previously investigated N-cadherin (Wanner *et al.*, 2006a; Wanner *et al.*, 2006b; Wanner & Wood, 2002), Sema4F (Parrinello *et al.*, 2008), L1-CAM (Seilheimer *et al.*, 1989) and NCAM (Hansen *et al.*, 2008), as well as a number of other CAMs not previously cited in Schwann cell/axonal interactions, for example cadherin-6, protocadherin-7, ninjurin and melanoma CAM (mCAM), which are useful candidates for future interaction studies. Interestingly, the transcription factors Sox2 and Sox10 were also found to

be down-regulated in LTD cells. However, Sox2 was not found to be responsible for the genetic lesion in LTD cells responsible for the broad dysregulation of CAM-related gene expression in LTD cells. For instance, the transcript levels of N-cadherin and Sema3B transcription were unaffected when Sox2 was over-expressed in Schwann cells and LTD cells. Unexpectedly, I found that Sox2 over-expression in Schwann cells resulted in the relocalisation of N-cadherin to homotypic Schwann cell-cell junctions and induced changes in the morphology of the adherens junctions. Sox2 over-expression also changed the behaviour of Schwann cells during encounters with other Schwann cells, switching the response from one of repulsion to one of attraction, mediated through N-cadherin, which we found resulted in increased Schwann cell clustering (Parrinello *et al.*, 2010).

In Chapter Four, I developed and utilised an siRNA approach to investigate the role of N-cadherin in homotypic Schwann cell-cell interactions. This work showed that N-cadherin was the functional cell adhesion molecule that bound Schwann cells together in groups. I also presented evidence that suggests homotypic *trans*-ligation of N-cadherin, between Schwann cells, conveys a cell-cycle inhibitory effect on Schwann cells. I next used a primary DRG/Schwann cell coculture system to investigate the functional role of N-cadherin in heterotypic Schwann cell/axonal interactions. Here, I showed that N-cadherin was necessary but not sufficient to instigate normal Schwann cell/axonal interactions. To determine how N-cadherin was functioning, and at which part of the interaction process, I studied N-cadherin immunofluorescence in conjunction with time-lapse analysis of normal Schwann cells and N-cadherin-depleted Schwann cells in coculture with DRG-axons. The immunofluorescence showed that N-cadherin was localised to the cytoplasmic ‘lamellipodia-like’ protrusions of the Schwann cells, even in Schwann cells that were not contacting axons. Moreover, the time-lapse analysis showed that Schwann cells recognise and ‘grab’ axons using these cytoplasmic protrusions, which were significantly disrupted in N-cadherin depleted Schwann cells, consistent with a role for N-cadherin as a mediator of these interactions. Importantly, work with perineural fibroblasts showed that this previously non-interacting cell-type could be driven to recognise and manipulate axons following heterologous N-cadherin expression. Together, these results showed that N-cadherin was necessary and sufficient for mediating Schwann cell/axonal recognition and early association with axons.

Previous studies have shown polarised N-cadherin expression along the adaxonal membrane interfacing the axonal axolemma in myelinating fibres (Chan *et al.*, 2006). Therefore, I investigated N-cadherin in mature myelinating Schwann cell/DRG cocultures in order to clarify its role in mature interactions. This work showed that loss of N-cadherin prior to initial Schwann cell/axonal interactions significantly impacted later myelination.

In Chapter Five, I describe the distinct roles played by N-cadherin and Sema4F in mediating Schwann cell/axonal interactions and also the affect of Raf/ERK-activation. Constitutive activation of Ras/Raf/ERK in Schwann cells is known to reverse the differentiated state of Schwann cells (Harrisingh & Lloyd, 2004), while dysregulation of the pathway is central to the aetiology of neurofibromatosis type 1 (Parrinello & Lloyd, 2009). Moreover, the associated downstream loss of Sema4F causes Schwann cell/axonal dissociation and impairs Schwann cell/axonal re-association and alignment *in vitro* (Parrinello *et al.*, 2008). Consistent with earlier work, sustained activation of Ras or Raf in Schwann cells impaired Schwann cell/axonal association and alignment despite strong expression of N-cadherin in these cells. Moreover, time-lapse analysis showed that although Raf-activated Schwann cells recognised and ‘grabbed’ axons, the resulting Schwann cell/axonal associations were generally unstable and short-lived. I advanced this finding by directly depleting Sema4F, a downstream target of the Ras/Raf/ERK pathway, from Schwann cells, which replicated the impairment displayed by either Ras or Raf activation. Finally, I showed that combined loss of Sema4F and N-cadherin from Schwann cells significantly disrupted cell interactions. These findings suggest that both N-cadherin and Sema4F are involved in normal Schwann cell/axonal interactions, but primarily function at different stages of the interaction: N-cadherin mediates recognition and initial association, while Sema4F facilitates the stabilisation of the association.

6.3 Homotypic Schwann cell-cell interactions

Homotypic Schwann cell-cell interactions play important roles in Schwann cell biology. In early development, prior to association with axons, homotypic interactions between SCPs facilitate the formation of sheets of interconnected cells

that migrate with, and are found in close proximity to, the developing and extending peripheral nerves (Woodhoo & Sommer, 2008). Homotypic interactions between SCPs are also important for capping and protecting sensitive axonal growth-cones as they traverse tissue to locate targets for innervation (Wanner *et al.*, 2006b). It has been suggested that homotypic interactions occur between juxtaposed Schwann cells along myelinated nerve fibres at the so-called microvilli fringe, i.e. in the region overlying the Node of Ranvier (Poliak *et al.*, 2002). However, Alanne *et al.* (2009) found no evidence for the involvement of E-cadherin, the most ideally placed CAM that could mediate this interaction, nor the presence of tight-junctional components, i.e. claudin family members, between Schwann cells. Thus, homotypic interactions in myelinated nerve - if they occur at all - remain poorly understood and require further clarification. In recent years, the role of homotypic interactions between denervated Schwann cells following nerve injury has been studied and their importance for nerve repair and regeneration has become clearer. For instance, injuries to the nerve can be in the form of nerve crush or nerve transection, where the latter tend to have less favourable outcomes in terms of repair. Despite this, a good proportion of sciatic nerve transections spontaneously reconnect with distal targets within 48-hours in rodents - importantly, homotypic Schwann cell-cell interactions have been shown to play a central role in facilitating the reconnection of the nerve (Parrinello *et al.*, 2010). In this study, we found that recently dissociated and dedifferentiated Schwann cells, at the proximal nerve stump (site of nerve injury), were clustering in a manner reminiscent of SCP-SCP sheets often observed during development, and which we showed, were important for guiding axons across otherwise intractable regions of the legion.

6.3.1 A role for N-cadherin

In the current thesis, I demonstrate a central role for N-cadherin in the mediation of homotypic Schwann cell-cell interactions between cultured denervated ‘injury’ Schwann cells *in vitro*. This finding is consistent with earlier studies, which suggested that N-cadherin mediates homotypic Schwann cell-cell interactions in cultured denervated Schwann cells (Fairless *et al.*, 2005; Wanner & Wood, 2002), as well as during development between SCPs (Wanner *et al.*, 2006a). Importantly, consistent with these studies and others, I confirmed that E-cadherin (an alternative

cadherin-type expressed by mature Schwann cells) was not expressed by denervated Schwann cells *in vitro* (Gess *et al.*, 2008; Wanner & Wood, 2002) and was therefore unlikely to be a mediator of Schwann cell/Schwann cell interactions.

During development, N-cadherin is expressed by Schwann cell progenitors, including NCCs and SCPs, while E-cadherin is not expressed in these progenitors, thus a role for N-cadherin in SCP clustering is highly plausible (Wanner *et al.*, 2006a; Wanner *et al.*, 2006b). Conversely, N-cadherin levels in peripheral nerve decline towards birth concordant with increasing levels of E-cadherin. N-cadherin is minimal and E-cadherin is maximal at around a week after birth (Crawford *et al.*, 2008). This is likely to reflect the changing requirement for stability in the nerve architecture that occurs during myelination and is initiated around birth (Jessen & Mirsky, 2005). As previously discussed, E-cadherin performs two major roles in myelinated nerve: first, in the formation of autotypic junctions between membrane lamellae of the glial paranodal loops, and second, in the stability of SLI channels (Salzer *et al.*, 2008). Interestingly, E-cadherin expression is up-regulated at the same time as genes involved in the myelination programme, notably the cAMP responsive gene Oct6, and has itself been shown to be a target of cAMP dependent PKA activation (Crawford *et al.*, 2008). The signals that drive the simultaneous down-regulation of N-cadherin remain to be elucidated. Cadherin switching is therefore, an important part of Schwann cell biology, changing the adhesive properties of adherens junctions to reflect the differing functional requirements of Schwann cells at specific stages of development. Cadherin-switching is observed in the early formation of NCCs, which undergo an EMT-like event that involves a switch in cadherin expression from E- to N-cadherin, thus allowing the delamination of fixed NCCs from the flanks of the neural tube to generate motile NCCs (Kuriyama & Mayor, 2008). Later Schwann cell progenitors mediate transient interactions via N-cadherin between themselves and axons, which is important for many processes, including neural crest migration and radial sorting. As Schwann cells make more stable interactions with the axons, the need for transient interactions is reduced and the requirement for stable interactions, mediated by E-cadherin and other CAMs with greater adhesive strength (Gumbiner, 2000), is increased and is necessary to generate the stable three-dimensional microarchitecture of the functional homeostatic nerve. This cadherin switch (from N- back to E-cadherin) is effectively a reverse of the

earlier neural EMT-like process involved in neural crest de-lamination. Interestingly, as previously discussed, dedifferentiated Schwann cells from injured nerve undergo another round of cadherin-switches, as they re-express N-cadherin and (presumably) down-regulate E-cadherin, take part in nerve repair and then re-express E-cadherin and down-regulate N-cadherin during re-myelination of the repaired axons. This is a further example of the versatility of Schwann cells.

Future work should aim to clarify the downstream components required for N-cadherin function in the mediation of homotypic interactions. In terms of the former, while the adhesive interactions of cadherins are well documented, the intracellular signalling components of cadherin function are less clear. Importantly, a number of cadherin binding partners can modulate the adhesive function of cadherins, for example p120-catenin (Perrin-Tricaud *et al.*, 2007), Merlin (Curto & McClatchey, 2008) as well as β -catenin (Davis *et al.*, 2003). Furthermore, cadherin function may be altered by binding in *cis* with other membrane proteins, for example RTKs (Doherty *et al.*, 2000). In Schwann cells, the role of these modulators of N-cadherin function is not well understood. For instance, Lewallen *et al.* (2011) show that N-cadherin and β -catenin colocalise, while immuno-precipitation (IP) experiments show a direct interaction between N-cadherin and β -catenin in Schwann cell/axonal cocultures. Furthermore, they demonstrate that β -catenin is required for N-cadherin function in Schwann cells as its ablation results in a delay to myelination. However, these findings are contradicted by Gess *et al.* (2008), who showed that β -catenin ablation in Schwann cells had no effect on the localisation of N-cadherin at cell-cell junctions and nor did it effect the morphology of Schwann cells, i.e. β -catenin was not required for mediating adhesive interactions between cells. In light of these findings, it would be advantageous to clarify the role of accessory molecules involved in the adhesive function of N-cadherin in Schwann cell-cell interactions. In order to address this, the Image-J quantification technique described in Chapter Four, could be adapted and employed as part of a RNAi screen to detect essential genes involved in all stages of homotypic Schwann cell-cell adhesion. For instance, Schwann cells could be cultured in multi-well plates and subjected to siRNA-mediated knockdown for an array of gene targets. Confluent plates could then be analysed to calculate extracellular area as a readout for the integrity of homotypic interactions. Implementation of such a screen would be relatively efficient as the

technique has been pre-optimised to permit rapid and reliable quantification of extracellular area in Schwann cell monocultures from fluorescent images.

6.3.2 Sox2 relocalises N-cadherin to cell-cell junctions and promotes Schwann cell-cell clustering

In the current thesis, I showed that Sox2 over-expression in Schwann cells resulted in substantially increased levels of N-cadherin at Schwann cell-cell junctions. Moreover, the gross morphology of the adherens junction (as viewed from immunofluorescence) was altered. In normal Schwann homotypic interactions, the junction is composed of short 'zipper-like' strands of N-cadherin arranged perpendicular to the cell-cell interface. In Sox2 over-expressing Schwann cells, this changed markedly, with substantially larger N-cadherin complexes residing at the cell junction where long-strands of N-cadherin appeared to project deep into the cell. Furthermore, we found that Sox2 was not acting to increase N-cadherin transcription, as mRNA levels remained unchanged between Sox2 and controls, indicating that N-cadherin gene was not a direct Sox2 target. Rather, Sox2 appeared to be directing the re-localisation of existing N-cadherin to Schwann cell-cell junctions (Parrinello *et al.*, 2010). Alternatively (or in addition), Sox2 effectors might be altering the stability of existing cell-surface expressed N-cadherin, i.e. by preventing degradation and/or internalisation of N-cadherin. The question as to how Sox2 might be mediating these changes to N-cadherin and through which cellular effectors, remains to be elucidated (see future work for strategies to address this). However, we recently showed that Sox2-dependent localisation of N-cadherin to cell-cell junctions was necessary for the formation and maintenance of Schwann cell-cell clusters *in vitro* and also following nerve transection *in vivo* (Parrinello *et al.*, 2010). In terms of the latter, we showed that fibroblasts present at the injury site play an important role by inducing the up-regulation of Sox2 expression in Schwann cells through heterotypic Fibroblast/Schwann cell interactions mediated by ephrin-B/EphB2 signalling (see **Figure 6.1**).

Importantly, Sox2 expression was found to promote Schwann cell-cell adhesion and furthermore, allowed directed and coordinated migration of Schwann cells from the proximal stump into and across the site of injury (nerve bridge) in injured nerve

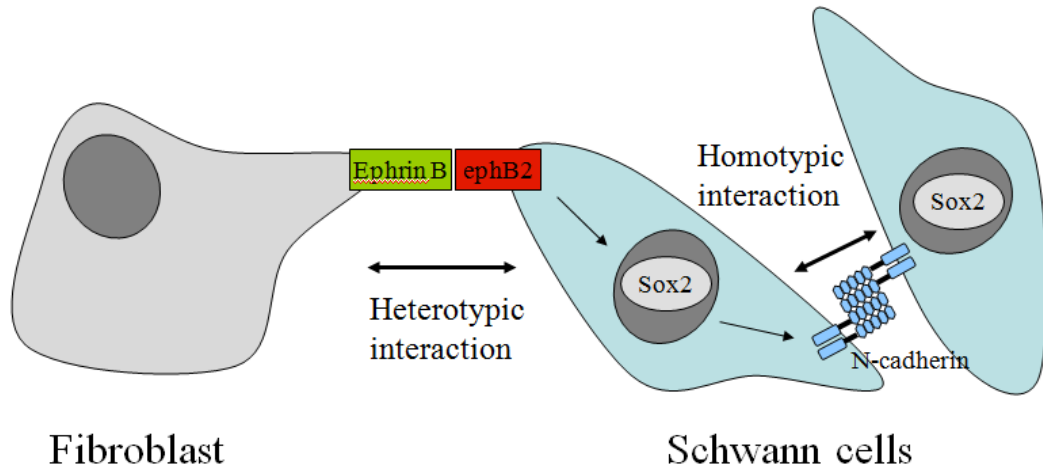


Figure 6.1 Schematic of the mechanism by which fibroblast/Schwann cell interactions promote Schwann cell-cell clustering after injury. Heterotypic interactions occur between fibroblasts and Schwann cells mediated by Ephrin B/ephB2 signalling, which initiates repulsion between these cells and induces Sox2 expression in Schwann cells. Sox2 mediates the redistribution of N-cadherin to cell junctions and enhances homotypic Schwann cell-cell interactions leading to Schwann cell clustering, which is important for Schwann cell-directed re-growth of axons across the lesion following nerve transection.

(Parrinello *et al.*, 2010) (see **Figure 6.2**). Consistent with these findings, a study by Seggio *et al.* (2010) demonstrated, in the absence of other cues, that Schwann cell orientation alone was sufficient to direct axonal re-growth *in vitro*. Thus, the collective migration of Schwann cells into the disorganised tissue milieu of the nerve-bridge (site of transection), which we showed occurs prior to axonal out-growth, is likely to aid regeneration by providing a favourable (guiding) substratum for axons to traverse the injury site in order to reconnect with distal targets, achieve re-innervation and complete the functional repair of the nerve (Parrinello *et al.*, 2010; Scherer & Salzer, 2001).

Sox2 is a transcription factor expressed early in the Schwann cell lineage, as well as after nerve injury, with a diverse range of transcriptional targets (Baer *et al.*, 2007; Le *et al.*, 2005a). It is best characterised as playing a key role in maintaining the

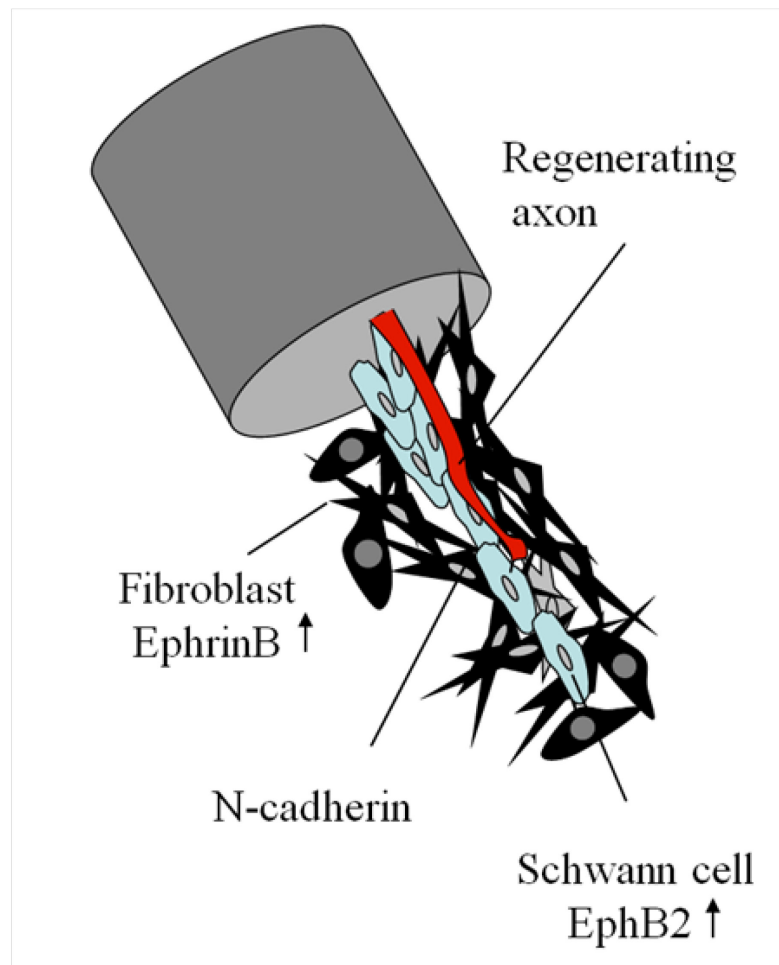


Figure 6.2. Schematic illustrating the importance of Sox2 mediated Schwann cell-cell interactions during nerve regeneration. Schwann cells present at the proximal stump up-regulate Sox2 following EphB2/EphrinB interactions with fibroblasts, which alters N-cadherin localisation at Schwann cell-cell junctions to promote clustering and drive a coordinated wave of Schwann cell migration across the nerve bridge. Regenerating axons use these Schwann cell strands to traverse the nerve bridge and reconnect with distal portion of the nerve (Parrinello *et al.*, 2010).

pluripotency and self-renewal capabilities of embryonic stem cells (Chambers & Tomlinson, 2009), and has also been shown to reprogram somatic cells to generate pluripotent stem cells (Chambers & Tomlinson, 2009; Takahashi & Yamanaka, 2006). However, to our knowledge, this was the first time that Sox2 activity has been linked to the regulation of N-cadherin function to effect long-term changes in cell behaviour, notably the switching between repulsion and attraction, in order to coordinate the mass-movement of cells in response to positional cues provided by fibroblasts (Parrinello *et al.*, 2010).

Future studies should aim to address the relationship between Sox2 and N-cadherin in Schwann cells. In particular, it would be interesting to discover how Sox2 was directing and organising the sub-cellular localisation of N-cadherin at cell junctions. It is most plausible that Sox2 directs this process via transcriptional control of target genes that are responsible redistributing N-cadherin. Therefore, an analysis of Sox2 binding sites would be a useful methodology for identifying Sox2 targets and thus, possible mediators in this process. In addition, a useful tool to develop would be an N-cadherin-GFP fusion protein, which could be transfected into Schwann cells and visualised in live-cells by spinning-disc confocal microscopy to achieve high-resolution video imaging of N-cadherin molecules in cells. The sub-cellular localisation of N-cadherin could then be tracked following induction of Sox2 expression, i.e. by using heterotypic Schwann cell/fibroblast cocultures, in order to discover how Sox2 remoulds N-cadherin junctions to enhance homotypic interactions. In addition, this approach would also be useful for visualising the dynamics of N-cadherin at Schwann cell protrusions and in DRG cocultures, where it could provide further evidence for the involvement of N-cadherin within these structures and also, in the dynamics of N-cadherin mediated Schwann cell/axonal recognition.

6.4 Homophilic N-cadherin ligation between Schwann cells elicits an inhibitory effect on the cell-cycle

The regulation of cell proliferation is of fundamental importance to Schwann cell biology throughout development and into adulthood. In contrast to most differentiated mammalian cells, adult Schwann cells lack a defined stem-cell population. They therefore retain an inherent capacity to dedifferentiate and re-enter the cell-cycle in order for Schwann cells to self-renew in response to nerve injury; however, this creates the potential for dysregulation and thus, Schwann cell proliferation is kept under tight regulatory control. Additionally, during development, Schwann cell proliferation is required to match the number of Schwann cells with the number of axons, which is especially important during radial sorting (Court *et al.*, 2006; Martin & Webster, 1973). As Schwann cells prepare to myelinate, proliferation is attenuated and ensheathed Schwann cells assume a quiescent state, which is an essential pre-requisite for myelination. The quiescent

state is maintained by close Schwann cell/axonal contact, in which the NRG1 signal is thought to play a role. Intriguingly, this signal can elicit both mitotic and, albeit indirectly, inhibitory effects on Schwann cell proliferation depending on the developmental context. In terms of the latter, this is mediated via NRG1 driving differentiation rather than inhibiting the cell-cycle *per se*. For instance, in early development, NRG1 Type III- β 1a acts as a potent mitogen for Schwann cell precursors and immature Schwann cells (Wolpowitz *et al.*, 2000), while later in development, the same isoform of NRG1 drives Schwann cell differentiation (Michailov *et al.*, 2004; Taveggia *et al.*, 2005). As discussed, the quiescent state of the myelinated Schwann cell is not permanent but rather is susceptible to reversal - as is observed in injured nerves, where dissociated Schwann cells are found in a proliferating state. Consistent with this, we have shown that loss of axonal-contact, following down-regulation of Sema4F, leads to a relaxation of cell-cycle inhibition in Schwann cells, which allows cell proliferation in non-associated Schwann cells in the presence of exogenous mitogens (Parrinello *et al.*, 2008).

In the current work, I show that N-cadherin mediated Schwann cell-cell interactions elicited a cell-cycle inhibitory effect on Schwann cells *in vitro*. In normal homotypic Schwann cell-cell interactions, as observed in cultured NS cells, the rate of proliferation attenuates as cultures reach confluence and importantly, the Schwann cell monolayer in these cultures is maintained despite increased cellular density. These observation can be explained in terms of a mechanism based on CIP (Tikoo *et al.*, 2000). Findings from the current work, in which N-cadherin was specifically depleted, showed that Schwann cell proliferation was not attenuated at confluence and furthermore, Schwann cells would often extend processes over one another rather than forming a tight monolayer, resulting in the appearance of disorganised Schwann cell monocultures *in vitro*. Together, these findings suggest a role for N-cadherin in Schwann cell CIP. This is not an unprecedented finding as cadherin mediated CIP has previously been reported. For instance, E-cadherin has been shown to mediate CIP in epithelial cells (Perrais *et al.*, 2007). In addition, a study by Levenberg *et al.* (1999), using Chinese Hamster Ovary (CHO) clones with incremental N-cadherin expression, showed that increasing N-cadherin expression resulted in a proportional decline in cell proliferation at confluence. They found that this effect was mediated through p27, which arrested the cell-cycle in G1. This work

appears to be contradictory to a study by Fairless *et al.* (2005), that found that Schwann cell proliferation, as measured by BrdU incorporation, was not affected in siRNA mediated N-cadherin knockdown Schwann cells *in vitro*. A possible explanation for this discrepancy, as acknowledged by the authors, was that the level of N-cadherin knockdown achieved was only partial, which they suggest was due to the incomplete transfection of N-cadherin siRNA into Schwann cells.

While cadherins mediate cell-cell adhesive contacts, it is still unclear how they (or associated intracellular and/or membrane proteins) signal to convey that information to the cell nucleus in order to effect cell-cycle inhibition (Perrais *et al.*, 2007). In addition, there is some degree of conjecture as to whether cadherin ligation promotes or inhibits proliferation. For example, a study by Gess *et al.* (2008) found that β -catenin signalling elicited a mitogenic effect on Schwann cells, where nuclear translocation of β -catenin was sufficient to transactivate various pro-mitotic genes including LEF/TCF transcription factors and cyclin-D1 (Shtutman *et al.*, 1999). However, these findings are contradictory to the earlier study by Perrais *et al.* (2007), who showed that cadherin homophilic ligation was inhibitory to cell proliferation through modulation (and subsequent inactivation) of growth factor receptors, for example the EGF receptor. In addition, the localisation of Merlin/NF2 to mature cadherin-based adherens junctions has also been shown to be inhibitory to cell proliferation (Curto *et al.*, 2007; McClatchey & Fehon, 2009). The importance of this tumour suppressor in Schwann cell proliferation is demonstrated by its loss, which is implicated in elevated proliferation in a number of cell-types (Lallemand *et al.*, 2009) as well as tumorigenicity, for example the formation of homogenous Schwann cell tumours termed schwannomas that are a hallmark of Neurofibromatosis Type II (Begnami *et al.*, 2007). Merlin/NF2 functions to suppress cell proliferation in addition to its shared role with other ERM (ezrin, radixin, moesin) proteins as an organiser of the actin cytoskeleton (Lallemand *et al.*, 2009). Importantly, a functional role for Merlin in CIP relies on extracellular cues to gauge cell-density, of which the cadherins, known to interact with Merlin, are ideally placed. Thus, it is plausible that loss of N-cadherin prevents correct Merlin function in Schwann cells, which might explain continued cell proliferation at cell confluence. Clearly, further studies are required to understand the complexities involved and indeed, the functional relevance of this to the nerve - although in terms of the latter,

it is clearly advantageous to have a cell-density dependent mechanism to attenuate hyper-proliferation.

6.5 Early mediators of heterotypic Schwann cell/axonal interactions

Heterotypic interactions between Schwann cells and axons are a central defining feature of Schwann cells. Initial interactions between Schwann cell and axons occur early in development and, in the healthy nerve, are maintained for life (Jessen & Mirsky, 2005). However, these interactions are recapitulated in damaged nerve, where dedifferentiated 'injury' Schwann cells are required to re-discover and re-associate with axons following axonal regeneration (Chen *et al.*, 2007). In the current thesis, I described the role of two early mediators of Schwann cell/axonal interactions, N-cadherin and Semaphorin-4F (Sema4F) and suggest how both CAMs are operating at distinct stages of the interaction process.

6.5.1 A role for N-cadherin

In the current thesis, I showed that homophilic *trans*-ligation between N-cadherin dimers, expressed on both Schwann cells and axons, was important for mediating an initial adhesive interaction between these cells. This initial interaction is fairly weak, consistent with N-cadherin mediating a transient cell-cell interaction, as reported in other cell systems (Gumbiner, 2005; Patel *et al.*, 2003), and later strengthens as the junction matures (Bayas *et al.*, 2006). The evidence I presented suggests that N-cadherin operates at cell protrusions as part of a mechanism, orchestrated by these sub-cellular structures, for mediating contact-dependent recognition between Schwann cells and axons.

The cellular environment of the nerve is heterogeneous, comprising of multiple cell-types all of which react differently to encounters with one another (homotypically) or with different cell-types (heterotypically). The behavioural response to an encounter depends on the repertoire of cell-surface expressed molecules, which can elicit neural, attractive or repulsive responses. For instance, in low-density cultures, Schwann cell/Schwann cell encounters generally lead to repulsion, Schwann

cell/axonal encounters lead to attraction, fibroblast/axonal encounters are neutral and fibroblast/Schwann cell encounters are repulsive. In addition, the behavioural response to cell encounters can be altered by previous heterotypic signalling, as demonstrated by Schwann cell/fibroblast interactions (discussed previously). Thus, there is a plausible case for recognition mechanism in order that Schwann cells can discern axons from other cell types in the nerve. Recognition is logically an important first-step in the Schwann cell/axonal interaction programme, both in development and following nerve injury. For instance, early Schwann cell progenitors, for example SCPs, need to distinguish axons from other cell-types present in the milieu of the prospective nerve. Similarly, dissociated Schwann cells, found in the injured nerve, need to identify new axonal targets from the heterogeneous environment of the lesion, in order to re-associate and regenerate myelinated fibres.

Evidence to support the role of N-cadherin and Schwann cell protrusions in contact recognition are several fold. First, the unique bi- and tri-polar morphology of non-associated Schwann cells, which typically project several expansive lamellipodia-like protrusions, is indicative of searching behaviour. As shown by time-lapse videos, when Schwann cells are seeded onto DRG-axonal cultures, they will migrate, apparently in random directions, in order to locate axons to associate with. The first point of contact is usually the tip of one of these Schwann cells protrusions, which elicits an immediate behavioural response by the Schwann cell, resulting in axonal-'grasping' followed by Schwann cell/axonal association. Therefore, it is likely that these structures primarily function in Schwann cell-directed acquisition and recognition of axons. Second, I showed that N-cadherin was asymmetrically localised to the cytoplasmic lamellipodia-like protrusions of non-associated Schwann cells prior to contacting axons, which implicates N-cadherin as playing a role in these structures for mediating interaction with axons. Consistent with this, I showed that the depletion of N-cadherin from Schwann cells severely affected their ability to associate and align with DRG-axons *in vitro* and time-lapse analysis showed that this defect was caused by a failure of Schwann cell recognition for axons in their cytoplasmic protrusions. Lastly, heterologous expression of N-cadherin in fibroblasts was sufficient to cause an otherwise non-axonal-interacting cell-type to radically alter its behaviour and grasp, manipulate and partially associate with axons.

Thus, N-cadherin expression alone is not only sufficient to change the behaviour of the fibroblast/axonal encounter from neutral to attractive but also allows the fibroblast to pull, grab and manipulate axons in a similar fashion to Schwann cells. This suggests that fibroblasts have all the necessary components to interact with axons apart from N-cadherin.

Collectively, these findings raises an intriguing question - if both Schwann cell/Schwann cell and Schwann cell/axonal interactions are initiated following homophilic N-cadherin-N-cadherin ligation, then how do Schwann cells differentiate their response to both encounters, i.e. repulsion in the case of the former and association in terms of the latter? Heterologous expression of N-cadherin in fibroblasts suggest that N-cadherin is sufficient for otherwise non-interacting cells to associate with axons. However, it is likely that other CAMs or the cylindrical morphology of the axon is required for the Schwann cell/axonal specific response whereas in the case of Schwann cell/Schwann cell encounters there are likely to be surface expressed molecules that instigate repulsion. If this were correct, then these molecules are likely to be inactivated or over-expressed upon Sox2 expression, which is permissive for Schwann cell cluster formation. Thus, there are likely to be other molecules involved in these interactions and future studies should aim to identify the additional molecules involved in mediating the distinct responses exhibited by Schwann cell/Schwann cell and Schwann cell/axonal interactions.

6.5.2 Distinct roles for Semaphorin-4F and N-cadherin

While N-cadherin is an important mediator of early Schwann cell/axonal interactions, its loss from Schwann cells only accounts for a 40% reduction in Schwann cell/axonal association. This implies that an additional CAM (or CAMs) were partially compensating for the loss of N-cadherin. In addition, time-lapse videos of N-cadherin-depleted Schwann cells, showed that a proportion of these cells were able to associate with axons, albeit with less efficiency, despite the ablation of Schwann cell/axonal 'grabbing-like' behaviour at Schwann cell protrusions. These interactions appeared to be mediated not by Schwann cell/axonal contact at cell protrusions but with the 'bulk' of the cell, which appears to adhere to the axon. In the current work, I investigated the dual roles of Sema4F, which is also down-regulated

in LTD cells, and N-cadherin in the normal Schwann cell/axonal interaction programme.

We previously showed that Sema4F expression by Schwann cells was important in both mediating interactions with axons and for the stability of existing interactions (Parrinello *et al.*, 2008). In terms of the latter, we found that Sema4F was down-regulated in Schwann cells upon Ras/Raf/ERK activation, a signalling pathway dysregulated in Neurofibromatosis type 1, and that loss of Sema4F was instrumental to loss of Schwann cell/axonal interactions, which is an important first stage in tumourgenesis. Importantly, Sema4F expression is lost from at least three different human neurofibroma cell-lines, NF88-3, NF90-8, and ST88-14, with all three tumour lines exhibiting defective Schwann cell/axonal interaction *in vitro* (Parrinello *et al.*, 2008). The semaphorins are a large family of axon guidance molecules that classically operate to direct axons by providing either attractive or repulsive signals to growing axonal growth-cones (Kruger *et al.*, 2005). The discovery that Sema4F was performing a cell-adhesion function by mediating relatively stable interactions between Schwann cells and axons was a surprising finding as they have not typically been reported in the literature as functioning as a CAM.

In the current work, I showed, consistent with Parrinello *et al.*, (2008)'s study, that depletion of Sema4F from Schwann cells was sufficient to disrupt axonal association and alignment to a similar extent to that observed in N-cadherin depleted Schwann cell/DRG-axon cocultures. Moreover, the action of both N-cadherin and Sema4F appeared to be mutually exclusive in that loss of both alone resulted in a similar degree of interaction impairment, while combined loss of N-cadherin and Sema4F resulted in an additive increase in phenotypic severity. This suggested that both molecules were mediating distinct parts of the interaction. As previously discussed, N-cadherin mediates the recognition of axons by Schwann cells; however, a proportion of N-cadherin depleted cells are able to associate, presumably through compensatory mechanisms, and these Schwann cell/axonal associations are generally maintained. On the other hand, depletion of Sema4F did not affect recognition as Schwann cells were still capable of grasping axons with their cytoplasmic protrusions. However, as with the Ras-activated Schwann cells, Sema4F depleted Schwann cells were prone to spontaneous dissociation from axons. Together, these

findings suggested that while N-cadherin mediates contact recognition between Schwann cells and axons, Sema4F is likely to be involved in stabilising early heterotypic interactions rather than mediating recognition. Importantly, Sema4F was not compensating by fulfilling the same functional role as N-cadherin, i.e. in axonal recognition at cell protrusions. Rather, Sema4F had a distinct role in stabilising the interaction, while N-cadherin had a distinct role at cytoplasmic protrusions to mediate recognition. In the absence of studies to determine the developmental expression of semaphorins in Schwann cells and axons, it still remains to be determined whether Sema4F plays a significant role in myelination and the homeostatic nerve; however, semaphorins are expressed in myelinated nerve (Spiegel *et al.*, 2006) and we have demonstrated that loss of Sema4F, following Ras/Raf/ERK signalling, initiates Schwann cell/axonal dissociation in NF1 patients - implicating its involvement in the stability of homeostatic nerve (Parrinello *et al.*, 2008).

A remaining question to address is whether N-cadherin and Sema4F are sufficient alone to mediate early Schwann cell/axonal interactions or whether other CAMs are needed. In the current work, I showed that combined loss of N-cadherin and Sema4F resulted in ca. 70% disruption in normal interactions, although approximately half of these double-knockdown Schwann cells were still associated (although not aligned). However, an important caveat for these experiments is that double siRNA knockdown transfections for N-cadherin and Sema4F may not result in the complete knockdown of both genes in Schwann cells. Thus, the reported 70% impairment might underplay the actual involvement of these CAMs. Nevertheless, when interactions were quantified for LTD (non-interacting) cells, the results show that over 95% of interactions were disrupted and, of these, 85% were found not associated with axons. Thus, while both N-cadherin and Sema4F are clearly the main mediators of early Schwann cell/axonal interactions, there are likely to be other CAMs which are compensating for their loss in the double knockdown condition. Given this, future studies should consider the role of additional CAMs in mediating Schwann cell/axonal interactions (discussed in the next section). In addition, in light of the caveat discussed earlier, it would be advantageous to study N-cadherin and Sema4F using Schwann cells derived from mouse knockout models where depletion of both N-cadherin and Sema4F can be guaranteed. In terms of the former, Lewallen

et al. (2011) have since developed a Schwann cell specific N-cadherin knockout mouse; however, to our knowledge, a Sema4F Schwann cell knockout has not been developed. Another useful tool would be to develop a Sema4F antibody, which would allow confirmation of Sema4F knockdown at the protein level, as well as provide clarity on its cellular localisation.

6.5.3 Identifying CAMs as mediators of heterotypic interaction

In Chapter Three, I described a microarray experiment to analyse expression changes between LT interacting Schwann cells (LTNS) and LT non-interacting Schwann cells (LTD). One important finding from this work was that a large group of CAMs had become dysregulated, including N-cadherin and Sema4F, both of which were investigated in this thesis. In order to examine these results further, I sought to validate my approach by cross-referencing my data with data from a screen conducted by Spiegel *et al.*, (2006), who used a signal-sequence-trap (SST) technique in order to identify the repertoire of CAMs expressed by axons and differentiated (myelinated) Schwann cells. In this pioneering work, the authors screened for mRNA that contained the eukaryotic cell-surface localisation signal, which encodes a short amino-terminal hydrophobic peptide thought to direct the transport of proteins towards the cell surface for membrane tethering or secretion. The authors obtained RNA from differentiated Schwann cells, which had been treated with the cAMP analogue dibutyryl cAMP (dbcAMP), and from rat sciatic nerve, and thus does not directly examine mediators of early Schwann cell/axonal interaction. There were some caveats to this work as discussed by the authors, for instance the SST method is less reliable at detecting some extracellular proteins, for example tetra-spanning transmembrane proteins. Nonetheless, the study expanded the number of putative candidates for Schwann cell/axonal interactions; for example, data from this study led the authors to identify the nectin-like (Necl/SynCAM) proteins, in which they and others later found that axonal expressed Necl-1 and Schwann cell expressed Necl-4 were essential mediators of Schwann cell/axonal interaction that were required for myelination (Maurel *et al.*, 2007; Spiegel *et al.*, 2007). In their SST screen, Spiegel *et al.* (2006) identified 159 cDNA clones corresponding to cell-surface expressed molecules, of which 36% were expressed exclusively in Schwann cells and 46% in sciatic nerve, while 18% were expressed by

both Schwann cells and axon. The study revealed a number of functional groups including genes involved in cell adhesion, extracellular matrix, receptor signalling, growth and differentiation, endoplasmic reticulum (ER), golgi and ectoenzymes. The two main groups of CAMs identified included tetraspanin proteins, for example PMP-22, Claudin-19, and the IgCAMs, for example MPZ/P0, MAG, neurofascin and nrCAM.

As this study provides an authoritative list of CAMs in myelinated Schwann cells, I decided to examine their findings in the context of my LT microarray data (described in Chapter Three). In particular I wanted to examine adhesion genes down-regulated in LTD cells as this implies that they are normally expressed by interacting Schwann cells. Prior to performing the analysis, I re-annotated the gene list from the CAM Table published by Spiegel *et al.* (2006), using DAVID (as described) in order to ensure that both datasets were using the most recent gene annotations. This process inevitably led to the removal of some genes (see Table 6.1 legend for full details). I then cross-referenced the Spiegel *et al.* (2006) CAM list with the significant gene list from the LT microarray (**Dataset E**) and presented the corresponding genes present in both studies (yellow highlight indicates correspondence) (**Table 6.1**).

Table 6.1 A comparison of CAMs identified in the Speigel et al., (2006) study against dysregulated genes in the LT microarray

Official Gene Name/Description	LT Array fold-change	FDR
CD24 molecule	n.s.	
CD34 molecule	-	
CD164 molecule, sialomucin	n.s.	
Endoglin	n.s.	
similar to cDNA sequence BC013529	n.s.	
similar to HTGN29 protein	n.s.	
syndecan 2	n.s.	
syndecan 3	n.s.	
syndecan 4	n.s.	
Cd63 molecule	n.s.	
Cd81 molecule	n.s.	
Cd82 molecule	n.s.	
claudin 19	-2.7890	0.00343
epithelial membrane protein 1	n.s.	
peripheral myelin protein 22	-140.8386	0.00050
Cd44 molecule	n.s.	
CD97 molecule	n.s.	

glycoprotein (transmembrane) nmb/Osteoactivin	6.0693	0.00579
[Obsolete Record 'similar to AU040320 (PKDI-like)]	-	
myelin protein zero	-189.8566	0.00112
inducible T-cell co-stimulator ligand	-	
Basigin	n.s.	
[obsolete record 'Zig-1']	-	
Neurotrimin	n.s.	
interleukin 1 receptor accessory protein	-3.8390	0.00195
cell adhesion molecule 3/Necl-1	n.s.	
cell adhesion molecule 1/Necl-2	2.2333	0.01138
cell adhesion molecule 4/Necl-4*	-10.6866	0.00073
myelin-associated glycoprotein	n.s.	
activated leukocyte cell adhesion molecule	n.s.	
melanoma cell adhesion molecule	-17.2076	0.00122
neuronal cell adhesion molecule	16.8809	0.00196
Neurofascin	n.s.	
DiGeorge syndrome critical region gene 2*	n.s.	
FXYD domain-containing ion transport regulator 5	-3.8938	0.00142
integrin alpha 7	4.1901	0.00573
integrin beta 8	-	
low density lipoprotein-related protein 12	n.s.	
milk fat globule-EGF factor 8 protein	n.s.	
cadherin 2/N-cadherin	-9.1274	0.00060
neuropilin 2	n.s.	
Notch homolog 2 (Drosophila)	n.s.	
olfactomedin-like 2B	-2.1604	0.05719
sema domain, immunoglobulin domain (Ig), short basic domain, secreted, (semaphorin) 3B	-8.4867	0.00221
sema domain, transmembrane domain (TM), and cytoplasmic domain, (semaphorin) 6D	-26.7105	0.00590
phosphoinositide-3-kinase interacting protein 1	-2.2706	0.03686
pituitary tumor-transforming 1 interacting protein	n.s.	
plexin domain containing 2	n.s.	
amyloid beta (A4) precursor protein	-6.4600	0.00100
Vasorin	n.s.	
delta-like 1 homolog (Drosophila)	n.s.	

Table of analysis: cross-referencing data from Spiegel *et al.*, (2006) study to the current microarray findings. Validating genes are highlighted in yellow. For completeness, the stringency of the FDR (false-discovery rate) has been lowered to 0.1 (the FDR for each gene is stated next to the Fold-Change value). (-): not-present (the gene was not included in the probesets for the Rat230-2 array; NS: not-significant (the gene was not significantly detected). [] denote genes from the Spiegel study which no longer have valid Entrez Ids and * denotes genes derived from ESTs (from the Spiegel *et al.*, (2006) study) with GenBank accession numbers that have since become obsolete or rescinded - however, they are included in the analysis for completeness.

This analysis showed that of the 51 CAMs identified in Spiegel *et al.*, (2006)'s SST screen as being expressed by myelinating Schwann cells and axons, 17 CAMs (33%) were also found to be significantly dysregulated in LTD cells. These include, N-

cadherin/cadherin-2, Sema3B, Sema6D, melanoma (m)CAM, nrCAM and Necl4/cell adhesion molecule-4 as well as a number of myelin genes: MPZ, PMP-22 and claudin-19. These findings validate the methodology and approach adopted in this thesis for identifying adhesion molecules, normally expressed by Schwann cells, that are also important for mediating Schwann cell/axonal interactions. Interestingly, while a number of semaphorins and their receptors, i.e. plexin and neuropilin-2, were identified, Sema4F was not detected in the SST screen. A significant finding from the SST screen was the asymmetric expression of Necl proteins between Schwann cells and axons, which led to the subsequent identification of this group of CAMs as mediators of Schwann cell/axonal interactions (Maurel *et al.*, 2007; Spiegel *et al.*, 2007). These studies showed that Schwann cell-expressed Necl-4 (cell adhesion molecule-4) and axonal-expressed Necl-1 (cell adhesion molecule-3), were important mediators of heterotypic Schwann cell/axonal interactions in myelinated nerves. Moreover, this interaction was required for myelination. Consistent with their findings, the LT microarray data indicate that Necl-4 was down-regulated 10-fold in LTD non-interacting cells. Therefore, Necl-4 (and other Necl members) are promising candidates for further study in relation to early mediators of Schwann cell/axonal interaction. It would also be interesting to investigate the function of mCAM, which has been shown to bind the ECM component laminin-411 (Flanagan *et al.*, 2012) as well as nrCAM, which is involved in Sodium channel clustering at the Node of Ranvier (Feinberg *et al.*, 2010).

In addition to CAMs validated by the SST screen, there were also a number of dysregulated CAMs in LTD cells that were not discovered by the SST screen, many of which have not previously been associated with Schwann cell/axonal interactions. These include a number of cadherins, for example cadherin-6 and cadherin-15, as well as protocadherins $\alpha 4$, $\alpha 7$ and $\alpha 21$. There were also two atypical flamingo-like cadherins identified (Celsr1/flamingo homolog-1 and Celsr2), which are seven-pass transmembrane adhesion proteins (Hadjantonakis *et al.*, 1997). Another interesting discovery was the identification of ninjurin 1 (down-regulated 3-fold in LTD cells), which has recently been implicated in leprosy (Graca *et al.*, 2012) - a disease whose aetiology is linked to Schwann cells. CD9 (down-regulated 2-fold in LTD cells) - a tetraspanin adhesion molecule - was also identified and has previously been shown to interact with various integrins, and moreover is expressed by denervated Schwann

cells in regenerating nerve (Cavalcanti *et al.*, 2009). Finally, two genes which were substantially down-regulated in LTD cells were periostin (osteoblast specific factor) (down-regulated 88-fold in LTD cells) and fibulin 5 (down-regulated 74-fold in LTD cells). Fibulin-5 is an extracellular glycoprotein, involved in the regulation of the ECM and is part of large number of ECM related genes dysregulated in LTD cells (functional cluster analysis showed that ECM genes were the second most dysregulated functional group after cell adhesion). Periostin is a secreted molecule that interacts with Wnt ligands to elevate Wnt signalling. Interestingly, a recent study has discovered an important role for the wnt/ β -catenin signalling pathway in Schwann cell myelination, with inhibition of the pathway leading to hypomyelinated nerves (Tawk *et al.*, 2011).

In terms of investigating these genes further in relation to early mediators of Schwann cell axonal interaction, it would be interesting to determine if any of these genes were acting with N-cadherin and Sema4F to mediate early interactions. Further studies could aim to clarify their role by adopting the siRNA approach and DRG association assay described in this thesis. In addition to this, future studies should also examine further the role played by transcription factors. In terms of the interaction defect exhibited by LTD cells, findings from this thesis suggest that Sox2 is most likely not responsible for the axonal interaction deficiency. However, dysregulation of transcription factors in LTD cells remains a plausible explanation as to how LTD cells possess an aberrant adhesion gene profile that is not permissive for axonal recognition and association. Future studies should attempt to identify the defective regulator in LTD cells by considering the other 54 genes dysregulated in LTD (refer to **Table 3.5**), which have a function in transcriptional regulation. Possible regulators could be selected for further study following analysis of transcription factor binding sites on genes involved in adhesion. However, one obvious example is Sox10, which was down-regulated 24-fold in LTD cells and is an important regulator of many aspects of Schwann cell biology. A role for Sox10 could be tested using an adenovirus expression system in order to drive Sox10 expression in LTD cells. DRG association assays could then be employed to determine if Sox10 re-expression could revert the LTD interaction impairment.

6.6 N-cadherin and stable Schwann cell/axonal interactions: polarisation and myelination

I have previously described a model for the various processes involved in Schwann cell/axonal interactions. Early interactions include recognition, association and alignment, where I have shown that N-cadherin mediates contact-recognition and is an important early mediator of association and alignment. Maturing interactions involve elongation, i.e. growth, and cellular polarisation, while later stable interactions are embodied by the differentiation of Schwann cells, the concentric wrapping of the axon by the Schwann cell and lastly the myelination of the axonal fibre. Previous studies have shown that N-cadherin is asymmetrically localised in Schwann cells during the radial polarisation of the nerve fibre, where N-cadherin was found colocalised with the Par-3 protein along the adaxonal (inner) Schwann cell membrane which interfaces the axon (Chan *et al.*, 2006; Lewallen *et al.*, 2011). Several studies have also shown that N-cadherin expression persists in the nerve up until myelination (Crawford *et al.*, 2008; Wanner *et al.*, 2006a). Moreover, N-cadherin, as well as other CAMs including NCAM, are re-expressed in denervated Schwann cells (Thornton *et al.*, 2005; Zelano *et al.*, 2006) and expression of N-cadherin during re-association and re-myelination is likely to mirror its role in development. Thus, collectively, there is a compelling case for the involvement of N-cadherin in all parts of the interaction programme.

Myelination is the culmination of a multi-step process of Schwann cell axonal interactions that includes polarisation but which is initiated by Schwann cell/axonal recognition. In terms of polarisation, a role for N-cadherin has previously been investigated. The aforementioned study by Chan *et al.* (2006) demonstrated the importance for the correct localisation of Par-3, which they found was required to enrich the adaxonal (axon-facing) membrane of the Schwann cell with the p75 neurotrophin receptor (p75^{NTR}), for which ligand-binding by BDNF is required for myelination (Chan *et al.*, 2001). Consistent with BDNF's function, they showed that disrupted Par-3 and therefore p75^{NTR} localisation inhibited myelination; however, importantly for the current thesis, they also observed that N-cadherin was colocalised with Par-3 along the longitudinal axis of the axo-glial interface. This was consistent with my findings, where I similarly found N-cadherin to be asymmetrically localised

at the Schwann cell/axonal interface of pre-myelinating cocultures. This raises the intriguing question as to whether N-cadherin was involved in Schwann cell/axonal polarisation. For instance, if homophilic N-cadherin ligation is required for initial contact between Schwann cells and axons, then it is plausible that this initial interaction could provide the first cellular cue as to the spatial orientation of the Schwann cell membrane with respect to the axon.

A key question I attempted to address in the current thesis, was to what extent N-cadherin loss in Schwann cells, prior to associating with axons, would have on the later myelination of axons. For instance, does loss of Schwann cell/axonal recognition impair the efficiency of myelination? To address this, I used an shRNA system to generate stable Schwann cell-lines in which N-cadherin was substantially reduced. In subsequent myelination assays with shRNA-Schwann cell/DRG-axon cocultures, I found that N-cadherin depleted Schwann cells myelinated significantly less-efficiently than controls, which suggested that N-cadherin was required for normal myelination *in vitro*. However, these findings were contradicted in a recent study by Lewallen *et al.* (2011), who also used an shRNA system to stably deplete N-cadherin from Schwann cells. In this study, N-cadherin shRNA cells appeared to align to axons and myelinate normally. In addition, they used an N-cadherin lentivirus to introduce N-cadherin shRNA into axons and, following coculture with normal Schwann cells, found that axonal N-cadherin depletion did not affect Par-3 localisation or myelination. While their results appear to suggest that N-cadherin was not required for polarisation or myelination, they did report, in shRNA experiments, that myelination was delayed in N-cadherin deficient Schwann cells. For instance, 10-day old myelinating N-cadherin shRNA Schwann cell/DRG cocultures exhibited a significant two-fold reduction in myelination compared to control cocultures. However, by day-15 this difference was no longer significant. Therefore, they concluded that the onset of myelination was delayed by at least five days in N-cadherin deficient Schwann cell/DRG cocultures *in vitro*.

There are several reasons that might explain the discrepancy between the shRNA results from the current work (stated in Chapter Four) and the N-cadherin shRNA/myelinating study conducted by (Lewallen *et al.*, 2011). First, the age at which the myelinating cocultures were fixed differed slightly and, moreover the

culture systems and conditions adopted between the studies were also different. For example, the study by Lewallen *et al.* (2011) used embryonic (E15) dissociated DRG cultures, while in the current thesis, I used postnatal (P1) explanted DRG cultures. These discrepancies may have impinged on the timing of myelination in the respective coculture systems. As discussed, in the Lewallen *et al.* (2011) paper, an important finding was that Schwann cell N-cadherin-loss was associated with the delayed-onset to myelination, with day-10 cocultures myelinating less-efficiently when compared to equivalent day-10 controls. In this study, cocultures were fixed at day-10 and day-15, while in the current study cocultures were fixed at day-14. Therefore, one explanation for this discrepancy could have been in the choice of time-points used in the respective studies, i.e. the time at which the cocultures were fixed and myelination assayed. Thus, in the current work, in which N-cadherin loss was shown to impair myelination, this might be mirroring the delayed myelination observed in the earlier day-10 cocultures of the Lewallen *et al.* (2011) study. Second, in the current study, although unlikely, it is possible that the selected shRNA N-cadherin Schwann cell line had unforeseen off-target effects not related to N-cadherin knockdown. Ideally, to control for this possibility, several shRNA cell lines should be incorporated into the experimental design; however, while three independent N-cadherin shRNA cell lines were developed, only one of these was found to reliably and efficiently knockdown N-cadherin (as discussed in Chapter Four) and thus, only one shRNA cell line was amenable for use in our myelination assay.

In addition to their *in vitro* investigations, the authors of the Lewallen *et al.* (2011) study also developed two separate mouse models to investigate N-cadherin in polarisation and myelination. The first model was a Schwann cell specific N-cadherin knockout, which was generated by introducing loxP sites that flanked the first intron of the N-cadherin gene. These mice were then crossed with *cre* (recombinase) mouse transgenics, in which *cre* expression was driven by the *Dhh* promoter. As *Dhh* expression is induced at the transition from neural crest to SCPs at about E10-11 (in rodent) (Jessen & Mirsky, 2005), all subsequent Schwann cell lineage progeny up to and including mature adult Schwann cells should carry the ablated N-cadherin gene. The data from these studies were found to replicate the previous *in vitro* shRNA analysis, in that myelination was delayed but overall was

unaffected. The second mouse model was a Schwann cell specific β -catenin knockout generated from loxP sites that flanked intron 2 to intron 6 of the β -catenin gene. These mice were similarly crossed with *cre* transgenics under the regulatory control of *Dhh*. In these mice the delay to myelination was greater than with N-cadherin ablation alone suggesting that β -catenin was compensating for N-cadherin loss although normal myelination was eventually achieved. Taken together, it is likely that N-cadherin is important for the timing of myelination but is not required for myelination. This suggests that while N-cadherin mediates contact recognition for axons, there are likely to be additional compensatory CAMs, for instance, Sema4F, that given sufficient time will allow Schwann cells to eventually associate with axons and achieve normal myelination.

6.8 Conclusion

The establishment of the complex, three-dimensional tissue architecture of the peripheral nerve, is critically dependent on cell-cell interactions mediated by the correct repertoire of cell-surface expressed CAMs. These adhesion molecules are required for early neural development, for instance directing processes of cell migration, cell-sorting and Schwann cell/axonal interactions, and are also later required for tissue homeostasis in the functional adult nerve, where they maintain stable Schwann cell/axonal associations. In addition, CAMs play pivotal roles during injury, in allowing the dissociation and re-association of Schwann cells with axons, which is fundamental to the repair process. Dysregulation of cellular signalling pathways - and resulting aberrant expression of CAMs - has significant implications for otherwise stable, Schwann cell/axonal associations, which is demonstrated by the phenotypic severity of de-myelinating inherited neuropathies and nerve sheath tumours, for example neurofibroma. In this thesis, I have highlighted a number of CAMs that play important roles in these processes, including N-cadherin and semaphorin-4F. Understanding how these, and other CAMs, interact will have implications for our understanding of neuropathies and tumours, and may yield insights into enhancing regenerative outcomes following nerve injury. Further work should continue to decipher the complexities of the reciprocal relationship between Schwann cells and axons, in order to truly understand their role in human health and disease.

References

- Aboussekhra, A. 2011. Role of cancer-associated fibroblasts in breast cancer development and prognosis. *The International journal of developmental biology*. 55:841-849.
- Adlkofer, K., Martini, R., Aguzzi, A., Zielasek, J., Toyka, K.V., and Suter, U. 1995. Hypermyelination and demyelinating peripheral neuropathy in Pmp22-deficient mice. *Nature genetics*. 11:274-280.
- Alanne, M.H., Pummi, K., Heape, A.M., Grenman, R., Peltonen, J., and Peltonen, S. 2009. Tight junction proteins in human Schwann cell autotypic junctions. *The journal of histochemistry and cytochemistry : official journal of the Histochemistry Society*. 57:523-529.
- Alberts, B., Jhonson, A., Lewis, J., Raff, M., Roberts, K., and Walter, P. 2008. *Molecular Biology of the Cell: Reference Edition, Volume 1*. Garland Science.
- Araki, T., Sasaki, Y., and Milbrandt, J. 2004. Increased nuclear NAD biosynthesis and SIRT1 activation prevent axonal degeneration. *Science*. 305:1010-1013.
- Armati, P.J. 2007. *The Biology of Schwann Cells: Development, Differentiation And Immunomodulation*. Cambridge University Press.
- Arthur-Farraj, P., Wanek, K., Hantke, J., Davis, C.M., Jayakar, A., Parkinson, D.B., Mirsky, R., and Jessen, K.R. 2011. Mouse schwann cells need both NRG1 and cyclic AMP to myelinate. *Glia*. 59:720-733.
- Avery, M.A., Sheehan, A.E., Kerr, K.S., Wang, J., and Freeman, M.R. 2009. Wld S requires Nmnat1 enzymatic activity and N16-VCP interactions to suppress Wallerian degeneration. *The Journal of cell biology*. 184:501-513.
- Bader, J.L. 1986. Neurofibromatosis and cancer. *Annals of the New York Academy of Sciences*. 486:57-65.
- Baer, K., Eriksson, P.S., Faull, R.L., Rees, M.I., and Curtis, M.A. 2007. Sox-2 is expressed by glial and progenitor cells and Pax-6 is expressed by neuroblasts in the human subventricular zone. *Experimental neurology*. 204:828-831.
- Balice-Gordon, R.J., Bone, L.J., and Scherer, S.S. 1998. Functional gap junctions in the schwann cell myelin sheath. *The Journal of cell biology*. 142:1095-1104.
- Ballester, R., Marchuk, D., Boguski, M., Saulino, A., Letcher, R., Wigler, M., and Collins, F. 1990. The NF1 locus encodes a protein functionally related to mammalian GAP and yeast IRA proteins. *Cell*. 63:851-859.
- Bard, L., Boscher, C., Lambert, M., Mege, R.M., Choquet, D., and Thoumine, O. 2008. A molecular clutch between the actin flow and N-cadherin adhesions drives growth cone migration. *The Journal of neuroscience : the official journal of the Society for Neuroscience*. 28:5879-5890.
- Baser, M.E., De Rienzo, A., Altomare, D., Balsara, B.R., Hedrick, N.M., Gutmann, D.H., Pitts, L.H., Jackler, R.K., and Testa, J.R. 2002. Neurofibromatosis 2 and malignant mesothelioma. *Neurology*. 59:290-291.
- Bayas, M.V., Leung, A., Evans, E., and Leckband, D. 2006. Lifetime measurements reveal kinetic differences between homophilic cadherin bonds. *Biophysical journal*. 90:1385-1395.
- Begnami, M.D., Rushing, E.J., Santi, M., and Quezado, M. 2007. Evaluation of NF2 gene deletion in pediatric meningiomas using chromogenic in situ hybridization. *International journal of surgical pathology*. 15:110-115.
- Benfey, M., and Aguayo, A.J. 1982. Extensive elongation of axons from rat brain into peripheral nerve grafts. *Nature*. 296:150-152.

- Benson, D.L., and Tanaka, H. 1998. N-cadherin redistribution during synaptogenesis in hippocampal neurons. *The Journal of neuroscience : the official journal of the Society for Neuroscience*. 18:6892-6904.
- Bermingham, J.R., Jr., Scherer, S.S., O'Connell, S., Arroyo, E., Kalla, K.A., Powell, F.L., and Rosenfeld, M.G. 1996. Tst-1/Oct-6/SCIP regulates a unique step in peripheral myelination and is required for normal respiration. *Genes & development*. 10:1751-1762.
- Bhat, M.A., Rios, J.C., Lu, Y., Garcia-Fresco, G.P., Ching, W., St Martin, M., Li, J., Einheber, S., Chesler, M., Rosenbluth, J., Salzer, J.L., and Bellen, H.J. 2001. Axon-glia interactions and the domain organization of myelinated axons requires neurexin IV/Caspr/Paranodin. *Neuron*. 30:369-383.
- Birchmeier, C., and Nave, K.A. 2008. Neuregulin-1, a key axonal signal that drives Schwann cell growth and differentiation. *Glia*. 56:1491-1497.
- Boyle, M.E., Berglund, E.O., Murai, K.K., Weber, L., Peles, E., and Ranscht, B. 2001. Contactin orchestrates assembly of the septate-like junctions at the paranode in myelinated peripheral nerve. *Neuron*. 30:385-397.
- Brannan, C.I., Perkins, A.S., Vogel, K.S., Ratner, N., Nordlund, M.L., Reid, S.W., Buchberg, A.M., Jenkins, N.A., Parada, L.F., and Copeland, N.G. 1994. Targeted disruption of the neurofibromatosis type-1 gene leads to developmental abnormalities in heart and various neural crest-derived tissues. *Genes & development*. 8:1019-1029.
- Britsch, S., Goerich, D.E., Riethmacher, D., Peirano, R.I., Rossner, M., Nave, K.A., Birchmeier, C., and Wegner, M. 2001. The transcription factor Sox10 is a key regulator of peripheral glial development. *Genes & development*. 15:66-78.
- Brummendorf, T., and Rathjen, F.G. 1995. Cell adhesion molecules 1: immunoglobulin superfamily. *Protein profile*. 2:963-1108.
- Bryne, J.H.e. 1997. Neuroscience Online: An Electronic Textbook for the Neurosciences. In <http://nba.uth.tmc.edu/neuroscience>. Department of Neurobiology and Anatomy, The University of Texas Medical School at Houston (UTHealth).
- Bunge, R.P., Bunge, M.B., and Eldridge, C.F. 1986. Linkage between axonal ensheathment and basal lamina production by Schwann cells. *Annual review of neuroscience*. 9:305-328.
- Carenini, S., Montag, D., Cremer, H., Schachner, M., and Martini, R. 1997. Absence of the myelin-associated glycoprotein (MAG) and the neural cell adhesion molecule (N-CAM) interferes with the maintenance, but not with the formation of peripheral myelin. *Cell and tissue research*. 287:3-9.
- Carroll, S.L., and Ratner, N. 2008. How does the Schwann cell lineage form tumors in NF1? *Glia*. 56:1590-1605.
- Cavalcanti, F., Kidd, T., Patitucci, A., Valentino, P., Bono, F., Nistico, R., and Quattrone, A. 2009. An axon regeneration signature in a Charcot-Marie-Tooth disease type 2 patient. *Journal of neurogenetics*. 23:324-328.
- Chambers, I., and Tomlinson, S.R. 2009. The transcriptional foundation of pluripotency. *Development*. 136:2311-2322.
- Chan, J.R., Cosgaya, J.M., Wu, Y.J., and Shooter, E.M. 2001. Neurotrophins are key mediators of the myelination program in the peripheral nervous system. *Proceedings of the National Academy of Sciences of the United States of America*. 98:14661-14668.

- Chan, J.R., Jolicoeur, C., Yamauchi, J., Elliott, J., Fawcett, J.P., Ng, B.K., and Cayouette, M. 2006. The polarity protein Par-3 directly interacts with p75NTR to regulate myelination. *Science*. 314:832-836.
- Chandross, K.J., Kessler, J.A., Cohen, R.I., Simburger, E., Spray, D.C., Bieri, P., and Dermietzel, R. 1996. Altered connexin expression after peripheral nerve injury. *Molecular and cellular neurosciences*. 7:501-518.
- Chen, J.J., Roberson, P.K., and Schell, M.J. 2010. The false discovery rate: a key concept in large-scale genetic studies. *Cancer control : journal of the Moffitt Cancer Center*. 17:58-62.
- Chen, S., Velardez, M.O., Warot, X., Yu, Z.X., Miller, S.J., Cros, D., and Corfas, G. 2006. Neuregulin 1-erbB signaling is necessary for normal myelination and sensory function. *The Journal of neuroscience : the official journal of the Society for Neuroscience*. 26:3079-3086.
- Chen, Z.L., Yu, W.M., and Strickland, S. 2007. Peripheral regeneration. *Annual review of neuroscience*. 30:209-233.
- Cheng, L., Khan, M., and Mudge, A.W. 1995. Calcitonin gene-related peptide promotes Schwann cell proliferation. *The Journal of cell biology*. 129:789-796.
- Chernousov, M.A., Rothblum, K., Stahl, R.C., Evans, A., Prentiss, L., and Carey, D.J. 2006. Glypican-1 and alpha4(V) collagen are required for Schwann cell myelination. *The Journal of neuroscience : the official journal of the Society for Neuroscience*. 26:508-517.
- Chernousov, M.A., Yu, W.M., Chen, Z.L., Carey, D.J., and Strickland, S. 2008. Regulation of Schwann cell function by the extracellular matrix. *Glia*. 56:1498-1507.
- Choi, Y.K., and Kim, K.W. 2008. Blood-neural barrier: its diversity and coordinated cell-to-cell communication. *BMB reports*. 41:345-352.
- Coleman, M.P., and Freeman, M.R. 2010. Wallerian degeneration, wld(s), and nmnat. *Annual review of neuroscience*. 33:245-267.
- Corfas, G., Velardez, M.O., Ko, C.P., Ratner, N., and Peles, E. 2004. Mechanisms and roles of axon-Schwann cell interactions. *The Journal of neuroscience : the official journal of the Society for Neuroscience*. 24:9250-9260.
- Cornejo, M., Nambi, D., Walheim, C., Somerville, M., Walker, J., Kim, L., Ollison, L., Diamante, G., Vyawahare, S., and de Bellard, M.E. 2010. Effect of NRG1, GDNF, EGF and NGF in the migration of a Schwann cell precursor line. *Neurochemical research*. 35:1643-1651.
- Court, F.A., Sherman, D.L., Pratt, T., Garry, E.M., Ribchester, R.R., Cottrell, D.F., Fleetwood-Walker, S.M., and Brophy, P.J. 2004. Restricted growth of Schwann cells lacking Cajal bands slows conduction in myelinated nerves. *Nature*. 431:191-195.
- Court, F.A., Wrabetz, L., and Feltri, M.L. 2006. Basal lamina: Schwann cells wrap to the rhythm of space-time. *Current opinion in neurobiology*. 16:501-507.
- Crawford, A.T., Desai, D., Gokina, P., Basak, S., and Kim, H.A. 2008. E-cadherin expression in postnatal Schwann cells is regulated by the cAMP-dependent protein kinase a pathway. *Glia*. 56:1637-1647.
- Cremona, C.A., and Lloyd, A.C. 2009. Loss of anchorage in checkpoint-deficient cells increases genomic instability and promotes oncogenic transformation. *Journal of cell science*. 122:3272-3281.

- Crossin, K.L., and Krushel, L.A. 2000. Cellular signaling by neural cell adhesion molecules of the immunoglobulin superfamily. *Developmental dynamics : an official publication of the American Association of Anatomists*. 218:260-279.
- Cui, X., and Churchill, G.A. 2003. Statistical tests for differential expression in cDNA microarray experiments. *Genome biology*. 4:210.
- Cui, X., and Loraine, A.E. 2009. Consistency analysis of redundant probe sets on affymetrix three-prime expression arrays and applications to differential mRNA processing. *PloS one*. 4:e4229.
- Curto, M., Cole, B.K., Lallemand, D., Liu, C.H., and McClatchey, A.I. 2007. Contact-dependent inhibition of EGFR signaling by Nf2/Merlin. *The Journal of cell biology*. 177:893-903.
- Curto, M., and McClatchey, A.I. 2008. Nf2/Merlin: a coordinator of receptor signalling and intercellular contact. *British journal of cancer*. 98:256-262.
- Dahme, M., Bartsch, U., Martini, R., Anliker, B., Schachner, M., and Mantei, N. 1997. Disruption of the mouse L1 gene leads to malformations of the nervous system. *Nature genetics*. 17:346-349.
- Davies, A.M. 1998. Neuronal survival: early dependence on Schwann cells. *Current biology : CB*. 8:R15-18.
- Davis, J.Q., Lambert, S., and Bennett, V. 1996. Molecular composition of the node of Ranvier: identification of ankyrin-binding cell adhesion molecules neurofascin (mucin+/third FNIII domain-) and NrCAM at nodal axon segments. *The Journal of cell biology*. 135:1355-1367.
- Davis, M.A., Ireton, R.C., and Reynolds, A.B. 2003. A core function for p120-catenin in cadherin turnover. *The Journal of cell biology*. 163:525-534.
- Decker, L., Desmarquet-Trin-Dinh, C., Taillebourg, E., Ghislain, J., Vallat, J.M., and Charnay, P. 2006. Peripheral myelin maintenance is a dynamic process requiring constant Krox20 expression. *The Journal of neuroscience : the official journal of the Society for Neuroscience*. 26:9771-9779.
- Denisenko, N., Cifuentes-Diaz, C., Irinopoulou, T., Carnaud, M., Benoit, E., Niwa-Kawakita, M., Chareyre, F., Giovannini, M., Girault, J.A., and Goutebroze, L. 2008. Tumor suppressor schwannomin/merlin is critical for the organization of Schwann cell contacts in peripheral nerves. *The Journal of neuroscience : the official journal of the Society for Neuroscience*. 28:10472-10481.
- Derycke, L.D., and Bracke, M.E. 2004. N-cadherin in the spotlight of cell-cell adhesion, differentiation, embryogenesis, invasion and signalling. *The International journal of developmental biology*. 48:463-476.
- Di Lullo, G.A., Sweeney, S.M., Korkko, J., Ala-Kokko, L., and San Antonio, J.D. 2002. Mapping the ligand-binding sites and disease-associated mutations on the most abundant protein in the human, type I collagen. *The Journal of biological chemistry*. 277:4223-4231.
- Doherty, J., and Freund, R. 1997. Polyomavirus large T antigen overcomes p53 dependent growth arrest. *Oncogene*. 14:1923-1931.
- Doherty, P., Williams, G., and Williams, E.J. 2000. CAMs and axonal growth: a critical evaluation of the role of calcium and the MAPK cascade. *Molecular and cellular neurosciences*. 16:283-295.
- Dong, Z., Brennan, A., Liu, N., Yarden, Y., Lefkowitz, G., Mirsky, R., and Jessen, K.R. 1995. Neu differentiation factor is a neuron-glia signal and regulates survival, proliferation, and maturation of rat Schwann cell precursors. *Neuron*. 15:585-596.

- Dor, Y., Brown, J., Martinez, O.I., and Melton, D.A. 2004. Adult pancreatic beta-cells are formed by self-duplication rather than stem-cell differentiation. *Nature*. 429:41-46.
- Dowsing, B.J., Morrison, W.A., Nicola, N.A., Starkey, G.P., Bucci, T., and Kilpatrick, T.J. 1999. Leukemia inhibitory factor is an autocrine survival factor for Schwann cells. *Journal of neurochemistry*. 73:96-104.
- Drees, F., Pokutta, S., Yamada, S., Nelson, W.J., and Weis, W.I. 2005. Alpha-catenin is a molecular switch that binds E-cadherin-beta-catenin and regulates actin-filament assembly. *Cell*. 123:903-915.
- Dreesmann, L., Mittnacht, U., Lietz, M., and Schlosshauer, B. 2009. Nerve fibroblast impact on Schwann cell behavior. *European journal of cell biology*. 88:285-300.
- Dupree, J.L., Girault, J.A., and Popko, B. 1999. Axo-glial interactions regulate the localization of axonal paranodal proteins. *The Journal of cell biology*. 147:1145-1152.
- Dyck, P.J., and Hopkins, A.P. 1972. Electron microscopic observations on degeneration and regeneration of unmyelinated fibres. *Brain : a journal of neurology*. 95:233-234.
- Eshed, Y., Feinberg, K., Poliak, S., Sabanay, H., Sarig-Nadir, O., Spiegel, I., Bermingham, J.R., Jr., and Peles, E. 2005. Gliomedin mediates Schwann cell-axon interaction and the molecular assembly of the nodes of Ranvier. *Neuron*. 47:215-229.
- Evans, D.G., Baser, M.E., McGaughan, J., Sharif, S., Howard, E., and Moran, A. 2002. Malignant peripheral nerve sheath tumours in neurofibromatosis 1. *Journal of medical genetics*. 39:311-314.
- Fairless, R., Frame, M.C., and Barnett, S.C. 2005. N-cadherin differentially determines Schwann cell and olfactory ensheathing cell adhesion and migration responses upon contact with astrocytes. *Molecular and cellular neurosciences*. 28:253-263.
- Fannon, A.M., Sherman, D.L., Ilyina-Gragerova, G., Brophy, P.J., Friedrich, V.L., Jr., and Colman, D.R. 1995. Novel E-cadherin-mediated adhesion in peripheral nerve: Schwann cell architecture is stabilized by autotypic adherens junctions. *The Journal of cell biology*. 129:189-202.
- Feinberg, K., Eshed-Eisenbach, Y., Frechter, S., Amor, V., Salomon, D., Sabanay, H., Dupree, J.L., Grumet, M., Brophy, P.J., Shrager, P., and Peles, E. 2010. A glial signal consisting of gliomedin and NrCAM clusters axonal Na⁺ channels during the formation of nodes of Ranvier. *Neuron*. 65:490-502.
- Feltri, M.L., Graus Porta, D., Previtali, S.C., Nodari, A., Migliavacca, B., Casseti, A., Littlewood-Evans, A., Reichardt, L.F., Messing, A., Quattrini, A., Mueller, U., and Wrabetz, L. 2002. Conditional disruption of beta 1 integrin in Schwann cells impedes interactions with axons. *The Journal of cell biology*. 156:199-209.
- Fernandez-Valle, C., Tang, Y., Ricard, J., Rodenas-Ruano, A., Taylor, A., Hackler, E., Biggerstaff, J., and Iacovelli, J. 2002. Paxillin binds schwannomin and regulates its density-dependent localization and effect on cell morphology. *Nature genetics*. 31:354-362.
- Filbin, M.T. 2003. Myelin-associated inhibitors of axonal regeneration in the adult mammalian CNS. *Nature reviews. Neuroscience*. 4:703-713.
- Finzsch, M., Schreiner, S., Kichko, T., Reeh, P., Tamm, E.R., Bosl, M.R., Meijer, D., and Wegner, M. 2010. Sox10 is required for Schwann cell identity and

- progression beyond the immature Schwann cell stage. *The Journal of cell biology*. 189:701-712.
- Flanagan, K., Fitzgerald, K., Baker, J., Regnstrom, K., Gardai, S., Bard, F., Mocchi, S., Seto, P., You, M., Larochelle, C., Prat, A., Chow, S., Li, L., Vandever, C., Zago, W., Lorenzana, C., Nishioka, C., Hoffman, J., Botelho, R., Willits, C., Tanaka, K., Johnston, J., and Yednock, T. 2012. Laminin-411 is a vascular ligand for MCAM and facilitates TH17 cell entry into the CNS. *PLoS one*. 7:e40443.
- Fraenzer, J.T., Pan, H., Minimo, L., Jr., Smith, G.M., Knauer, D., and Hung, G. 2003. Overexpression of the NF2 gene inhibits schwannoma cell proliferation through promoting PDGFR degradation. *International journal of oncology*. 23:1493-1500.
- Garbay, B., Heape, A.M., Sargueil, F., and Cassagne, C. 2000. Myelin synthesis in the peripheral nervous system. *Progress in neurobiology*. 61:267-304.
- Garratt, A.N., Britsch, S., and Birchmeier, C. 2000. Neuregulin, a factor with many functions in the life of a schwann cell. *BioEssays : news and reviews in molecular, cellular and developmental biology*. 22:987-996.
- Gates, J., and Peifer, M. 2005. Can 1000 reviews be wrong? Actin, alpha-Catenin, and adherens junctions. *Cell*. 123:769-772.
- Gavard, J., Lambert, M., Grosheva, I., Marthiens, V., Irinopoulou, T., Riou, J.F., Bershadsky, A., and Mege, R.M. 2004. Lamellipodium extension and cadherin adhesion: two cell responses to cadherin activation relying on distinct signalling pathways. *Journal of cell science*. 117:257-270.
- Gess, B., Halfter, H., Kleffner, I., Monje, P., Athauda, G., Wood, P.M., Young, P., and Wanner, I.B. 2008. Inhibition of N-cadherin and beta-catenin function reduces axon-induced Schwann cell proliferation. *Journal of neuroscience research*. 86:797-812.
- Ghislain, J., and Charnay, P. 2006. Control of myelination in Schwann cells: a Krox20 cis-regulatory element integrates Oct6, Brn2 and Sox10 activities. *EMBO reports*. 7:52-58.
- Ghislain, J., Desmarquet-Trin-Dinh, C., Jaegle, M., Meijer, D., Charnay, P., and Frain, M. 2002. Characterisation of cis-acting sequences reveals a biphasic, axon-dependent regulation of Krox20 during Schwann cell development. *Development*. 129:155-166.
- Gibbs, R.A., Weinstock, G.M., Metzker, M.L., Muzny, D.M., Sodergren, E.J., Scherer, S., Scott, G., Steffen, D., Worley, K.C., Burch, P.E., Okwuonu, G., Hines, S., Lewis, L., DeRamo, C., Delgado, O., Dugan-Rocha, S., Miner, G., Morgan, M., Hawes, A., Gill, R., Celera, Holt, R.A., Adams, M.D., Amanatides, P.G., Baden-Tillson, H., Barnstead, M., Chin, S., Evans, C.A., Ferreria, S., Fosler, C., Glodek, A., Gu, Z., Jennings, D., Kraft, C.L., Nguyen, T., Pfannkoch, C.M., Sitter, C., Sutton, G.G., Venter, J.C., Woodage, T., Smith, D., Lee, H.M., Gustafson, E., Cahill, P., Kana, A., Doucette-Stamm, L., Weinstock, K., Fectel, K., Weiss, R.B., Dunn, D.M., Green, E.D., Blakesley, R.W., Bouffard, G.G., De Jong, P.J., Osoegawa, K., Zhu, B., Marra, M., Schein, J., Bosdet, I., Fjell, C., Jones, S., Krzywinski, M., Mathewson, C., Siddiqui, A., Wye, N., McPherson, J., Zhao, S., Fraser, C.M., Shetty, J., Shatsman, S., Geer, K., Chen, Y., Abramzon, S., Nierman, W.C., Havlak, P.H., Chen, R., Durbin, K.J., Egan, A., Ren, Y., Song, X.Z., Li, B., Liu, Y., et al. 2004. Genome sequence of the Brown Norway rat yields insights into mammalian evolution. *Nature*. 428:493-521.

- Giese, K.P., Martini, R., Lemke, G., Soriano, P., and Schachner, M. 1992. Mouse P0 gene disruption leads to hypomyelination, abnormal expression of recognition molecules, and degeneration of myelin and axons. *Cell*. 71:565-576.
- Gillespie, C.S., Sherman, D.L., Fleetwood-Walker, S.M., Cottrell, D.F., Tait, S., Garry, E.M., Wallace, V.C., Ure, J., Griffiths, I.R., Smith, A., and Brophy, P.J. 2000. Peripheral demyelination and neuropathic pain behavior in periaxin-deficient mice. *Neuron*. 26:523-531.
- Giovannini, M., Robanus-Maandag, E., van der Valk, M., Niwa-Kawakita, M., Abramowski, V., Goutebroze, L., Woodruff, J.M., Berns, A., and Thomas, G. 2000. Conditional biallelic Nf2 mutation in the mouse promotes manifestations of human neurofibromatosis type 2. *Genes & development*. 14:1617-1630.
- Göhlmann, H., and Talloen, W. 2009. Gene Expression Studies Using Affymetrix Microarrays. CRC Press.
- Gottfried, O.N., Viskochil, D.H., and Couldwell, W.T. 2010. Neurofibromatosis Type 1 and tumorigenesis: molecular mechanisms and therapeutic implications. *Neurosurgical focus*. 28:E8.
- Graca, C.R., Paschoal, V.D., Cordeiro-Soubhia, R.M., Tonelli-Nardi, S.M., Machado, R.L., Kouyoumdjian, J.A., and Baptista Rossit, A.R. 2012. NINJURIN1 single nucleotide polymorphism and nerve damage in leprosy. *Infection, genetics and evolution : journal of molecular epidemiology and evolutionary genetics in infectious diseases*. 12:597-600.
- Guertin, A.D., Zhang, D.P., Mak, K.S., Alberta, J.A., and Kim, H.A. 2005. Microanatomy of axon/glia signaling during Wallerian degeneration. *The Journal of neuroscience : the official journal of the Society for Neuroscience*. 25:3478-3487.
- Gumbiner, B.M. 2000. Regulation of cadherin adhesive activity. *The Journal of cell biology*. 148:399-404.
- Gumbiner, B.M. 2005. Regulation of cadherin-mediated adhesion in morphogenesis. *Nature reviews. Molecular cell biology*. 6:622-634.
- Gupta, S.K., Poduslo, J.F., and Mezei, C. 1988. Temporal changes in PO and MBP gene expression after crush-injury of the adult peripheral nerve. *Brain research*. 464:133-141.
- Hadjantonakis, A.K., Sheward, W.J., Harmar, A.J., de Galan, L., Hoovers, J.M., and Little, P.F. 1997. Celsr1, a neural-specific gene encoding an unusual seven-pass transmembrane receptor, maps to mouse chromosome 15 and human chromosome 22qter. *Genomics*. 45:97-104.
- Halbleib, J.M., and Nelson, W.J. 2006. Cadherins in development: cell adhesion, sorting, and tissue morphogenesis. *Genes & development*. 20:3199-3214.
- Hall, H., Bozic, D., Fauser, C., and Engel, J. 2000. Trimerization of cell adhesion molecule L1 mimics clustered L1 expression on the cell surface: influence on L1-ligand interactions and on promotion of neurite outgrowth. *Journal of neurochemistry*. 75:336-346.
- Hall, S. 2005. The response to injury in the peripheral nervous system. *The Journal of bone and joint surgery. British volume*. 87:1309-1319.
- Haney, C.A., Sahenk, Z., Li, C., Lemmon, V.P., Roder, J., and Trapp, B.D. 1999. Heterophilic binding of L1 on unmyelinated sensory axons mediates Schwann cell adhesion and is required for axonal survival. *The Journal of cell biology*. 146:1173-1184.

- Hansen, S.M., Berezin, V., and Bock, E. 2008. Signaling mechanisms of neurite outgrowth induced by the cell adhesion molecules NCAM and N-cadherin. *Cellular and molecular life sciences : CMLS*. 65:3809-3821.
- Harrisingh, M.C., and Lloyd, A.C. 2004. Ras/Raf/ERK signalling and NF1. *Cell Cycle*. 3:1255-1258.
- Harrisingh, M.C., Perez-Nadales, E., Parkinson, D.B., Malcolm, D.S., Mudge, A.W., and Lloyd, A.C. 2004. The Ras/Raf/ERK signalling pathway drives Schwann cell dedifferentiation. *The EMBO journal*. 23:3061-3071.
- Hartline, D.K., and Colman, D.R. 2007. Rapid conduction and the evolution of giant axons and myelinated fibers. *Current biology : CB*. 17:R29-35.
- Hasegawa, M., Seto, A., Uchiyama, N., Kida, S., Yamashita, T., and Yamashita, J. 1996. Localization of E-cadherin in peripheral glia after nerve injury and repair. *Journal of neuropathology and experimental neurology*. 55:424-434.
- Hoschuetzky, H., Aberle, H., and Kemler, R. 1994. Beta-catenin mediates the interaction of the cadherin-catenin complex with epidermal growth factor receptor. *The Journal of cell biology*. 127:1375-1380.
- Howe, D.G., and McCarthy, K.D. 2000. Retroviral inhibition of cAMP-dependent protein kinase inhibits myelination but not Schwann cell mitosis stimulated by interaction with neurons. *The Journal of neuroscience : the official journal of the Society for Neuroscience*. 20:3513-3521.
- Hu, X., Hicks, C.W., He, W., Wong, P., Macklin, W.B., Trapp, B.D., and Yan, R. 2006. Bace1 modulates myelination in the central and peripheral nervous system. *Nature neuroscience*. 9:1520-1525.
- Huang, W., Sherman, B.T., and Lempicki, R.A. 2009. Systematic and integrative analysis of large gene lists using DAVID bioinformatics resources. *Nature protocols*. 4:44-57.
- Irizarry, R.A., Bolstad, B.M., Collin, F., Cope, L.M., Hobbs, B., and Speed, T.P. 2003b. Summaries of Affymetrix GeneChip probe level data. *Nucleic acids research*. 31:e15.
- Irizarry, R.A., Hobbs, B., Collin, F., Beazer-Barclay, Y.D., Antonellis, K.J., Scherf, U., and Speed, T.P. 2003a. Exploration, normalization, and summaries of high density oligonucleotide array probe level data. *Biostatistics*. 4:249-264.
- Jaegle, M., Ghazvini, M., Mandemakers, W., Piirsoo, M., Driegen, S., Levavasseur, F., Raghoenath, S., Grosveld, F., and Meijer, D. 2003. The POU proteins Brn-2 and Oct-6 share important functions in Schwann cell development. *Genes & development*. 17:1380-1391.
- Jessen, K.R. 2004. Glial cells. *The international journal of biochemistry & cell biology*. 36:1861-1867.
- Jessen, K.R., and Mirsky, R. 1999. Schwann cells and their precursors emerge as major regulators of nerve development. *Trends in neurosciences*. 22:402-410.
- Jessen, K.R., and Mirsky, R. 2005. The origin and development of glial cells in peripheral nerves. *Nature reviews. Neuroscience*. 6:671-682.
- Jessen, K.R., and Mirsky, R. 2008b. Negative regulation of myelination: relevance for development, injury, and demyelinating disease. *Glia*. 56:1552-1565.
- Jessen, K.R., Mirsky, R., and Salzer, J. 2008a. Introduction. Schwann cell biology. *Glia*. 56:1479-1480.
- Joseph, N.M., Mosher, J.T., Buchstaller, J., Snider, P., McKeever, P.E., Lim, M., Conway, S.J., Parada, L.F., Zhu, Y., and Morrison, S.J. 2008. The loss of Nf1 transiently promotes self-renewal but not tumorigenesis by neural crest stem cells. *Cancer cell*. 13:129-140.

- Joseph, N.M., Mukouyama, Y.S., Mosher, J.T., Jaegle, M., Crone, S.A., Dormand, E.L., Lee, K.F., Meijer, D., Anderson, D.J., and Morrison, S.J. 2004. Neural crest stem cells undergo multilineage differentiation in developing peripheral nerves to generate endoneurial fibroblasts in addition to Schwann cells. *Development*. 131:5599-5612.
- Juarez, P., and Palau, F. 2012. Neural and molecular features on charcot-marie-tooth disease plasticity and therapy. *Neural plasticity*. 2012:171636.
- Kawauchi, T. 2011. Regulation of cell adhesion and migration in cortical neurons: Not only Rho but also Rab family small GTPases. *Small GTPases*. 2:36-40.
- Kioussi, C., Gross, M.K., and Gruss, P. 1995. Pax3: a paired domain gene as a regulator in PNS myelination. *Neuron*. 15:553-562.
- Kiryushko, D., Berezin, V., and Bock, E. 2004. Regulators of neurite outgrowth: role of cell adhesion molecules. *Annals of the New York Academy of Sciences*. 1014:140-154.
- Kiselyov, V.V., Berezin, V., Maar, T.E., Soroka, V., Edvardsen, K., Schousboe, A., and Bock, E. 1997. The first immunoglobulin-like neural cell adhesion molecule (NCAM) domain is involved in double-reciprocal interaction with the second immunoglobulin-like NCAM domain and in heparin binding. *The Journal of biological chemistry*. 272:10125-10134.
- Kruger, R.P., Aurandt, J., and Guan, K.L. 2005. Semaphorins command cells to move. *Nature reviews. Molecular cell biology*. 6:789-800.
- Kuhlbrodt, K., Herbarth, B., Sock, E., Hermans-Borgmeyer, I., and Wegner, M. 1998. Sox10, a novel transcriptional modulator in glial cells. *The Journal of neuroscience : the official journal of the Society for Neuroscience*. 18:237-250.
- Kuhn, G., Lie, A., Wilms, S., and Muller, H.W. 1993. Coexpression of PMP22 gene with MBP and P0 during de novo myelination and nerve repair. *Glia*. 8:256-264.
- Kuriyama, S., and Mayor, R. 2008. Molecular analysis of neural crest migration. *Philosophical transactions of the Royal Society of London. Series B, Biological sciences*. 363:1349-1362.
- Kursula, P. 2008. Structural properties of proteins specific to the myelin sheath. *Amino acids*. 34:175-185.
- Lallemand, D., Saint-Amaux, A.L., and Giovannini, M. 2009. Tumor-suppression functions of merlin are independent of its role as an organizer of the actin cytoskeleton in Schwann cells. *Journal of cell science*. 122:4141-4149.
- Le Douarin, N.M., and Kalcheim, C. 1999. The neural crest. Cambridge University Press, Cambridge, UK.
- Le, N., Nagarajan, R., Wang, J.Y., Araki, T., Schmidt, R.E., and Milbrandt, J. 2005a. Analysis of congenital hypomyelinating Egr2Lo/Lo nerves identifies Sox2 as an inhibitor of Schwann cell differentiation and myelination. *Proceedings of the National Academy of Sciences of the United States of America*. 102:2596-2601.
- Le, N., Nagarajan, R., Wang, J.Y., Svaren, J., LaPash, C., Araki, T., Schmidt, R.E., and Milbrandt, J. 2005b. Nab proteins are essential for peripheral nervous system myelination. *Nature neuroscience*. 8:932-940.
- Leblanc, S.E., Srinivasan, R., Ferri, C., Mager, G.M., Gillian-Daniel, A.L., Wrabetz, L., and Svaren, J. 2005. Regulation of cholesterol/lipid biosynthetic genes by Egr2/Krox20 during peripheral nerve myelination. *Journal of neurochemistry*. 93:737-748.

- Lemke, G. 2001. Glial control of neuronal development. *Annual review of neuroscience*. 24:87-105.
- Lemke, G., Lamar, E., and Patterson, J. 1988. Isolation and analysis of the gene encoding peripheral myelin protein zero. *Neuron*. 1:73-83.
- Lemke, G.E., and Brockes, J.P. 1984. Identification and purification of glial growth factor. *The Journal of neuroscience : the official journal of the Society for Neuroscience*. 4:75-83.
- Leskovar, A., Moriarty, L.J., Turek, J.J., Schoenlein, I.A., and Borgens, R.B. 2000. The macrophage in acute neural injury: changes in cell numbers over time and levels of cytokine production in mammalian central and peripheral nervous systems. *The Journal of experimental biology*. 203:1783-1795.
- Letourneau, P.C., Roche, F.K., Shattuck, T.A., Lemmon, V., and Takeichi, M. 1991. Interactions of Schwann cells with neurites and with other Schwann cells involve the calcium-dependent adhesion molecule, N-cadherin. *Journal of neurobiology*. 22:707-720.
- Levenberg, S., Yarden, A., Kam, Z., and Geiger, B. 1999. p27 is involved in N-cadherin-mediated contact inhibition of cell growth and S-phase entry. *Oncogene*. 18:869-876.
- Lewallen, K.A., Shen, Y.A., De la Torre, A.R., Ng, B.K., Meijer, D., and Chan, J.R. 2011. Assessing the role of the cadherin/catenin complex at the Schwann cell-axon interface and in the initiation of myelination. *The Journal of neuroscience : the official journal of the Society for Neuroscience*. 31:3032-3043.
- Li, C., Tropak, M.B., Gerlai, R., Clapoff, S., Abramow-Newerly, W., Trapp, B., Peterson, A., and Roder, J. 1994. Myelination in the absence of myelin-associated glycoprotein. *Nature*. 369:747-750.
- Li, C., and Wong, W.H. 2001. Model-based analysis of oligonucleotide arrays: expression index computation and outlier detection. *Proceedings of the National Academy of Sciences of the United States of America*. 98:31-36.
- Li, Y., Gonzalez, M.I., Meinkoth, J.L., Field, J., Kazanietz, M.G., and Tennekoon, G.I. 2003. Lysophosphatidic acid promotes survival and differentiation of rat Schwann cells. *The Journal of biological chemistry*. 278:9585-9591.
- Lloyd, A.C., Obermuller, F., Staddon, S., Barth, C.F., McMahon, M., and Land, H. 1997. Cooperating oncogenes converge to regulate cyclin/cdk complexes. *Genes & development*. 11:663-677.
- Lunn, E.R., Perry, V.H., Brown, M.C., Rosen, H., and Gordon, S. 1989. Absence of Wallerian Degeneration does not Hinder Regeneration in Peripheral Nerve. *The European journal of neuroscience*. 1:27-33.
- Lustig, M., Zanazzi, G., Sakurai, T., Blanco, C., Levinson, S.R., Lambert, S., Grumet, M., and Salzer, J.L. 2001. Nr-CAM and neurofascin interactions regulate ankyrin G and sodium channel clustering at the node of Ranvier. *Current biology : CB*. 11:1864-1869.
- Mack, T.G., Reiner, M., Beirowski, B., Mi, W., Emanuelli, M., Wagner, D., Thomson, D., Gillingwater, T., Court, F., Conforti, L., Fernando, F.S., Tarlton, A., Andressen, C., Addicks, K., Magni, G., Ribchester, R.R., Perry, V.H., and Coleman, M.P. 2001. Wallerian degeneration of injured axons and synapses is delayed by a Ube4b/Nmnat chimeric gene. *Nature neuroscience*. 4:1199-1206.
- Mai, J.K., and Paxinos, G. 2011. The Human Nervous System. Elsevier Science.

- Maitra, S., Kulikaukas, R.M., Gavilan, H., and Fehon, R.G. 2006. The tumor suppressors Merlin and Expanded function cooperatively to modulate receptor endocytosis and signaling. *Current biology : CB*. 16:702-709.
- Mandemakers, W., Zwart, R., Jaegle, M., Walbeehm, E., Visser, P., Grosveld, F., and Meijer, D. 2000. A distal Schwann cell-specific enhancer mediates axonal regulation of the Oct-6 transcription factor during peripheral nerve development and regeneration. *The EMBO journal*. 19:2992-3003.
- Martin, J.R., and Webster, H.D. 1973. Mitotic Schwann cells in developing nerve: their changes in shape, fine structure, and axon relationships. *Developmental biology*. 32:417-431.
- Martini, R., and Schachner, M. 1997. Molecular bases of myelin formation as revealed by investigations on mice deficient in glial cell surface molecules. *Glia*. 19:298-310.
- Mathon, N.F., Malcolm, D.S., Harrisingh, M.C., Cheng, L., and Lloyd, A.C. 2001. Lack of replicative senescence in normal rodent glia. *Science*. 291:872-875.
- Maurel, P., Einheber, S., Galinska, J., Thaker, P., Lam, I., Rubin, M.B., Scherer, S.S., Murakami, Y., Gutmann, D.H., and Salzer, J.L. 2007. Nectin-like proteins mediate axon Schwann cell interactions along the internode and are essential for myelination. *The Journal of cell biology*. 178:861-874.
- Maurel, P., and Salzer, J.L. 2000. Axonal regulation of Schwann cell proliferation and survival and the initial events of myelination requires PI 3-kinase activity. *The Journal of neuroscience : the official journal of the Society for Neuroscience*. 20:4635-4645.
- McClatchey, A.I., and Fehon, R.G. 2009. Merlin and the ERM proteins--regulators of receptor distribution and signaling at the cell cortex. *Trends in cell biology*. 19:198-206.
- McDonald, D., Cheng, C., Chen, Y., and Zochodne, D. 2006. Early events of peripheral nerve regeneration. *Neuron glia biology*. 2:139-147.
- Meier, C., Parmantier, E., Brennan, A., Mirsky, R., and Jessen, K.R. 1999. Developing Schwann cells acquire the ability to survive without axons by establishing an autocrine circuit involving insulin-like growth factor, neurotrophin-3, and platelet-derived growth factor-BB. *The Journal of neuroscience : the official journal of the Society for Neuroscience*. 19:3847-3859.
- Melendez-Vasquez, C.V., Rios, J.C., Zanazzi, G., Lambert, S., Bretscher, A., and Salzer, J.L. 2001. Nodes of Ranvier form in association with ezrin-radixin-moesin (ERM)-positive Schwann cell processes. *Proceedings of the National Academy of Sciences of the United States of America*. 98:1235-1240.
- Menichella, D.M., Arroyo, E.J., Awatramani, R., Xu, T., Baron, P., Vallat, J.M., Balsamo, J., Lilien, J., Scarlato, G., Kamholz, J., Scherer, S.S., and Shy, M.E. 2001. Protein zero is necessary for E-cadherin-mediated adherens junction formation in Schwann cells. *Molecular and cellular neurosciences*. 18:606-618.
- Meyer, D., Yamaai, T., Garratt, A., Riethmacher-Sonnenberg, E., Kane, D., Theill, L.E., and Birchmeier, C. 1997. Isoform-specific expression and function of neuregulin. *Development*. 124:3575-3586.
- Michailov, G.V., Sereda, M.W., Brinkmann, B.G., Fischer, T.M., Haug, B., Birchmeier, C., Role, L., Lai, C., Schwab, M.H., and Nave, K.A. 2004. Axonal neuregulin-1 regulates myelin sheath thickness. *Science*. 304:700-703.

- Min, Y., Kristiansen, K., Boggs, J.M., Husted, C., Zasadzinski, J.A., and Israelachvili, J. 2009. Interaction forces and adhesion of supported myelin lipid bilayers modulated by myelin basic protein. *Proceedings of the National Academy of Sciences of the United States of America*. 106:3154-3159.
- Monk, K.R., Naylor, S.G., Glenn, T.D., Mercurio, S., Perlin, J.R., Dominguez, C., Moens, C.B., and Talbot, W.S. 2009. A G protein-coupled receptor is essential for Schwann cells to initiate myelination. *Science*. 325:1402-1405.
- Montag, D., Giese, K.P., Bartsch, U., Martini, R., Lang, Y., Bluthmann, H., Karthigasan, J., Kirschner, D.A., Wintergerst, E.S., Nave, K.A., and et al. 1994. Mice deficient for the myelin-associated glycoprotein show subtle abnormalities in myelin. *Neuron*. 13:229-246.
- Monuki, E.S., Weinmaster, G., Kuhn, R., and Lemke, G. 1989. SCIP: a glial POU domain gene regulated by cyclic AMP. *Neuron*. 3:783-793.
- Morgan, L., Jessen, K.R., and Mirsky, R. 1991. The effects of cAMP on differentiation of cultured Schwann cells: progression from an early phenotype (04+) to a myelin phenotype (P0+, GFAP-, N-CAM-, NGF-receptor-) depends on growth inhibition. *The Journal of cell biology*. 112:457-467.
- Morris, J.H., Hudson, A.R., and Weddell, G. 1972. A study of degeneration and regeneration in the divided rat sciatic nerve based on electron microscopy. IV. Changes in fascicular microtopography, perineurium and endoneurial fibroblasts. *Z Zellforsch Mikrosk Anat*. 124:165-203.
- Morrison, H., Sperka, T., Manent, J., Giovannini, M., Ponta, H., and Herrlich, P. 2007. Merlin/neurofibromatosis type 2 suppresses growth by inhibiting the activation of Ras and Rac. *Cancer research*. 67:520-527.
- Morrison, S.J., White, P.M., Zock, C., and Anderson, D.J. 1999. Prospective identification, isolation by flow cytometry, and in vivo self-renewal of multipotent mammalian neural crest stem cells. *Cell*. 96:737-749.
- Murphy, P., Topilko, P., Schneider-Maunoury, S., Seitanidou, T., Baron-Van Evercooren, A., and Charnay, P. 1996. The regulation of Krox-20 expression reveals important steps in the control of peripheral glial cell development. *Development*. 122:2847-2857.
- Nagaraj, S.H., Gasser, R.B., and Ranganathan, S. 2007. A hitchhiker's guide to expressed sequence tag (EST) analysis. *Briefings in bioinformatics*. 8:6-21.
- Napoli, I., Noon, L.A., Ribeiro, S., Kerai, A.P., Parrinello, S., Rosenberg, L.H., Collins, M.J., Harrisingh, M.C., White, I.J., Woodhoo, A., and Lloyd, A.C. 2012. A central role for the ERK-signaling pathway in controlling Schwann cell plasticity and peripheral nerve regeneration in vivo. *Neuron*. 73:729-742.
- Nave, K.A. 2010a. Myelination and the trophic support of long axons. *Nature reviews. Neuroscience*. 11:275-283.
- Nave, K.A. 2010b. Myelination and support of axonal integrity by glia. *Nature*. 468:244-252.
- Nave, K.A., and Salzer, J.L. 2006. Axonal regulation of myelination by neuregulin 1. *Current opinion in neurobiology*. 16:492-500.
- Noe, V., Willems, J., Vandekerckhove, J., Roy, F.V., Bruyneel, E., and Mareel, M. 1999. Inhibition of adhesion and induction of epithelial cell invasion by HAV-containing E-cadherin-specific peptides. *Journal of cell science*. 112 (Pt 1):127-135.
- Ogata, T., Iijima, S., Hoshikawa, S., Miura, T., Yamamoto, S., Oda, H., Nakamura, K., and Tanaka, S. 2004. Opposing extracellular signal-regulated kinase and

- Akt pathways control Schwann cell myelination. *The Journal of neuroscience : the official journal of the Society for Neuroscience*. 24:6724-6732.
- Oinuma, I., Ishikawa, Y., Katoh, H., and Negishi, M. 2004. The Semaphorin 4D receptor Plexin-B1 is a GTPase activating protein for R-Ras. *Science*. 305:862-865.
- Overturf, K., al-Dhalimy, M., Ou, C.N., Finegold, M., and Grompe, M. 1997. Serial transplantation reveals the stem-cell-like regenerative potential of adult mouse hepatocytes. *The American journal of pathology*. 151:1273-1280.
- Owens, G.C., Boyd, C.J., Bunge, R.P., and Salzer, J.L. 1990. Expression of recombinant myelin-associated glycoprotein in primary Schwann cells promotes the initial investment of axons by myelinating Schwann cells. *The Journal of cell biology*. 111:1171-1182.
- Owens, G.C., and Bunge, R.P. 1991. Schwann cells infected with a recombinant retrovirus expressing myelin-associated glycoprotein antisense RNA do not form myelin. *Neuron*. 7:565-575.
- Parkinson, D.B., Bhaskaran, A., Arthur-Farraj, P., Noon, L.A., Woodhoo, A., Lloyd, A.C., Feltri, M.L., Wrabetz, L., Behrens, A., Mirsky, R., and Jessen, K.R. 2008. c-Jun is a negative regulator of myelination. *The Journal of cell biology*. 181:625-637.
- Parkinson, D.B., Bhaskaran, A., Droggiti, A., Dickinson, S., D'Antonio, M., Mirsky, R., and Jessen, K.R. 2004. Krox-20 inhibits Jun-NH2-terminal kinase/c-Jun to control Schwann cell proliferation and death. *The Journal of cell biology*. 164:385-394.
- Parmantier, E., Lynn, B., Lawson, D., Turmaine, M., Namini, S.S., Chakrabarti, L., McMahon, A.P., Jessen, K.R., and Mirsky, R. 1999. Schwann cell-derived Desert hedgehog controls the development of peripheral nerve sheaths. *Neuron*. 23:713-724.
- Parrinello, S., and Lloyd, A.C. 2009. Neurofibroma development in NF1--insights into tumour initiation. *Trends in cell biology*. 19:395-403.
- Parrinello, S., Napoli, I., Ribeiro, S., Wingfield Digby, P., Fedorova, M., Parkinson, D.B., Doddrell, R.D., Nakayama, M., Adams, R.H., and Lloyd, A.C. 2010. EphB signaling directs peripheral nerve regeneration through Sox2-dependent Schwann cell sorting. *Cell*. 143:145-155.
- Parrinello, S., Noon, L.A., Harrisingh, M.C., Wingfield Digby, P., Rosenberg, L.H., Cremona, C.A., Echave, P., Flanagan, A.M., Parada, L.F., and Lloyd, A.C. 2008. NF1 loss disrupts Schwann cell-axonal interactions: a novel role for semaphorin 4F. *Genes & development*. 22:3335-3348.
- Parrinello, S., Samper, E., Krtolica, A., Goldstein, J., Melov, S., and Campisi, J. 2003. Oxygen sensitivity severely limits the replicative lifespan of murine fibroblasts. *Nature cell biology*. 5:741-747.
- Patel, S.D., Chen, C.P., Bahna, F., Honig, B., and Shapiro, L. 2003. Cadherin-mediated cell-cell adhesion: sticking together as a family. *Current opinion in structural biology*. 13:690-698.
- Perlin, J.R., and Talbot, W.S. 2007. Putting the glue in glia: Necls mediate Schwann cell axon adhesion. *The Journal of cell biology*. 178:721-723.
- Perrais, M., Chen, X., Perez-Moreno, M., and Gumbiner, B.M. 2007. E-cadherin homophilic ligation inhibits cell growth and epidermal growth factor receptor signaling independently of other cell interactions. *Molecular biology of the cell*. 18:2013-2025.

- Perrin-Tricaud, C., Rutishauser, U., and Tricaud, N. 2007. P120 catenin is required for thickening of Schwann cell myelin. *Molecular and cellular neurosciences*. 35:120-129.
- Perron, J.C., and Bixby, J.L. 1999. Distinct neurite outgrowth signaling pathways converge on ERK activation. *Molecular and cellular neurosciences*. 13:362-378.
- Pina-Oviedo, S., and Ortiz-Hidalgo, C. 2008. The normal and neoplastic perineurium: a review. *Advances in anatomic pathology*. 15:147-164.
- Podratz, J.L., Rodriguez, E., and Windebank, A.J. 2001. Role of the extracellular matrix in myelination of peripheral nerve. *Glia*. 35:35-40.
- Poliak, S., Gollan, L., Martinez, R., Custer, A., Einheber, S., Salzer, J.L., Trimmer, J.S., Shrager, P., and Peles, E. 1999. Caspr2, a new member of the neurexin superfamily, is localized at the juxtaparanodes of myelinated axons and associates with K⁺ channels. *Neuron*. 24:1037-1047.
- Poliak, S., Matlis, S., Ullmer, C., Scherer, S.S., and Peles, E. 2002. Distinct claudins and associated PDZ proteins form different autotypic tight junctions in myelinating Schwann cells. *The Journal of cell biology*. 159:361-372.
- Poliak, S., and Peles, E. 2003. The local differentiation of myelinated axons at nodes of Ranvier. *Nature reviews. Neuroscience*. 4:968-980.
- Poliak, S., Salomon, D., Elhanany, H., Sabanay, H., Kiernan, B., Pevny, L., Stewart, C.L., Xu, X., Chiu, S.Y., Shrager, P., Furley, A.J., and Peles, E. 2003. Juxtaparanodal clustering of Shaker-like K⁺ channels in myelinated axons depends on Caspr2 and TAG-1. *The Journal of cell biology*. 162:1149-1160.
- Polyak, K., and Kalluri, R. 2010. The role of the microenvironment in mammary gland development and cancer. *Cold Spring Harbor perspectives in biology*. 2:a003244.
- Pummi, K.P., Heape, A.M., Grenman, R.A., Peltonen, J.T., and Peltonen, S.A. 2004. Tight junction proteins ZO-1, occludin, and claudins in developing and adult human perineurium. *The journal of histochemistry and cytochemistry : official journal of the Histochemistry Society*. 52:1037-1046.
- Purves, D., Augustine, G.J., Fitzpatrick, D., and Hall, W.C. 2001. Neuroscience. Sinauer Associates, Sunderland (MA).
- Quintes, S., Goebbels, S., Saher, G., Schwab, M.H., and Nave, K.A. 2010. Neuron-glia signaling and the protection of axon function by Schwann cells. *Journal of the peripheral nervous system : JPNS*. 15:10-16.
- Ramesh, V. 2004. Merlin and the ERM proteins in Schwann cells, neurons and growth cones. *Nature reviews. Neuroscience*. 5:462-470.
- Ranscht, B. 2000. Cadherins: molecular codes for axon guidance and synapse formation. *International journal of developmental neuroscience : the official journal of the International Society for Developmental Neuroscience*. 18:643-651.
- Reilly, K.M. 2009. Neurofibromatosis and lessons for the war on cancer. *EMBO molecular medicine*. 1:198-200.
- Ribeiro-Resende, V.T., Koenig, B., Nichterwitz, S., Oberhoffner, S., and Schloschauer, B. 2009. Strategies for inducing the formation of bands of Bungner in peripheral nerve regeneration. *Biomaterials*. 30:5251-5259.
- Riccardi, V.M., and Lewis, R.A. 1988. Penetrance of von Recklinghausen neurofibromatosis: a distinction between predecessors and descendants. *American journal of human genetics*. 42:284-289.

- Riethmacher, D., Sonnenberg-Riethmacher, E., Brinkmann, V., Yamaai, T., Lewin, G.R., and Birchmeier, C. 1997. Severe neuropathies in mice with targeted mutations in the ErbB3 receptor. *Nature*. 389:725-730.
- Rosenbluth, J. 1999. A brief history of myelinated nerve fibers: one hundred and fifty years of controversy. *Journal of neurocytology*. 28:251-262.
- Rosoff, W.J., Urbach, J.S., Esrick, M.A., McAllister, R.G., Richards, L.J., and Goodhill, G.J. 2004. A new chemotaxis assay shows the extreme sensitivity of axons to molecular gradients. *Nature neuroscience*. 7:678-682.
- Rozen, S., and Skaletsky, H. 2000. Primer3 on the WWW for general users and for biologist programmers. *Methods Mol Biol*. 132:365-386.
- Ryu, E.J., Wang, J.Y., Le, N., Baloh, R.H., Gustin, J.A., Schmidt, R.E., and Milbrandt, J. 2007. Misexpression of Pou3f1 results in peripheral nerve hypomyelination and axonal loss. *The Journal of neuroscience : the official journal of the Society for Neuroscience*. 27:11552-11559.
- Saher, G., Brugger, B., Lappe-Siefke, C., Mobius, W., Tozawa, R., Wehr, M.C., Wieland, F., Ishibashi, S., and Nave, K.A. 2005. High cholesterol level is essential for myelin membrane growth. *Nature neuroscience*. 8:468-475.
- Salzer, J.L. 2003. Polarized domains of myelinated axons. *Neuron*. 40:297-318.
- Salzer, J.L. 2008. Switching myelination on and off. *The Journal of cell biology*. 181:575-577.
- Salzer, J.L., Brophy, P.J., and Peles, E. 2008. Molecular domains of myelinated axons in the peripheral nervous system. *Glia*. 56:1532-1540.
- Samuels, M.L., Weber, M.J., Bishop, J.M., and McMahon, M. 1993. Conditional transformation of cells and rapid activation of the mitogen-activated protein kinase cascade by an estradiol-dependent human raf-1 protein kinase. *Molecular and cellular biology*. 13:6241-6252.
- Schafer, D.P., and Rasband, M.N. 2006. Glial regulation of the axonal membrane at nodes of Ranvier. *Current opinion in neurobiology*. 16:508-514.
- Scherer, S., and Salzer, J.L. 2001. Axon-Schwann cell interactions during peripheral nerve degeneration and regeneration. Oxford University Press, Oxford.
- Scherer, S.S., Wang, D.Y., Kuhn, R., Lemke, G., Wrabetz, L., and Kamholz, J. 1994. Axons regulate Schwann cell expression of the POU transcription factor SCIP. *The Journal of neuroscience : the official journal of the Society for Neuroscience*. 14:1930-1942.
- Schmid, R.S., Graff, R.D., Schaller, M.D., Chen, S., Schachner, M., Hemperly, J.J., and Maness, P.F. 1999. NCAM stimulates the Ras-MAPK pathway and CREB phosphorylation in neuronal cells. *Journal of neurobiology*. 38:542-558.
- Schmid, R.S., Pruitt, W.M., and Maness, P.F. 2000. A MAP kinase-signaling pathway mediates neurite outgrowth on L1 and requires Src-dependent endocytosis. *The Journal of neuroscience : the official journal of the Society for Neuroscience*. 20:4177-4188.
- Schreiner, S., Cossais, F., Fischer, K., Scholz, S., Bosl, M.R., Holtmann, B., Sendtner, M., and Wegner, M. 2007. Hypomorphic Sox10 alleles reveal novel protein functions and unravel developmental differences in glial lineages. *Development*. 134:3271-3281.
- Seggio, A.M., Narayanaswamy, A., Roysam, B., and Thompson, D.M. 2010. Self-aligned Schwann cell monolayers demonstrate an inherent ability to direct neurite outgrowth. *Journal of neural engineering*. 7:046001.

- Seilheimer, B., Persohn, E., and Schachner, M. 1989. Antibodies to the L1 adhesion molecule inhibit Schwann cell ensheathment of neurons in vitro. *The Journal of cell biology*. 109:3095-3103.
- Shapiro, L., Fannon, A.M., Kwong, P.D., Thompson, A., Lehmann, M.S., Grubel, G., Legrand, J.F., Als-Nielsen, J., Colman, D.R., and Hendrickson, W.A. 1995. Structural basis of cell-cell adhesion by cadherins. *Nature*. 374:327-337.
- Shaw, R.J., Paez, J.G., Curto, M., Yaktine, A., Pruitt, W.M., Saotome, I., O'Bryan, J.P., Gupta, V., Ratner, N., Der, C.J., Jacks, T., and McClatchey, A.I. 2001. The Nf2 tumor suppressor, merlin, functions in Rac-dependent signaling. *Developmental cell*. 1:63-72.
- Sherman, D.L., and Brophy, P.J. 2005. Mechanisms of axon ensheathment and myelin growth. *Nature reviews. Neuroscience*. 6:683-690.
- Sherman, D.L., Fabrizi, C., Gillespie, C.S., and Brophy, P.J. 2001. Specific disruption of a schwann cell dystrophin-related protein complex in a demyelinating neuropathy. *Neuron*. 30:677-687.
- Sherman, D.L., Tait, S., Melrose, S., Johnson, R., Zonta, B., Court, F.A., Macklin, W.B., Meek, S., Smith, A.J., Cottrell, D.F., and Brophy, P.J. 2005. Neurofascins are required to establish axonal domains for saltatory conduction. *Neuron*. 48:737-742.
- Shewan, A.M., Maddugoda, M., Kraemer, A., Stehbens, S.J., Verma, S., Kovacs, E.M., and Yap, A.S. 2005. Myosin 2 is a key Rho kinase target necessary for the local concentration of E-cadherin at cell-cell contacts. *Molecular biology of the cell*. 16:4531-4542.
- Shi, P., Nedelec, S., Wichterle, H., and Kam, L.C. 2010. Combined microfluidics/protein patterning platform for pharmacological interrogation of axon pathfinding. *Lab on a chip*. 10:1005-1010.
- Shibuya, Y., Mizoguchi, A., Takeichi, M., Shimada, K., and Ide, C. 1995. Localization of N-cadherin in the normal and regenerating nerve fibers of the chicken peripheral nervous system. *Neuroscience*. 67:253-261.
- Shtutman, M., Zhurinsky, J., Simcha, I., Albanese, C., D'Amico, M., Pestell, R., and Ben-Ze'ev, A. 1999. The cyclin D1 gene is a target of the beta-catenin/LEF-1 pathway. *Proceedings of the National Academy of Sciences of the United States of America*. 96:5522-5527.
- Simons, M., and Trotter, J. 2007. Wrapping it up: the cell biology of myelination. *Current opinion in neurobiology*. 17:533-540.
- Spiegel, I., Adamsky, K., Eisenbach, M., Eshed, Y., Spiegel, A., Mirsky, R., Scherer, S.S., and Peles, E. 2006. Identification of novel cell-adhesion molecules in peripheral nerves using a signal-sequence trap. *Neuron glia biology*. 2:27-38.
- Spiegel, I., Adamsky, K., Eshed, Y., Milo, R., Sabanay, H., Sarig-Nadir, O., Horresh, I., Scherer, S.S., Rasband, M.N., and Peles, E. 2007. A central role for Necl4 (SynCAM4) in Schwann cell-axon interaction and myelination. *Nature neuroscience*. 10:861-869.
- Srinivasan, R., Sun, G., Keles, S., Jones, E.A., Jang, S.W., Krueger, C., Moran, J.J., and Svaren, J. 2012. Genome-wide analysis of EGR2/SOX10 binding in myelinating peripheral nerve. *Nucleic acids research*.
- Stewart, H.J., Brennan, A., Rahman, M., Zoidl, G., Mitchell, P.J., Jessen, K.R., and Mirsky, R. 2001. Developmental regulation and overexpression of the transcription factor AP-2, a potential regulator of the timing of Schwann cell generation. *The European journal of neuroscience*. 14:363-372.

- Stewart, H.J., Zoidl, G., Rossner, M., Brennan, A., Zoidl, C., Nave, K.A., Mirsky, R., and Jessen, K.R. 1997. Helix-loop-helix proteins in Schwann cells: a study of regulation and subcellular localization of Ids, REB, and E12/47 during embryonic and postnatal development. *Journal of neuroscience research*. 50:684-701.
- Stoll, G., Jander, S., and Myers, R.R. 2002. Degeneration and regeneration of the peripheral nervous system: from Augustus Waller's observations to neuroinflammation. *Journal of the peripheral nervous system : JPNS*. 7:13-27.
- Suter, U., and Scherer, S.S. 2003. Disease mechanisms in inherited neuropathies. *Nature reviews. Neuroscience*. 4:714-726.
- Svaren, J., and Meijer, D. 2008. The molecular machinery of myelin gene transcription in Schwann cells. *Glia*. 56:1541-1551.
- Swirnoff, A.H., Apel, E.D., Svaren, J., Severson, B.R., Zimonjic, D.B., Popescu, N.C., and Milbrandt, J. 1998. Nab1, a corepressor of NGFI-A (Egr-1), contains an active transcriptional repression domain. *Molecular and cellular biology*. 18:512-524.
- Tait, S., Gunn-Moore, F., Collinson, J.M., Huang, J., Lubetzki, C., Pedraza, L., Sherman, D.L., Colman, D.R., and Brophy, P.J. 2000. An oligodendrocyte cell adhesion molecule at the site of assembly of the paranodal axo-glial junction. *The Journal of cell biology*. 150:657-666.
- Takahashi, K., and Yamanaka, S. 2006. Induction of pluripotent stem cells from mouse embryonic and adult fibroblast cultures by defined factors. *Cell*. 126:663-676.
- Tang, S., Shen, Y.J., DeBellard, M.E., Mukhopadhyay, G., Salzer, J.L., Crocker, P.R., and Filbin, M.T. 1997. Myelin-associated glycoprotein interacts with neurons via a sialic acid binding site at ARG118 and a distinct neurite inhibition site. *The Journal of cell biology*. 138:1355-1366.
- Taveggia, C., Feltri, M.L., and Wrabetz, L. 2010. Signals to promote myelin formation and repair. *Nature reviews. Neurology*. 6:276-287.
- Taveggia, C., Zanazzi, G., Petrylak, A., Yano, H., Rosenbluth, J., Einheber, S., Xu, X., Esper, R.M., Loeb, J.A., Shrager, P., Chao, M.V., Falls, D.L., Role, L., and Salzer, J.L. 2005. Neuregulin-1 type III determines the ensheathment fate of axons. *Neuron*. 47:681-694.
- Tawk, M., Makoukji, J., Belle, M., Fonte, C., Trousson, A., Hawkins, T., Li, H., Ghandour, S., Schumacher, M., and Massaad, C. 2011. Wnt/beta-catenin signaling is an essential and direct driver of myelin gene expression and myelinogenesis. *The Journal of neuroscience : the official journal of the Society for Neuroscience*. 31:3729-3742.
- Thornton, M.R., Mantovani, C., Birchall, M.A., and Terenghi, G. 2005. Quantification of N-CAM and N-cadherin expression in axotomized and crushed rat sciatic nerve. *Journal of anatomy*. 206:69-78.
- Tikoo, R., Zanazzi, G., Shiffman, D., Salzer, J., and Chao, M.V. 2000. Cell cycle control of Schwann cell proliferation: role of cyclin-dependent kinase-2. *The Journal of neuroscience : the official journal of the Society for Neuroscience*. 20:4627-4634.
- Todaro, G.J., Green, H., and Goldberg, B.D. 1964. Transformation of Properties of an Established Cell Line by Sv40 and Polyoma Virus. *Proceedings of the National Academy of Sciences of the United States of America*. 51:66-73.

- Tofaris, G.K., Patterson, P.H., Jessen, K.R., and Mirsky, R. 2002. Denervated Schwann cells attract macrophages by secretion of leukemia inhibitory factor (LIF) and monocyte chemoattractant protein-1 in a process regulated by interleukin-6 and LIF. *The Journal of neuroscience : the official journal of the Society for Neuroscience*. 22:6696-6703.
- Topilko, P., Schneider-Maunoury, S., Levi, G., Baron-Van Evercooren, A., Chennoufi, A.B., Seitanidou, T., Babinet, C., and Charnay, P. 1994. Krox-20 controls myelination in the peripheral nervous system. *Nature*. 371:796-799.
- Traka, M., Dupree, J.L., Popko, B., and Karagogeos, D. 2002. The neuronal adhesion protein TAG-1 is expressed by Schwann cells and oligodendrocytes and is localized to the juxtaparanodal region of myelinated fibers. *The Journal of neuroscience : the official journal of the Society for Neuroscience*. 22:3016-3024.
- Tricaud, N., Perrin-Tricaud, C., Bruses, J.L., and Rutishauser, U. 2005. Adherens junctions in myelinating Schwann cells stabilize Schmidt-Lanterman incisures via recruitment of p120 catenin to E-cadherin. *The Journal of neuroscience : the official journal of the Society for Neuroscience*. 25:3259-3269.
- Uemura, K., Kihara, T., Kuzuya, A., Okawa, K., Nishimoto, T., Ninomiya, H., Sugimoto, H., Kinoshita, A., and Shimohama, S. 2006. Characterization of sequential N-cadherin cleavage by ADAM10 and PS1. *Neuroscience letters*. 402:278-283.
- Vander, A.J., Sherman, J.H., and Luciano, D.S. 2001. Human physiology: the mechanisms of body function. McGraw-Hill, New York, USA.
- Wanner, I.B., Guerra, N.K., Mahoney, J., Kumar, A., Wood, P.M., Mirsky, R., and Jessen, K.R. 2006a. Role of N-cadherin in Schwann cell precursors of growing nerves. *Glia*. 54:439-459.
- Wanner, I.B., Mahoney, J., Jessen, K.R., Wood, P.M., Bates, M., and Bunge, M.B. 2006b. Invariant mantling of growth cones by Schwann cell precursors characterize growing peripheral nerve fronts. *Glia*. 54:424-438.
- Wanner, I.B., and Wood, P.M. 2002. N-cadherin mediates axon-aligned process growth and cell-cell interaction in rat Schwann cells. *The Journal of neuroscience : the official journal of the Society for Neuroscience*. 22:4066-4079.
- Webber, C., and Zochodne, D. 2010. The nerve regenerative microenvironment: early behavior and partnership of axons and Schwann cells. *Experimental neurology*. 223:51-59.
- Williams, E.J., Furness, J., Walsh, F.S., and Doherty, P. 1994. Activation of the FGF receptor underlies neurite outgrowth stimulated by L1, N-CAM, and N-cadherin. *Neuron*. 13:583-594.
- Wolpowitz, D., Mason, T.B., Dietrich, P., Mendelsohn, M., Talmage, D.A., and Role, L.W. 2000. Cysteine-rich domain isoforms of the neuregulin-1 gene are required for maintenance of peripheral synapses. *Neuron*. 25:79-91.
- Wong, M.H., and Filbin, M.T. 1996. Dominant-negative effect on adhesion by myelin Po protein truncated in its cytoplasmic domain. *The Journal of cell biology*. 134:1531-1541.
- Wood, P.M., Schachner, M., and Bunge, R.P. 1990. Inhibition of Schwann cell myelination in vitro by antibody to the L1 adhesion molecule. *The Journal of neuroscience : the official journal of the Society for Neuroscience*. 10:3635-3645.

- Woodhoo, A., Alonso, M.B., Droggiti, A., Turmaine, M., D'Antonio, M., Parkinson, D.B., Wilton, D.K., Al-Shawi, R., Simons, P., Shen, J., Guillemot, F., Radtke, F., Meijer, D., Feltri, M.L., Wrabetz, L., Mirsky, R., and Jessen, K.R. 2009. Notch controls embryonic Schwann cell differentiation, postnatal myelination and adult plasticity. *Nature neuroscience*. 12:839-847.
- Woodhoo, A., and Sommer, L. 2008. Development of the Schwann cell lineage: from the neural crest to the myelinated nerve. *Glia*. 56:1481-1490.
- Wu, J., Williams, J.P., Rizvi, T.A., Kordich, J.J., Witte, D., Meijer, D., Stemmer-Rachamimov, A.O., Cancelas, J.A., and Ratner, N. 2008. Plexiform and dermal neurofibromas and pigmentation are caused by Nf1 loss in desert hedgehog-expressing cells. *Cancer cell*. 13:105-116.
- Yamada, S., Pokutta, S., Drees, F., Weis, W.I., and Nelson, W.J. 2005. Deconstructing the cadherin-catenin-actin complex. *Cell*. 123:889-901.
- Yang, D., Bierman, J., Tarumi, Y.S., Zhong, Y.P., Rangwala, R., Proctor, T.M., Miyagoe-Suzuki, Y., Takeda, S., Miner, J.H., Sherman, L.S., Gold, B.G., and Patton, B.L. 2005. Coordinate control of axon defasciculation and myelination by laminin-2 and -8. *The Journal of cell biology*. 168:655-666.
- Yang, F.C., Ingram, D.A., Chen, S., Zhu, Y., Yuan, J., Li, X., Yang, X., Knowles, S., Horn, W., Li, Y., Zhang, S., Yang, Y., Vakili, S.T., Yu, M., Burns, D., Robertson, K., Hutchins, G., Parada, L.F., and Clapp, D.W. 2008. Nf1-dependent tumors require a microenvironment containing Nf1+/- and c-kit-dependent bone marrow. *Cell*. 135:437-448.
- Yin, X., Crawford, T.O., Griffin, J.W., Tu, P., Lee, V.M., Li, C., Roder, J., and Trapp, B.D. 1998. Myelin-associated glycoprotein is a myelin signal that modulates the caliber of myelinated axons. *The Journal of neuroscience : the official journal of the Society for Neuroscience*. 18:1953-1962.
- Young, P., Boussadia, O., Berger, P., Leone, D.P., Charnay, P., Kemler, R., and Suter, U. 2002. E-cadherin is required for the correct formation of autotypic adherens junctions of the outer mesaxon but not for the integrity of myelinated fibers of peripheral nerves. *Molecular and cellular neurosciences*. 21:341-351.
- Yu, W.M., Yu, H., and Chen, Z.L. 2007. Laminins in peripheral nerve development and muscular dystrophy. *Molecular neurobiology*. 35:288-297.
- Zalc, B., Goujet, D., and Colman, D. 2008. The origin of the myelination program in vertebrates. *Current biology : CB*. 18:R511-512.
- Zanazzi, G., Einheber, S., Westreich, R., Hannocks, M.J., Bedell-Hogan, D., Marchionni, M.A., and Salzer, J.L. 2001. Glial growth factor/neuregulin inhibits Schwann cell myelination and induces demyelination. *The Journal of cell biology*. 152:1289-1299.
- Zelano, J., Wallquist, W., Hailer, N.P., and Cullheim, S. 2006. Expression of nectin-1, nectin-3, N-cadherin, and NCAM in spinal motoneurons after sciatic nerve transection. *Experimental neurology*. 201:461-469.
- Zheng, H., Chang, L., Patel, N., Yang, J., Lowe, L., Burns, D.K., and Zhu, Y. 2008. Induction of abnormal proliferation by nonmyelinating schwann cells triggers neurofibroma formation. *Cancer cell*. 13:117-128.
- Zhu, Y., Ghosh, P., Charnay, P., Burns, D.K., and Parada, L.F. 2002. Neurofibromas in NF1: Schwann cell origin and role of tumor environment. *Science*. 296:920-922.
- Zhu, Y., and Parada, L.F. 2002. The molecular and genetic basis of neurological tumours. *Nature reviews. Cancer*. 2:616-626.

Appendix

Media & datasets located on the attached CD-ROM at the back of this thesis

Time-lapse videos

- Video 3.1** NS interactions with DRGs
- Video 3.2** LTD interactions with DRGs
- Video 4.1** NS Ncad siRNA interactions with DRGs
- Video 4.2** Fb AdGFP interactions with DRGs
- Video 4.3** Fb AdNcad interactions with DRGs
- Video 5.1** NR Tmx Scram interactions with DRGs
- Video 5.2** NR Tmx siNcad interactions with DRGs

Array datasets

- Dataset-A** Full array list
- Dataset-B** Annotated array
- Dataset-C** Annotated array with reduced redundancy
- Dataset-D** Significant genes: $FDR < 0.01$, $FC > 2$ (up/down)
- Dataset-E** Unique significant genes
- Dataset-F** Gene cluster analysis
- Dataset-G** Functional enrichment analysis

Appendix Tables

(A) Table showing the first 120 genes with (i) the greatest down-regulation and (ii) the greatest up-regulation (from Dataset-E)

Accession ID	Gene	Fold-change
<u>(i) 120 most down-regulated genes</u>		
NM_017027	myelin protein zero	-189.9
AA943163	peripheral myelin protein 22	-140.8
AI412746	tweety homolog 1 (Drosophila)	-117.9
AW532566	PDZ domain containing RING finger 3	-113.8
NM_012610	nerve growth factor receptor (TNFR superfamily, member 16)	-111.3
AA925924	cytokine receptor-like factor 1	-103.5
BI283881	actin filament associated protein 1-like 2	-91.4
BM389026	periostin, osteoblast specific factor	-87.6
NM_019153	fibulin 5	-74.2
AI599143	collagen, type XIV, alpha 1	-73.2
NM_013191	S100 calcium binding protein B	-67.1
NM_130738	SNRPN upstream reading frame	-64.9
BF285019	sodium channel, voltage-gated, type VII, alpha	-64.1
AJ131902	growth arrest specific 7	-60.1
AA892798	sclerostin domain containing 1	-57.2
AA925717	apoptosis-associated tyrosine kinase	-54.2
X57764	endothelin receptor type B	-53.1
BM389001	procollagen, type IX, alpha 3	-51.6
AW530272	EGF-like-domain, multiple 8	-48.1
AW144676	similar to RNA binding motif, single stranded interacting protein 3 isoform 1	-44.9
AW144660	secreted frizzled-related protein 1	-44.3
AI385260	hypothetical LOC310540	-44.1
AI059603	DEP domain containing 6	-43.9
AF228917	zinc finger, DHHC-type containing 2	-43.5
BF406693	laminin, alpha 4	-42.2
BI288690	ectonucleoside triphosphate diphosphohydrolase 2	-42.1
NM_031069	NEL-like 1 (chicken)	-36.7
BI286015	Ras association (RalGDS/AF-6) domain family member 4	-36.2
AI230625	similar to Protein C8orf4 (Thyroid cancer protein 1) (TC-1)	-35.5
NM_022297	dimethylarginine dimethylaminohydrolase 1	-35.1
M29294	small nuclear ribonucleoprotein polypeptide N	-34.2
AI717472	tyrosinase-related protein 1	-33.0
AI071251	glypican 4	-32.4
BF388057	hairy/enhancer-of-split related with YRPW motif 2	-30.3
AI705040	CKLF-like MARVEL transmembrane domain containing 5	-30.2
NM_017009	glial fibrillary acidic protein	-29.6

NM_017229	phosphodiesterase 3B, cGMP-inhibited	-29.5
NM_012886	TIMP metalloproteinase inhibitor 3	-29.2
AA996943	phosphatase and actin regulator 1	-28.8
AI598833	LIM domain 7	-28.8
AI171093	protein kinase C, theta	-28.5
BM386525	sema domain, transmembrane domain (TM), and cytoplasmic domain, (semaphorin) 6D	-26.7
BM389302	nidogen 2	-25.7
AI043817	pellino 2	-25.2
NM_031783	neurofilament, light polypeptide	-24.0
NM_019193	SRY (sex determining region Y)-box 10	-23.8
AI235948	nidogen 1	-22.9
AI058424	leucine-rich repeat LGI family, member 4	-22.1
AI176034	tenascin C	-21.9
BE108345	collagen, type XII, alpha 1	-20.8
AI556075	frizzled homolog 8 (Drosophila)	-20.6
AW919178	Palmdelphin	-20.1
AI177031	phosphatidic acid phosphatase type 2B	-19.5
NM_012750	GDNF family receptor alpha 2	-19.5
NM_012935	crystallin, alpha B	-19.4
BM387419	matrilin 2	-18.8
BM388456	collagen, type XI, alpha 1	-18.7
AW535310	ADAM metalloproteinase with thrombospondin type 1 motif, 5	-18.6
BE111706	myristoylated alanine rich protein kinase C substrate	-18.4
BF557676	family with sequence similarity 19 (chemokine (C-C motif)-like), member A5	-18.4
AW533483	peripheral myelin protein 2	-18.1
BI296384	KN motif and ankyrin repeat domains 4	-17.8
AB035507	melanoma cell adhesion molecule	-17.2
AF081582	pleckstrin homology domain containing, family B (evectins) member 1	-16.9
AW529672	zinc finger protein 536	-16.5
NM_012880	superoxide dismutase 3, extracellular	-16.4
BG379319	transforming growth factor, beta induced	-16.4
BG380570	similar to RIKEN cDNA 1200009O22; EST AI316813	-16.3
AA944398	fibulin 2	-16.3
NM_021760	collagen, type V, alpha 3	-15.9
AI013730	similar to hypothetical protein	-15.4
AI233246	insulin-like growth factor binding protein 7	-15.3
BM388427	transmembrane protein 45A	-15.2
AF159103	tumor necrosis factor alpha induced protein 6	-15.0
BE116590	adherens junction associated protein 1	-14.6
NM_130429	lymphoid enhancer binding factor 1	-14.5
AI179828	kelch-like 13 (Drosophila)	-14.5
BF283122	SH3 domain and tetratricopeptide repeats 2	-14.1
BI287851	collagen, type VI, alpha 2	-14.0
NM_017345	L1 cell adhesion molecule	-14.0
BI284296	G protein-coupled receptor 126	-13.5
BG377201	Rho GTPase activating protein 24	-13.5

BI294932	similar to uncharacterized hypothalamus protein HSMNP1	-13.3
AW522302	similar to Galactosylceramide sulfotransferase (GalCer sulfotransferase) (Cerebroside sulfotransferase) (3-phosphoadenylylsulfate:galactosylceramide 3-sulfotransferase) (3-phosphoadenosine-5-phosphosulfate:GalCer sulfotransferase)	-13.0
BG381587	beta-site APP-cleaving enzyme 2	-12.9
BG663483	protocadherin alpha 4	-12.8
M94043	RAB38, member RAS oncogene family	-12.8
BI295963	similar to Protein C20orf158	-12.6
BI295878	kynurenine aminotransferase III	-12.1
AA800701	similar to limb-bud and heart	-12.0
X04440	protein kinase C, beta	-12.0
AW529714	desert hedgehog homolog (Drosophila)	-11.8
BI274101	prostate transmembrane protein, androgen induced 1	-11.7
NM_012817	insulin-like growth factor binding protein 5	-10.9
BG671865	necdin homolog (mouse)	-10.8
BF407272	RPE-spondin	-10.8
NM_012959	GDNF family receptor alpha 1	-10.7
AA943034	cell adhesion molecule 4	-10.7
NM_053927	erythrocyte protein band 4.1-like 3	-10.5
AI407898	immunoglobulin superfamily, member 11	-10.5
AI176393	collagen, type IV, alpha 1	-10.5
BE107450	neuronal regeneration related protein	-10.3
Z78279	collagen, type I, alpha 1	-10.3
AW521619	ubiquitin specific protease 13 (isopeptidase T-3)	-10.3
L02530	frizzled homolog 2 (Drosophila)	-10.2
AB000779	phospholipase D1	-10.0
BE108253	kinesin family member 5C	-9.8
BI302544	tandem C2 domains, nuclear	-9.8
AI180408	feline leukemia virus subgroup C cellular receptor family, member 2	-9.7
BM389644	ras homolog gene family, member J	-9.7
BF546934	leucine rich repeat containing 4B	-9.7
U44948	cysteine and glycine-rich protein 2	-9.4
AI072336	naked cuticle homolog 2 (Drosophila)	-9.2
NM_031333	cadherin 2	-9.1
BI281705	collagen, type IV, alpha 2	-9.0
BG380414	chemokine (C-X-C motif) ligand 14	-8.9
NM_054008	response gene to complement 32	-8.8
AW252169	lipoma HMGIC fusion partner	-8.7
BI295776	sorbin and SH3 domain containing 1	-8.6
BI275485	sema domain, immunoglobulin domain (Ig), short basic domain, secreted, (semaphorin) 3B	-8.5

(ii) 120 most up-regulated Genes

U22520	chemokine (C-X-C motif) ligand 10	83.2
NM_031518	Cd200 molecule	79.1
AA819034	putative ISG12(b) protein	72.4
AI409634	radical S-adenosyl methionine domain containing 2	62.1

AB001382	secreted phosphoprotein 1	58.2
NM_053352	chemokine (C-X-C motif) receptor 7	50.8
BF419319	2'-5'-oligoadenylate synthetase-like	48.8
BI289546	brain expressed gene 4	47.6
NM_017043	prostaglandin-endoperoxide synthase 1	47.5
BE096523	interferon, alpha-inducible protein (clone IFI-15K)	43.1
NM_016991	adrenergic, alpha-1B-, receptor	39.5
NM_033237	galanin prepropeptide	37.8
BE107296	ribosomal protein S6 kinase polypeptide 6	34.8
NM_053779	serine (or cysteine) peptidase inhibitor, clade I, member 1	34.6
AI603408	serum deprivation response	32.5
BI290559	microsomal glutathione S-transferase 2	31.9
AI072459	Eph receptor A4	30.2
AI579422	brain expressed gene 1	28.2
NM_030856	leucine rich repeat neuronal 3	28.1
NM_053502	ATP-binding cassette, sub-family G (WHITE), member 1	27.7
L09752	cyclin D2	26.5
AI175048	SIX homeobox 1	25.7
NM_133523	matrix metalloproteinase 3	25.6
NM_053572	protocadherin 21	24.8
AI716912	pop-eye domain-containing 3	22.0
BG664080	similar to transmembrane 4 superfamily member 10	21.9
D88250	complement component 1, s subcomponent	21.7
BI303019	Periplakin	21.2
L32601	aldo-keto reductase family 1, member C18	21.0
AI716211	hypothetical LOC302884	19.6
NM_031556	caveolin 1, caveolae protein	18.9
AA901088	family with sequence similarity 167, member A	17.5
AF177430	heparan sulfate (glucosamine) 3-O-sulfotransferase 1	16.7
BI290063	pleiomorphic adenoma gene 1	16.1
AA819788	receptor (chemosensory) transporter protein 4	16.1
BI286417	SIX homeobox 4	16.0
BI275896	adipocyte-specific adhesion molecule	16.0
BE098317	tumor necrosis factor receptor superfamily, member 26	15.8
AI178793	mannosidase, alpha, class 2A, member 1	15.2
BI276370	insulin-like growth factor 2 mRNA binding protein 1	14.9
NM_032069	glutamate receptor interacting protein 1	14.8
BI289459	similar to apolipoprotein L2; apolipoprotein L-II	14.8
AA964219	lipase, endothelial	14.8
AA963184	melanoma associated antigen (mutated) 1-like 1	14.6
BI303853	DEAD (Asp-Glu-Ala-Asp) box polypeptide 60	14.4
NM_053843	Fc fragment of IgG, low affinity IIa, receptor (CD32)	14.2
NM_057191	kelch repeat and BTB (POZ) domain containing 10	14.0
AI408343	similar to hypothetical protein LOC340061	13.6
NM_013004	phosphate regulating endopeptidase homolog, X-linked	13.3
NM_053573	olfactomedin 1	13.3

BG380684	reticulon 2	13.2
AW526982	toll-like receptor 2	12.5
NM_031544	adenosine monophosphate deaminase 3	12.5
AF323608	fibrinogen-like 2	11.9
BF419320	WNT1 inducible signaling pathway protein 1	11.3
BF291123	similar to KIAA1217	11.2
NM_012527	cholinergic receptor, muscarinic 3	11.2
AA819458	chromodomain protein, Y chromosome-like 2	10.9
AI599177	teashirt zinc finger homeobox 3	10.8
NM_053897	coagulation factor II (thrombin) receptor-like 1	10.7
U18772	neuronal pentraxin 1	10.7
L07268	aquaporin 1	10.7
BF289229	phospholipase A2 receptor 1	10.5
BF288508	transmembrane protein 16A	10.1
AI101388	B cell RAG associated protein	10.0
BF281337	keratin 8	10.0
AW530225	neuropeptide W	10.0
AI233740	aldo-keto reductase family 1, member B8	9.7
AW534737	basonuclin 2	9.6
NM_080688	phospholipase C, delta 4	9.4
D78610	protein tyrosine phosphatase, receptor type, E	9.2
NM_134455	chemokine (C-X3-C motif) ligand 1	8.9
AI234287	MAM domain containing 2	8.8
AW523000	cadherin 15	8.6
BF282370	cytidine monophosphate (UMP-CMP) kinase 2, mitochondrial	8.5
NM_053346	neuritin 1	8.4
AI575264	DEAD (Asp-Glu-Ala-Asp) box polypeptide 58	8.2
AA963276	ets variant 1	8.1
BE101834	laminin, beta 3	7.9
BF393945	Ral GEF with PH domain and SH3 binding motif 2	7.9
BI298356	four and a half LIM domains 1	7.9
AW140991	regulator of G-protein signaling 17	7.8
BI283829	transmembrane 6 superfamily member 1	7.7
BF284360	X-linked Kx blood group (McLeod syndrome) homolog	7.4
AA012755	tropomyosin 2	7.3
BI289088	heat shock transcription factor 2 binding protein	7.2
NM_021693	SNF1-like kinase	7.2
AI232036	ATPase, Na ⁺ /K ⁺ transporting, beta 1 polypeptide	7.1
NM_053968	metallothionein 3	6.6
NM_053530	twist homolog 1 (Drosophila)	6.5
NM_012627	protein kinase inhibitor beta, (cAMP-dependent, catalytic) inhibitor beta	6.4
BI288816	Ras-related GTP binding D	6.4
BF398531	B-cell CLL/lymphoma 11B (zinc finger protein)	6.4
AW531805	interferon-induced protein with tetratricopeptide repeats 3	6.4
AF075704	solute carrier family 38, member 1	6.3
BI279663	desmocollin 2	6.2

AI232065	Rho GTPase activating protein 18	6.1
NM_133298	glycoprotein (transmembrane) nmb	6.1
AI555447	RGD1565975	6.0
AI179321	dual specificity phosphatase 9	6.0
BE102693	solute carrier family 35, member F2	5.9
NM_012673	Thy-1 cell surface antigen	5.9
BE109193	translocation associated membrane protein 1-like 1	5.9
NM_012528	cholinergic receptor, nicotinic, beta 1 (muscle)	5.8
AI717736	apolipoprotein L 9a	5.7
NM_031802	gamma-aminobutyric acid (GABA) B receptor 2	5.7
AI716026	myotubularin related protein 11	5.7
BG371594	fibroblast growth factor 9	5.6
BI292425	complement component 1, r subcomponent	5.6
AI410264	tetraspanin 12	5.5
AW915529	schlafen 2	5.4
AF474979	cyclin-dependent kinase inhibitor 2B (p15, inhibits CDK4)	5.4
BF414160	insulin-like growth factor 2 mRNA binding protein 3	5.4
BM384457	Rho GTPase activating protein 22	5.3
BE117444	teashirt zinc finger homeobox 1	5.3
BE099622	obscurin-like 1	5.3
NM_012907	apolipoprotein B mRNA editing enzyme, catalytic polypeptide 1	5.3
NM_130419	discoïdin, CUB and LCCL domain containing 2	5.3
M37394	epidermal growth factor receptor	5.2
NM_053687	schlafen 3	5.2

Gene list illustrating (part i) the greatest 120 down-regulated genes, and (part ii) the greatest 120 up-regulated genes. (FDR<0.01, FC>2 up/down). Genes of special interest are highlighted in yellow.

(B) Analysis of probesets and target sequences comprising the Rat 230-2 array

Code	Source	Type	Entire dataset		Non-annotated only		Annotated only	
				%		%		%
AA	GenBank	EST	2341	7.5	875	8.1	1466	7.2
AB	DDBJ	Direct sub	132	0.4	2	0.0	130	0.6
AF	GenBank	Direct sub	494	1.6	8	0.1	486	2.4
AI	GenBank	EST	6821	22.0	2579	23.9	4242	20.9
AJ	EMBL	Direct sub	65	0.2	1	0.0	64	0.3
AT	DDBJ	EST	7	0.0	7	0.1	0	0.0
AW	GenBank	EST	2229	7.2	963	8.9	1266	6.2
AY	GenBank	Direct sub	35	0.1	0	0.0	35	0.2
BE	GenBank	EST	2958	9.5	1324	12.3	1634	8.1
BF	GenBank	EST	5728	18.5	3082	28.6	2646	13.1
BG	GenBank	EST	1453	4.7	482	4.5	971	4.8

BI	GenBank	EST	3155	10.2	957	8.9	2198	10.8
BM	GenBank	EST	1474	4.7	417	3.9	1057	5.2
C	DDBJ	EST	10	0.0	5	0.0	5	0.0
D	DDBJ	Direct sub	100	0.3	2	0.0	98	0.5
H	GenBank	EST	108	0.3	36	0.3	72	0.4
J	GenBank	GSDB direct sub	40	0.1	1	0.0	39	0.2
K	GenBank	GSDB direct sub	4	0.0	0	0.0	4	0.0
L	GenBank	GSDB direct sub	106	0.3	5	0.0	101	0.5
M	GenBank	GSDB direct sub	208	0.7	5	0.0	203	1.0
N	GenBank & DDBJ	EST, since been removed	1	0.0	0	0.0	1	0.0
NM	RefSeq	mRNA validated	3170	10.2	5	0.0	3165	15.6
R	GenBank	EST	2	0.0	1	0.0	1	0.0
S	GenBank	Journal scanning	5	0.0	1	0.0	4	0.0
U	GenBank	Direct sub	274	0.9	6	0.1	268	1.3
V	EMBL	Direct sub	1	0.0	0	0.0	1	0.0
X	EMBL	Direct sub	86	0.3	5	0.0	81	0.4
Y	EMBL	Direct sub	25	0.1	0	0.0	25	0.1
Z	EMBL	Direct sub	10	0.0	2	0.0	8	0.0
Totals:			31042	100	10771	100	20271	100

Depositories include EMBL (European Molecular Biology Laboratory), DDBJ (DNA Data Bank of Japan), GenBank (Genetic Sequence database) and RefSeq (Reference Sequence) database.

(C) List of databases/resources used for functional annotation

Database/resource	Genes with term	%
Functional categories		
*COG_ONTOLOGY	71	7.8%
PIR_SEQ_FEATURE	59	6.5%
SP_COMMENT_TYPE	503	55.3%
*SP_PIR_KEYWORDS	541	59.5%
*UP_SEQ_FEATURE	459	50.5%
Gene ontology		
GOTERM_BP_1	611	67.2%
GOTERM_BP_2	609	67.0%
GOTERM_BP_3	573	63.0%
GOTERM_BP_4	560	61.6%
GOTERM_BP_5	523	57.5%
GOTERM_BP_ALL	613	67.4%
*GOTERM_BP_FAT	583	64.1%
GOTERM_CC_1	648	71.3%
GOTERM_CC_2	626	68.9%
GOTERM_CC_3	625	68.8%
GOTERM_CC_4	585	64.4%
GOTERM_CC_5	570	62.7%
GOTERM_CC_ALL	648	71.3%
*GOTERM_CC_FAT	546	60.1%
GOTERM_MF_1	688	75.7%

GOTERM_MF_2	674	74.1%
GOTERM_MF_3	560	61.6%
GOTERM_MF_4	503	55.3%
GOTERM_MF_5	409	45.0%
GOTERM_MF_ALL	688	75.7%
*GOTERM_MF_FAT	561	61.7%
PANTHER_BP_ALL	646	71.1%
PANTHER_MF_ALL	651	71.6%
General annotations		
CHROMOSOME	906	99.7%
CYTOBAND	897	98.7%
ENTREZ_GENE_SUMMARY	382	42.0%
HOMOLOGOUS_GENE	840	92.4%
OFFICIAL_GENE_SYMBOL	908	99.9%
PIR_SUMMARY	297	32.7%
SP_COMMENT	498	54.8%
Literature		
GENERIF_SUMMARY	346	38.1%
PUBMED_ID	692	76.1%
Main accessions		
ENSEMBL_GENE_ID	845	93.0%
ENTREZ_GENE_ID	908	99.9%
Pathways		
*BBID	1	0.1%
EC_NUMBER	129	14.2%
*KEGG_PATHWAY	257	28.3%
PANTHER_PATHWAY	197	21.7%
Protein domains		
BLOCKS	295	32.5%
COG_NAME	71	7.8%
*INTERPRO	603	66.3%
PANTHER_FAMILY	813	89.4%
PANTHER_SUBFAMILY	643	70.7%
PFAM	592	65.1%
*PIR_SUPERFAMILY	280	30.8%
PRINTS	213	23.4%
PRODOM	92	10.1%
PROFILE	319	35.1%
PROSITE	387	42.6%
SCOP_CLASS	25	2.8%
SCOP_FAMILY	25	2.8%
SCOP_FOLD	25	2.8%
SCOP_SUPERFAMILY	24	2.6%
*SMART	339	37.3%
SSF	153	16.8%
TIGRFAMS	45	5.0%
Protein interactions		
BIND	37	4.1%
DIP	14	1.5%
MINT	38	4.2%
REACTOME_INTERACTION	4	0.4%
Tissue expression		
PIR_TISSUE_SPECIFICITY	135	14.9%
UP_TISSUE	579	63.7%

The gene list contained 912 entries, which were cross-references against the ten database ontology and annotation resources (asterisk in bold). The table also shows the number and percentage of genes that could be annotated by all the given resources available to DAVID.

(D) Expanded summary of functional annotation analysis c.f. Table 3.4

Category	Term	No.	%	P-value	BG	Fold
Annotation Cluster 1	Enrichment Score: 14.5					
GOTERM_BP_FAT	GO:0022610~biological adhesion	71	7.81	3.53E-18	463	3.18
GOTERM_BP_FAT	GO:0007155~cell adhesion	71	7.81	3.53E-18	463	3.18
SP_PIR_KEYWORDS	cell adhesion	35	3.85	1.67E-09	180	3.23
Annotation Cluster 2	Enrichment Score: 13.48					
GOTERM_CC_FAT	GO:0031012~extracellular matrix	55	6.05	2.96E-20	252	4.31
GOTERM_CC_FAT	GO:0005578~proteinaceous extracellular matrix	48	5.28	1.05E-17	220	4.31
GOTERM_CC_FAT	GO:0044420~extracellular matrix part	30	3.30	2.15E-15	97	6.10
GOTERM_CC_FAT	GO:0044421~extracellular region part	83	9.13	1.76E-13	693	2.36
GOTERM_CC_FAT	GO:0005604~basement membrane	24	2.64	3.74E-13	72	6.58
GOTERM_CC_FAT	GO:0005576~extracellular region	123	13.53	9.53E-13	1281	1.90
SP_PIR_KEYWORDS	extracellular matrix	20	2.20	1.01E-06	89	3.73
Annotation Cluster 3	Enrichment Score: 7.14					
GOTERM_BP_FAT	GO:0032989~cellular component morphogenesis	49	5.39	5.00E-10	376	2.70
GOTERM_BP_FAT	GO:0048666~neuron development	45	4.95	3.32E-09	347	2.69
GOTERM_BP_FAT	GO:0030182~neuron differentiation	53	5.83	5.63E-09	457	2.41
GOTERM_BP_FAT	GO:0031175~neuron projection development	38	4.18	1.04E-08	273	2.89
GOTERM_BP_FAT	GO:0048812~neuron projection morphogenesis	33	3.63	1.09E-08	215	3.18
GOTERM_BP_FAT	GO:0030030~cell projection organization	45	4.95	1.14E-08	361	2.59
GOTERM_BP_FAT	GO:0000902~cell morphogenesis	43	4.73	1.68E-08	340	2.62
GOTERM_BP_FAT	GO:0032990~cell part morphogenesis	35	3.85	3.13E-08	248	2.93
GOTERM_BP_FAT	GO:0048858~cell projection morphogenesis	34	3.74	3.80E-08	238	2.96
GOTERM_BP_FAT	GO:0000904~cell morphogenesis involved in differentiation	32	3.52	5.92E-07	242	2.74
GOTERM_BP_FAT	GO:0048667~cell morphogenesis involved in neuron differentiation	27	2.97	6.90E-06	207	2.71
GOTERM_BP_FAT	GO:0007409~axonogenesis	25	2.75	9.78E-06	186	2.79
GOTERM_BP_FAT	GO:0007411~axon guidance	16	1.76	1.44E-04	105	3.16
Annotation Cluster 4	Enrichment Score: 6.62					
GOTERM_BP_FAT	GO:0007517~muscle organ development	28	3.08	3.43E-08	169	3.44
GOTERM_BP_FAT	GO:0060537~muscle tissue development	24	2.64	1.62E-07	138	3.61
GOTERM_BP_FAT	GO:0014706~striated muscle tissue development	23	2.53	2.62E-07	131	3.64
GOTERM_BP_FAT	GO:0060538~skeletal muscle organ development	17	1.87	7.20E-07	78	4.52

GOTERM_BP_FAT	GO:0007519~skeletal muscle tissue development	17	1.87	7.20E-07	78	4.52
Annotation Cluster 5	Enrichment Score: 5.64					
GOTERM_MF_FAT	GO:0005539~glycosaminoglycan binding	22	2.42	7.65E-09	102	4.60
GOTERM_MF_FAT	GO:0030247~polysaccharide binding	23	2.53	1.66E-08	116	4.23
GOTERM_MF_FAT	GO:0001871~pattern binding	23	2.53	1.66E-08	116	4.23
GOTERM_MF_FAT	GO:0008201~heparin binding	15	1.65	5.00E-06	72	4.44
GOTERM_MF_FAT	GO:0030246~carbohydrate binding	29	3.19	0.0023379	337	1.84
SP_PIR_KEYWORDS	heparin-binding	8	0.88	0.00581103	37	3.59
Annotation Cluster 6	Enrichment Score: 4.43					
GOTERM_CC_FAT	GO:0005624~membrane fraction	63	6.93	1.81E-05	716	1.74
GOTERM_CC_FAT	GO:0005626~insoluble fraction	65	7.15	2.61E-05	755	1.70
GOTERM_CC_FAT	GO:0000267~cell fraction	76	8.36	1.03E-04	967	1.55
Annotation Cluster 7	Enrichment Score: 3.82					
GOTERM_BP_FAT	GO:0001944~vasculature development	29	3.19	1.01E-05	237	2.54
GOTERM_BP_FAT	GO:0001568~blood vessel development	28	3.08	1.63E-05	230	2.52
GOTERM_BP_FAT	GO:0048514~blood vessel morphogenesis	23	2.53	8.70E-05	186	2.56
GOTERM_BP_FAT	GO:0001525~angiogenesis	12	1.32	0.03477	123	2.02
Annotation Cluster 8	Enrichment Score: 3.67					
GOTERM_MF_FAT	GO:0019901~protein kinase binding	20	2.20	1.34E-04	157	2.72
GOTERM_MF_FAT	GO:0019899~enzyme binding	42	4.62	2.35E-04	492	1.82
GOTERM_MF_FAT	GO:0019900~kinase binding	21	2.31	2.90E-04	180	2.49
Annotation Cluster 9	Enrichment Score: 3.22					
GOTERM_BP_FAT	GO:0010033~response to organic substance	71	7.81	9.93E-05	928	1.59
GOTERM_BP_FAT	GO:0048545~response to steroid hormone stimulus	29	3.19	3.76E-04	291	2.07
GOTERM_BP_FAT	GO:0009719~response to endogenous stimulus	47	5.17	4.36E-04	573	1.70
GOTERM_BP_FAT	GO:0009725~response to hormone stimulus	42	4.62	8.70E-04	510	1.71
GOTERM_BP_FAT	GO:0043627~response to estrogen stimulus	16	1.76	0.00509	148	2.24
Annotation Cluster 10	Enrichment Score: 3.13					
GOTERM_BP_FAT	GO:0006928~cell motion	44	4.84	1.74E-06	416	2.19
GOTERM_BP_FAT	GO:0016477~cell migration	26	2.86	7.28E-04	259	2.08
GOTERM_BP_FAT	GO:0051674~localization of cell	26	2.86	0.01513	327	1.65
GOTERM_BP_FAT	GO:0048870~cell motility	26	2.86	0.01513	327	1.65
Annotation Cluster 11	Enrichment Score: 3.08					
SP_PIR_KEYWORDS	Signal	139	15.29	9.44E-08	1517	1.52
SP_PIR_KEYWORDS	Glycoprotein	169	18.59	9.68E-08	1949	1.44
UP_SEQ_FEATURE	signal peptide	139	15.29	5.65E-07	1516	1.46
UP_SEQ_FEATURE	glycosylation site:N-linked (GlcNAc...)	155	17.05	1.27E-05	1831	1.35
SP_PIR_KEYWORDS	disulfide bond	116	12.76	2.68E-05	1340	1.44
UP_SEQ_FEATURE	disulfide bond	105	11.55	0.00154	1272	1.32
SP_PIR_KEYWORDS	Secreted	66	7.26	0.00242	765	1.43
SP_PIR_KEYWORDS	Membrane	215	23.65	0.00329	3063	1.16
UP_SEQ_FEATURE	topological domain:Extracellular	95	10.45	0.00616	1181	1.28

UP_SEQ_FEATURE	topological domain:Cytoplasmic	113	12.43	0.02556	1516	1.19
SP_PIR_KEYWORDS	Transmembrane	162	17.82	0.12788	2478	1.09
UP_SEQ_FEATURE	transmembrane region	143	15.73	0.13745	2097	1.09
GOTERM_CC_FAT	GO:0031224~intrinsic to membrane	193	21.23	0.99902	4467	0.85
GOTERM_CC_FAT	GO:0016021~integral to membrane	178	19.58	0.99995	4336	0.81
Annotation Cluster 12	Enrichment Score: 2.97					
GOTERM_BP_FAT	GO:0030029~actin filament-based process	21	2.31	5.15E-04	183	2.38
GOTERM_BP_FAT	GO:0030036~actin cytoskeleton organization	20	2.20	7.64E-04	175	2.37
GOTERM_BP_FAT	GO:0007010~cytoskeleton organization	28	3.08	0.00302	318	1.83

E) Gene cluster analysis (showing first 13 out of 28 gene groups)

Affy ID	Gene Name	Fold-change
Gene Group 1	Enrichment Score: 9.04	
BF406693	laminin, alpha 4	-42.18
BE108345	collagen, type XII, alpha 1	-20.83
BM387419	matrilin 2	-18.76
BM388456	collagen, type XI, alpha 1	-18.73
BG379319	transforming growth factor, beta induced	-16.40
NM_021760	collagen, type V, alpha 3	-15.88
AI176393	collagen, type IV, alpha 1	-10.47
BI281705	collagen, type IV, alpha 2	-8.97
AI598402	collagen, type VI, alpha 1	-8.03
AA817826	similar to Glypican-6 precursor	-7.65
NM_134452	collagen, type V, alpha 1	-7.24
AA997129	laminin, gamma 1	-3.45
AA891834	collagen, type IV, alpha 5	-2.59
BF392901	collagen, type XXVII, alpha 1	-2.38
AI179399	collagen, type V, alpha 2	-2.27
BF412281	ADAMTS-like 5	-2.04
BF412784	Fras1 related extracellular matrix 1; tetratricopeptide repeat domain 39B	4.35
BE101834	laminin, beta 3	7.93
Gene Group 2	Enrichment Score: 7.90	
AI235948	nidogen 1	-22.91
AI144872	EGF-like, fibronectin type III and laminin G domains	-8.39
BF413643	similar to ribosomal protein L27a; von Willebrand factor A domain containing 1	-7.58
AI235465	coiled-coil domain containing 80	-5.24
AA958001	collagen triple helix repeat containing 1	-3.21
AF065438	lectin, galactoside-binding, soluble, 3 binding protein	2.11
AI407838	hypothetical gene supported by NM_017187; extracellular matrix protein 1	4.38
NM_022230	stanniocalcin 2	4.98
Gene Group 3	Enrichment Score: 6.79	
BM389026	periostin, osteoblast specific factor	-87.60
AA944162	olfactomedin-like 2A	-7.55
AI235465	coiled-coil domain containing 80	-5.24
AF109674	cysteine-rich secretory protein LCCL domain containing 2	-2.24

Gene Group 4	Enrichment Score: 6.01	
AA892798	sclerostin domain containing 1	-57.23
AI113146	acid phosphatase-like 2	-3.97
AW251360	C1q and tumor necrosis factor related protein 6	-3.54
AF140346	secreted frizzled-related protein 4	-2.93
BM384311	platelet-derived growth factor receptor-like	-2.08
NM_022230	stanniocalcin 2	4.98
Gene Group 5	Enrichment Score: 5.64	
NM_017027	myelin protein zero	-189.86
AI412746	tweety homolog 1 (Drosophila)	-117.93
AI385260	hypothetical LOC310540	-44.10
AI556075	frizzled homolog 8 (Drosophila)	-20.56
AB035507	melanoma cell adhesion molecule	-17.21
BG380570	similar to RIKEN cDNA 1200009O22; EST AI316813	-16.33
BE116590	adherens junction associated protein 1	-14.57
NM_017345	L1 cell adhesion molecule	-14.00
BG663483	protocadherin alpha 4	-12.80
NM_012959	GDNF family receptor alpha 1	-10.75
AA943034	cell adhesion molecule 4	-10.69
AI407898	immunoglobulin superfamily, member 11	-10.52
AI180408	feline leukemia virus subgroup C cellular receptor family, member 2	-9.70
BF546934	leucine rich repeat containing 4B	-9.67
NM_031333	cadherin 2	-9.13
AW252169	lipoma HMGIC fusion partner	-8.69
NM_053492	CDW92 antigen	-8.30
L15011	cortexin 1	-7.81
BI301193	tyrosylprotein sulfotransferase 2	-6.81
AF387513	BMP and activin membrane-bound inhibitor, homolog (Xenopus laevis)	-6.23
BG671466	F-box only protein 23	-6.18
NM_013016	signal-regulatory protein alpha	-5.69
NM_031521	neural cell adhesion molecule 1	-5.21
BE103601	cadherin, EGF LAG seven-pass G-type receptor 2 (flamingo homolog, Drosophila)	-5.04
AA956340	protocadherin 7	-4.55
BG665934	membrane bound O-acyltransferase domain containing 2	-4.34
NM_021909	FXYD domain-containing ion transport regulator 5	-3.89
NM_012968	interleukin 1 receptor accessory protein	-3.84
AA891414	ST6 (alpha-N-acetyl-neuraminyl-2,3-beta-galactosyl-1,3)-N-acetylgalactosaminide alpha-2,6-sialyltransferase 2	-3.69
BM390970	fibroblast growth factor receptor-like 1	-3.51
BF283018	DnaJ (Hsp40) homolog, subfamily C, member 22	-3.32
NM_017087	Biglycan	-3.30
AA851945	similar to Tetraspanin-15 (Tspan-15) (Transmembrane 4 superfamily member 15) (Tetraspan NET-7)	-3.28
BG380515	transmembrane protein 59-like	-3.18
BI300274	leucine-rich repeat-containing G protein-coupled receptor 4	-3.02
BE113263	metallophosphoesterase 1	-2.93
D25290	cadherin 6	-2.91
M83143	ST6 beta-galactosamide alpha-2,6-sialyltransferase 1	-2.87
BG378563	claudin 19	-2.79
NM_031337	ST3 beta-galactoside alpha-2,3-sialyltransferase 5	-2.66
AI412938	G protein-coupled receptor 56	-2.53
U72660	ninjurin 1	-2.53
NM_139107	transmembrane protein 150	-2.43
AI232414	peroxisomal membrane protein 4	-2.08
BM384311	platelet-derived growth factor receptor-like	-2.08
BG668228	integral membrane protein 2C	-2.06
AA851939	FXYD domain-containing ion transport regulator 6	-2.04
BF402765	cadherin 10	2.05
BI296264	glycosyltransferase-like 1B	2.13
AI408279	CKLF-like MARVEL transmembrane domain containing 8	2.18

BI275715	transmembrane protein 19	2.22
NM_031646	receptor (G protein-coupled) activity modifying protein 2	2.25
NM_134459	CD99 molecule-like 2	2.26
AI180275	angiotensin II receptor-associated protein	2.30
BF415817	neogenin homolog 1 (chicken)	2.34
BF413152	similar to chromosome 20 open reading frame 39	2.54
AI408095	small cell adhesion glycoprotein	2.55
NM_022926	UDP-N-acetyl-alpha-D-galactosamine:polypeptide N-acetylgalactosaminyltransferase 7 (GalNAc-T7)	2.62
BI296215	solute carrier family 24 (sodium/potassium/calcium exchanger), member 6	2.68
NM_053714	ankylosis, progressive homolog (mouse)	2.68
BG376410	epithelial cell adhesion molecule	2.78
NM_031738	solute carrier family 29 (nucleoside transporters), member 2	2.89
BI295949	stomatin; ABO-family member 5	3.16
NM_031740	UDP-Gal:betaGlcNAc beta 1,4-galactosyltransferase, polypeptide 6	3.36
AW525904	TLC domain containing 1	3.43
NM_057118	contactin 1	3.59
NM_030834	solute carrier family 16, member 3 (monocarboxylic acid transporter 4)	4.12
X74293	integrin alpha 7	4.19
NM_031645	receptor (G protein-coupled) activity modifying protein 1	4.80
NM_130419	discoidin, CUB and LCCL domain containing 2	5.27
AI410264	tetraspanin 12	5.45
NM_031802	gamma-aminobutyric acid (GABA) B receptor 2	5.73
NM_133298	glycoprotein (transmembrane) nmb	6.07
BI279663	desmocollin 2	6.19
BF284360	X-linked Kx blood group (McLeod syndrome) homolog	7.37
NM_053346	neuritin 1	8.35
AW523000	cadherin 15	8.55
AI101388	B cell RAG associated protein	9.98
L07268	aquaporin 1	10.66
BI275896	adipocyte-specific adhesion molecule	15.99
NM_053572	protocadherin 21	24.81
NM_030856	leucine rich repeat neuronal 3	28.15
NM_031518	Cd200 molecule	79.07
Gene Group 6	Enrichment Score: 4.90	
NM_019153	fibulin 5	-74.16
AW530272	EGF-like-domain, multiple 8	-48.07
NM_031069	NEL-like 1 (chicken)	-36.69
BM389302	nidogen 2; similar to nidogen 2 protein	-25.71
AA944398	fibulin 2	-16.28
NM_057100	growth arrest specific 6	-2.73
AB012139	bone morphogenetic protein 1	-2.51
NM_031825	fibrillin 1	-2.18
BI292425	complement component 1, r subcomponent	5.58
Gene Group 7	Enrichment Score: 3.00	
BI275818	serine (or cysteine) peptidase inhibitor, clade E, member 2	-5.85
NM_017200	tissue factor pathway inhibitor (lipoprotein-associated coagulation inhibitor)	-3.38
AI411527	WAP four-disulfide core domain 2	-2.11
NM_053779	serine (or cysteine) peptidase inhibitor, clade I, member 1	34.59
Gene Group 8	Enrichment Score: 2.85	
BI283881	actin filament associated protein 1-like 2	-91.35
BF388057	hairy/enhancer-of-split related with YRPW motif 2	-30.28
NM_019193	SRY (sex determining region Y)-box 10	-23.76
NM_130429	lymphoid enhancer binding factor 1	-14.54
AI177143	homeo box D9	-6.69
BI284495	transcription factor AP-2, gamma	-5.35
NM_013154	CCAAT/enhancer binding protein (C/EBP), delta	-5.04
BE107033	ecotropic viral integration site 1	-4.40

BF415939	FBJ osteosarcoma oncogene	-3.47
NM_053369	transcription factor 4	-3.45
BE104219	myocyte enhancer factor 2C	-3.36
AI045857	Kruppel-like factor 13	-3.21
BF548737	SRY (sex determining region Y)-box 2	-3.19
BM390477	similar to CCAAT displacement protein isoform b; cut-like homeobox 1	-3.06
BI289559	SRY (sex determining region Y)-box 6	-2.98
NM_053894	Jun dimerization protein 2	-2.39
BE104098	Meis homeobox 2	-2.36
BM386654	SCAN domain-containing 1	-2.33
BE113920	signal transducer and activator of transcription 3	-2.17
BM392093	WW domain containing transcription regulator 1	-2.12
AI175992	catenin, beta-interacting protein 1	2.12
AA998296	recombination signal binding protein for immunoglobulin kappa J region; recombining binding protein suppressor of hairless (Drosophila)	2.14
NM_031789	nuclear factor, erythroid derived 2, like 2	2.33
NM_053412	interleukin enhancer binding factor 3	2.35
BE099050	nuclear factor I/B	2.48
NM_053720	apoptosis antagonizing transcription factor	2.50
BE108745	nucleosomal binding protein 1; similar to Nucleosome binding protein 1 (Nucleosome binding protein 45) (NBP-45) (GARP45 protein); nucleosome binding protein 1 (predicted)	2.90
NM_053349	SRY (sex determining region Y)-box 11	4.36
NM_013060	inhibitor of DNA binding 2	4.85
BF398531	B-cell CLL/lymphoma 11B (zinc finger protein)	6.39
AA963276	ets variant 1	8.06
BI286417	SIX homeobox 4	16.04
AI175048	SIX homeobox 1	25.73
Gene Group 9	Enrichment Score: 2.51	
AW532566	PDZ domain containing RING finger 3	-113.78
AF228917	zinc finger, DHHC-type containing 2	-43.53
AI598833	LIM domain 7	-28.81
BM387419	matrilin 2	-18.76
AW535310	ADAM metallopeptidase with thrombospondin type 1 motif, 5	-18.59
AI013730	similar to hypothetical protein	-15.41
U44948	cysteine and glycine-rich protein 2	-9.42
BG373522	MICAL-like 2	-7.83
BM386413	tripartite motif protein 2	-7.51
AI104117	PDZ and LIM domain 7	-7.12
BM384701	peroxidasin homolog (Drosophila)	-6.54
BG673169	similar to SMAD-interacting zinc finger protein 2	-4.75
AA962978	family with sequence similarity 149, member A	-4.75
BF416285	a disintegrin-like and metalloprotease (reprolysin type) with thrombospondin type 1 motif, 9	-4.10
BE109520	family with sequence similarity 134, member B	-3.77
NM_017062	reversion induced LIM gene	-3.63
AI030916	similar to arginyl aminopeptidase (aminopeptidase B)-like 1	-3.47
NM_017148	cysteine and glycine-rich protein 1	-2.96
BE113263	metallophosphoesterase 1	-2.93
BI284849	vesicle amine transport protein 1 homolog (T californica)	-2.52
BG375362	latent transforming growth factor beta binding protein 4	-2.32
NM_031975	Parathyrosin	-2.27
AW527799	LIM domain containing preferred translocation partner in lipoma	-2.17
AW528458	zinc finger, DHHC-type containing 8	-2.13
BM383785	zinc finger, AN1-type domain 3	-2.06
BF412281	ADAMTS-like 5	-2.04
BI296586	zinc finger, DHHC-type containing 14	2.03
NM_053681	S100 calcium binding protein A3	2.20
AI028875	tripartite motif-containing 26	2.20
AW533683	zinc finger protein 770	2.32
AW522661	ligand of numb-protein X 1	2.40

BE102096	jumonji domain containing 1C	2.42
BE104149	testis derived transcript	2.46
BM390663	dystrobrevin, beta	2.73
U66322	prostaglandin reductase 1	2.81
BF391522	ring finger protein 139	2.95
BF416560	ring finger protein 217	3.26
BG375352	carbonic anhydrase 5b, mitochondrial	4.15
BF412784	tetratricopeptide repeat domain 39B	4.35
BI298356	four and a half LIM domains 1	7.86
AW534737	basonuclin 2	9.59
NM_013004	phosphate regulating endopeptidase homolog, X-linked	13.29
Gene Group 10	Enrichment Score: 2.49	
BE107450	neuronal regeneration related protein	-10.32
AF069525	ankyrin 3, epithelial	-4.04
AF389425	dihydropyrimidinase-like 3	-3.67
NM_031066	fasciculation and elongation protein zeta 1 (zygin I)	-2.38
NM_017195	growth associated protein 43	3.51
AA963276	ets variant 1	8.06
Gene Group 11	Enrichment Score: 2.47	
AI412746	tweety homolog 1 (Drosophila)	-117.93
BF285019	sodium channel, voltage-gated, type VII, alpha	-64.10
NM_017348	solute carrier family 6 (neurotransmitter transporter, creatine), member 8	-5.48
AY028605	potassium large conductance calcium-activated channel, subfamily M, beta member 4	-4.06
NM_021909	FXYD domain-containing ion transport regulator 5	-3.89
NM_139107	transmembrane protein 150	-2.43
NM_053327	chloride channel Ka	-2.33
AA851939	FXYD domain-containing ion transport regulator 6	-2.04
BI296215	solute carrier family 24 (sodium/potassium/calcium exchanger), member 6	2.68
AB013454	solute carrier family 34 (sodium phosphate), member 1	3.07
NM_013125	sodium channel, voltage-gated, type V, alpha subunit	3.17
NM_030834	solute carrier family 16, member 3 (monocarboxylic acid transporter 4)	4.12
AF075704	solute carrier family 38, member 1	6.29
AI232036	ATPase, Na ⁺ /K ⁺ transporting, beta 1 polypeptide	7.08
Gene Group 12	Enrichment Score: 2.32	
AW433901	cadherin, EGF LAG seven-pass G-type receptor 1 (flamingo homolog, Drosophila)	-5.63
AI028942	cordons-bleu homolog (mouse)	-4.10
AI406386	LIM domain only 4	-3.90
BF410961	shroom family member 3	-3.12
AW917849	frizzled homolog 6 (Drosophila)	3.50
NM_053530	twist homolog 1 (Drosophila)	6.46
Gene Group 13	Enrichment Score: 1.94	
NM_012610	nerve growth factor receptor (TNFR superfamily, member 16)	-111.28
AF016296	neuropilin 1	-6.18
NM_019272	semaphorin-4F	-2.92
NM_017310	semaphorin-3A	3.37

312 genes were analysed and 311 were organised into 28 clusters of genes enriched for similar function (shown are the first 13 such related groups ranked by enrichment score).